THE DESIGN OF BENTONITE-SAND MIXTURES

by

Lee Hamilton Mollins

Submitted in accordance with the requirements for the degree of Doctor of Philosophy

Department of Civil Engineering
The University of Leeds

April 1996

The candidate confirms that the work submitted is his own and that appropriate credit has been given where reference is made to the work of others

Abstract

One-dimensional and isotropic swelling tests, hydraulic conductivity tests and triaxial compression tests have been performed at applied stresses up to 450kPa on sodium bentonite powder, sand and compacted sodium bentonite-sand mixtures (5, 10, and 20% bentonite by dry weight). This was done to investigate the use of bentonite improved soils for waste containment, and study the fundamental geotechnical properties of bentonite-sand mixtures using a classical soil mechanics approach.

It was found that air dried bentonite powder swells to reach a state described by a single straight line on a plot of void ratio against the logarithm of vertical effective stress, regardless of preparation technique. The gradient of this line was intermediate between a normal consolidation and rebound line for the same material indicating a different sample fabric when allowed to reach equilibrium from an initially dry state rather than the conventional fully saturated state. Swelling of bentonite-sand mixtures expressed in terms of the clay void ratio show a deviation from bentonite behaviour above a threshold stress which depends on the bentonite content. From this behaviour, a modified principle of effective stress has been proposed. Similar swelling relationships were found for samples under an isotropic confining stress.

Hydraulic conductivity data for bentonite and mixtures indicate an approximately linear relationship between the logarithm of hydraulic conductivity and the logarithm of void ratio. Observed differences in hydraulic conductivity between bentonite and mixtures, when represented in terms of the clay void ratio, are attributed to the sand porosity and tortuosity.

From a stress-dilatancy analysis of triaxial data, the peak strength of mixtures has been shown to depend on the sand relative density. This parameter indicates how the material will behave during shear. A threshold sand relative density has been postulated, which is dependent on the axial strain. Below the threshold value, it is likely that the stress-strain behaviour will be characteristic of the bentonite alone.

A design model based on the clay void ratio, sand porosity and tortuosity, and sand relative density is presented, enabling the hydraulic conductivity or strength of a mixture to be estimated.

TABLE OF CONTENTS

CHAPTER 3

EQUIPMENT AND MATERIALS

CHAPTER 4
EXPERIMENTAL METHODS

CHAPTER 5
RESULTS AND DISCUSSION

CHAPTER 6
FURTHER DISCUSSION

LIST OF FIGURES

Figure **page**

Chapter 2

Chapter 3

Chapter 4

Chapter 5

Chapter 6

Appendix 3

Appendix 5

LIST OF TABLES

LIST OF ABBREVIATIONS

A - R	net electrical attractive pressure
A	cross-sectional area of soil sample
A_e	effective cross-sectional area available for flow
B	pore water pressure coefficient
C	crystobalite
C'	effective contact stress
C_0	pore size term
C_c	compression index
CD	consolidated drained
C_r	rebound index
CU	consolidated undrained
D_{10}	effective particle size
E'	drained stiffness
E_u	undrained stiffness
FH	falling head
G_s	specific gravity
I_D	relative density
I_R	relative dilatancy index
K	earth pressure coefficient
K	permeability
L	length of sample
LL	liquid limit
M	montmorillonite
M_s	specific surface area of solid matrix
N	solution molarity
NCL	normal consolidation line
Q	flow rate
Q	quartz
R - A	net electrical repulsive pressure
RC	Rowe cell
S	number of bonds per unit area
S	settlement
SEL	swelling equilibrium line
S_r	degree of saturation
U	theoretical degree of consolidation
U_f	average degree of consolidation at failure
V_c	volume of clay

V_s	volume of sand
V_{solids}	volume of solids
V_T	total volume
V_v	volume of voids
a	cross-sectional area of burette or standpipe
a_m	fraction of the total area in mineral-to-mineral contact
b	lattice dimensions (or effective particle size)
b	scale factor
c	height of unit cell
c'	effective cohesion intercept
c'_{cv}	cohesion intercept at zero dilatancy
c_v	coefficient of consolidation
d	effective clay particle spacing
e	void ratio
e_c	clay void ratio
e_g	granular void ratio
e_l	void ratio at the liquid limit
e_{max}	maximum void ratio
e_{min}	minimum void ratio
e_s	sand void ratio
g	acceleration due to gravity
h	hydraulic head
h	sample height
i	hydraulic gradient
i	offset constant
k	hydraulic conductivity
k_{clay}	clay hydraulic conductivity
k_{mix}	mixture hydraulic conductivity
m_v	coefficient of volume compressibility
n	porosity
n'_w	effective porosity
n_s	sand porosity
p'	mean effective stress
p'	swelling (osmotic) pressure
q	required physical quantity
q'	deviator stress
r	electrical signal
r^2	coefficient of correlation

r_{vc}	volume ratio
t	elapsed time
t_{50}	time for 50% primary consolidation
t_{90}	time for 90% primary consolidation
t_f	time to failure
u	pore water pressure
u'	equivalent pore water pressure
u_{max}	maximum pore water pressure
v	specific discharge (or superficial flow velocity)
v	specific volume
v_c	clay specific volume
w	moisture content
x	volumetric fraction of dry solids occupied by bentonite in a mixture
Δ_{BB}	base bedding
Δ_{BT}	top bedding
Δ_L	load cell deflection
ΔL	macroscopic length over which flow takes place
ΔL_e	average length of a flow tube through sand
Δ_{ram}	loading system deflection
Δ_S	sample compression
Δ_T	top cap sample reorientation
α	fluidity (or mobility) factor
$\delta\Delta$	horizontal displacement
δV	volume increase
ε_1	major principal strain
ε_A	axial strain
ε_h	horizontal strain
ε_v	volumetric strain
ϕ	piezometric head
ϕ'_{cv}	constant volume angle of shearing resistance
ϕ'_{max}	maximum angle of shearing resistance
ϕ'_r	residual angle of shearing resistance
γ	anion exclusion factor
γ_c	effective clay dry density
γ_w	unit weight of water
η	a factor depending upon drainage conditions at triaxial sample boundaries
μ	viscosity
ρ	density

ρ_d	dry density
ρ_w	density of water
σ	applied external normal stress (total stress)
σ_m	mineral-to-mineral contact stress
σ'	effective normal stress
σ''	intrinsic effective stress
σ'_1	major principal effective stress
σ'_3	minor principal effective stress (effective cell pressure)
σ'_c	clay effective stress
σ'_D	deviator stress
σ'_h	horizontal effective stress
σ'_s	sand effective stress
σ'_v	vertical effective stress
τ	actual geometric tortuosity
τ_a	apparent tortuosity factor
τ_{max}	maximum shear stress
τ_s	sand tortuosity factor
υ	angle of dilation
υ	kinematic viscosity

Acknowledgements

I would firstly like to recognise the support of my supervisors Dr. T. W. Cousens and Dr. D. I. Stewart. Their advice, interest, and encouragement throughout the duration of this project has been invaluable. I also gratefully acknowledge EPSRC for a research scholarship

A great deal of technical support was needed for the construction and repair of laboratory apparatus, and for various computer related problems. I would like to thank all the technical staff of the Civil Engineering Department, in particular, Dave Webster, Dave Wade, Ronnie Keane, Pete Richards, Brian Tomlinson, Ben Hudson and Andy Stewart.

The help which I have received from others within the department is much appreciated, including Phil Studds, Emily Richardson, Matthew Tait, Jack Noble and Marcus Gronqvist. Many thanks to Engineering Geology 93/94 (the Wykeham Wanderers) and the Civil Engineering posse 94-96.

I am truly indebted to my parents for their financial assistance and continual support. Finally, I would like to thank Clare for all her encouragement, belief and reassurance that the end would finally arrive.

CHAPTER 1
INTRODUCTION

1.1 General introduction

On disposal of hazardous waste, the concentration of harmful substances can be much higher than is acceptable from an environmental and health perspective. Therefore, it is necessary to minimise leakage from the disposal site, so that external concentrations of chemicals in the groundwater will not reach unacceptable values. This problem can be solved in several ways. One solution is to bury waste in thick deposits of practically impervious soil or rock. Another solution is to design hydraulic barriers of low hydraulic conductivity. Horizontal or sloping barriers called liners may be artificial (geomembranes) or composed of natural materials such as bentonite-sand mixtures (e.g., Chapuis, 1981).

Bentonite-sand mixtures are often used for landfill liners because the bentonite has the ability to fill the sand pores, due to its high swelling potential, producing a material with a low hydraulic conductivity. Typical design criteria specify only a hydraulic conductivity, typically less than 10^{-9} m/s (e.g., Cowland and Leung, 1991). However, the design of such a liner must also consider the strength and swelling behaviour of the mixture.

Although the geotechnical properties of bentonite and sand individually are well documented, little appears to be known of the behaviour of such materials when mixed together in varying proportions. In addition, classical studies of volume change behaviour, hydraulic conductivity and the strength of clays usually begin with the clay in a fully saturated state from which it is compressed to the desired effective stress for testing. As bentonite-sand liners are constructed with the clay in a relatively dry state, it is unknown how the properties differ when the material is initially on the "dry" side of equilibrium conditions[1]. Therefore, in addition to the application of these materials to waste containment, it is of fundamental interest to understand how initially dry clay-sand mixtures behave in terms of classical soil mechanics. In this dissertation the emphasis is on the latter aspect.

1.2 Aims and approaches

The main objectives of this research were to investigate the volume change behaviour (swelling, normal consolidation and rebound) of bentonite, the swelling of bentonite-sand

[1] If equilibrium conditions are defined by the final void ratio of a sample under a particular applied stress when its pore water pressure is at steady state, then a 'dry' sample has an initial moisture content lower than its fully saturated equilibrium value under the same applied stress.

mixtures and the hydraulic conductivity and strength of bentonite, sand and bentonite-sand mixtures. The aim was to produce a coherent framework of the material behaviour thus enabling a design method for hydraulic conductivity and strength criteria to be suggested. This was achieved by conducting a laboratory test programme on the selected mixtures to accurately determine the properties of engineering interest. Methods of analysis were also developed to enable a quantitative interpretation of the data.

Materials used in the study were sodium Wyoming bentonite and Knapton Quarry sand individually, and 20, 10, and 5% bentonite-sand mixtures (by dry weight). The types of apparatus used for the testing of samples were: consolidometer cells for swelling, normal consolidation and rebound tests (and for indirect measurement of hydraulic conductivity), Rowe, triaxial permeameter and compaction permeameter cells for hydraulic conductivity tests, and triaxial cells for strength tests. The objective was to quantify the behaviour of the mixtures in effective stress terms enabling standard geotechnical approaches to be applied. This was achieved by considering the contributions of the individual phases of the material.

1.3 Structure of the report

In chapter 2, a general description of landfill liner types, construction details and considerations for design are given. The remainder of the chapter focuses on the geotechnical properties of clays and sands individually, and relevant work on artificial soil mixtures and natural soils which contain clay. Since the behaviour of a mixture is likely to be largely influenced by the fine fraction, there is considerable discussion on the behaviour of clays. Possible swelling models, fabric models and strength generating mechanisms are reviewed with particular emphasis on the interaction between clay particles and surface water. In chapter 3, the laboratory equipment and test materials are described. Necessary calibrations to test cells and associated measuring instrumentation are detailed. Experimental methods and possible errors in triaxial test data are given in chapter 4. In addition, saturation techniques, sample preparation and measurement of material parameters are discussed. Results, general discussion of data trends and some data analysis are presented in chapter 5. The soil parameters which are used for interpretation of the behaviour are also defined. A further discussion of the results from chapter 5, and the analysis of triaxial strength data are given in chapter 6. In both chapters 5 and 6 predictive equations for the behaviour of the material are presented and, based on these equations, a design method is proposed in chapter 7. Conclusions and recommendations for both engineering practice and for further research are given in chapter 8.

CHAPTER 2
LITERATURE REVIEW

2.1 Introduction

This chapter is divided into four main sections. As bentonite-sand mixtures have a real application in waste containment, section 2.2 discusses landfill liners in general, considerations for design and the differences between laboratory measured values of hydraulic conductivity, and between laboratory and field values. The remainder of the chapter focuses on the reported properties of bentonite and sand of relevance to the design of bentonite-sand mixtures. In section 2.3, a basic outline of clay mineralogy is given, followed by a detailed review of the proposed mechanisms controlling the swelling of clay soils. Section 2.4 focuses on hydraulic conductivity. Darcy's law is the most widely used equation describing hydraulic flow, this is defined and possible deviations discussed, and the influences of mechanical and physico-chemical effects on clay hydraulic conductivity are described. The principle of effective stress is introduced in section 2.5. This is expanded to cover proposed modified principles of effective stress which account for physico-chemical effects in clay soils. Finally the strength of sand, clay and soil mixtures are discussed. A brief outline of soil stiffness is given in 2.5.7 as this is important when considering the ductility of a liner.

Bentonite is highly active and sand relatively inert, and therefore the majority of discussion focuses on clay alone. Due to the lack of literature the behaviour of clay and sand are considered separately in most cases and previous work on mixtures is included where relevant.

Quoted clay contents are all by dry weight, and unless otherwise stated, full saturation is assumed throughout.

2.2 Landfill Liners

2.2.1 Types of liners, materials and construction

Three types of liner are used in the containment of waste, namely flexible membrane liners, natural liners, and double liner systems which are a composite of a flexible membrane and natural soil. These are discussed in this section and typical construction details are given.

Flexible membrane liners of various geosynthetic materials are commonly used to prevent the migration of leachate from landfills. Final covers also incorporate membranes, preventing water percolating into the waste. The barrier is normally placed on a slope,

with a drainage layer of coarse granular material placed over it. Liquids percolate downwards into a zone over the barrier and flow laterally into a collection system, usually a perforated pipe (McEnroe, 1992). The hydraulic conductivity to water is in the range of about 3×10^{-15} to 300×10^{-15} m/s for several polymer types, and decreases with increasing pressure difference across the membrane. However, transit time for flow may be very short because of its small thickness, typically 0.5-2mm (Mitchell, 1991), and the membrane can be easily punctured. Chapuis (1990b) reports that a defective area smaller than 1% of the total area can increase the leakage by a factor of 1000-10000.

Natural liners can be constructed from compacted clays (e.g., Daniel, 1984), silty soils (e.g., Holtz, 1985), mine tailings (e.g., Jessberger and Beine, 1981), and bentonite-soil mixes (e.g., Chapuis, 1981). The positive properties of clays as barrier materials are supposed to be a low hydraulic conductivity, and high sorption capacity of both organic and inorganic substances (Lundgren and Söderblom, 1985). Several types of clay have been proposed; kaolinite and various bentonites (calcium and sodium for example), which may be processed or unprocessed. Bentonite (a montmorillonitic clay) is one of the more frequently used clays.

Pure clay materials have some undesirable properties such as shrinkage and cracking (if dried) and insufficiently high bearing capacities leading to consolidation or creep and cracking (Dixon and Gray, 1985). Therefore it is usual practice to mix the selected clay material with a local soil. Mitchell's data (1976) indicate that mixing a sand sized fine aggregate with a clay enhances the compaction, thermal and mechanical properties. Dixon et al. (1985) showed the volumetric shrinkage (determined by oven drying) of compacted clay-sand mixtures increases with the compaction water content but decreases with decreasing clay content. For compacted bentonite-sand mixtures, at dry densities of approximately $1.7 Mg/m^3$, they found the volumetric shrinkage is reduced to insignificant values at all water contents when the clay content is 50% or less. However, at lower densities the clay content may need to be much less to prevent shrinkage. Therefore, for natural liners, variations in the clay content, density and placement water content may significantly affect the overall performance. As a consequence, a modern landfill usually incorporates a double liner system.

The concept of double liner systems is that the geomembrane acts as the main barrier to fluid and chemical transport, and the underlying compacted clay serves as a back-up barrier to retard, by virtue of its low hydraulic conductivity and adsorption properties, any flow that has made its way through the membrane (Mitchell, 1991). Such flow may

result from both holes in the membrane and conduction through the intact membrane material by various means.

A typical section of a modern landfill containment system is shown in figure 2.1 (after Oakley, 1987). Outward seepage of leachates from the structure is impeded or controlled by the bentonite-soil layer. The leachate collection and removal system conveys fluids off the earthen liner to collection sumps where it is removed and treated. A final cover placed over the waste, impedes or eliminates infiltration of water into the refuse, controlling leachate generation. The usual mix thickness is 60-300 cm after compaction (Garlanger et al., 1987, Oakley, 1987) and the bentonite content is commonly in the range 5-15%.

A typical construction method involves grading and placement of the sand, spreading the bentonite, mixing the sand and bentonite and adding and mixing in the water (Garlanger et al., 1987). Mixing is done on the site using various techniques such as a rotary tiller or other agricultural mixing equipment, a pulverising mixer, and sometimes a cement mixer. The literature suggests that the cement mixer and the pulverising mixer give the most homogeneous mixes. Installation originally involved sprinkling the dry powder on the borrow soil and mixing by rotivator. Moisture was then added by rainfall or sprinkled. This method produced non homogeneous mixes. Therefore, more recently, the soil is excavated and thoroughly mixed with the bentonite and water (Cowland and Leung, 1991), which avoids bentonite segregation (Chapuis, 1990b). Cowland and Leung (1991) suggest compacting the liner by a vibrating roller in 2 layers with 10 passes per layer to minimise the potential for defects penetrating the entire thickness. O'Sadnick et al. (1995) found no difference in compacted density between 4 and 6 passes of the compactor, but specify a minimum of 6 passes per lift.

2.2.2 Considerations for design

The composition of the mix involves the selection of the soil and the bentonite appropriate for the type of wastes or chemicals to be controlled, and consideration of the possible physico-chemical interactions between the waste and the total layer (bentonite-soil layer plus filter and protection layers, etc.). For example, ionic exchange may occur between sodium and calcium, which lowers the swelling ability of bentonite, hence the performance of the liner. Chapuis (1990a) states that any testing method must verify the long term stability of the total layer and not only that of the bentonite-soil mix. The latter, which may be stable in a long term laboratory test, may have a poor field performance simply because of a filter layer or protective layer made of crushed limestone, which may induce a slow ionic exchange between sodium and calcium.

Depending on its composition, bentonite has an unconfined swelling capacity between 2 to 12ml of water per gram of dry bentonite (Cowland and Leung, 1991). When mixed with soil, therefore, it has the capacity to swell and fill the voids producing a material of low hydraulic conductivity. A number of hazardous waste disposal regulations currently in force in the US stipulate maximum values of hydraulic conductivity, typically in the range of 10^{-8} to 10^{-10} m/s, above which a clay material is considered unacceptable for use in isolation of toxic waste materials (Dunn, 1985).

Laboratory tests are performed to minimise the cost of the mix, which is spread over a large surface area on site (typically between 2 and 25 acres). Due to the various methods of determining the hydraulic conductivity in the laboratory, the exact percentage of bentonite required is difficult to establish. Results of Garlanger et. al (1987) show hydraulic conductivity decreases with increasing bentonite content. They suggest 6% bentonite for a hydraulic conductivity of 10^{-10}m/s and recommend 7.5% is used for actual production to account for content variation. Data from Daniel (1987) show a decrease in hydraulic conductivity with increasing bentonite content in a bentonite-silty sand mix, from 10^{-6}m/s at 0% to approximately 10^{-10}m/s at 16%, with a constant value at about 20% bentonite content. Cowland and Leung (1991) found no noticeable differences using the falling head method and suggest a 7% bentonite content is adequate for a hydraulic conductivity specification of 10^{-9}m/s. O'Sadnick et al. (1995) performed hydraulic conductivity tests on Wyoming bentonite-sand mixtures. Samples containing 10% bentonite all had measured hydraulic conductivities less than 10^{-9}m/s. In addition to the method of measurement, the homogeneity of the mix is also likely to affect its hydraulic conductivity. Slurry trench mixes have hydraulic conductivity values comparable with those of "dry" soil-bentonite liners at much lower bentonite contents. According to Chapuis (1990a) this is due to the natural fines content, and construction method, which produces a more homogeneous mix.

The success of the bentonite-soil liner is dependent on the mixture having the right moisture content at the time of compaction. O'Sadnick et al. (1995) found measured hydraulic conductivities decreased with moisture content ranging from 0.6% below to 4% above optimum for a given bentonite content. Their data indicate that a 9% mix compacted with a Cat 815B compactor, at moisture contents between 0 to +4 percent of optimum and 95% dry density conditions, fulfilled a hydraulic conductivity specification of 10^{-9} m/s. Low compactive effort combined with low moisture content led to marginal hydraulic conductivity values. The same placement moisture content is also recommended by Cowland and Leung (1991). They thought that the hydraulic conductivity would be reduced if compacted at high moisture content, due to swelling.

2.2.3 Laboratory and field measurement

Evaluation of clay barriers and estimates of contaminant flow quantities and patterns can only be as accurate as the values of hydraulic conductivity used to make them. Unfortunately, in many cases these values are quite inaccurate due to the test methods used to determine them: typical variations in hydraulic conductivity were discussed in 2.2.2. Two types of laboratory sample container are most commonly employed; fixed wall and flexible wall. In fixed wall permeameters soils may be compacted inside the container. However, there may not be full contact between the sample and cell wall resulting in side wall leakage. In addition, samples can shrink and pull away from the wall. Flexible wall permeameters minimise sidewall leakage and there is control over vertical and horizontal effective stresses. However, if the effective stress exceeds that in the field, hydraulic conductivity values may be too low (Cowland and Leung, 1991). Cowland and Leung (1991) found mixtures with low bentonite contents (5 & 7%) had hydraulic conductivities up to 2 orders of magnitude higher in a Rowe cell than in a compaction permeameter, using tap water as the permeant. They thought that this was due to large particles (10mm) in a 20mm high sample and, therefore, preferential flow paths. Daniel et al. (1985) found the measured hydraulic conductivity of kaolinite was similar using both types of cell with distilled water as the permeant.

Discrepancy between field and laboratory values of hydraulic conductivity is commonly attributed to the non-representative nature of laboratory samples, i.e., not containing hydraulic defects such as cracks, fissures, poor bonding between clods of clay, zones of inadequate compaction or local heterogeneities in the clay liner (e.g. Day and Daniel, 1985, Chapuis, 1990b). It has been suggested that well compacted liners do not contain such hydraulic defects, but there are few published data to support such hypotheses. Daniel (1984) performed laboratory and field tests on two clay liners. He found that field hydraulic conductivities were generally 10-1000 times larger than values obtained from laboratory tests on either undisturbed or recompacted samples of the clay liner[1]. Recompacted specimens may be non-representative due to variations in the compaction water content, method of compaction, compactive effort, size of clay clods, degree of hydration of clay clods, and various other parameters may not match conditions in the field.

Field studies have indicated that diffusion may be the controlling mechanism of solute transport in many fine-grained soils (e.g., Goodhall and Quigley, 1977, Quigley and Rowe, 1986, Quigley et al., 1987). Permeants also pass through geomembranes by a diffusion process and not as a liquid (Mitchell, 1991). According to Haxo (1990), the

[1]The highest field hydraulic conductivity was 9×10^{-8} m/s.

process involves three steps: solution or absorption of the permeant at the upstream face, diffusion of the dissolved material through the geomembrane (at steady state this process follows Fick's law), and evaporation or desorption from the downstream surface. As a result, it is becoming necessary to evaluate the migration of chemicals through earthen barriers due to diffusion in addition to advection (Shackleford and Daniel, 1991).

2.3 Bentonite volume change behaviour

2.3.1 Introduction

Bentonite is a highly plastic swelling clay which predominantly consists of the clay mineral montmorillonite (typically 85-90%). The name bentonite is generally used to cover the entire family of clays that have montmorillonite as their chief constituent. Bentonites may be divided into two general classes: (1) those that adsorb large quantities of water, swelling greatly in the process; (2) those that adsorb only slightly more water than ordinary plastic clays. Of the former, it is the sodium (Wyoming) type which has received the greatest attention in application to containment of waste from landfills.

This section attempts to draw the literature together, to offer a consistent model for the volume change behaviour of bentonite. Mechanisms of swelling are discussed, and also the factors and properties which control the amount of swelling. The behaviour of clay during consolidation is discussed and the current knowledge regarding the swelling of clay-sand mixtures.

For convenience, the term swelling will be used in a generic sense to describe an increase in volume of clay soils by any mechanism. If, for example, the increase in volume is specifically associated with unloading of a consolidated sample (i.e. rebound), this will be stated.

2.3.2 Mineralogy

The basic structural units of clay comprise tetrahedral and octahedral sheets. These are shown in figure 2.2 (after Mitchell, 1993). The silica sheet is composed of silica tetrahedra; the octahedral sheet is composed of magnesium or aluminium cations co-ordinated octahedrally with oxygens or hydroxyls (Mitchell, 1976). As a result of the lateral extension and vertical stacking of these sheets, a flat platelike structure is formed (e.g., Pellissier and Maree, 1991).

Montmorillonite is an aluminium dioctahedral smectite, and its occurrence in soils of engineering interest is very common. Montmorillonite is a 2:1 layer mineral because its crystals consist of two silica sheets bonded to a central alumina sheet; these three sheets together are referred to as the unit cell. A diagrammatic sketch of the montmorillonite structure is shown in figure 2.3 (after Mitchell, 1993). The height (c dimension) of the unit cell is approximately 10Å; this unit does not expand. Mitchell (1976) states that particles may range in thickness from 10Å (unit cell) upwards to about 1/100 of the width (usually less than 1 or 2μm). Particles with a thickness larger than 10Å consist of

stacks of unit cells. An electron photomicrograph of Wyoming bentonite is shown in figure 2.4 (after Mitchell, 1976).

Interactions between mineral particles, cations and water arise because there are unbalanced forces at the interfaces between mineral contacts due to imperfections in the crystal lattice (e.g., Moore, 1991). Exchange reactions, known as isomorphous substitution, involve the replacement of intersheet cations (within unit cells) with other cations (Helferrich, 1962). Although the exchange process does not affect the structure of the clay minerals themselves, a large negative surface charge is produced which is balanced by cations adsorbed to the clay mineral crystal surfaces in the presence of water (e.g., Mitchell, 1976).

Swelling and shrinkage of clays was first discussed by Terzaghi and Peck (1948). It is thought the distinction between expanding and non-expanding clays is a matter of degree rather than difference in nature. Montmorillonitic and illitic clay layers (unit cells) are roughly 10Å in thickness. Illite particles consist, in general, of layers of 10Å each which are bonded by chemical forces. The volume of water adsorbed by illite particles during swelling is associated with the external surface area of the particle only, and is therefore relatively small. In contrast, the surface area available for adsorption of water in montmorillonite is large, and may increase further if interlayer bonds between individual sheets within the clay particle are broken. As a result the swelling, which implies an increase of the distance between the particles, is large. The swelling of illite is comparatively much less, although is thought to be of a similar nature.

Sections 2.3.4-2.3.6 present explanations for swelling of clay soils found in the literature, described here as interlayer, interparticle and inter-aggregate swelling. Interlayer swelling refers to the water adsorption between the stack of layers (each of 10Å thickness) which make up the clay particle, thereby increasing the particle thickness. Interparticle swelling is the increase in volume caused by water adsorption between the particles, and inter-aggregate swelling describes an increase in volume between clusters of particles. The interaction between clay mineral surfaces and water is important when considering the swelling behaviour of clays, a brief outline is given in section 2.3.3. A proposed model of overall swelling is summarised in section 2.3.7.

2.3.3 Clay-water interaction

Possible mechanisms of soil-water interaction which most likely contribute to the swelling of bentonite are as follows:

1. Hydration of exchangeable cations. Since cations are attracted to negatively charged clay surfaces, their water of hydration will also be. Mitchell (1976) states that this mechanism is most important at low water contents.

2. Hydrogen bonding. The surfaces of clay minerals are usually composed of a layer of either oxygens or hydroxyls. Hydrogen bonding develops, with oxygens attracting the positive corners and hydroxyls the negative corners of water molecules.

3. Attraction by osmosis. The concentration of cations increases as negatively charged clay surfaces are approached. Water molecules tend to diffuse towards the surface in an attempt to equalise concentrations.

These three mechanisms of water adsorption are shown in figure 2.5 (after Mitchell, 1993). Cation hydration and hydrogen bonding are important when considering interlayer swelling, and osmotic attraction is important for interparticle and inter-aggregate swelling.

2.3.4 Interlayer swelling

Water molecules penetrate between layers of montmorillonite clays when in contact with water. If the clay is initially dry, this first stage of hydration (swelling) involves water adsorption in successive monolayers on the interlayer surfaces, which pushes them apart. The principal driving power is the adsorption energy of the water layers on the clay surface. This interlayer swelling causes an increase in the basal spacing to definite values of the order of 12.5 to 20Å, depending on the type of clay and cation (van Olphen, 1977). Studds (personal communication, 1996) has shown the increase in basal spacing to be approximately 10Å (approximately three layers of water molecules) for air-dried Wyoming bentonite in distilled water. Therefore, interlayer swelling leads to at most a doubling of the volume of the dry clay (van Olphen, 1977).

Two alternative mechanisms are proposed, involving cation hydration and hydrogen bonding respectively. In the former, interlayer cations become hydrated and the large hydration energy involved is able to overcome the attractive forces between the layers. Alternatively, it has been proposed that the penetrating water does not hydrate the cations between the layers but becomes adsorbed on the oxygen surfaces by establishing hydrogen bonds. Both these mechanisms are outlined below.

As a result of the uneven charge distribution and dipolar character of water molecules, they are attracted to ions in solution leading to ion hydration. Exchangeable cations between the sheets of a dry clay particle will hydrate when exposed to water (the positive charge of the cation attracts the negative corners of the water molecules). Water molecules will move from their normal structure in free solution into positions in the

hydration shell of a cation, and the energy released forces the clay sheets apart causing swelling (Mitchell, 1976).

Low, and various co-workers have proposed an alternative swelling mechanism relating the properties of surface water to interlayer swelling. It is proposed that the structure of hydrogen bonded water is strained to match that of the montmorillonite, and as a result, the potential energy of the water is altered (e.g., Davidtz and Low, 1970). The lattice (*b*) dimensions (or effective particle size) of the montmorillonite determine the degree of strain introduced into the water structure and, ultimately, the amount of swelling. Data from Low and Margheim (1979) show a linear relation between swelling (defined as the mass ratio of water to montmorillonite at equilibrium) and *b* dimension for montmorillonites having widely different cation exchange capacities.

Pusch (1982) indicates that swelling pressure (i.e., the pressure required to prevent a clay from swelling) is primarily due to crystal/water interaction when the bulk density exceeds about 2 Mg/m^3 and below this density, electrical double layers develop. According to van Olphen (1977), at plate distances beyond about 10Å (approximately 3 water layers), the surface hydration energy is no longer important, and osmotic repulsion becomes the major repulsive force between the plates. This is discussed in 2.3.5.

2.3.5 Interparticle swelling (double layer theory)

The most commonly cited mechanism controlling swelling is osmotic attraction of water molecules to clay particle surfaces. This is known as the osmotic pressure concept of volume change (e.g., Mitchell, 1976). The amount of water which enters the clay can be calculated from the spacing between particles based on double layer theory. Before describing this swelling mechanism it is pertinent to outline briefly the ion distributions in clay-water systems.

Attraction of exchangeable cations to the negatively charged clay particle is opposed by the tendency of the cations to distribute themselves evenly throughout the system (to equalise concentrations throughout). The escaping tendency due to diffusion and the opposing electrostatic attraction lead to a cation distribution adjacent to a clay particle in suspension as shown in figure 2.6 (after Mitchell, 1993). Since the negative charge of the particle and the positive charge of the counter ions are spatially separated, this system can be regarded as an electric double layer. In order to indicate the diffuse character of the counter charge, the term "diffuse double layer" is used (Bolt, 1956). The diffuse double-layer thickness of montmorillonite is a function of the exchangeable sodium content owing to the ions' greater ease of dissociation from the clay surface in

the presence of water. The other exchangeable cations, namely calcium, magnesium, and potassium, are strongly adsorbed by the clay surface and do not contribute significantly to the diffuse double-layer thickness (Sridharan et al., 1990). The interaction of like charged diffuse double layers causes the clay to expand and is generally considered to be the primary force which is responsible for repulsion between two clay particles (e.g., Sridharan and Rao, 1979).

When a clay specimen comes into contact with water, the ionic concentration in the vicinity of clay particles exceeds the concentration in "free" solution, giving rise to an osmotic pressure difference. Since the exchangeable cations stay with the clay (due to electrostatic attraction), a specimen consisting of pure clay can be regarded as an osmometer, the semi-permeable membrane of which is formed by the clay particles themselves (Bolt, 1956). Figure 2.7 (after Mitchell, 1993) shows the interaction of double layers between two adjacent clay particles. The osmotic pressure (or suction) draws water into the zone of high concentration, the clay swells, the inter-particle distance increases, and the suction decreases. At equilibrium, when the clay is neither expanding nor compressing, the external pressure will balance the osmotic pressure (e.g., Graham et al., 1986). Although the osmotic pressure within the double layer decreases continuously with distance from the particle surface, the effective osmotic pressure of the system is determined by the concentration of the ions in the central plane between the interacting double layers (Verwey and Overbeek, 1948).

Calculation of the swelling (osmotic) pressure, based on double-layer theory, was introduced by Schofield (1946), using the Gouy theory of the electrical double layer (Gouy, 1910, Schofield, 1946, Verwey and Overbeek, 1948, and Bolt, 1954). The factors involved in double layer theory are the soil properties, represented by cation exchange capacity and surface area, and the fluid properties, i.e., ion concentration, cation valency, dielectric constant and temperature.

Extensive research has been performed to verify quantitatively the accuracy of double layer theory. Mesri and Olson (1971) performed consolidation and rebound tests on Wyoming bentonite at various electrolyte concentrations. They found double layer theory predicts compression and swelling (rebound) of the right order of magnitude but at low pressures specimens establish equilibrium at a void ratio smaller than predicted, suggesting some sort of potential minimum. The theoretical and experimental curves are shown in figure 2.8. This correlates with work by Nagaraj and Murthy (1986) who found there is practically no force exerted beyond a distance of about 200-300 Å particle separation. Mitchell (1960) performed compression tests on Na-kaolinite, Na-illite and

Na-montmorillonite to study the applicability of the double layer theory to the compression of clays. Based on the test results, he concluded that double layer theory is not applicable to clays containing particles greater than some size between 0.2 and 1.0μm diameter unless the particles have parallel arrangement[2]. Low (1980) argues that less than 1% of exchangeable sodium is dissociated from the montmorillonite particle surfaces, and therefore the primary cause of swelling is the difference in potential energy between the internal and external solutions. However, this surface force effect relates to interlayer swelling (see 2.3.4) and only accounts for a doubling in volume of dry clay, it cannot account for the large swelling observed between individual particles.

Attractive forces (principally London van der Waals forces) are ignored in the theory. Sridharan and Jayadeva (1982) found no difference in the theoretical swelling relationship when the contribution from van der Waals-Hamaker attractive pressure was taken into account. It is thought that attractive forces become significant at a separation of about 20 Å. Hence if the particles come closer than 20 Å, they get attracted to form clusters or aggregates which act as a single unit. Then the externally applied pressure is transferred across two such units or aggregates and the distance between them will be governed by double layer considerations to mobilise the required repulsive force (Nagaraj and Murthy, 1990). This proposed behaviour is the basis for the model of inter-aggregate swelling and is discussed next.

2.3.6 Inter-aggregate swelling

The work of Olsen (1962), Pusch (1970, 1973) and Yong and Sheeran (1973) show that in many soils, clay structure is formed by aggregations of particles, generally defining two types of pore; intra-aggregate and inter-aggregate, the latter involving large distances between the structural units (or clusters). Using mercury intrusion porosimetry[3] on a variety of clays Griffiths and Joshi (1989) propose two types of porosity; the free porosity and entrapped porosity, corresponding to the intra and inter-aggregate pore space (shown in figure 2.9). Delage and Lefebvre (1983) showed that compressibility hence swelling was governed by inter-aggregate pores. The distances involved, in the 1μm range, could not be governed by double layer phenomena. Griffiths and Joshi (1989) also found that only the largest pores are affected during consolidation.

---

[2]This is interpreted as meaning that because montmorillonite particles are so small, the swelling is large whatever the particle arrangement because the water in the diffuse double layer will always be in close proximity to an adjacent particle. This may not apply for clays of larger particle size. Therefore, for clays such as illite and kaolinite the behaviour is controlled by initial particle orientations and physical interactions rather than osmotic repulsive pressures.

[3]The mercury intrusion technique is based on the principle that a non-wetting liquid will not intrude into the pores of a solid unless forced under pressure. The amount of pressure required for mercury intrusion determines the pore radius.

Bolt (1956) using double layer theory on pure clays showed that the initial compression curve deviates somewhat from the expected curve; structural effects are thought to be the cause. As double layer theory assumes parallel alignment of clay particles, this implies that during the first compression (normal consolidation) parallel arrangement is only gradually completed.

As theoretical equations for swelling pressures assume parallel particle orientation, lateral swelling pressures of zero are predicted. At dry densities less than $1.7Mg/m^3$, Gray et al. (1985) found the swelling pressure of bentonite was approximately 1/3 the value predicted by double layer theory[4]. However, at higher dry densities, the swelling pressure along the axis of compaction was found to exceed the pressure orthogonal to it. They proposed that at low densities, samples consist of clusters of particles which develop the theoretical swelling pressure. However, they are randomly arranged and therefore at the macroscale, the mean swelling pressure is developed. As the density increases a more anisotropic fabric is produced, and the swelling pressure tends to that predicted by double layer theory. Pusch and Carlsson (1985) suggested deviation from parallel orientation becomes dominant at dry densities below approximately $1.3Mg/m^3$ with edge to face association. The different limiting density to that found by Gray et al. (1985) may be due the type of bentonite considered.

2.3.7 Summary of swelling mechanisms

To summarise, it appears that three types of swelling can be characterised which collectively contribute to the overall volume increase of bentonite. Firstly, swelling within the clay particle between unit cells appears to be due to either the structure of hydrogen bonded water or hydration of exchangeable cations, both mechanisms causing a potential energy difference between the surface water and the external solution; interlayer swelling. Interlayer swelling is most important at low moisture contents. Secondly, the concentration difference between the solution within the diffuse double layer and the free solution causes osmotic swelling between individual clay particles; interparticle swelling. Clay fabric is likely to be composed of clusters of particles, and double layer type swelling occurs between individual clusters with relatively large pore volumes in the inter-aggregate pores. As the influence of the clay particles on the pore solution decreases with distance from the surface, the water in the centre of the inter-aggregate pores is probably similar in nature to the external solution.

---

[4]Initially dry samples were statically compacted, confined and allowed access to water without allowing volume increase. Swelling pressure was measured both along and orthogonal to the axis of compaction.

If the clay is initially in a dry state at a high confining stress (or density), it is likely that interlayer swelling dominates until approximately 3 water layers have been adsorbed. At this stage the particle diameter is doubled because the unit cell and adsorbed water thicknesses are both approximately 10Å. Any tendency to further separate at this stage is likely to be opposed by van der Waals attractive forces, therefore the layers separate no further, and the particles have a constant thickness[5]. With reducing stress, double layer swelling is expected to dominate with large separation between the particles.

When discussing the swelling of bentonite, many authors fail to distinguish between interlayer and interparticle volume change and the literature is often vague. In addition, quantitative swelling predictions are sometimes based on consolidation data only and it is likely that the behaviour is much different during rebound or swelling from a dry state.

2.3.8 Mechanical and physico-chemical volume change

Swelling is analogous to the process of consolidation. Seed et. al (1962) found the shape of the swelling curve for compacted clays to mirror the consolidation curve, on a volume change versus logarithm of time plot. The compressibility, hence swelling, of clay soils under external load depends on the mechanical properties of the clay minerals and the physico-chemical properties of the pore fluid (e.g. Bolt, 1956, Sridharan and Jayadeva, 1982). Mechanically, compressibility of a clay is controlled primarily by the shearing resistance at the region where two adjacent particles come closest together. This resistance is not equal at all points of contact and volume changes occur by shear displacements and/or sliding between particles (Sridharan and Rao, 1973). Second, compressibility is governed by long-range electrical repulsive forces, which are mainly double layer type.

Mechanical concepts of volume change behaviour appear to be of minor significance in the compressibility and swelling of bentonite. When a coarse grained material such as sand is unloaded there is a resulting deficit in hydrostatic pressure between the particles (a negative pore water pressure), this pressure equalises by water entering the sample. Bolt (1956) found void ratios greater than 20 in the early stages of normal consolidation of bentonite, implying very little contact between clay particles. Since hydrostatic pressure changes occur as a result of mechanical forces (i.e., direct contact) between the grains, this implies that swelling of clay must be of a different nature than in coarse grained soils. Bolt (1956) concluded that compression, hence swelling, was mainly of an osmotic nature. Since the osmotic pressure difference between the pore fluid and the

[5]The attractive forces may be sufficient to prevent further swelling when the sample is in a static state. However if a sample is sheared, for example, the energy input may be enough to overcome attractive forces creating a larger quantity of particles with reduced thicknesses.

"free" solution must equal the external stress on the sample, unloading results in pore fluid entering a sample to regain equilibrium, hence, causing swelling; a physico-chemical effect (see 2.3.5).

Olson and Mesri (1970) found large differences in gradient between virgin and rebound curves of montmorillonite, indicating that particle rearrangement is the major source of virgin compression. They interpreted the very flat rebound curves as indicating that mechanical swelling is a minor component and the major contribution is osmotic adsorption of fluid and formation of diffuse double layers.

2.3.9 Consolidation and rebound

Consolidation is the time dependent positive volumetric straining of soils resulting from dissipation of pore water pressures and consequent transfer of stress to the soil skeleton. Rebound refers to an increase in volume, and results from unloading a previously consolidated soil[6]. The time required for pore water pressure equalisation in both phenomena is related to the soil hydraulic conductivity (Gibson and Henkel, 1953). The consolidation and rebound characteristics of clay soils are important in understanding the fabric of the soil for a particular state of stress and stress history, and consequently the hydraulic conductivity and strength. Other considerations are double layer attractive and repulsive forces.

Parry (1960) recognised that irrecoverable interparticle attractive forces are mobilised in clay-water systems during first consolidation, causing a reduction in the net repulsive forces. Mitchell et al. (1969) conceptualise overconsolidation as a considerable increase in the number of interparticle bonds. These effects are observed as a marked reduction in effective external stress to keep the system in equilibrium in its rebound state at the same void ratio as in the normally consolidated state, thus accounting for the large spatial separation between normal consolidation and rebound lines. From the evidence of consolidation and rebound cycles the interparticle forces are considered to oppose the separation of particles during rebound (Nagaraj and Murthy, 1983). Thus, some bonds formed during normal consolidation are retained after removal of much of the consolidation pressure.

Using double layer theory Klausner and Shainberg (1971) postulated that during normal consolidation the number of particles in a cluster (see 2.3.6) increases with an increase in effective stress thus causing a reduction in both operating specific surface and net osmotic repulsive pressure. The operating specific surface is the difference between the

[6]A clay soil under a stress less than its maximum previous stress is referred to as overconsolidated.

total specific surface and the specific surface within the cluster. The swelling pressure causing rebound upon unloading is proposed to be an inverse function of the average half space distance between the clusters, which depends on the operating specific surface (or the maximum past pressure). This causes a rebound upon unloading from a virgin line and nearly equal recompression upon reloading within the preconsolidation pressure range, since the number of particles in a cluster is unlikely to alter (Nagaraj and Murthy, 1987). This hypothesis goes far in explaining the elastic nature of rebound and recompression lines. However, Griffiths and Joshi (1989), on consolidation of montmorillonite, found that pore volumes for radii less than 0.1μm remain nearly constant regardless of consolidation stress, indicating that consolidation affects only inter-aggregate pores. They found no evidence of aggregate or cluster formation due to consolidation.

It appears, therefore, that consideration of the clay fabric is essential when interpreting swelling and consolidation behaviour. If a sample is initially swollen from a rather dry state where a more flocculated structure is likely, the cluster concept of swelling, where the clay structure consists of intra and inter-aggregate pores, seems reasonable. However, the conflicts in the literature occur over the effects of consolidation on the clay fabric. Some authors suggest that the cluster concept holds and pore fluid is expelled from the inter-aggregate pores only. The alternative view to this is that consolidation causes parallel alignment of clay particles producing a dispersed fabric. Once the inter-aggregate pores can compress no further, compression will still occur with increasing load. Therefore, the degree of particle alignment must be dependent on the effective stress. A subsequent reduction in stress will result in swelling (rebound[7]) either between clusters or individual aligned particles.

2.3.10 Clay-sand mixtures

Kenney (1977) states that in a mixture of clay mineral particles, quartz particles and water, the clay minerals and water form a cohesive matrix and the quartz particles are discrete inclusions in the matrix (above a threshold clay content dependent on the clay type[8]). Scanning electron micrographs by Graham et al. (1989) on 50% bentonite-sand mixtures show sand particles separated from each other by a matrix of clay particles only. Whatever the interaction of the sand particles within a mixture, its presence is expected to have an effect on the mechanical properties. The presence of coarse grained material is considered to dilute the effects of the clay with a resultant reduction in surface activity (Nagaraj and Murthy, 1983). It has been shown that adding sand to bentonite improves

[7]Rebound is likely to be due to both hydrostatic and osmotic pressure deficiencies (see section 2.6).
[8]The threshold was found to be approximately 20% bentonite (by dry weight) for bentonite-sand mixtures.

the soil strength properties (Mitchell, 1976), and the maximum attainable dry density is increased (Dixon et al., 1985). The self-healing capability (i.e. completely clay filled voids) is dependent on the quantity of sand in the mix (Gray et al., 1985). Gray et al., (1985) performed swelling tests on compacted bentonite-sand mixtures. To achieve a given swelling pressure, they found a higher sample dry density was required as the sand content increased (up to 50%).

Graham et al. (1986) suggest a possible development of the critical state model for describing the behaviour of expansive clays. A swelling equilibrium line (SEL) is proposed on the assumption that there is a unique relationship (Cheung et al., 1987) between swelling (osmotic) pressure p' and dry density (or v) of a clay-sand mix. The line is in principle similar to the normal consolidation line (NCL) in the critical state model. Graham et al. (1986, 1989) performed one dimensional compression tests on different bentonite-sand mixtures[9]. Mixtures containing 25 to 100% bentonite show a good correlation when clay specific volume is plotted against vertical effective stress. Their results show similarity with confined swelling pressure tests on similar mixtures by Gray et al. (1985), suggesting that both tests may be measuring the same relationship between the clay specific volume and the equilibrium effective pressure, whether expressed as swelling pressure or as externally applied pressure.

The clay phase appears to determine the swelling of clay-sand mixes, and the sand can be regarded solely as an inert filler (e.g., Dixon et al. 1985, Gray et al., 1985). Gray et al. (1985) have shown that moisture contents of bentonite-sand mixtures are directly proportional to the clay content and swelling pressures are independent of the sand content. Separation between clay particles is inversely related to the effective clay dry density, γ_c (mass of clay/(volume clay + voids)). Assuming that the sand serves only to limit the space available for clay compaction, the effective clay dry density will determine the swelling pressure of the system. Graham et al. (1989) define a clay specific volume, v_c, they use this parameter to relate to swelling rather than the overall specific volume. Plotting v_c against effective stress simplified the swelling of various bentonite-sand mixtures to a single relationship.

An effective way of separating the individual components of a clay-sand mixture is by the use of phase diagrams. Chapuis (1990a) and Wu and Khera (1990) represent a saturated bentonite-sand mixture as a four phase model consisting of sand, clay, adsorbed water and free water. The amount of adsorbed water is a function of the amount and type of

[9]Mixtures were prepared at approximately 30% moisture content and allowed to equilibrate under an applied stress range of 50-5000kPa.

bentonite and the liquid. Gray et al. (1985) also suggest the water in the system is subdivided into surface, or adsorbed, water and free, or interstitial, water. Phase relationships for bentonite-sand mixtures are further discussed in chapter 5.

2.3.11 Swelling of dry bentonite

On exposure to water, a long time is required for the development of full swell of dry bentonite. This is a result of initial interlayer swelling (see 2.3.7), and the time required to effect the stress transfer in the water from a large negative value, existing before exposure of the sample to water, up to the zero value that must exist throughout the system at equilibrium (an osmotic effect). The rate decreases with increasing time because of the continually decreasing gradient tending to draw-in water (Seed et al., 1962). The extent to which dry bentonite will swell has been shown by Pusch (1980) to depend on pore water chemistry, initial density and temperature. Seed and Chan (1959) found that clay samples compacted dry of optimum exhibit higher swelling characteristics than samples compacted wet of optimum, this was attributed to fabric differences. At a given clay density, processed bentonite exhibits a greater swelling capacity than unprocessed, this is attributed to the partial cementation of the unprocessed clay (Oscarson et al., 1990).

2.3.12 Representation of clay volume change behaviour

The swelling, consolidation and rebound of clay soils can be idealised on a plot of void ratio (or specific volume) versus the logarithm of effective confining stress (e-log p' plots). Sridharan and Jayadeva (1982) found that the swelling lines for three pure clays were spatially separated in e-log p' space. However, the effect of clay type on the d-log p' relationship, where d is particle separation, is negligible. The clay type is reflected in the e-log p' relationship by the surface area. They also found that at small pore fluid concentration the data were best represented in logarithmic space and at large cation concentration in semi-logarithmic space. Typical curves for d-log p' and e-log p' relationships of montmorillonite, illite and kaolinite are shown in figure 2.10.

From the results of one-dimensional volume change tests, a plot of void ratio against the logarithm of vertical effective stress can be used to determine the rebound index, C_i, and the compression index, C_c (a plot similar to figure 2.10 is produced where σ'_v replaces p'). The ratio $a = C_i/C_c$ is a good indicator of the relative importance of the influence of the osmotic forces in clay soils regarding swelling and compression (Bolt, 1956). Low values of a would be expected for clay soils, as rebound lines are usually much flatter than normal consolidation lines, whereas a value close to unity would be typical for sand.

2.3.13 Summary of volume change behaviour

The volume change behaviour of clay soils is most pronounced when the particle size of the clay fraction is small and appears to be strongly influenced by the initial soil fabric, which, in turn, is influenced by the initial moisture content, state of stress and stress history. For clay-sand mixtures, the initial soil fabric and percentage of sand are likely to influence the magnitude of volume change caused by variations in the pore fluid or applied stress. Conversely, the sand content, and stress history, i.e., previous consolidation, rebound and swelling paths, will affect the soil fabric, hence the engineering properties.

2.4 Hydraulic conductivity

2.4.1 Darcy's law

Darcy (1856) investigated the flow of water in vertical homogeneous sand filters. From his experiments, Darcy concluded that the rate of flow, Q, is proportional to the cross - sectional area, A, the difference in water level elevations in the inflow and outflow reservoirs of the filter (h_1-h_2), and the filters length, L. When combined, these conclusions gave the Darcy formula (or law)

$$Q=k\,A(h_1 - h_2)/L \qquad 2.1$$

Flow takes place from a higher piezometric head, ϕ, to a lower one, where piezometric head is the sum of the elevation and pressure heads (e.g., Bear and Verruijt, 1987). The quotient (ϕ_1 - ϕ_2)/L is the hydraulic gradient, i, and therefore Q = kAi. In Darcy's law the kinetic energy of the water is neglected as, in general, changes in piezometric head along the flow path are much larger than changes in the kinetic energy. Inertial effects have also been neglected.

Linearity of flow rates versus hydraulic gradients for clays has been reported by numerous investigators (e.g. Terzaghi, 1925, Macey, 1942). Low (1960) presented data showing linearity for sodium montmorillonite.

2.4.2 Properties of porous media

The hydraulic conductivity, k, expresses the ease with which a fluid is transported through a porous matrix. It depends therefore on both matrix and fluid properties (Bear, 1972). Fluid properties are density, ρ, and viscosity, μ, or combined as kinematic viscosity, υ. Solid properties are grain (or pore) size distribution, shape of grains (or pores), tortuosity of flow path, specific surface and porosity. The simplest theoretical models of porous media (Lamb, 1932) show that the hydraulic conductivity is directly proportional to the 2nd power of the diameter of the flow channel.

In the literature hydraulic conductivity and permeability are often used to indicate the same property, i.e. the coefficient in Darcy's law. Modern terminology refers to k in Darcy's law as the hydraulic conductivity and it has units LT^{-1}. The permeability, K, on the other hand has units L^2 and depends solely on the properties of the solid matrix. The relationship between hydraulic conductivity and permeability is given by:

$$k=\frac{K\gamma}{\mu}=\frac{Kg}{\upsilon} \qquad 2.2$$

where γ/μ represents the influence of the fluid.

Cheung et al. (1987) suggest that some of the pore fluid cannot be mobilised for flow in clay soils, and the fractional volume of water available for flow, termed the effective porosity, is less than the overall porosity of the soil. This is attributed to the anomalous properties of surface water. Surface water may have a significant influence on the hydraulic flow and is discussed in sections 2.4.3 and 2.4.5.

2.4.3 Deviations from Darcy's law

In fine grained soils there are indications that there exists a lower limit to the validity of Darcy's law, due to a minimum, or threshold, gradient below which there is practically no flow. Von Englehardt and Tunn (1955) and Lutz and Kemper (1959) show considerable deviations from linearity between flow rates and hydraulic gradients. Hansbo's (1960) data are consistent with this at hydraulic gradients less than 10. Swarzendruber (1962) found greater than proportional increases for flow velocity versus hydraulic gradient and showed that Darcy's law was obeyed in porous media not subject to the effects associated with clay. It is important to know how the hydraulic conductivity of a soil varies with the hydraulic gradient and therefore possible deviations from Darcy's law are discussed below.

Work by Low (1960, 1961) shows that water properties near clay surfaces are not the same as those of normal bulk water (see 2.3.4). According to Low, surface water possesses a more crystalline structure so that it exhibits a viscosity that exceeds the bulk liquid value by an amount that decreases with distance from the surface. Data from Kemper et al. (1964) from diffusion tests show that the viscosity of the first three layers of water adsorbed on sodium saturated mineral surfaces was about 10, 1.5, and 1.1 times that of bulk water. Due to the increased viscosity, a minimum hydraulic gradient is required to cause water movement, and Darcy's law is not obeyed. Kemper et al. (1964) incorporated a "fluidity" or "mobility" factor, α, in Fick's law to account for the increased viscosity near to the particle surface. Oscarson and Cheung (1983) suggest hydraulic conductivity is dependent on an "effective porosity" for flow, n'_w, assuming that no flow occurs in the surface water. Poiseuille's law (used in the derivation of the Kozeny-Carman equation, a flow model) assumes that the pore liquid viscosity is a constant throughout and equal to the bulk liquid value. Olsen (1962) conducted hydraulic conductivity tests on six different clays and found discrepancies in Poiseuille's law. However, he concluded that none of the discrepancies could be described by high viscosity.

As water moves near the clay surface, it carries along some cations in the diffuse layer. The cations are electrically attracted to the clay particles and their movement is impeded.

This, in turn, produces a drag on the moving water. A potential difference is established due to the migration of cations and electrokinetic coupling is thought to occur between hydraulic and electrical flows (Elton, 1948). The coupling gives rise to an induced electrical gradient called the streaming potential which acts in the opposite direction to the flow (Bear, 1972). Streaming potentials of up to a few tens of millivolts per atmosphere pressure difference have been measured in clays (Mitchell, 1991). Olsen (1962) has shown that this counter-flow is negligible in most cases, but may become significant relative to the true hydraulic conductivity for soils of hydraulic conductivity less than 10^{-10} m/s.

Von Engelhardt and Tunn (1955) propose that adsorbed immobile water layers on the particle surfaces possess non - Newtonian (shear rate dependent) viscosity, and that Newtonian conditions prevail elsewhere. It is proposed that with increasing applied head difference, the increased shear stress imposed on the immobile water layers decreases their thickness, so the effective cross section for flow increased with the hydraulic gradient. Swarzendruber (1962) also attributes deviations in Darcy's law to non - Newtonian liquid viscosity or a yield value Bingham plasticity[10] caused by clay water interaction. Pusch and Carlsson (1985) also associate the flow of pore water in dense montmorillonite with shear displacement of organised water.

Large seepage forces due to high hydraulic gradients may induce internal migration of soil particles resulting in clogging of pore spaces or erosion of sample material. Results from Dunn (1985) show that hydraulic conductivity decreased irreversibly with increasing gradient (20 to 200). Larger decreases in less dense samples are consistent with particle migration. The denser the sample the larger the interparticle bond strengths and therefore, the greater the percentage of particles incorporated in the load carrying framework of the soil are not available for migration. Swarzendruber (1962), on the other hand, found increasing gradients increased the effective cross section for flow and suggested reversible particle orientations may occur.

Stearns (1927) proposes an alternative form of Darcy's law, $q = C_1 i + C_2$, where q is the one dimensional mass flow rate of water, i is the hydraulic gradient, and C_1 and C_2 are constants. Swarzendruber (1962) gives the formula, $v = B[i - J(1 - e^{-Ci})]$, where v is the flow velocity, B, J and C are constants, for hydraulic gradients above a threshold value, below which there is no flow.

---

[10]The Bingham yield stress is a threshold shear stress at which yielding of the more viscous adsorbed water occurs. Above the threshold shear stress, rate of shear is linearly proportional to shear stress as in Newtonian flow.

To conclude, it seems that deviations from Darcy's law will be of most significance at low void ratios (or high applied stresses) and low hydraulic gradients.

2.4.4 Mechanical effects on hydraulic conductivity

Particle interaction increases with increasing consolidation pressure (or decreasing void ratio) causing a reduction in hydraulic conductivity (Bolt, 1956, Mitchell, 1956, Lambe, 1958). The flocculation of clay particles, which influences the distribution of void sizes and shapes, was recognised by Mesri and Olson (1971) as the most important variable influencing hydraulic conductivity. Terzaghi (1925) emphasised the importance of the nonuniformity of the voids on clay hydraulic conductivity and the substantial dependence of the hydraulic conductivity on the void ratio. Terzaghi and Peck (1967) suggest a linear relationship between the logarithm of hydraulic conductivity and the logarithm of void ratio for a particular soil type. This relationship is shown for three sodium clays in figure 2.11 using experimental data from Mesri and Olson (1971). For soils with a similar general history and fabric the hydraulic conductivity-void ratio relationships are also expected to be similar (Little et al. 1992).

In one proposed fabric model which accounts for the reduction in hydraulic conductivity with increasing applied stress, the reduced fluid flow is attributed to a more dispersed clay structure with channels that are all nearly the same size. This causes an increase in the length of the flow path (tortuosity) as the sample becomes more anisotropic under increasing consolidation stress. Shelley and Daniel (1993) performed tests on compacted kaolinite and found that hydraulic conductivity generally decreases with increasing moulding water content and reaches a minimum just wet of optimum (indicating a decrease in hydraulic conductivity as the fabric becomes more dispersed).

The cluster concept (see 2.3.6) provides a more satisfactory explanation of the fabric effects on hydraulic conductivity. It postulates that the total porosity is distributed among inter- and intra-aggregate pores. These groupings lead to the existence of many tiny flow channels through which there is likely to be little flow, and a smaller number of relatively large channels through which the main flow occurs. Flow through these pores will be much greater than through the intra-aggregate pores, since the hydraulic conductivity varies with the square of the pore radius (e.g., Bear and Verruijt, 1987). Compression causes the clusters to approach a density corresponding to the densest possible packing of spheres and the hydraulic conductivity decreases due to the reduction in inter-aggregate void space. At a threshold stress, the clusters themselves begin to compress causing a reduction in both the inter- and intra-aggregate void spaces, and the

hydraulic conductivity decreases further. This model also accounts for anisotropy because as clusters begin to compress the clay fabric becomes more dispersed.

Another effect of soil fabric on hydraulic conductivity has been discussed by Bear and Verruijt (1987). They propose that 'dead end pores' in the solid matrix reduce the area available for flow and define an effective porosity with respect to the flow through the medium. The effective porosity is less than the calculated porosity. Similarly, Chapuis (1990a), using a predictive method, shows a decrease in hydraulic conductivity of 5 orders of magnitude when the degree of saturation of a clay soil falls from 100 to 40%. He relates the hydraulic conductivity to a parameter called the efficient porosity which accounts for the degree of saturation of the soil. However, since Darcy's law assumes full saturation the relevance of this parameter is questionable.

2.4.5 Physico-chemical effects on hydraulic conductivity

The hydraulic conductivity of montmorillonite is recognised to be influenced strongly by the diffuse double layer associated with the clay particles (e.g., Yong and Warkentin, 1975). The concentration of the pore fluid can have a large effect on the double layer thickness hence the available cross-section for flow (Olsen, 1962, Dunn, 1985). Mesri and Olson (1971) found the hydraulic conductivity of montmorillonite to be consistently lower when the electrolyte concentration in the pore water is lower. The thicker double layer associated with dilute solutions constricts the available void space for water flow, and the confining stress determines to what degree double layers interact. Fernandez and Quigley (1988) showed the hydraulic conductivity of compacted clay permeated with differing contents of domestic waste landfill leachate was virtually unaffected at 160kPa vertical confining stress. However, when the samples were unconfined, the hydraulic conductivity increased up to three orders of magnitude for high concentration leachate.

Montmorillonite in non-polar fluids, such as benzene, is flocculated into very tight, more or less spherical domains (Mesri and Olson, 1971), leaving large pores through which the fluid can flow. These pores are not constricted either by the presence of adsorbed layers of fluid molecules or by the presence of diffuse double layers, and are thus completely open for fluid flow. Experimental curves for the hydraulic conductivity of sodium bentonite in four different pore fluids are shown in figure 2.12 (after Mesri and Olson, 1971).

The chemical compositions of the clay and permeant affect the viscosity of the fluid adjacent to the clay particle; a low fluid viscosity promotes more rapid flow. Macey

(1942) attributes the lower hydraulic conductivity of clay to water to be the anomalous viscosity of water near the clay surface.

Therefore, assigning a unique value of hydraulic conductivity to a clay soil is far from justified because the ease of fluid flow is dependent on factors which determine the size and distribution of void spaces within the soil, i.e., mechanical and physico-chemical effects. It is of great importance to recognise the significance of these factors when interpreting laboratory and field values of hydraulic conductivity.

2.4.6 Effects of coarse particles on fine grained soil hydraulic conductivity

Adding coarse grained particles to clay for use in hydraulic barriers strengthens the material, reduces shrink-swell potential, and reduces hydraulic conductivity due to the nearly impermeable particles blocking flow paths (e.g., Gray et al., 1984, Holtz, 1985). The range of moulding water content at which minimum hydraulic conductivity is achieved is also broadened (Shelley and Daniel, 1993). Dixon et al. (1985) found increasing sand content up to 50% (in bentonite-sand mixtures) reduced the effective porosity, n_{eff}, available for flow: above 50%, only marginal changes in values of n_{eff} were found. Daniel (1990), on use of gravel, cautions that too much is undesirable in a hydraulic barrier because if the voids between the gravel particles are not entirely filled with clay then a large amount of flow may occur through these pore volumes. Daniel (1990) recommends that liner materials be restricted to soils containing less than 10-20% gravel-size particles.

Jones (1954) found the hydraulic conductivity of sand-gravel mixes was significantly less than the sand alone for gravel contents less than 65%. Above this value voids between gravel particles were not completely filled. Holtz and Lowitz (1957) performed compaction tests on clayey soils containing varying amounts of gravel, as the gravel content approached two-thirds of the total material, there was often insufficient fine material to completely fill the voids between the larger particles. The results of hydraulic conductivity tests on silty clay-gravel mixtures by Shakoor and Cook (1990) show a large increase in hydraulic conductivity for gravel contents greater than 50%. Chapuis (1990a) found the hydraulic conductivity of sand decreases when the total fines content is increased. These findings have an important analogy with bentonite-sand mixtures where the sand content and void ratio of the bentonite may have an important influence on the hydraulic conductivity.

2.4.7 Hydraulic conductivity of bentonite-sand mixtures

For a bentonite-sand mixture, Hoeks et al. (1987) suggest that the hydraulic conductivity depends on the bentonite content and type, grain size distribution of the sand, degree of compaction and quality of permeating water. They argue that Darcy's law is only valid when water molecules can move freely within the pores of the medium. Wu and Khera (1990) investigated the effects of the expanded volume of bentonite on hydraulic conductivity by performing consolidation tests on 10% bentonite-sand mixtures. Their results indicate that during consolidation only free liquid drains initially until the soil has been consolidated to contain essentially solid particles and adsorbed liquid. At this point the hydraulic conductivity becomes very low because the solid particles and the semi-rigid adsorbed liquids are relatively impermeable. Chapuis (1990a) proposes a volume of slow-moving (adsorbed) water proportional to the volume of bentonite in the mix and considers this to be unavailable for flow. He defines the total pore space available for fast moving water as the efficient porosity; the difference between the porosity and the volume of adsorbed water. Mixtures with high bentonite contents have negative efficient porosities, meaning all pore water is slow moving. In this case, the hydraulic conductivity of the mix is similar to that of bentonite alone that is regularly distributed to fill all void spaces.

Gray et al. (1985) and Cheung et al. (1987) propose that the hydraulic conductivity of a bentonite-sand mixture depends on the effective clay dry density (mass of clay/volume of clay plus voids). Dixon and Gray (1985) show that hydraulic conductivity decreases with increasing effective clay dry density and is virtually independent of the sand content. Holopainen (1985) found hydraulic conductivity decreases with increasing degree of compaction, and increasing bentonite content up to 15% (using hydraulic gradients greater than 33).

The quantitative effects of bentonite content on the hydraulic conductivity of mixtures appear to be largely unknown and different authors report widely varying values (see 2.2.2). This is largely because of a failure to recognise the important soil parameters and poor experimental technique. For example, if a mixture is not allowed to reach equilibrium before testing, time dependent hydraulic conductivity is likely due to gradual closure of flow paths as the bentonite swells. Methods of hydraulic conductivity measurement are discussed in 2.4.8.

2.4.8 Methods of hydraulic conductivity measurement

Presently, there are no standards available for laboratory hydraulic conductivity tests, except ASTM-D2434-68 which applies only to clean sands and gravels, and the opinions

on which test to use to measure hydraulic conductivity are diverse. Tests can be performed in rigid wall or flexible wall permeameters. Authors usually agree that a triaxial test (flexible wall method) is preferable because it is faster (3-7 days) and it gives control of effective stresses and the degree of saturation by back pressure (Black and Lee, 1973). The potential for leakage between the sample and confining membranes is minimised. However, the decreasing diameter in a triaxial cell during consolidation is inconsistent with field boundary conditions (Sällfors and Peirce, 1985) and at high chemical concentrations the latex membrane cannot be prevented from being damaged (Wu and Khera, 1990). A rigid wall permeameter, however, can provide results similar to those of a triaxial cell (Lundgren, 1981, Chapuis, 1981) if sidewall leakage is controlled (for example by a fine coating of bentonite). A fixed wall cell has boundary conditions and an effective stress distribution resembling field conditions (no lateral deformation and one-dimensional flow). Sällfors and Peirce (1985) report fixed wall cells have a tendency to yield higher values than triaxial cells. However, Boynton and Daniel (1985), using kaolinite and fire clay, found the type of permeameter did not have a large effect on the measured hydraulic conductivity.

For soils with very low hydraulic conductivities it is impractical to test the specimen at low hydraulic gradients. Wu and Khera (1990) recommend that a specimen of small thickness is used. However, the time period required to reach equilibrium conditions prior to testing can still be extensive. Chapuis (1990a) found the time to saturate, consolidate and reach steady state seepage conditions of bentonite-soil mixtures (3-5cm thick) was 2-7 days in triaxial cell and 7-12 days in a fixed wall cell.

Variation of results in hydraulic conductivity measurement are attributed to differing grain-size distributions, total porosities, degrees of saturation, amounts of swelling allowed, hydration and inflow and outflow conditions (Dunn, 1985, Chapuis, 1990a). One of the major difficulties in interpreting reported hydraulic conductivity data is that these parameters are very rarely measured or given.

2.4.9 Summary

A common error in the literature is that a measured value of hydraulic conductivity is taken as absolute for a particular material, which is an inaccurate assumption. For example, Chapuis (1990a) reports a variation in laboratory measured hydraulic conductivity of a 10% bentonite-sand mixture from 5×10^{-8} m/s to 9×10^{-10} m/s. From the previous sections it is apparent that many factors affect the hydraulic conductivity of clay soils, most notably effective stress, fabric and type of pore fluid (all of which influence the void ratio). If these factors are not accounted for, the performance of a

landfill liner may be overestimated. Therefore, in addition to quoting a hydraulic conductivity value, the material and pore fluid properties at which it was measured are essential. Failure to report, measure or account for such parameters, is likely to prevent a quantitative interpretation of the effects of sand content on the hydraulic conductivity of bentonite-sand mixtures.

Terminology is also confusing. Hydraulic conductivity and permeability are generally used interchangeably. However, as discussed in 2.4.2 they are entirely different material properties. When discussing materials not susceptible to physico-chemical reactions, the term effective porosity refers to the available volume for flow due to the effects of 'dead end pores'. Oscarson and Cheung (1983) use the same term to account for immobile surface water unavailable for flow, which Chapuis (1990a) defines as the efficient porosity. The tortuosity is sometimes defined as the ratio of the length of 'tortuous' flow path to actual sample thickness, and has a value greater than one. The inverse of this value is also defined as tortuosity, this is preferred as the value is less than one and therefore relates to the reduction in flow caused by the extra length of flow path. Other definitions refer to tortuosity as the square of either of these values.

The chosen method of measurement is the largest source of debate for determining hydraulic conductivity values. If the volume of a fully saturated sample is constant, and inflow and outflow produced by a constant head difference are identical, then, assuming Darcian flow[11], the true hydraulic conductivity can be calculated for the specific material and pore fluid properties. The test type should only alter the property of the material (i.e., void ratio), which, consequently, will change the hydraulic conductivity and this can be accounted for. A further, equally important issue, is ensuring that the type of test performed on a laboratory sample is comparable to the field conditions. Alternatively, if values obtained from laboratory testing are to be used for design purposes, the constructed liner should be as similar to the laboratory sample as possible.

[11]This may not be true for all material types (see 2.4.3).

2.5 Strength

2.5.1 Principle of effective stress

It is widely accepted that Terzaghi's concept of effective stress (Terzaghi, 1923) provides a satisfactory basis for understanding the strength and deformation characteristics of saturated soils. The principle of effective stress can be stated as:

$$\sigma = \sigma' + u \qquad 2.3$$

where σ' = effective normal stress

σ = applied external normal stress (total stress)

u = pore water pressure

The principle assumes that the area through which the intergranular stress acts is negligible. It also states that all measurable effects of changes in stress, such as distortion, compression or expansion, arise from a change in effective stress. Interparticle contacts, which are effectively solid-to-solid, are the only significant region between soil grains where effective normal stress and shear stresses can be transmitted (Mitchell et al., 1969). Effective and total shear stresses are always equal as pore fluids cannot support shear stress.

Sridharan and Rao (1973) propose that volume change in clays is governed by the shearing resistance at interparticle level, and by diffuse double layer repulsive forces, which operate simultaneously. The latter is thought to dominate the volume change behaviour of expanding clays like montmorillonite (see 2.3.8). Mitchell (1976) and Lambe and Whitman (1979) suggest that for expanding clays, where particles are small and carry repulsive charges, it is unlikely that there any significant interparticle contact. Several authors have modified Terzaghi's principle of effective stress to account for the observed behaviour of montmorillonitic clays. These are discussed in section 2.5.2.

2.5.2 Modified principle of effective stress

Electrical attractive and repulsive forces at particle level in clays are thought to influence the engineering behaviour. As a consequence, the principle of effective stress has been modified by various authors (Lambe, 1960, Sridharan, 1968, Sridharan and Rao, 1973, Mitchell, 1976).

Lambe (1960) introduced an equation relating the total external load to the internal stress in the particulate soil system. His generalised equation could be stated as

$$\sigma = \sigma_m a_m + u' + (R - A) \qquad 2.4$$

where, σ_m is the mineral-to-mineral contact stress, a_m the fraction of the total interparticle contact area that is in mineral-to-mineral contact, u' the equivalent pore

water pressure and (R - A) the interparticle attraction and repulsion divided by the total interparticle area. The conventional effective stress is

$$\sigma - u' = \sigma_m a_m + (R - A) \qquad 2.5$$

Mitchell's (1976) modified principle of effective stress for soils containing expanding clay minerals at water content (and void ratio) equilibrium is:

$$\sigma = \sigma' + (R - A) + u \qquad 2.6$$

σ' is the traditional effective stress associated with interparticle contact, (R - A) is the magnitude of the intrinsic effective stress derived from the electrochemical charge fields around the particles, and u is the pore water pressure in the unbound (or "free") water in larger pore spaces. Graham et al (1989) modify this equation further assuming montmorillonite particles are not in mineral-to-mineral contact. The modified equation becomes

$$\sigma = (R - A) + u \qquad 2.7$$

From this equation they conclude that the electrochemical forces between particles balance the difference between externally applied pressures and the free water pressure in the clay, and the apparent effective stress, $(\sigma - u)$, controls strength, compressibility, etc. The net repulsive pressure, (R - A), is larger when external stresses are large and the occupied volume is small. Dixon et al. (1986) increased the pore water pressure at the base of a 50% bentonite-sand sample after the swelling pressure had been allowed to fully develop. They found the total stress increased linearly and equally with the applied pore pressure and concluded that the total stress is equal to the sum of the swelling (osmotic) pressure and the pore water pressure.

Sridharan (1990) believes that although mineral to mineral contact may not exist in the literal sense, contact stress exists through adsorbed water and entanglement of particles. If σ' is zero, as suggested by equation 2.7, then shear strength will be zero. Sridharan and Rao (1973, 1979) and Sridharan (1990) state that an effective stress of (R -A) is contrary to the behaviour. An increase in R or a decrease in A should bring about a reduction in shear strength. They rewrote the modified effective stress concept expressed as

$$C' = \sigma' + \sigma'' \qquad 2.8$$

where C' is the effective contact stress which controls the shearing resistance, σ' is the conventional effective stress and σ'' is the intrinsic effective stress, (A - R), equal to the net electrical attractive pressure. Repulsive forces tend to separate the clay particles away from each other in the same way as the positive pore water pressure does, and the attractive forces tend to bring the clay particles closer together in the same way as the external normal force does. When C' becomes zero the shear strength is zero.

Chatterji and Morgenstern (1990) propose a modified effective stress law:

$$\sigma^*_n = \sigma'_n - (R - A) \qquad 2.9$$

where σ^*_n is the true effective stress and σ'_n the apparent effective stress $(\sigma_n - u_w)$, equal to the classical definition of effective stress. They performed shear box tests on bentonite samples containing different pore fluids. At the same apparent effective stress, σ'_n, the effect of a change in pore fluid salinity is believed to change the net repulsive stress, (R - A), of the clay system, thus bringing about a change in the true effective stress, σ^*_n. They found that if the measured residual shear strength values are divided by the corresponding estimated true effective stress, similar values of residual friction angles are obtained irrespective of the pore fluid salt content.

Of the modified principles proposed, those after Sridharan (1990) and Chatterji and Morgenstern (1990) seem the most tenable. As pore fluid has no shear strength, frictional strength can only occur through effective stresses transmitted through particle contacts[12]. For example, at the liquid limit the void ratio of bentonite is very large and yet the soil still has shear strength. If the concept of clusters of clay particles is again considered, it is easy to visualise how the clay fabric can support such large void ratios. Although some of the clay particles at the intra-aggregate level may not be in contact, individual clusters may be acting as larger 'granular' particles in contact with one another, thus transmitting the effective stress throughout the soil structure.

It therefore seems logical to assume that some form of particle contact exists, the degree of which is determined by pore fluid concentration and externally applied stress. For example, an increase in pore fluid concentration of a sample initially at equilibrium decreases the double layer repulsive force between particles, with a resultant increase in particle contact and effective stress. A subsequent reduction in externally applied stress causes swelling, resulting in less particle contact and a decrease in effective stress. At equilibrium, if the final and initial soil states are identical, the effective stress has its original value because the degree of particle contact is the same. This is essentially the same as Terzaghi's theory, which predicts the effective stress is constant at a particular soil state. For a material such as sand, where there is no contribution to volume change from electro-chemical forces, the effective stress at any state is simply the difference between the externally applied (total) stress and the pore water pressure.

---

[12]Section 2.4.3 discussed the likelihood of highly viscous adsorbed water on particle surfaces, which may possess shear strength. Data from Kemper (1964) suggests that any contribution to shear strength would be limited to the first monolayer of water. Therefore, although mineral-to-mineral contact may not exist, contact between particles is reasonable if the first water layer and particle are considered to be a single unit.

2.5.3 Strength of sand

The physical property from which a sand achieves its strength is interparticle friction. According to Bowden and Tabor (1954), interparticle friction depends on the nature of the mineral, the properties of its surface and roughness and on the size of the load per particle[13]. Skinner (1969) demonstrated that the angle of shearing resistance of glass ballotini sheared at constant volume was independent of the coefficient of interparticle friction. He attributed this to a failure mechanism involving particle rolling and translation, rather than direct sliding, as this was prevented by interlocking of the particles. Rowe (1962) found that interlocking between sand particles increases with angularity of particle shape and the uniformity coefficient of the grading.

Casagrande with Terzaghi and Peck (1948) and Taylor (1948) demonstrated the basic shear characteristics of sands. Typical deviator stress-axial strain curves and volumetric strain-axial strain curves for dense and loose sand are shown in figure 2.13 (after Bishop and Henkel, 1962). As a dense sand shears it increases in volume (dilates). The point of peak strength is usually associated with the maximum rate of dilation as shown in figure 2.13a. Deformations to failure are small, and a brittle type failure occurs resulting in a slip plane with little previous remoulding (Rowe, 1962). The peak strength of dense sand is represented on a Mohr-Coulomb failure envelope by the angle of shearing resistance, ϕ'_{max}. At considerably greater strains, shearing occurs at constant volume where the corresponding angle of shearing resistance is denoted as ϕ'_{cv}. Evidence from Roscoe (1970) suggests that soil in rupture zones will dilate fully to achieve a critical state, at which shear deformation can continue in the absence of volume change.

Loose sand reaches its maximum, equal to ϕ'_{cv}, at large strains without passing a previous peak with a corresponding decrease in volume as shown in figure 2.13b. A plastic type failure occurs with no clear slip plane. Roscoe, Schofield and Wroth (1958) proved that assemblies of particles attain a single final porosity for a given normal pressure, the value of which depends on particle shape and grading. This ultimate condition (or critical state) is associated with ϕ'_{cv} and is reached whatever the initial porosity of the sample. The behaviour of dense and loose sands is conceptualised in figure 2.14 (after Bolton, 1979).

The conventional Mohr-Coulomb plot for peak strength gives different plots for each state of packing. Furthermore, with dense sands the envelope is not straight. For a particular void ratio, dilatancy decreases with increasing pressure due to the smaller

---

[13]Sand interparticle friction was measured by Rowe (1962) by shearing blocks of quartz against each other.

changes in void ratio necessary to reach the critical state and crushing at the grain contacts, which decreases the degree of interlocking (e.g., Rowe, 1962, Bishop, 1966). Tests on dense sand under extreme stresses mimic the normal behaviour of very loose sand. The peak phenomena is suppressed and the sample volume contracts rather than dilates (Bolton, 1986). The dilation of soils during shear is discussed further in 2.5.6.

2.5.4 Strength of clay

The behaviour of clay soils during shear is much more complex than that of coarse grained or granular soils. Many factors, such as clay mineral type, water content, pore fluid concentration, stress history, drainage during shear, stress path, rate of loading, temperature and soil fabric influence the strength and deformation of clays (e.g., Sridharan and Rao, 1979). Mitchell (1976) states that the frictional coefficient decreases with increasing in specific surface area (or decreasing particle size). Haefeli (1951) found that the magnitude of the drop in strength from peak to residual in clays increased with liquid limit. Moore (1991) shows that clays saturated with monovalent sodium cations consistently resulted in lower residual strengths than clays saturated with calcium divalent cations. Seed and Chan (1959) found strength increases with density provided the structure remains the same, and at large strains samples behave the same regardless of structure. The drained behaviour of overconsolidated clays is broadly analogous to that of dense sands, whereas, normally consolidated clays behave like sands at less than critical densities.

At very large strains frictional sliding occurs between strongly oriented clay particles at which point the residual strength, ϕ'_r, is mobilised, which is much lower than the constant volume strength. The effect of loss of strength in clays due to preferred particle orientation is not predicted by the critical state theory. The critical state for clay soils is envisaged as shear at constant volume but with random particle orientation (Lupini et al., 1981).

Clays soils are often referred to as cohesive. Rowe (1962) states that no strong evidence for cohesion exists, and a cohesion term is usually the result of pore pressures which are unaccounted for in data analysis. Mitchell et al. (1969) performed consolidation and strength tests on San Francisco Bay mud, illite and sand. They found a linear variation between number of bonds per unit area, S, and effective consolidation pressure, and postulated that the bonds represented by the intercept on the S axis (at zero stress) are the source of true cohesion. All materials showed the same proportionality between strength and number of interparticle bonds which passed through the origin. They suggest the basic strength generating mechanism, i.e., interparticle bonding between

atoms at interparticle contacts, is the same for both sands and clays. The increased strength of overconsolidated clays is attributed to bonds formed during normal consolidation, which do not disappear when the effective consolidation pressure is reduced (i.e., the higher density, for a particular stress, yields a dilitant component of strength).

Sridharan and Rao (1979) found a decrease in cohesion intercept, tending to zero, with an increase in dielectric constant for statically compacted and hand-remoulded samples of kaolinite and montmorillonite. Using their modified equation (equation 2.8) they argue that an increase in effective stress occurs due to a positive value of (A - R), this acts in the same way as a negative pore pressure. When this is taken into account, as in the determination of effective stress plots from total stress plots, the true effective stress is known and the cohesion intercept is essentially zero. This is interpreted as meaning the shearing resistance in the soil is of a frictional nature. Chatterji and Morgenstern (1990) postulate purely frictional strength with the seat of friction at the solid interparticle contacts.

2.5.5 Strength of soil mixtures

For soil mixtures, such as a clay-sand mixture, Kenney (1977) suggests that the clay mineral and water form a cohesive matrix which is either distributed within the voids of a sand skeleton, or surrounds discrete sand particles. The strength will therefore depend on the relative volumes of matrix and sand. For small volumes of sand the behaviour is controlled by the clay-mineral matrix, and increasing volumes of sand inhibit to an increasing extent the clay-mineral particles becoming oriented parallel to the direction of shear displacement, thus causing increased shear resistance. Beyond a certain volume, the sand particles will form a continuous structure which resists applied forces, with the clay mineral matrix acting only to fill the voids. Georgiannou (1988) performed fabric studies aimed at establishing the distribution of clay in clayey sands (7-8% clay content). He showed that clay particles tend to concentrate at the contacts between sand grains, to form clay bridges, and at irregularities on sand grain surfaces. In this overall arrangement, sand grains are fixed by clay at most contacts. At clay contents in excess of 10%, the physico-chemical properties of the clay may exert an influence on shear strength far in excess of its relative abundance (Yong and Warkentin, 1975, Mitchell, 1976). The amount of clay in soils is very important when determining shear strength.

As the clay content of a soil increases, a change in shearing mechanism occurs. Borowicka (1965) performed reversal shear box tests on different artificially produced clay soils. He found brittleness increased and the residual shearing angle decreased with

increasing clay fraction. Vaughan et al. (1978) suggested that the discontinuous change in residual friction angle with increasing clay fraction might be due to the existence of two shearing mechanisms, turbulent shear and sliding shear, with a relatively sudden change between them. Turbulent shear involves shear at constant volume without preferred particle orientation; the strength essentially that of the coarse particles. A higher proportion of platy particles, perhaps involving separation of the contacts between the coarse particles, results in a reduction in strength, although still without preferred orientation of the clay. Sliding shear behaviour occurs when the clay fraction is sufficiently high for a well formed, polished sliding surface of strongly orientated clay to develop. Evidence for particle orientation has been established using optical microscope techniques (e.g., Mitchell, 1956) and using the electron microscope (e.g., Yong and McKyes, 1971). Lupini et al. (1981) working on natural and artificial clays found a relatively smooth transition with increasing clay content from a residual strength equivalent to $\sigma'_n \tan \phi'_{cv}$ for a granular soil to a strength related to sliding of clay particles. Their electron micrographs show transitional behaviour involves discontinuous sliding shear surfaces and pockets of soil behaving in the turbulent mode, both contained within a thick shear zone (about 2mm). Transitional shearing behaviour was shown over a range of clay fractions between about 23% and 43%. Peak and residual friction coefficients against clay fraction for bentonite-sand mixtures are shown in figure 2.15 (after Lupini et al., 1981), showing the change in strength with clay fraction. Skempton (1985) found transitional behaviour of bentonite-sand mixtures at clay fractions between 25% and 50% under 350kPa vertical stress. Storr (1992) performed ring shear tests on 20% bentonite-sand mixtures and found an ultimate angle of friction midway between ϕ'_{cv} for a sand and ϕ'_r of a clay . The observed value is considered to represent clay type behaviour, but with the churning action of sand grains along the shear plane preventing the development of true residual strength behaviour.

Ring shear tests on natural soils by Lupini et al. (1981) show a decrease in residual friction coefficient with increasing normal stress (90 - 900kPa) when the clay content is sufficient for sliding shear only to occur. At lower clay contents the opposite behaviour is expected because increasing compression due to increasing normal stress will bring the granular fraction of a mixture to a closer packing, and so promote interference and interlocking between the coarse particles. If both turbulent and sliding shear are playing a part in the shear mechanism, then the two effects are in opposition and may partly cancel out.

To account for the two soil phases in a clay-sand mixture, Kenney (1977) relates strength to the volume ratio, r_{vc} (volume of clay plus water/total volume). Lupini et al.

(1981) found residual strength correlates best with the void ratio of the granular phase of the soil, e_g (volume of clay and water/volume of coarse particles). This parameter reflects changes in packing due to compression directly hence the interference between the coarse particles. For sands and clayey sands of the same bulk unit weight, Georgiannou et al. (1990) found an increase in granular void ratio with increase in clay content and for a fixed initial granular void ratio there was no significant change in the slope of the compression curves with clay contents between 3.5 and 7%. It therefore appears that consideration of the individual phases of the soils is best in interpreting the strength of soil mixtures.

In bentonite-sand mixtures, Graham et al. (1986) propose that effective stresses will result from a combination of interparticle forces between sand grains and osmotic pressure between clay particles. The relationship between these two sets of forces will depend on factors such as the ratio of sand to clay, the homogeneity of the mixture, and its degree of compaction or density. Graham et al. (1986) performed triaxial tests on 50% bentonite-sand mixtures. Their results suggest that at high stresses (~0.5MPa) there is sufficient compression of the clay matrix that the sand particles are beginning to support some of the externally applied stress. Graham et al. (1989) have developed a conceptual behavioural model based on critical state soil mechanics, using results from swelling pressure and oedometer compression tests. Their results predict that long term behaviour of bentonite-sand mixtures (defined as samples allowed to swell fully to equilibrium) will be like strain hardening clay. In samples of this type the clay supports all the stress and therefore shearing results in compression. The short term behaviour, where samples have not fully swollen and the sand supports the effective stress, is expected to be more like strain softening clay.

2.5.6 Stress-dilatancy theory

The peak strength of soils can be considered to be composed of two components; the strength due to friction and the additional strength due to dilation (e.g., Bolton, 1986). Several relationships have been derived to account for the phenomena of dilation. Some of the more important, and relevant, relationships are discussed in this section.

The saw blades model of dilation, shown in figure 2.16 (after Bolton, 1979), is the simplest. The peak strength, ϕ'_{max}, is given by

$$\phi'_{max} = \phi'_{cv} + \upsilon \qquad 2.10$$

where ϕ'_{cv} is the angle of shearing on soil loose enough to be in a critical state, with zero dilation and υ is the angle of dilation.

Taylor, followed by Skempton and Bishop (1950) performed direct shear tests on sand and separated the strength component due to friction from that due to dilation. They found that the frictional strength was the difference between the peak and dilatant strengths, or

$$\tan \phi'_{cv} = \tan \phi'_{max} - (\delta V/\delta \Delta) \qquad 2.11$$

where δV is volume increase over a horizontal displacement $\delta \Delta$

In these relations no attempt has been made to optimise the failure mechanism or to correlate the directions of principal stress and strain increments.

Rowe (1962) performed triaxial tests on packings of steel shot and sand. His results lead to the stress-dilatancy relation

$$\frac{\sigma'_1}{\sigma'_3} = \left(\frac{\sigma'_1}{\sigma'_3}\right)_{cv} \left(1 - \frac{d\varepsilon_v}{d\varepsilon_1}\right) \qquad 2.12$$

Where ε_V and ε_1 are the volumetric and axial strains respectively. This equation was obeyed over a wide range of negative and positive dilatancies, including the case of zero dilatancy and accounts for the sum of the energy absorbed in friction and that in dilation. Rowe (1962) found that packings in a state intermediate between the loose and dense state undergo a degree of rearranging prior to failure which varies from a maximum in the loose state to almost zero in the dense state. Reloaded samples subject to stresses less than the previous maximum show very little rearranging until the previous maximum is approached.

Bolton (1986) uses a relative dilatancy index $I_R = I_D(10 - \ln p') - 1$, where I_D is the relative density and p' the mean effective stress at failure. This offered a unique set of correlations for the dilatancy related behaviour of each of 17 sands. For triaxial strain in the range $0 < I_R < 4$, Bolton found that

$$\phi'_{max} - \phi'_{cv} = 3I_R^\circ \qquad 2.13$$

and

$$-\left|\frac{d\varepsilon_v}{d\varepsilon_1}\right|_{max} = 0.3I_R \qquad 2.14$$

The expression $\phi'_{max} = \phi'_{cv} + 0.8\upsilon$, was found to be operationally indistinguishable from Rowe's stress dilatancy equation.

It is known that the deformation and failure characteristics of clays with respect to effective stresses are very similar to those of granular materials and evidence suggests that the stress-dilatancy relation may be of general application (Rowe, 1962). Rowe et al. (1963) proposed a modified stress-dilatancy equation for soils containing clay as

$$\frac{\sigma_1'}{\left(1-\frac{d\varepsilon_v}{d\varepsilon_1}\right)} = \sigma_3' \tan^2\left(45+\frac{\phi_{cv}'}{2}\right) + 2c_{cv}' \tan\left(45+\frac{\phi_{cv}'}{2}\right) \qquad 2.15$$

Where ϕ'_{cv} and c'_{cv} are the angle of shearing resistance and cohesion intercept at zero dilatancy respectively. Equation 2.15 was investigated experimentally on two natural clay soils. It was found that the stress-dilatancy data lay on a theoretical line given by $\phi'_{cv} = 28°$ and $c'_{cv} = 0$, in which case equation 2.15 reduces to Rowe's stress-dilatancy relation for granular materials (equation 2.12). The variable dilatancy of specimens tested at different pressures under different overconsolidation ratios was shown to be the cause of a cohesion intercept on the Mohr-Coulomb envelope. These findings indicate that stress-dilatancy relationships for granular materials have a general application, and any contribution to the shearing resistance of soil from 'true cohesion' is minor.

2.5.7 Elasticity, plasticity and stiffness

In an ideal (but not necessarily isotropic, linear or homogeneous) elastic material the deformations are recoverable on unloading and the energy supplied to the material over a closed loading cycle is zero. In addition, deformations are dependent on the stress increments causing them and are independent of the current states of stress and strain. The stress-strain relationship for a perfectly elastic material is shown in figure 2.17a. The deformations of an ideal plastic material are stress independent and irrecoverable, and the energy supplied during a loading increment is dissipated within the material. Plastic and elastic-plastic behaviour is shown in figure 2.17b.

The stress-strain behaviour of soils can take many different forms between the idealised elastic and plastic relationships. Figure 2.17c is typical of the brittle properties of dense sands and overconsolidated clays, and figure 2.17d represents the ductile behaviour of very loose sands and normally consolidated clays (plastic deformation). Although elastic theory may apply reasonably well for monotonic loading, many soil stress-strain unloading-reloading curves have substantial hysteresis and the corresponding elastic strains are not fully recoverable over the whole range of unloading (Atkinson and Richardson, 1985).

There are indications that soil behaviour should be considered as inelastic even at relatively small strains and that the stiffness[14] is greatest at the start of loading when the increments of stress and strain are small. Jardine et al. (1984) performed undrained

[14]Soil stiffness usually refers to Young's modulus, E, equal to $d\sigma/d\varepsilon$. The undrained stiffness is denoted by E_u and the drained stiffness by E'.

triaxial tests on clay and found the stress-strain behaviour to be non-linear, and very stiff undrained behaviour was observed below 0.1% axial strain. Each test departed from straight line behaviour over its small strain range. Atkinson et al. (1990), also performing triaxial tests, found that within the regions of loading examined (strains in excess of 0.1%) both the stress-strain curves and strain paths were non-linear.

Soil stiffness will depend on the soil, which may be described by the grading, mineralogy and plasticity, and for a given soil, by the current state of stress and the stress history. For a given soil at a given state and with a particular stress history, the measured stiffness is often different for different stress paths such as compression or extension, drained or undrained, loading or unloading (Atkinson et al., 1990). An additional influence on stiffness is the recent history of the soil described by the most recent loading, which may take the form of an extended period of rest or a sudden change in the direction of the stress path (Atkinson, 1973). However, these effects are only significant at small strains (<0.5%). Atkinson et al. (1990) indicate that the variation of stiffness, following a given stress path rotation, increases with increasing plasticity.

When considering clay-sand mixtures, the stiffness will be governed by the clay matrix at high clay contents, the sand matrix at low clay contents, or a combination of both. Georgiannou et al. (1990) performed undrained triaxial compression tests on kaolinite-sand mixtures. At a fixed granular void ratio (or sand density) approximately equal to 0.8, small variations in clay content did not appear to have a significant effect on the measured stiffness for a normally consolidated soil. The stiffness increased with a reduction in the granular void ratio and an increase in overconsolidation ratio, and was less dependent on the overconsolidation ratio as the axial strain increased.

Conventionally, the determination of the axial stiffness of a triaxial sample is based on external measurements of displacement which include a number of extraneous movements. For example, the true soil strains developed in triaxial tests can be masked by deflections which originate in compliances of the loading system and the load measuring system. In addition, the difficulty in trimming samples with perpendicular faces and a variety of sample bedding effects can give a poor definition of the stress-strain behaviour of the material under test, particularly over the small strain range (Jardine et al., 1984). Most triaxial tests therefore tend to give apparent soil stiffnesses far lower than those inferred from field behaviour. The measurement of stiffness of the bentonite-sand mixtures in the testing programme is discussed in 4.5.7.

2.6 Summary and conclusions

Volume change behaviour, hydraulic conductivity and strength and stiffness of clays, and the strength of sands have been detailed. Literature which cites the engineering behaviour of clay-sand mixtures is also included. Since it is likely that the mechanical properties are dominated by the clay fraction in bentonite-sand mixtures this chapter has been heavily weighted as a discussion on bentonite and the factors which contribute to its varying behaviour. It has been shown that swelling of bentonite appears to be controlled largely by physico-chemical effects and a three level swelling model is likely: interlayer swelling (within particles), interparticle swelling (between particles) and inter-aggregate swelling (between clusters of particles). The contribution of each type of swelling to the total volume change will be strongly influenced by the applied stress and/or pore fluid concentration, and, in addition to the stress history, will determine the fabric of the clay. As hydraulic conductivity and strength of clays are also dependent on the fabric it is essential to understand the swelling behaviour before consideration of other properties[15].

The factors which affect the hydraulic conductivity of clay soils have been discussed. Hydraulic conductivity has been shown to significantly vary with mechanical and physico-chemical changes. In addition, deviations from Darcy's law are possible due to interactions between clay particles and water, and these have been listed. Methods of measurement compound the problem of quantifying the behaviour of soils with low hydraulic conductivity because different techniques can yield wide ranges of values. However, if all the parameters of the sample are known, measured and controlled, it seems that reasonable correlations between various methods can be achieved.

The principle of effective stress has been modified by several authors to account for the electrochemical attractive and repulsive forces which govern the volume change behaviour in expanding clay soils, these modifications have been summarised. Since friction between particles must exist for a soil to have shear strength, it seems reasonable to state that the total stress is equal to the effective stress plus a water pressure term. In sands and clays of large particle size where mechanical effects dominate, the water pressure term is equal to the excess pore water pressure in Terzaghi's principle of effective stress (equation 2.3). For montmorillonite, a pore water pressure increase and/or an increase in the net electrical repulsive force will tend to force particles apart, a pore water pressure decrease and/or an increase in the net electrical attractive force will tend to bring the particles closer together. Therefore, a water pressure term is likely to

[15]The osmotic concept of swelling due to physico-chemical interactions appears to be significant only for clay particles of very small diameter, namely montmorillonite.

consist of both hydrostatic and osmotic pressures, determined by load and concentration differences respectively.

The cluster concept relating to inter and intra-aggregate pores provides a useful conceptual fabric model for understanding the swelling and hydraulic conductivity of clays. It may also be useful in interpreting behaviour during shear. For example, the peak angle of shearing resistance is generally much higher than that at the residual state[16]. Peak strength may be due to clusters of clay particles initially acting as more granular particles. At the residual state this fabric effect is largely removed because clay particles are aligned along the shear plane and as a consequence the shear strength is less.

As sand is added to clay the activity of the soil decreases and the swelling of the sample as a whole reduces. The effects of this on the hydraulic conductivity and strength have received relatively little attention. There are conflicting data on the changes in hydraulic conductivity with clay content, usually because the state of the sample (i.e., stress, void ratio etc.) is unknown. The strength of soil mixtures has been discussed. It is known that the ultimate angle of shearing resistance decreases with increasing clay content, however, much of the reported test data are interpreted qualitatively. In addition, very little is reported on the peak strength of soil mixtures. The actual effects on varying clay content on swelling, hydraulic conductivity and strength of clay-sand mixtures are not fully understood quantitatively (in engineering terms) and there appears to be no coherent framework for understanding the behaviour of two soil phase materials.

The material which has been discussed in this chapter is considered to be essential background in understanding the behaviour of bentonite-sand mixtures and some of the methods described will be used in the analysis of the laboratory test data in chapters 5 and 6.

[16]Lupini et al. (1981) found peak and residual angles of shearing resistance of a sodium bentonite to be 20° and 6° respectively when tested on a ring shear apparatus.

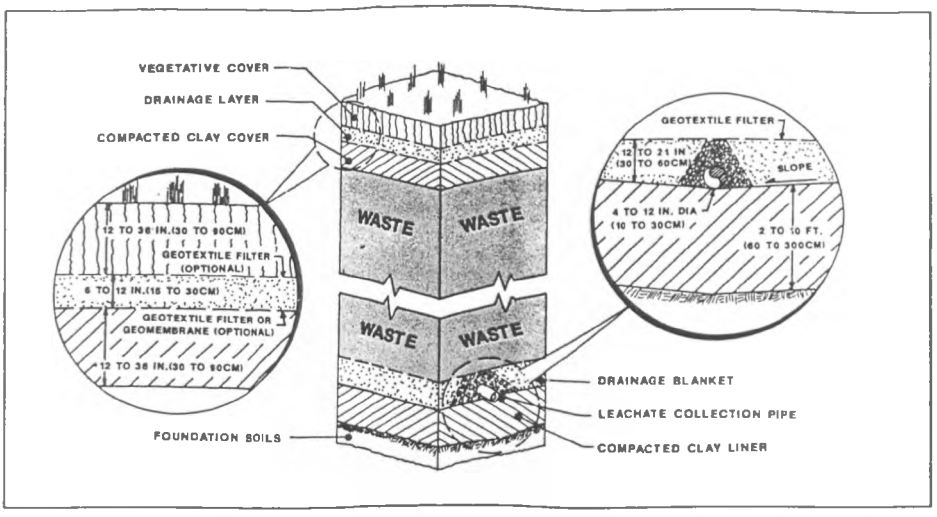

Figure 2.1a: Typical landfill section and component dimensions (after Oakley, 1987).

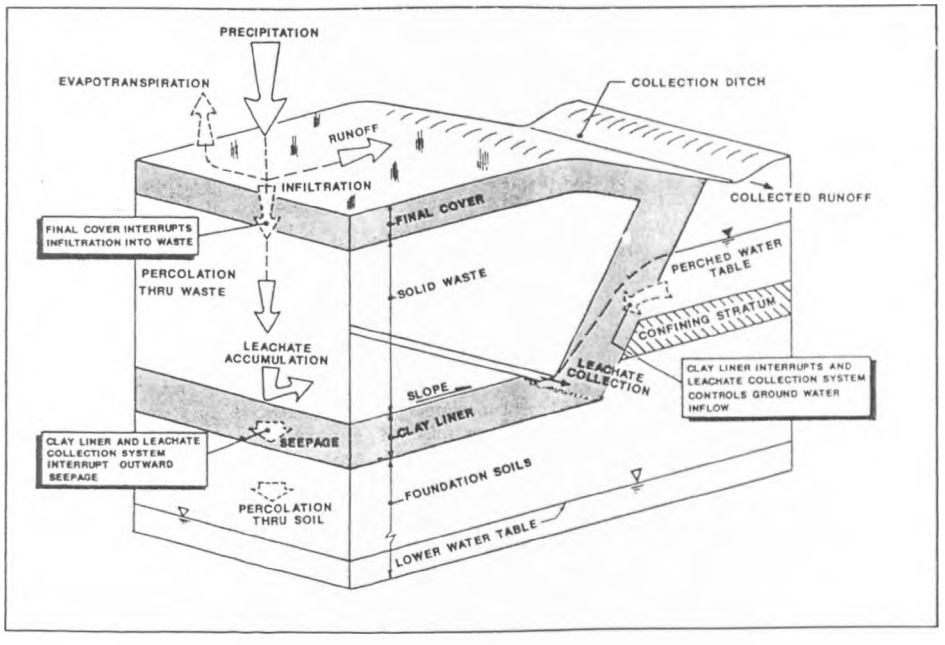

Figure 2.1b: Hydrological cycle as applied to landfill containment system (after Oakley, 1987).

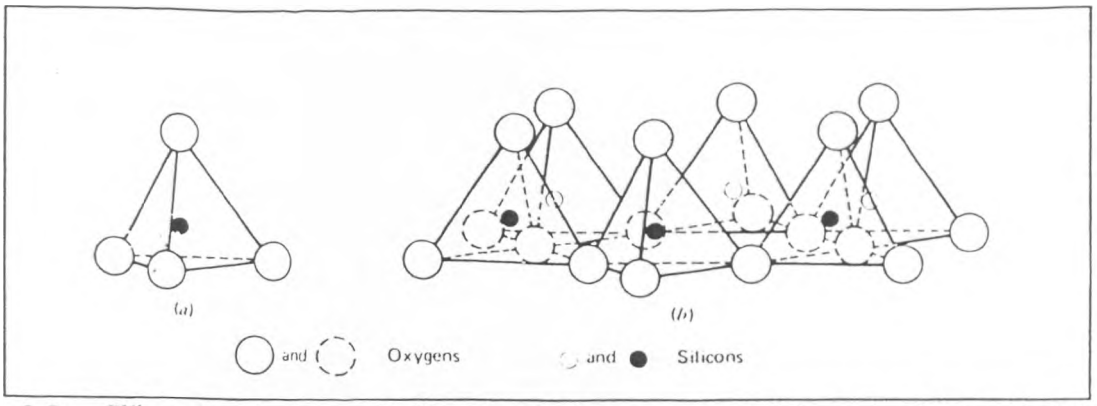

2.2a: Silicon tetrahedron and silica tetrahedra arranged in a hexagonal network (after Mitchell, 1993).

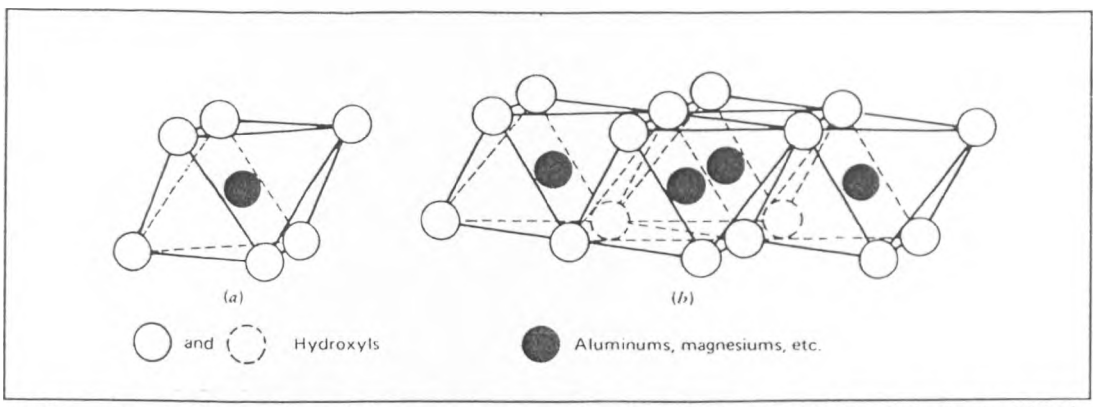

2.2b: Octahedral unit and sheet structure of octahedral units (after Mitchell, 1993).

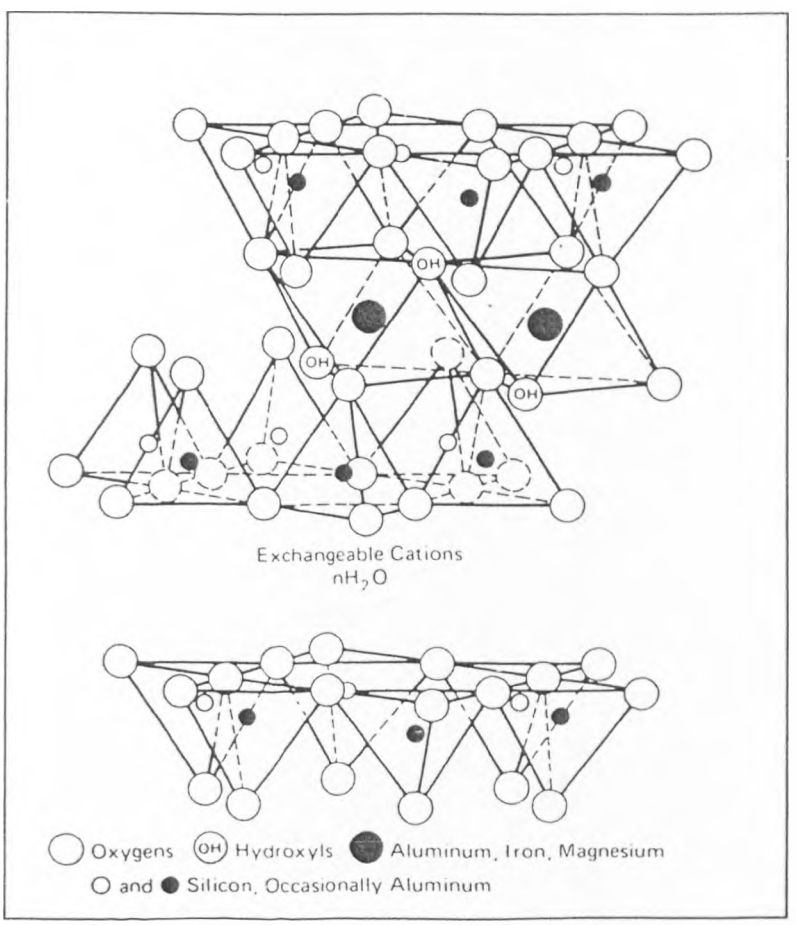

Figure 2.3: Diagrammatic sketch of the montmorillonite structure (after Mitchell, 1993).

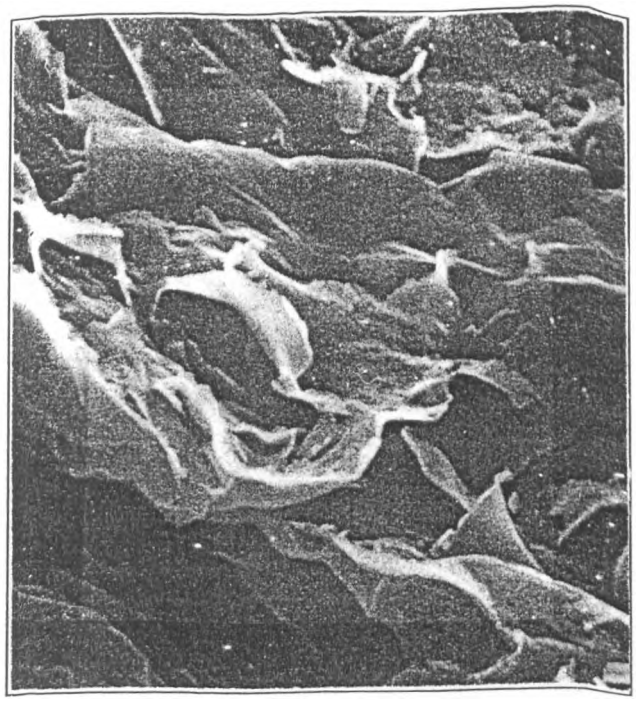

Note: Picture width is 7.5μm.

Figure 2.4: Electron photomicrograph of montmorillonite (after Mitchell, 1993).

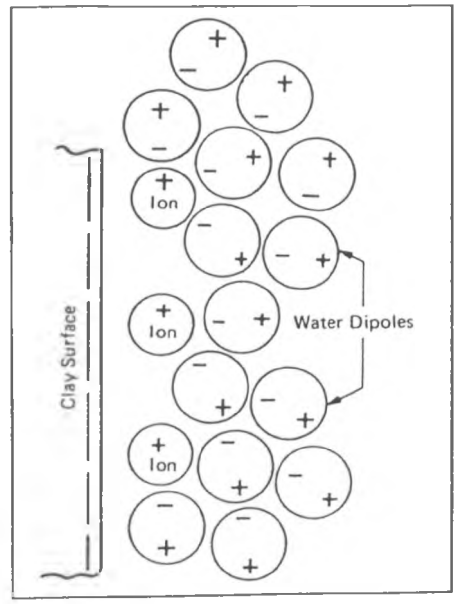

2.5a

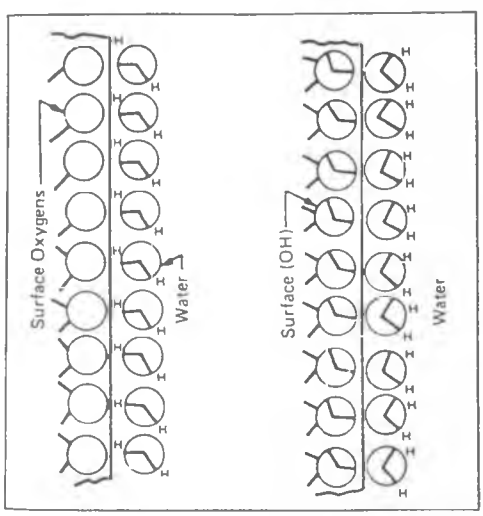

2.5b

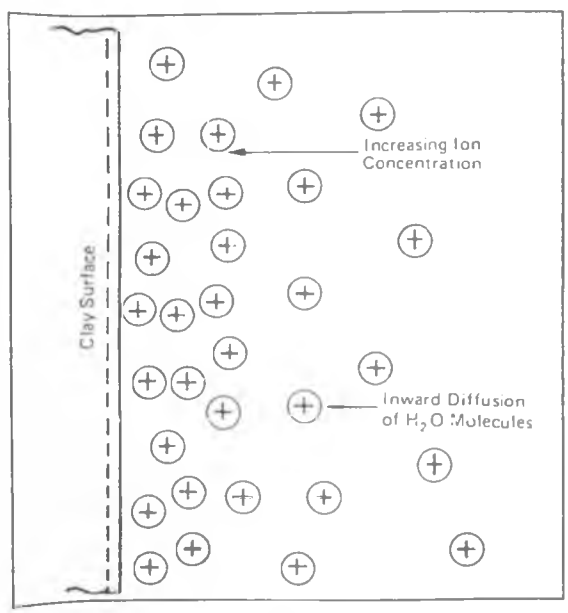

2.5c

Figure 2.5: Possible mechanisms of water adsorption by clay surfaces (after Mitchell, 1993). (a) Ion hydration. (b) Hydrogen bonding. (c) Attraction by osmosis.

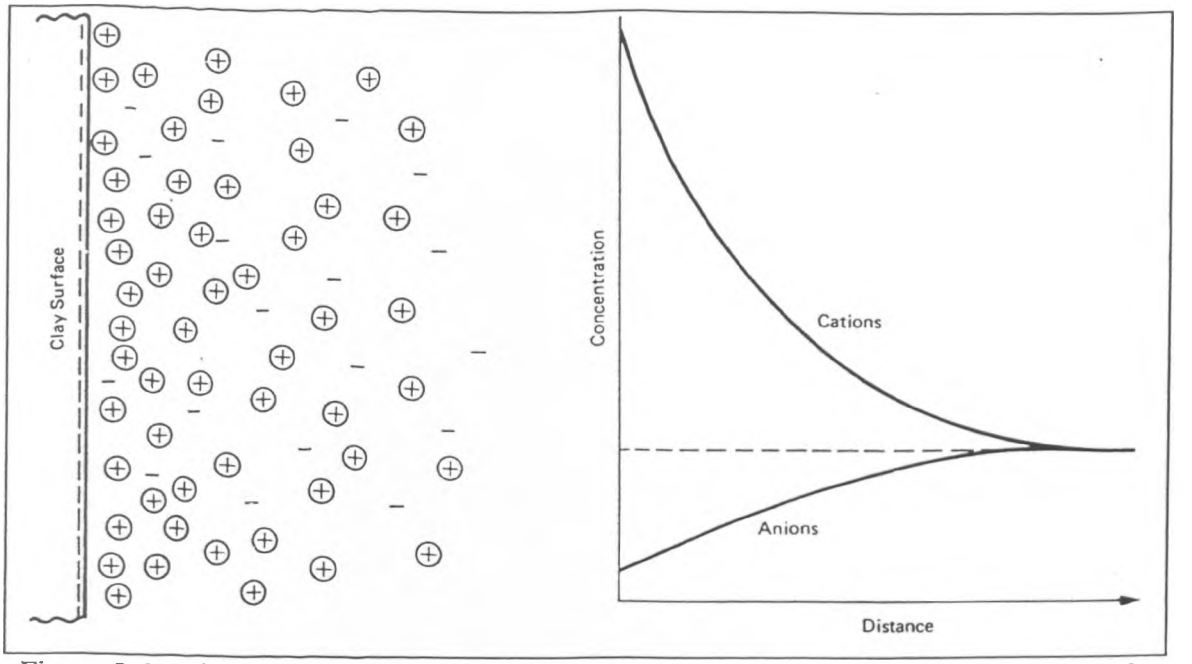

Figure 2.6: Distributions of ions adjacent to a clay surface according to the concept of the diffuse double layer (after Mitchell, 1993).

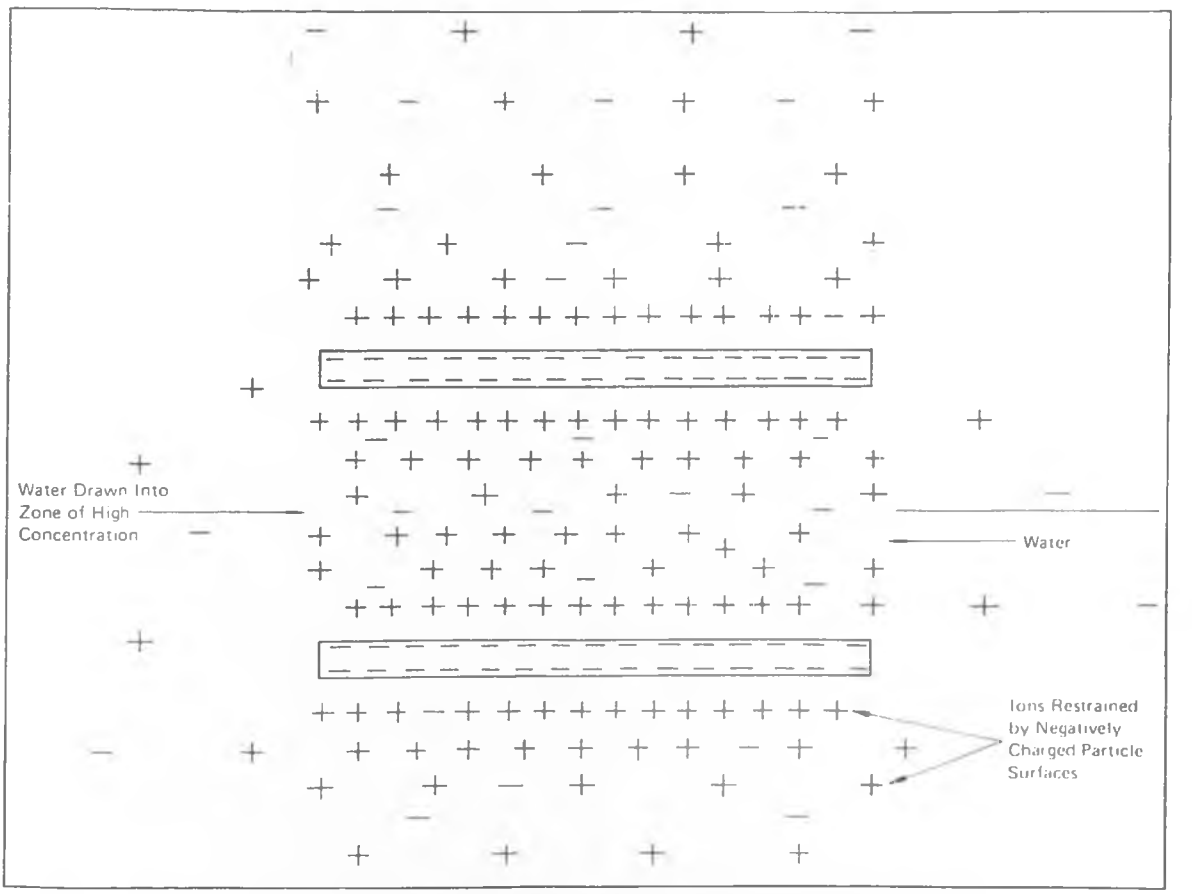

Figure 2.7: Mechanism of osmotic swelling pressure generation in clay (after Mitchell, 1993).

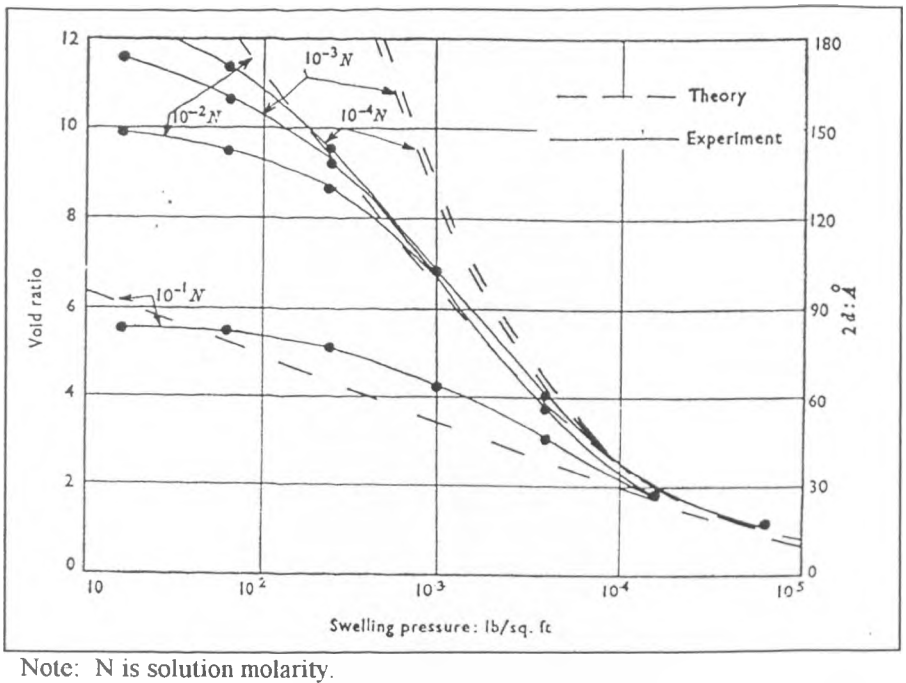

Note: N is solution molarity.

Figure 2.8: Theoretical and experimental swelling curves for consolidation and rebound of sodium montmorillonite (after Mesri and Olson, 1971).

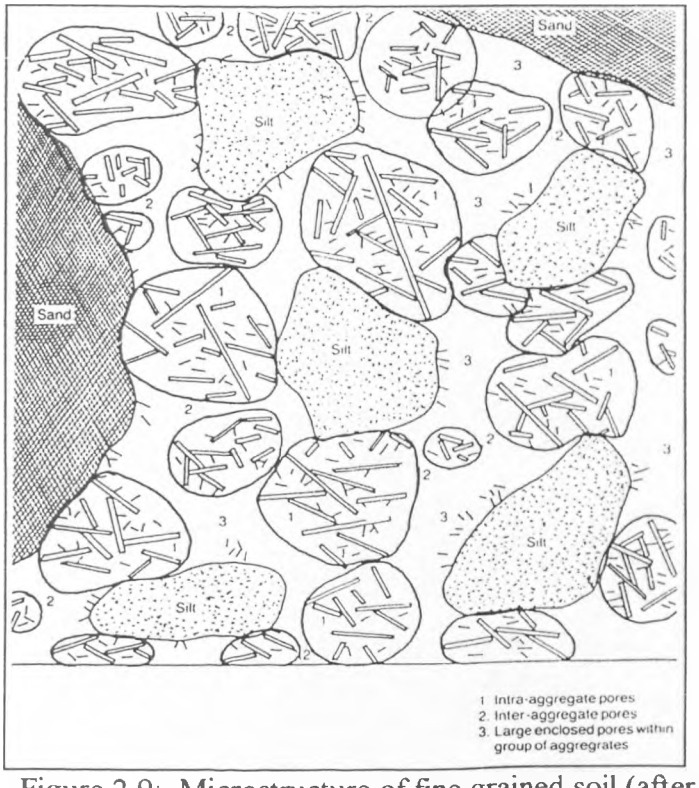

Figure 2.9: Microstructure of fine grained soil (after Griffiths and Joshi, 1989).

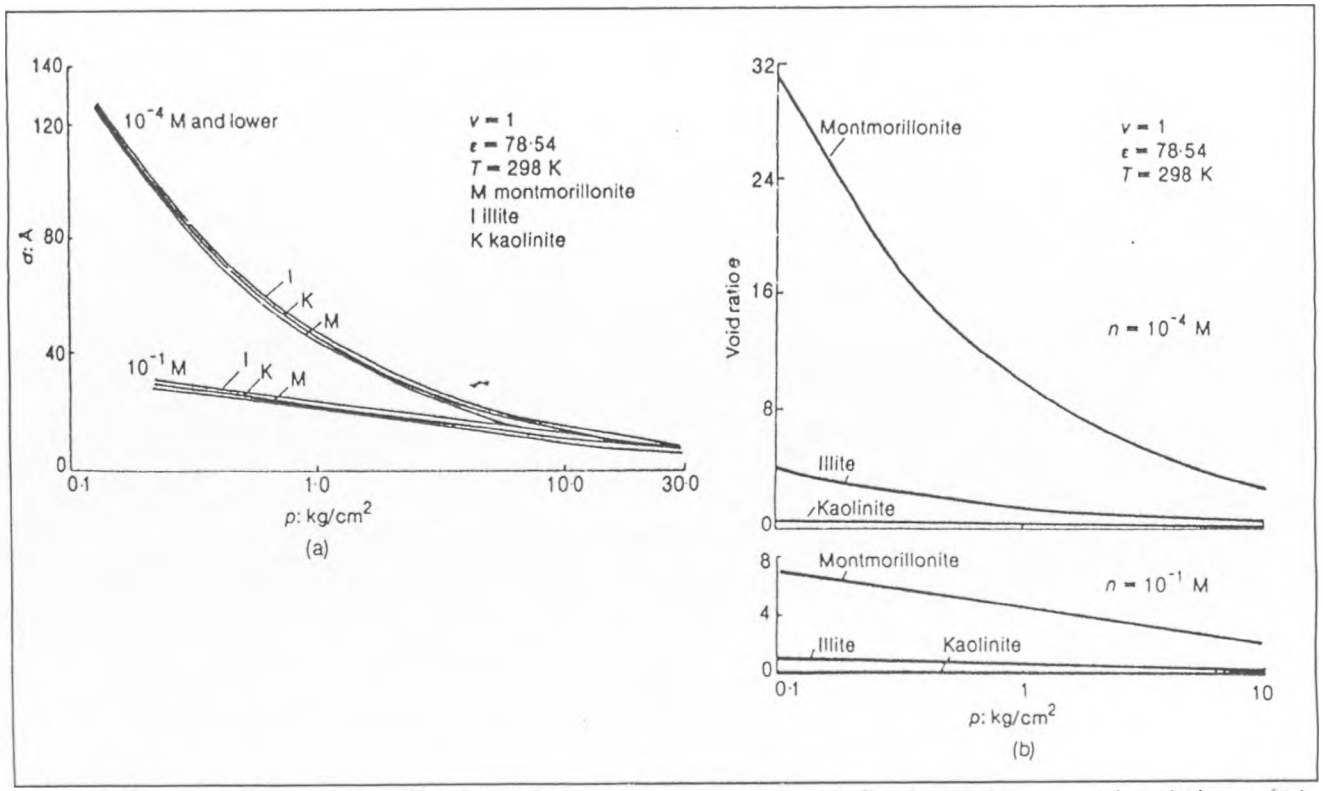

Note: v is cation valence, ε the dielectric constant of the pore fluid, T the absolute temperature and n the solution molarity.

Figure 2.10: (a) d plotted against log p for various clay types and concentrations; (b) e plotted against log p for various clay types and concentrations (after Sridharan and Jayadeva, 1982).

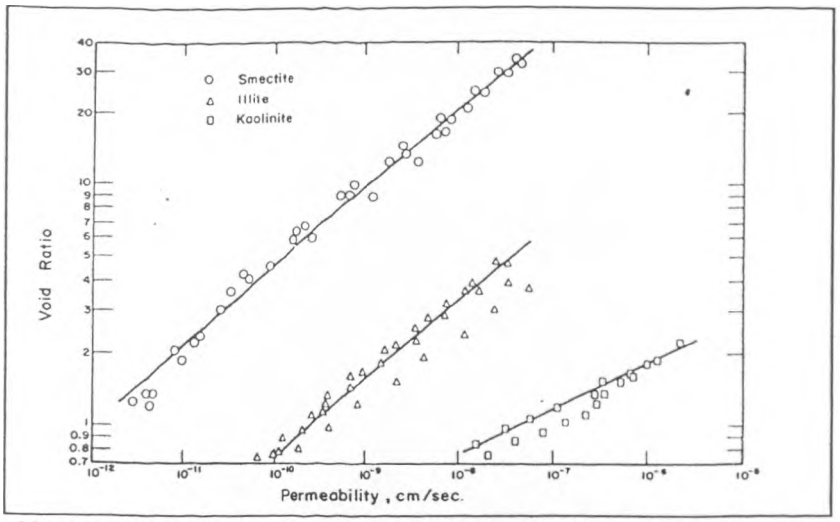

Note: Permeability (used in the figure) is identical to the hydraulic conductivity defined in 2.4.2.

Figure 2.11: Hydraulic conductivity of three sodium clays in water (after Mesri and Olson, 1971).

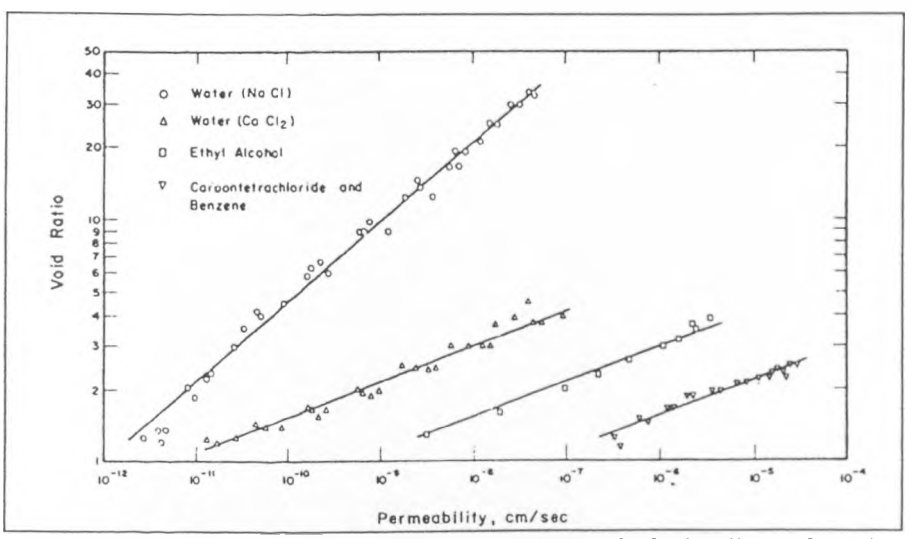

Note: Permeability (used in the figure) is identical to the hydraulic conductivity defined in 2.4.2.

Figure 2.12: Hydraulic conductivity of smectite in four pore fluids (after Mesri and Olson, 1971).

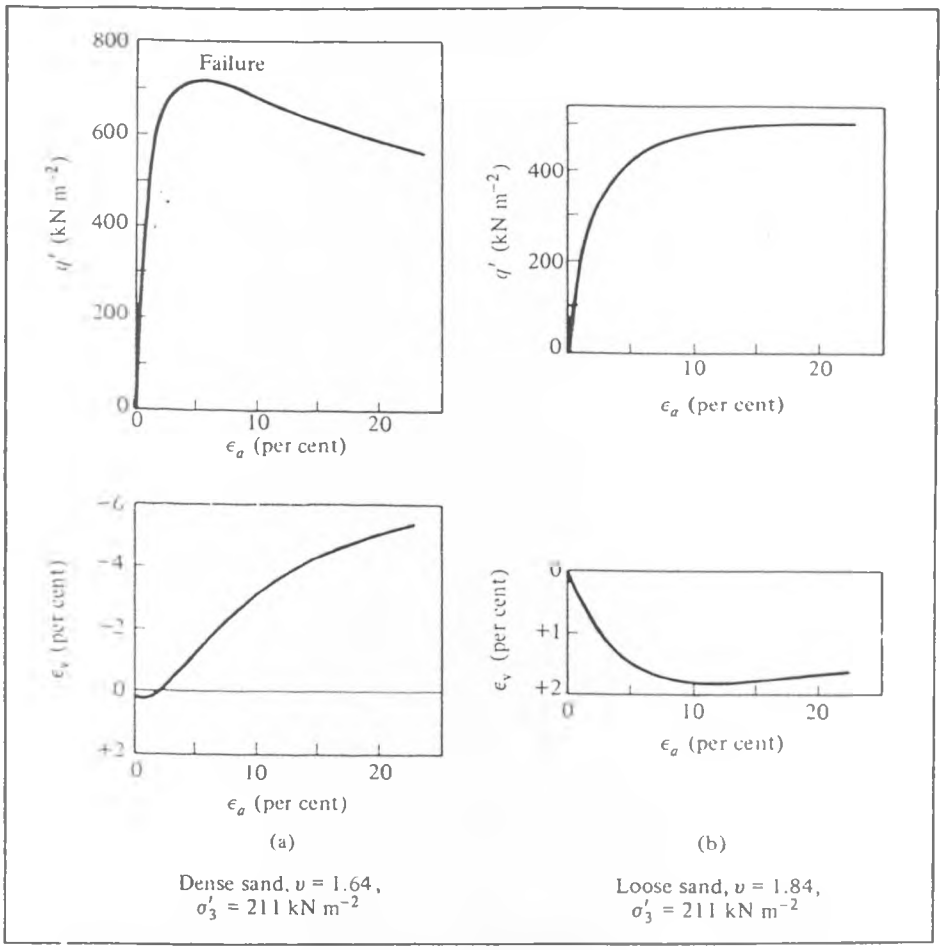

Note: q' is the deviator stress and υ the specific volume.

Figure 2.13: Results of drained triaxial test on (a) a dense sample and (b) loose sample of sand (after Bishop and Henkel, 1962).

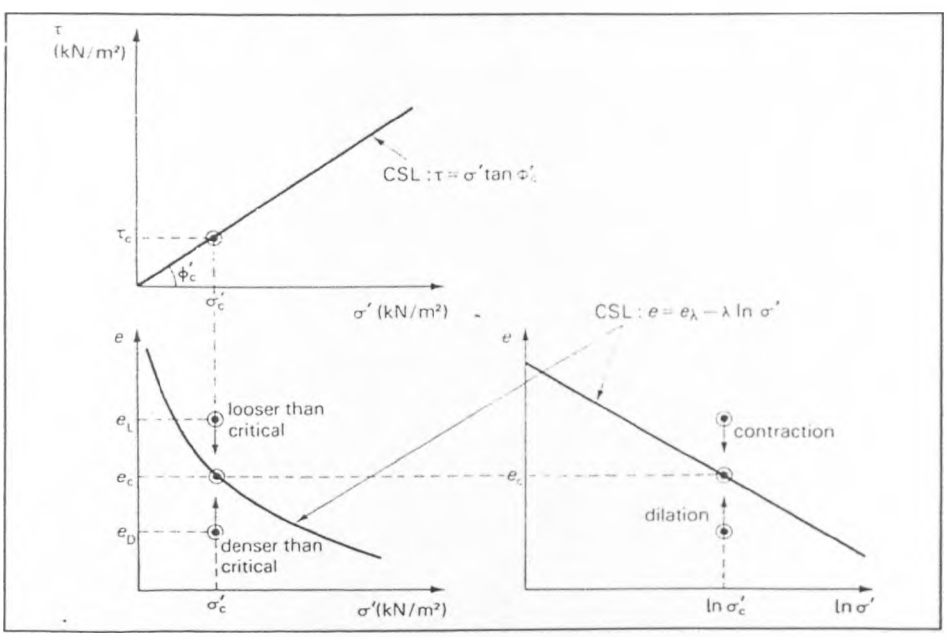

Note: τ_c, σ'_c, e_c and ϕ'_c are the shear stress, effective normal stress, void ratio and effective angle of shearing resistance, all at the critical state, respectively.

Figure 2.14: Critical state line (CSL) in (τ, σ', e) space (after Bolton, 1979).

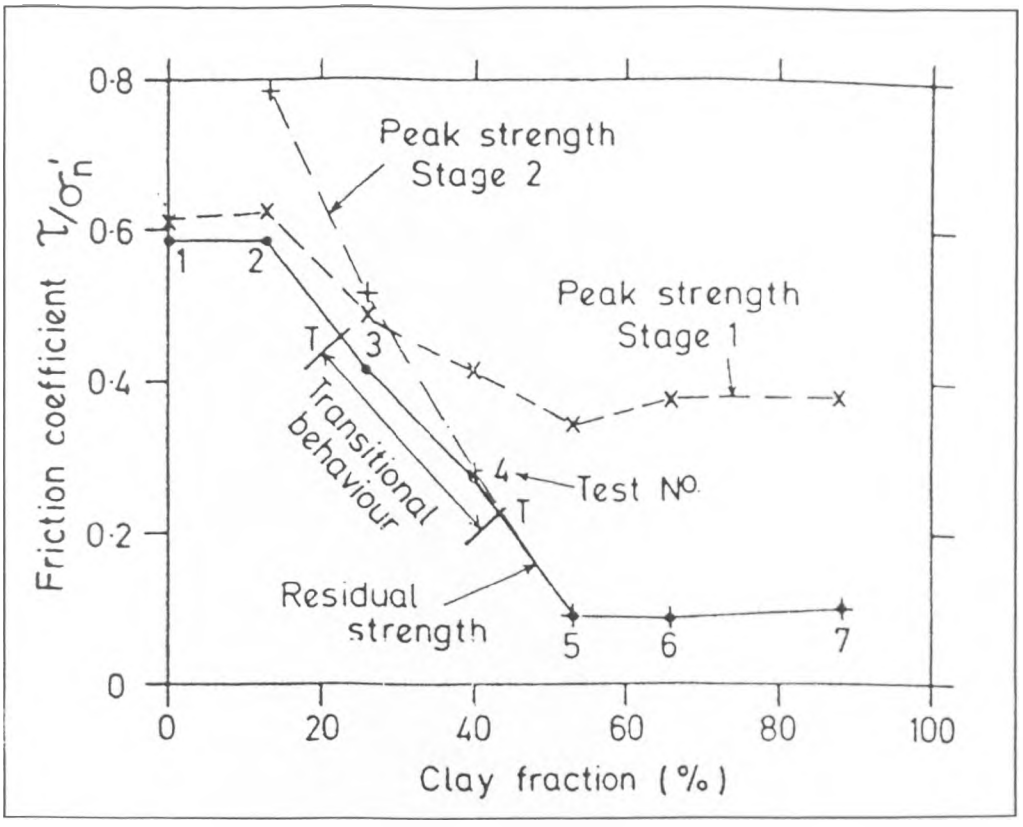

Figure 2.15: Sand-bentonite mixtures, peak and residual friction coefficients against clay fraction (after Lupini et al., 1981).

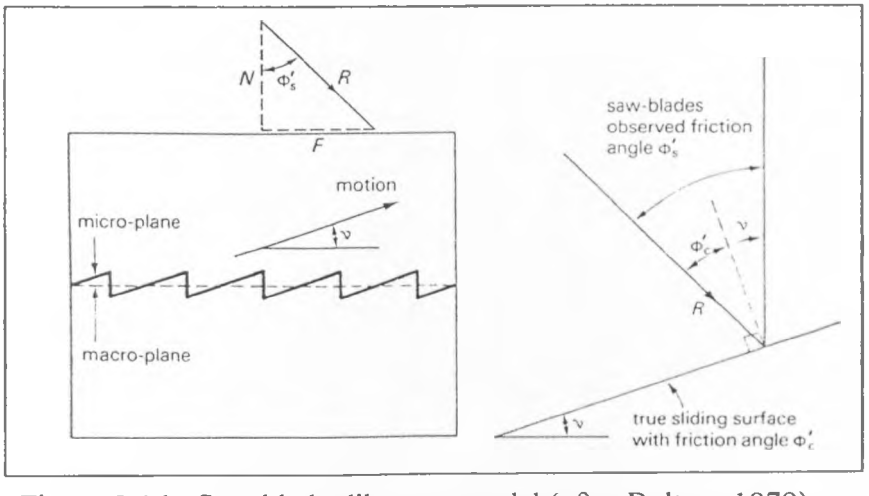

Figure 2.16: Saw-blade dilatancy model (after Bolton, 1979).

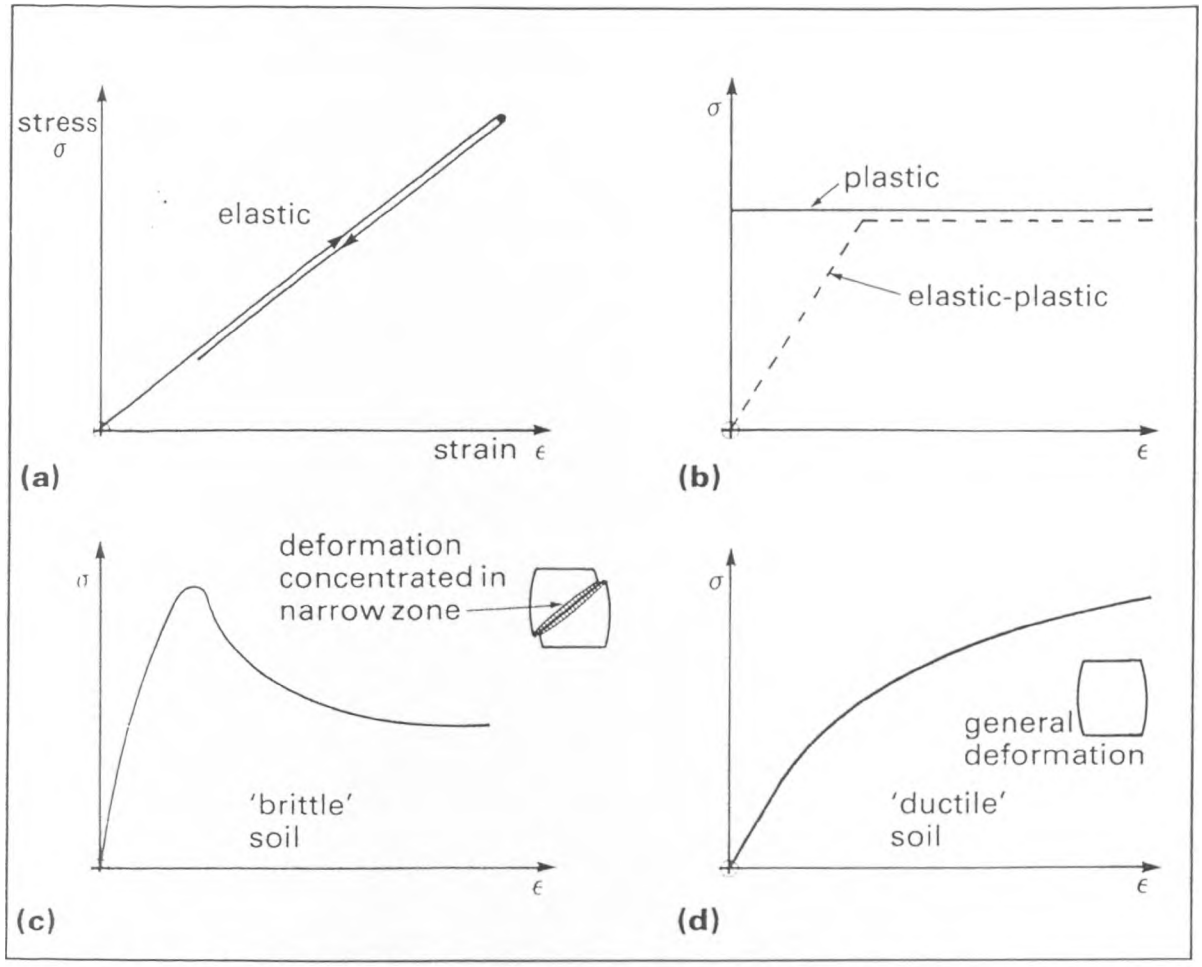

Figure 2.17: Stress-strain relationships for: (a) perfectly elastic material, (b) plastic and elastic/plastic material, (c) typical 'brittle' soil, (d) typical 'ductile' soil (after Head, 1986).

CHAPTER 3
EQUIPMENT AND MATERIALS

3.1 Introduction

This chapter describes the equipment and instrumentation used for volume change, hydraulic conductivity and strength tests, followed by a description of the materials used in the experimental programme. Experimental methods are discussed in chapter 4. Equipment includes test cells and associated pressure systems, which were set up in the laboratory for accurate testing to determine the mechanical behaviour of bentonite-sand mixtures. Measurement of physical quantities was predominantly by use of electronic transducers, however, when existing equipment was used measurement was by mechanical means (dial gauges, proving rings, etc.) . The calibration and accuracy of transducers are covered in sections 3.5.3 to 3.5.5.

3.2 Volume change tests

Standard floating ring oedometer consolidation cells (for 70mm or 100mm diameter samples) were used for the swelling, normal consolidation and rebound tests. Where a large stress was applied the samples were loaded by means of a mechanical lever system.

3.3 Hydraulic conductivity tests

3.3.1 Introduction and test cells

Due to the low hydraulic conductivity of the material (84% of all samples $< 10^{-9}$ m/s), four types of test were conducted to maximise the amount of data acquired: Rowe cell, triaxial cell, falling head using a compaction permeameter and an indirect method using oedometer consolidation test data.

Two sizes of Rowe cell (supplied by ELE) were utilised for hydraulic conductivity testing, 75mm and 250mm. The general arrangement of the cell is shown in figure 3.1. Rowe cells were originally designed to perform consolidation tests; the advantage over conventional oedometers being pore water pressure measurement and drainage control. Rowe cells differ from conventional oedometers in that the test sample is loaded hydraulically by water pressure acting on a flexible diaphragm, instead of by a mechanical lever system, enabling samples of large diameter to be tested under high stresses. A spindle, which is attached to the diaphragm, passes through the cell top so that the change in sample height can be monitored, this also allows pore fluid to drain from the sample to the top flow line. Conditions of equal strain are maintained by a rigid plate which is situated between the diaphragm and top porous disc.

The most important feature of the Rowe cell is the ability to measure and control drainage, one aspect of which is the ease in applying a back pressure, therefore, it is ideal for hydraulic conductivity testing. Further, the large sample diameter to thickness ratio gives a larger area available for flow, hence, more representative sample, and the time for swelling and/or saturation is reduced due to the decreased thickness (compared to standard triaxial, for example). Other advantages are: Teflon lining of the cell walls which minimises wall friction and the error in settlement measurement caused by compression of the loading system is negligible even with stiff samples. The absence of water pressure acting over the area of the spindle results in an average error in the applied pressure of 1.5% with a 75mm cell and 0.14% with a 250mm cell, however, this can be automatically corrected for by calibration (see 3.5.1).

A triaxial permeameter was used to test 100mm diameter samples (see figure 3.2). The cell has no piston for axial loading and therefore an isotropic confining stress is applied from the cell fluid. The base and top cap connections are similar to those provided in a standard triaxial cell.

The compaction permeameter and oedometer are standard laboratory equipment, a description of these test cells can be found in any standard text such as Head (1981), no further discussion is therefore necessary.

3.3.2 Pressure system and measurement

For the Rowe cells, three independent pressure lines apply vertical stress and pressure to the inflow and outflow lines to the sample. A stainless steel air/water interface provided the vertical stress system. This consists of a stainless steel tube (water side) large enough to contain a rubber bladder (air side) of approximately 2000ml capacity. When pressure is applied to the bladder, water is forced out of the cylinder through a drainage line connected to the diaphragm of the Rowe cell. The air/water interface to the inflow and outflow lines was provided by volume change units, an example unit is shown schematically in figure 3.3. Volume change units consist of a 10ml burette with an outer perspex pressure tube, which enables the burette to be pressurised (for back pressure application) as the pressure relative to the outer tube is zero. The arrangement enabled the use of the burettes only for samples of very low hydraulic conductivity (10^{-10} to 10^{-12} m/s) or when relatively large flow volumes occurred ($k > 10^{-10}$ m/s) valve A. was opened and the full bore (flow from both burette and tube) was used. Calibration of volume change units is discussed in 3.5.1.

The same pressure system as above was used for triaxial permeameter tests, the stainless steel air/water interface was used to apply the cell pressure.

Pressure was supplied to each system from the laboratory airline, which has a maximum pressure of approximately 600kPa. Watson Smith pressure regulators (referred to hereafter as Manostats) with a nominal output of 14-830kPa provided the required pressure to each line. The Manostat specifications, supplied by the manufacturer, indicate an accuracy of 0.02%, this corresponds to a pressure of 0.2kPa. Two types of instrumentation were used for pressure measurement, Druck and TransInstruments pressure transducers connected to calibrated signal conditioning/readout units, and Druck integral pressure transducer/readout units. In the latter, the transducer is situated inside the unit which is connected to the required pressure outlet via nylon pressure tubing. The pressure measuring instrumentation for Rowe cell tests was considered to be accurate to ±1kPa.

The arrangement of Rowe and triaxial cells for hydraulic conductivity tests with vertical flow are shown in figures 3.1 and 3.2 respectively. Figure 3.2 indicates the cell connections to the three pressure systems used for triaxial permeameter tests, the layout is similar for Rowe cell tests.

3.4 Triaxial compression and direct shear test equipment

3.4.1 Test cells

Standard triaxial cells and a Bishop-Wesley stress path cell[1] were used for strength testing of 38mm diameter samples. Standard cells were mounted on a Wykeham Farrance 50kN load frame with a motorised loading platen[2]. As the platen is driven upwards, the submersible load cell (which replaces the conventional loading ram) is restrained by a crosshead and forced further into the cell, hence causing compression of the sample. Bishop-Wesley cells differ by having a pneumatically driven loading ram. Although this system is self-contained, the stress which can be applied to the sample is limited by the maximum available airline pressure, because the pressure forcing the ram upwards is opposed by the cell pressure. Stress range is further restricted with back pressure application, as the back pressure value must be added the required effective stress to give the applied cell pressure (see appendix 1). The bases of both types of cell were modified by connecting the top and bottom pore pressure/volume change lines enabling a vacuum to be simultaneously applied to both ends of the sample for de-airing purposes.

---

[1]Both types of cell were supplied by Wykeham Farrance with maximum working capacities of 1700kPa and 1000kPa respectively.

[2]The maximum applied load was approximately 2% of the frame capacity.

Standard Wykeham Farrance direct shear box equipment was modified by raising the height of the carriage in which the shear box is placed. The box was therefore completely submerged, enabling conditions of double drainage throughout saturation and allowing fully drained shear testing. The size of the shear box used was 60 x 60 x 40mm, however, the box was packed with porous discs to allow a sample of smaller thickness to be tested (see 4.5.8).

3.4.2 Instrumentation and measurement

Both types of triaxial cell system used electronic instrumentation for measurement of cell and back pressure, deviator load, axial displacement and volume change/or pore water pressure. Cell and back pressure/or pore water pressure were measured by TransInstruments and Druck pressure transducers. Wykeham Farrance submersible load cells, mounted inside the cell to eliminate the effects of piston friction, were used for axial load measurement. Two types of volume change unit, rolling diaphragm and Imperial College type (e.g., Head, 1986), measured volume change. They both work on the same principal of a piston sealed in a pressure chamber connected to the armature of a displacement transducer (LVDT[3]). Both types of volume change unit were supplied by Wykeham Farrance. The units are calibrated enabling a known piston displacement to be converted to a volume change (see 3.5.3). Piston displacement was measured by a Schlumberger submersible LVDT (rolling diaphragm) or RDP LVDT (Imperial College type). All other LVDT's measuring axial displacement were supplied by RDP.

Transducers were connected from the cell to a data acquisition unit (built in house) containing one or more power supplies which were required to energise each transducer (typically 10-12V). The range of output of all instrumentation was from 20mV to 5V for full scale deflection. For transducers with small outputs, high quality integrated instrumentation amplifiers (built in house) with filtering were used to amplify the signal such that sufficient voltage was output from the transducer during testing. A gain of 100 was used on load cells and Druck pressure transducers to increase the full scale output to 2V and 3V respectively (see 3.5.4). Each transducer was assigned a specific input connection (or channel) on a terminal board within the data acquisition unit. Each channel was linked to computer via an Advantech analogue to digital (A/D) board which accepts 8 analogue inputs. The A/D board converts a continuous electrical input to an equivalent digital output. The main features of the board are 12-bit resolution A/D conversion and programmable analogue input ranges from ± 0.3125V to ± 5V. Electrical noise, inherent in any electronic device, was reduced to a minimum by placing capacitors across the terminal board for each channel.

---

[3]Linear variable differential transformer.

Data were automatically logged using Advantech LabTech Notebook, an integrated, general purpose software package for data acquisition, monitoring and real time control. Notebook has a graphical interface known as ICONview from which data acquisition and control setups can be created by moving and connecting icons. An icon (or block) may represent an analogue input, digital output, data file or a calculated block such as a moving average. The setup for data acquisition consisted of 5 analogue input blocks, reading cell pressure, back pressure, deviator load, axial displacement and volume change/or pore water pressure. The scale factors and offset constants for each transducer were input into their respective blocks (determined by calibration, see 3.5.3), converting electrical signals into engineering units. A block average of 10 data points logged in a 1 second period was performed on each analogue input block to smooth the output signal from the transducer as some noise was still evident even with integrated circuits. For manageable output files, data was written to file at a slower predetermined rate which depended on the overall test duration.

3.4.3 Pressure systems

Cell and back pressures were applied to the standard triaxial cell and Bishop-Wesley cell manually using Manostat pressure regulators and stainless steel air/water cylinders as described in 3.3.2.

As the Bishop-Wesley cell does not have a motorised loading platen, an additional pressure line was required to drive the pneumatic loading ram vertically up onto the sample. For this triaxial system, the data acquisition unit contained an additional board which enabled automatic control of all three pressure lines by pulsing digital outputs to stepper motor controllers. The stepper motor controller contains an anti-backlash gearbox connected to a Manostat, which is adjusted to either increase or decrease the pressure, producing directional control of the ram or a change in cell and/or back pressure[4]. Only the ram pressure was varied during testing, to maintain a similarity as close as possible to a standard consolidated-drained test. Control was achieved with LabTech Notebook (see 4.5.4).

3.5 Calibration

3.5.1 Rowe cell and volume change unit calibrations

Due to stiffness of the diaphragm and friction between the diaphragm and cell wall, the pressure exerted by the Rowe cell diaphragm is less than the pressure applied by the airline, and this becomes more significant as the cell size decreases. The difference varies with both the applied pressure and diaphragm extension, and is greatest at low pressures.

[4]The Bishop-Wesley cell was designed in this manner so that stress path testing is possible.

The calibration procedure for each Rowe cell was as follows. The cell top was fitted to the body and the space above the diaphragm filled with water. Without the cell base, the assembly was placed upside-down on the platen of a loading frame. A rigid circular plate was placed on the diaphragm and spacers inserted up to a calibrated load ring mounted on the load frame. The arrangement is indicated in figure 3.4 (after Head, 1986). The water content of the diaphragm was adjusted to make the extension about the same as when in contact with a sample. A pressure system fitted with an accurately calibrated pressure transducer was connected to the diaphragm pressure line. The diaphragm pressure was incrementally increased up to the maximum airline pressure and the load ring reading noted at each stage. The true pressure on the sample area was calculated as the load ring force plus the weight of the plate divided by the area of the cell. The diaphragm pressure correction is the difference between the applied pressure measured by the transducer and the calculated true pressure.

Figures 3.5 and 3.6 are plots of diaphragm pressure correction against true pressure on the sample for 75mm and 250mm Rowe cells respectively. All points are plotted on the same figure from a series of tests. The diaphragm was unlubricated during testing and so was calibrated in the same state. Although the pressure correction is minimised with the diaphragm lubricated, it was thought that lubricant on the cell wall may alter the swelling characteristics of initially dry samples[5] and consequently the hydraulic conductivity. Therefore, for consistency, all tests were performed with the diaphragm unlubricated.

The pressure correction to be added to the required pressure for loading or unloading[6] directions can be read off the best fit lines for the 75mm cell. For application of stresses up to 100kPa, the pressure was first increased above the required value and proceeded by an unloading stage to the required pressure (with a 0-5kPa correction), as the percentage error increases at low stresses for loading increments. Above a pressure of 100kPa the scatter in unloading data is greater than for loading, therefore above this stress, the pressure was applied by loading the diaphragm. For the large Rowe cell, figure 3.6 shows a cyclic response in the pressure correction with true pressure which is more pronounced on unloading. It is thought that this may be due to stick-slip behaviour between the diaphragm and cell wall and/or between the spindle and seal in the cell top.

---

[5]Bentonite particles may become inadvertently attached or coated in grease near the cell wall, causing changes in fabric or even preventing swelling at the periphery of the sample which may have an unknown effect throughout the whole of the sample.

[6]In multi-stage tests, where hydraulic conductivity was calculated at several vertical effective stresses, the loading sequence involved reducing the stress in increments from the initial value. This ensured no consolidation of the sample occurred during the stress history. Unloading and reloading of the diaphragm was performed with drainage lines closed, leaving the effective stress on the sample unchanged. Additionally, any changes in stress over a time period of a few seconds would have a negligible effect on the sample due to the low hydraulic conductivity.

Due to non-uniformity of the unloading calibration curve, only loading stages were used with a pressure correction of 25kPa each time. This calibration automatically allows for the small non-pressurised area under the drainage stem.

Rowe cells can distort when subjected to high internal pressures which influences the measured settlements. With the diaphragm supported on a rigid disc inside the cell, both sides of the diaphragm were pressurised equally in increments using the diaphragm pressure line and the inflow pressure line (see figure 3.1). Over the applied stress range (0-500kPa), the resulting effect on the settlement dial gauge was found to have no measurable value.

Losses of pressure head due to friction and turbulence in the connecting tubing, porous discs, and constrictions in valves, tube connectors and cell ports can be considered negligible when testing materials of low hydraulic conductivity (Head, 1986). Therefore, no calibration for head loss was considered necessary.

Volume change measuring burettes were calibrated to enable the full bore to be used when testing samples with relatively high flow rates ($k > 10^{-10}$ m/s). The sample drainage lines (see figure 3.3) of both inflow and outflow volume change units were hydraulically connected. At the inflow side (with valve A. open) valve B. was opened allowing full bore drainage into the outflow side. Since valve A. was closed on the outflow volume change unit, water drained into the burette only. When the levels in each unit were equal, water was drained from the burette to re-establish a head difference. The burettes have a 10ml capacity and can be read accurately to 0.01ml, therefore the drop in "full bore" water level was converted to volume in ml per ml change of the inner burette. A similar procedure was repeated for the outflow volume change unit. For both units, a full bore volume change of 14ml per 1ml drop in burette level were found, giving each unit a capacity of 140ml.

3.5.2 Triaxial cell calibrations

When the pressure in a triaxial cell is increased the cell walls expand. This introduces an error if sample volume change measurements are made on the cell pressure line. Since volume change was measured on the back pressure line this calibration was unnecessary. Triaxial tests were conducted at constant cell pressure, therefore a correction for vertical deformation of the cell (causing an error in the measured axial displacement) with changing pressure was also unnecessary.

As in Rowe cell tests, pipeline head losses are considered negligible when testing soils of low hydraulic conductivity.

3.5.3 Calibration of measuring instruments

Transducers which measure load and pressure have a clearly defined zero point corresponding to zero load or atmospheric pressure respectively. Displacement measurement depends upon the position of an arbitrarily chosen datum point, determined by the position of the transducer at the start of calibration or test. The electrical signal produced at a datum point for any transducer is referred to as an offset constant, i. The relationship between the transmitted signal and the physical quantity being measured is known as the scale factor, b. Therefore, assuming a linear transducer response, the relationship to determine the required physical quantity, q, from an electrical signal, r, is given by:

$$q = b(r - i) \qquad 3.1$$

The purpose of calibration is to determine scale factors and offset constants, and also the accuracy and resolution of transducers and measuring instruments. Transducer outputs were measured by a data acquisition unit linked to a computer via an A/D board, for automatically logged triaxial tests. When data acquisition was manual, either a signal conditioning/readout unit, or digital voltmeter was used[7]. Values of i and b were input into LabTech Notebook for data logged tests immediately before testing commenced, offsets were removed from electronic signal conditioning/readout units under initial conditions. Where output measurement was by use of a digital voltmeter, values of i and b were used in equation 3.1 to calculate the required physical quantity from the indicated voltage.

On manually logged tests, a pressure was indicated by connecting a transducer to an RDP signal conditioning/readout unit. The readout and pressure transducer were calibrated together using a Druck precision calibration unit, which has a resolution of 0.1kPa over a range of 1000kPa. Pressure was applied to the transducer by the Druck unit over the full range (this was 1000kPa for all pressure transducers). Gain and zero offset controls were available on the RDP unit, these were adjusted until the indicated pressure was consistently equal to the known applied pressure over the full range. It was thought an accuracy of ±1kPa was reasonable for pressure measurement by this system (the manufacturers specification for the Manostats is approximately ±0.1kPa).

---

[7]Transducers were calibrated on their respective testing systems, i.e. using the same data acquisition unit as during the test etc. The calibration, therefore, gives an indication of the accuracy and resolution of each system as a whole and not a summation of the individual components.

The calibration check for triaxial system pressure transducers was as follows: With the pressure lines open to the atmosphere, the voltage was determined by averaging 100 data points logged in Notebook for cell and back pressure transducers, hence offset constants were determined. This was repeated several times and the mean values, plus the scale factors (as supplied by the manufacturer), were input into Notebook for both transducers. The pressure lines were hydraulically connected such that the same pressure could be applied to each transducer from one Manostat. The pressure was incrementally increased up to the maximum value (600kPa), and the value indicated by each transducer noted. No difference was observed between the two recorded pressures over the full range, and as other similar transducers had been calibrated against a precision calibration unit and found to comply to the manufacturers specification, the manufacturers scale factors were deemed satisfactory.

Load transducers were calibrated using both dead weights and a reference load cell traceable back to a national standard. In the latter, load was applied by placing the reference cell on the platen of a 50kN triaxial load frame and forcing it against the load transducer. In both types of calibration the load cell was connected to its designated data acquisition unit and voltages read in LabTech Notebook. Three load/unload cycles were performed over a range of 0-600N. The maximum load of approximately 80% of the triaxial tests fell within this load range, and of the remaining tests the maximum load was about 1kN. Since no measurable deviation from linearity was found, it was thought reasonable that the scale factors determined would apply up to 1kN. The manufacturers specifications indicate a non-linearity less than 0.1% of full scale (3kN and 5kN) and repeatability to within 0.05% of the indicated load.

A vernier height gauge with readout was used for calibration of displacement transducers. The transducer was rigidly clamped with the armature against the gauge, which was laterally displaced across the calibration range. The transducer output was recorded for every gauge displacement of 1mm to a resolution of 0.001mm. The calibration range was ±10mm either side of the zero output displacement as this is the most linear range of the transducer and the maximum displacement required for triaxial testing. Each calibration was performed 3 times. The calculated coefficient of correlation, r^2, of displacement against voltage for all transducers was greater than 0.98.

Volume change indicators were calibrated as follows. With the piston initially fully upwards the LVDT output was noted. A deairing valve on the triaxial cell was opened allowing water to drain from the volume change unit into a beaker and the mass of water was measured along with the corresponding transducer output. This procedure was

repeated until all water had drained from the chamber. Small volumes of water were drained at each stage to produce sufficient data points for linear regression analysis to determine the scale factor. The mass of water was converted to ml giving the scale factor in ml/V. This procedure was repeated 3 times. The problem in draining the entire chamber is that the range of the transducer used in calibration is much larger than during testing. However, it was considered more accurate to drain a relatively large volume of water at each stage, in case any slight loss of water occurred at the valve. In addition, no significant deviation from linearity was found over the full range of volume change.

3.5.4 Resolution of electronic measurement systems

The accuracy of electronic instrumentation is most significant when the physical quantity measured by the transducer is small compared to the full working range. No measurable deviation from linearity was found over the calibration range for all transducers (as discussed in 3.5.3), and therefore, scale factors were used in the software with a high degree of confidence. Resolution of measurement is also of importance. This is determined by the A/D converter, the selected analogue input range (programmable gain on A/D board), which determines the proportion of full scale output over which the transducer will meaningfully operate[8], and the calculated scale factor.

A 12-bit A/D board was used for conversion of analogue signals. This means that with 1-bit accuracy, the signal can be read to 1/4096 (2^{12}) of the selected analogue input range. Analogue input ranges were conservatively selected, based on the estimated range required for measurement by the transducer. By reducing the input range, the resolution of voltage measurement is increased. For example, if a ±50mm displacement transducer with a corresponding output of ±5V was required to measure a maximum displacement of 20mm, then an analogue input range of ±1.25V would be used. The resolution in mm would be equal to 1.25/4096V multiplied by the scale factor of the transducer in mm/V.

In the Bishop-Wesley cell, the load transducer has a capacity of 5kN, and for standard triaxial tests a 3kN load transducer was used. The scale factors determined by calibration were found to be approximately 2400N/V and 1700N/V for Bishop-Wesley and standard triaxial load transducers respectively. The nominal output of each load cell was 20mV, and an integrated amplifier with a gain of 100 increased this to approximately 2V. With a selected analogue input range of ±1.25V, the corresponding resolutions are 0.7N and 0.5N for 5kN and 3kN transducers respectively.

---

[8]For example, a ±50mm transducer with a full scale output of ±5V will only measure between ±10mm if the selected analogue input range is ±1V.

The resolution of volume change measurement is dependent on the resolution of the LVDT which measures displacement of the piston armature (displacement is then converted to volume change). Resolution of displacement and volume change measurement was calculated as 0.003mm and 0.008ml respectively.

Since a back pressure was used for all tests, pressure transducers were all approximately at the middle of their working range (0-1000kPa) during testing, and the programmable gain on the A/D board was not required. Analogue input ranges were set at ±5V for all Druck and TransInstruments pressure transducers with corresponding resolutions of 0.1kPa and 0.2kPa respectively.

3.5.5 Accuracy of measurement

The resolutions quoted in 3.5.4 assume that the combination of transducer, signal conditioning (including amplification) and readout comply exactly to specifications. Even with integrated circuits, effects such as electrical noise and repeatability of measurement have a significant effect on the accuracy to which a data point can be confidently stated. For example, taking electrical noise into account, and from the manufacturers specifications, it is reasonable to assume that the A/D board can measure accurately only to within ±2 bits. Since testing periods were of durations up to ten weeks, temperature changes also affect accuracy by altering the characteristics of the transducer.

The accuracy and repeatability of readings was investigated on setting up of the equipment and monitored throughout the triaxial testing programme[9]. A fixed load, displacement or pressure was applied to each transducer, and the signal logged in LabTech Notebook. Typical curves for load and displacement transducers over a 10 day logging period are shown in figures 3.7a and 3.7b. The figures show that temperature has a significantly greater effect on accuracy than electrical noise with a cyclic variation in reading over a 24hr period. The smaller changes at any particular time are presumed to be due to electrical noise. Even though the difference between minimum and maximum values is relatively large, the reading returns almost to its original value after 24 hours (some time lag is evident, probably due general temperature change rather than diurnal). Similar behaviour was exhibited by all other transducers for logging periods up to 4 weeks, each response was monitored a minimum of 3 times.

---

[9]Prior to shear testing, an isotropic confining stress was applied to samples for periods up to four weeks until swelling equilibrium was reached. The stability of all the transducers could therefore be monitored for this time period with the exception of volume change, which was monitored during undrained testing.

Accuracy of physical quantities (in engineering units) and the corresponding percentage of the maximum measured values during testing are shown in table 3.1.

Physical quantity	**Units**	**Accuracy**	**% of maximum measured value**
load	N	±2	0.2 - 4.3
displacement	mm	±0.01	0.07 - 0.6
volume	ml	±0.05	1.2 - 6
pressure	kPa	±1	0.2 - 0.3

Table 3.1. Accuracy of triaxial system measurements.

3.6 Materials

3.6.1 Description of test clay

The clay used in the study was Conquest Wyoming bentonite supplied by Colin Stewart MinChem. Conquest grade Wyoming bentonite originates from Newcastle, Wyoming, and is ground, dried and air classified during processing. The X-ray diffraction spectra (after Mollins et al., in print) shown in figure 3.8 indicate that it is predominantly a montmorillonite with some quartz and trace cristobalite. Table 3.2 shows the composition obtained from a chemical analysis and confirms that the soil is predominantly a sodium montmorillonite.

Chemical Compound		Percentage by weight
Silica	SiO_2	62.91
Titania	TiO_2	0.15
Alumina	Al_2O_3	20.63
Ferric Oxide	Fe_2O_3	3.75
Magnesia	MgO	2.45
Lime	CaO	1.16
Soda	Na_2O	2.29
Potash	K_2O	0.57
Loss on ignition (1000°C for 1 hr)		5.83
		99.74

Note: Sample dried at 105°C prior to testing

Table 3.2. Chemical composition of Conquest Wyoming bentonite determined by X-ray fluorescence spectroscopy (after Mollins et al., in print).

The properties of Wyoming bentonite are as follows[†] :

Liquid limit = 407%

Plastic limit = 48%

Specific gravity = 2.76

Moisture content ~ 14% (as supplied)

Free swell[#] = 833% (oven dried), 1233% (as supplied).

Cation exchange capacity[x] = 90meq/100g

Specific surface[x] ~ 800m^2/g

[†] Tests performed in accordance with B.S. 1377: Part 2: 1990 (see 4.6) unless otherwise indicated.

[#] The volume increase when unconfined bentonite powder is inundated, divided by the volume of the original dry loose powder (Head, 1980).

[x] Studds (personal communication, 1996).

3.6.2 Description of test sand

The sand used in the study was Knapton Quarry sand from Knapton, North Yorkshire. It is a slightly silty fine angular quartz sand, containing some iron oxides and silicate minerals. Figure 3.9 is the particle size distribution curve of Knapton Quarry sand, other properties are as follows[†] :

Fines = 7%

Particle shape - sub-angular to angular

Effective size (D_{10}) = 0.07mm

Maximum void ratio* = 0.978

Minimum void ratio* = 0.451

As supplied moisture content ~ 5%

Specific gravity = 2.67

3.7 Summary

Laboratory test equipment, pressure systems, electronic instrumentation, and hardware and software have been described. Calibration procedures have been outlined for both the test equipment and instrumentation. The resolution of measurement and an indication of accuracy, as a percentage of the maximum physical quantities measured in the triaxial test programme, have been reported. Finally, a description of the test materials has been given.

[†]Tests performed in accordance with B.S. 1377: Part 2: 1990 (see 4.6) unless otherwise indicated.
*Determined by methods described in Head (1980).

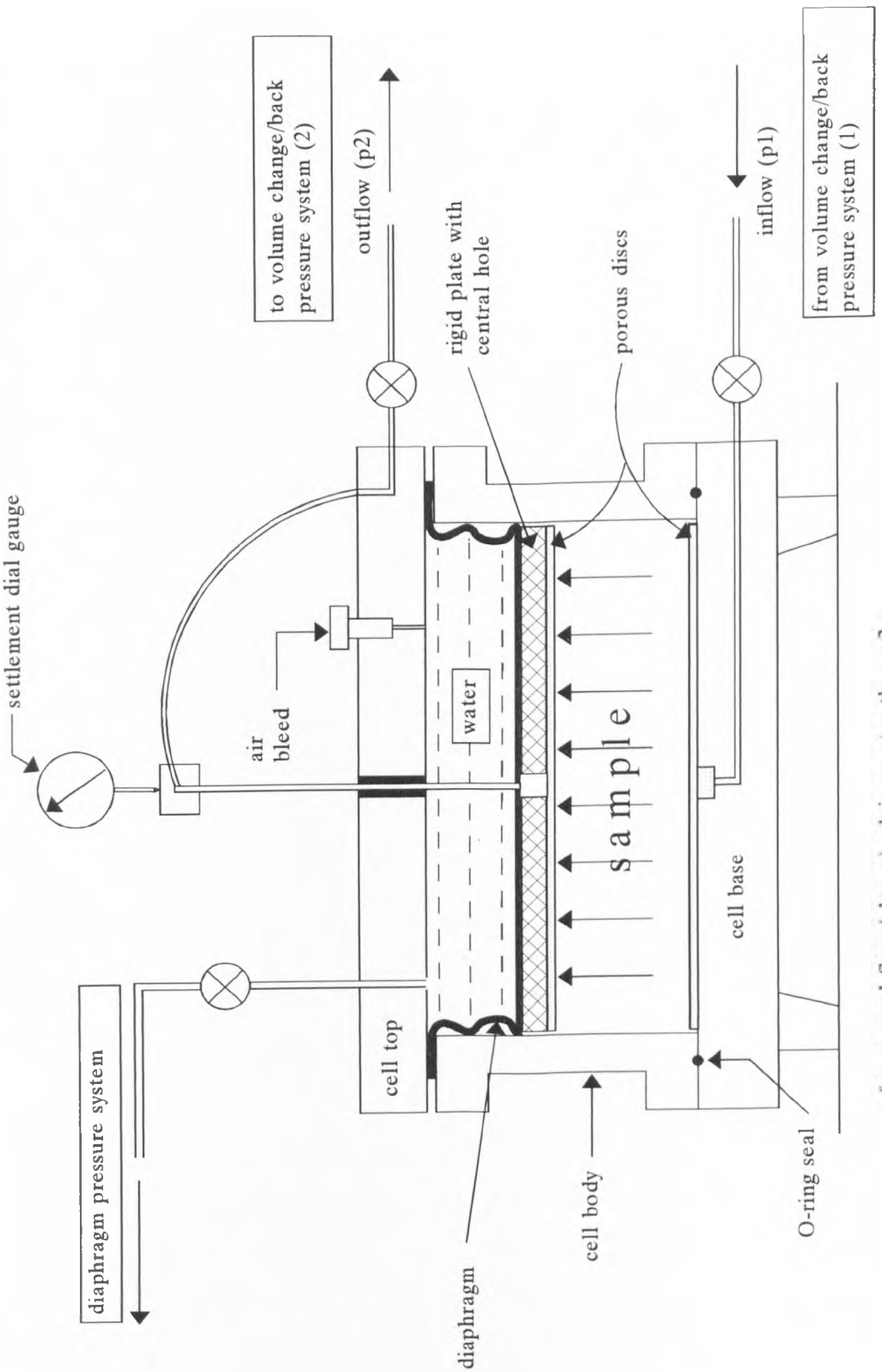

Figure 3.1: Arrangement of Rowe cell for hydraulic conductivity tests with vertical flow.

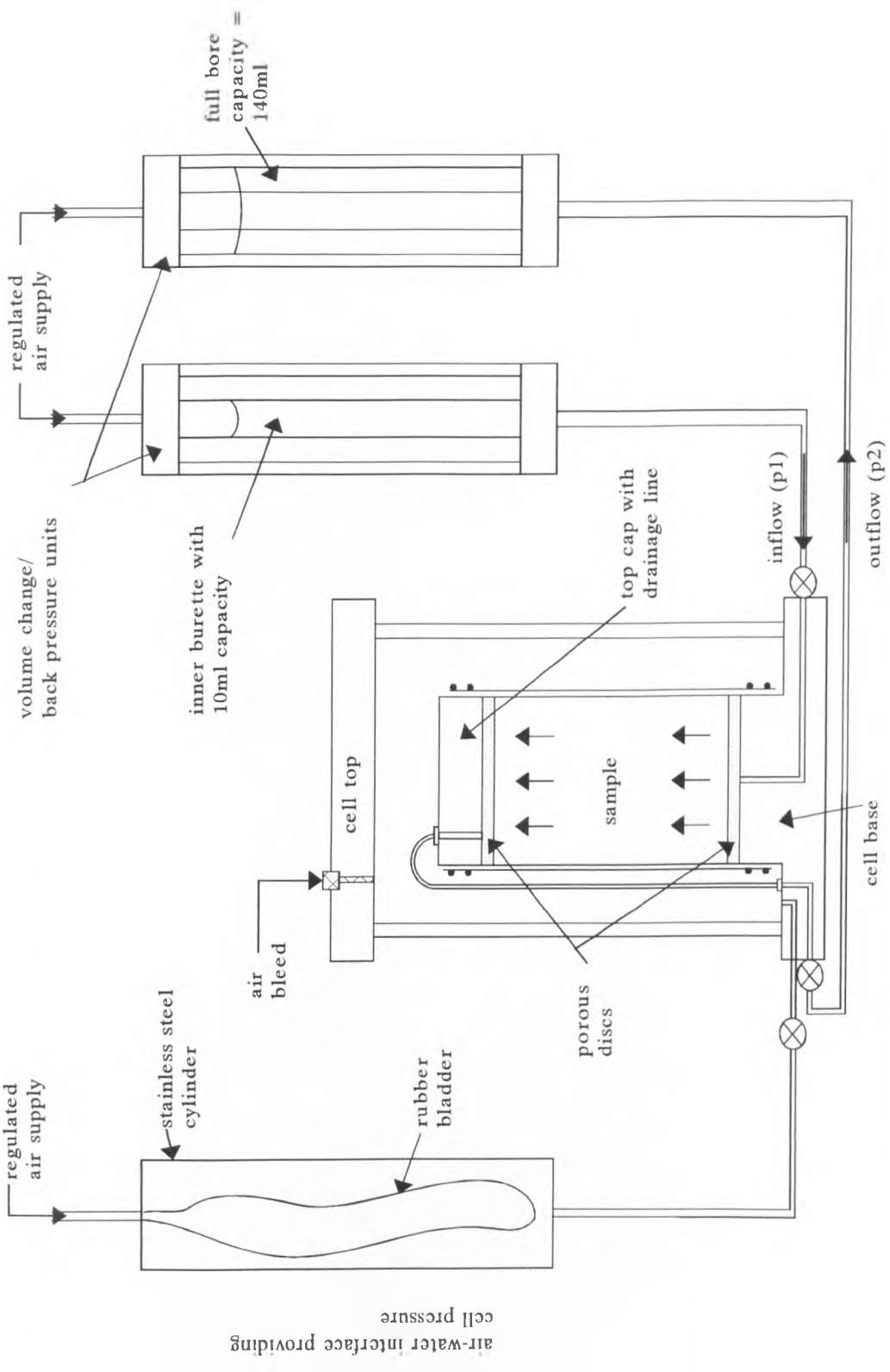

For upward flow (shown) p1 is greater than p2

Figure 3.2: Arrangement of triaxial cell for hydraulic conductivity tests with vertical flow.

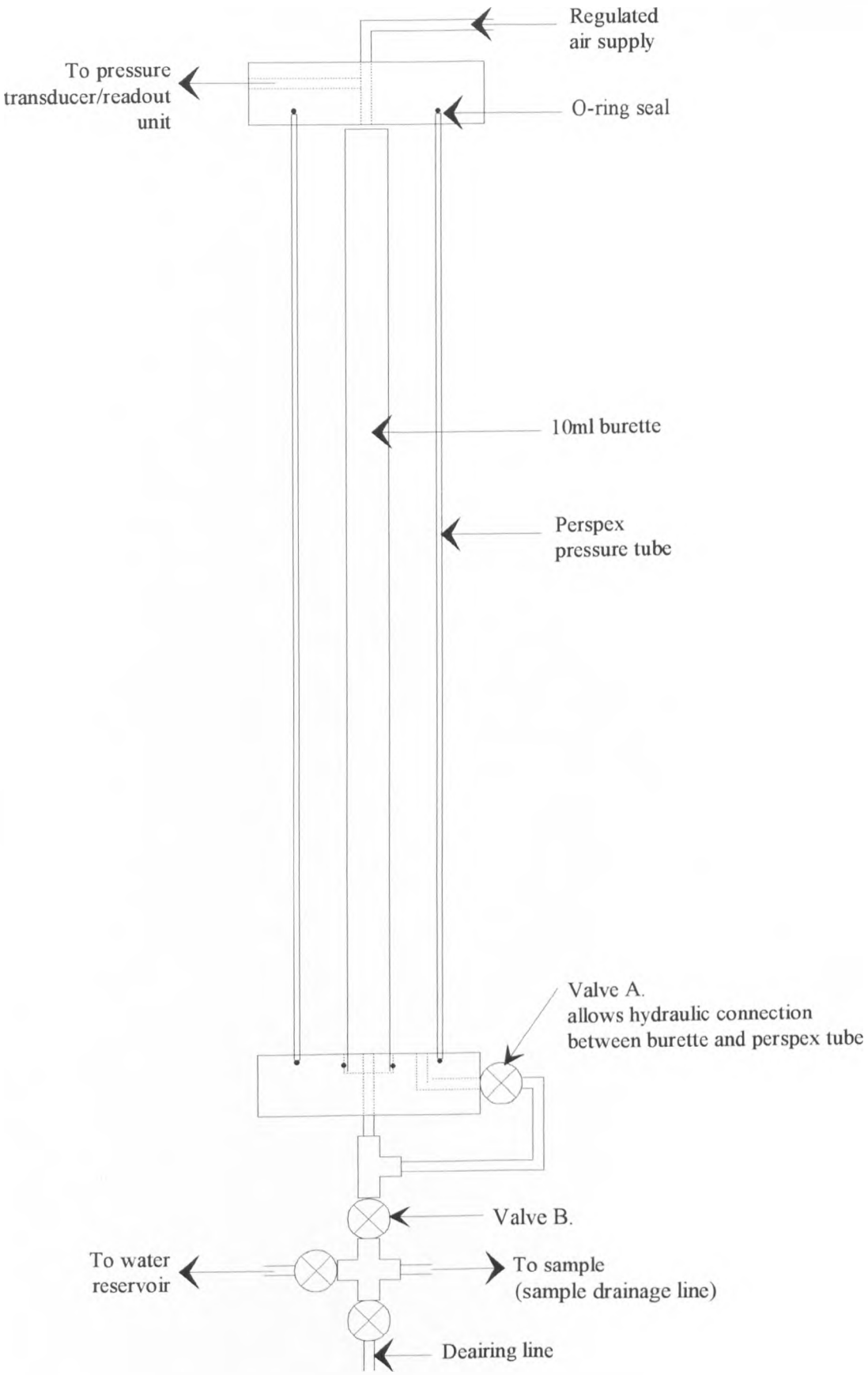

Figure 3.3: Volume change unit for inflow/outflow measurement in hydraulic conductivity tests.

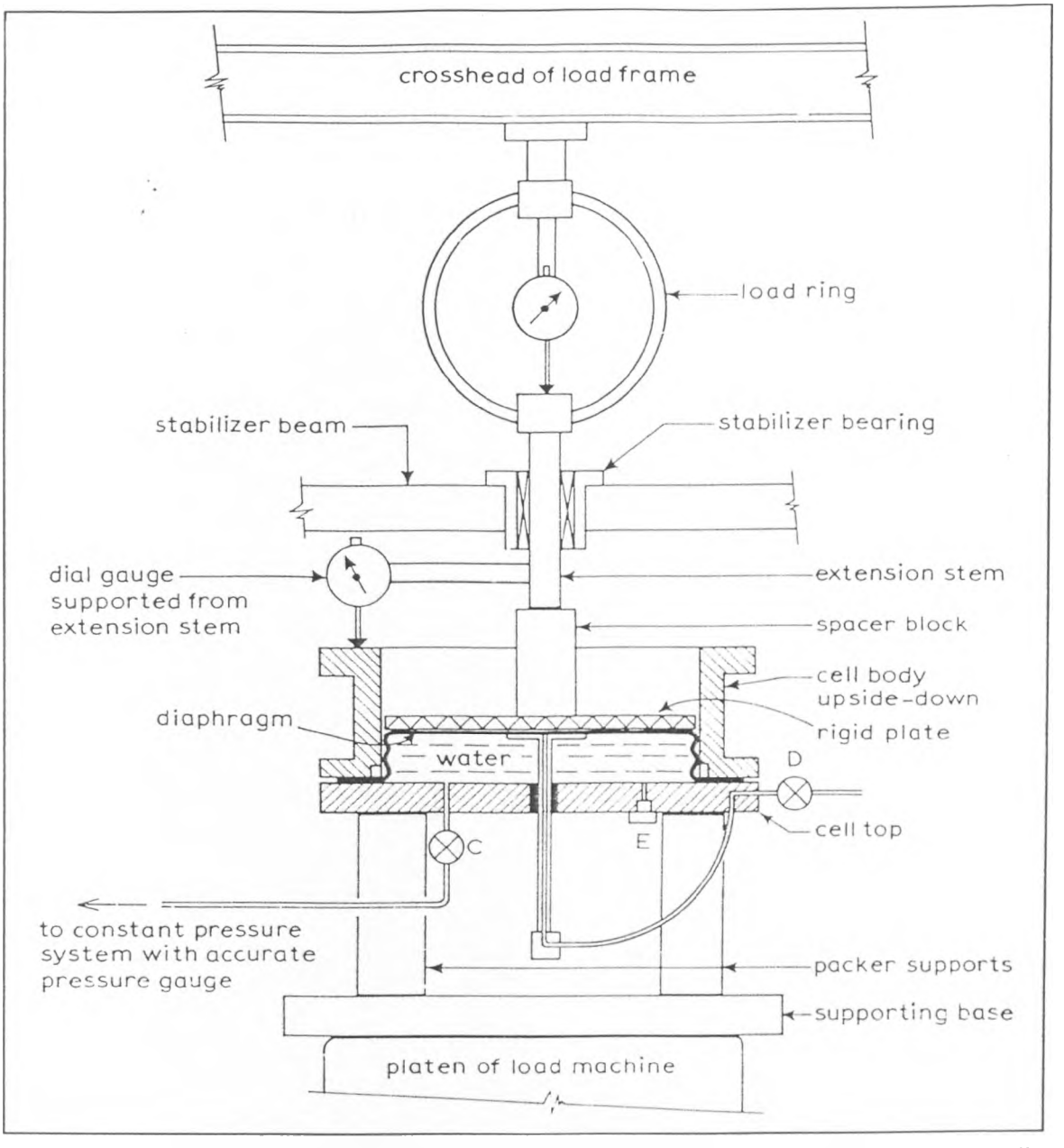

Figure 3.4: Arrangement for calibration of load transmitted by diaphragm of Rowe cell (after Head, 1986).

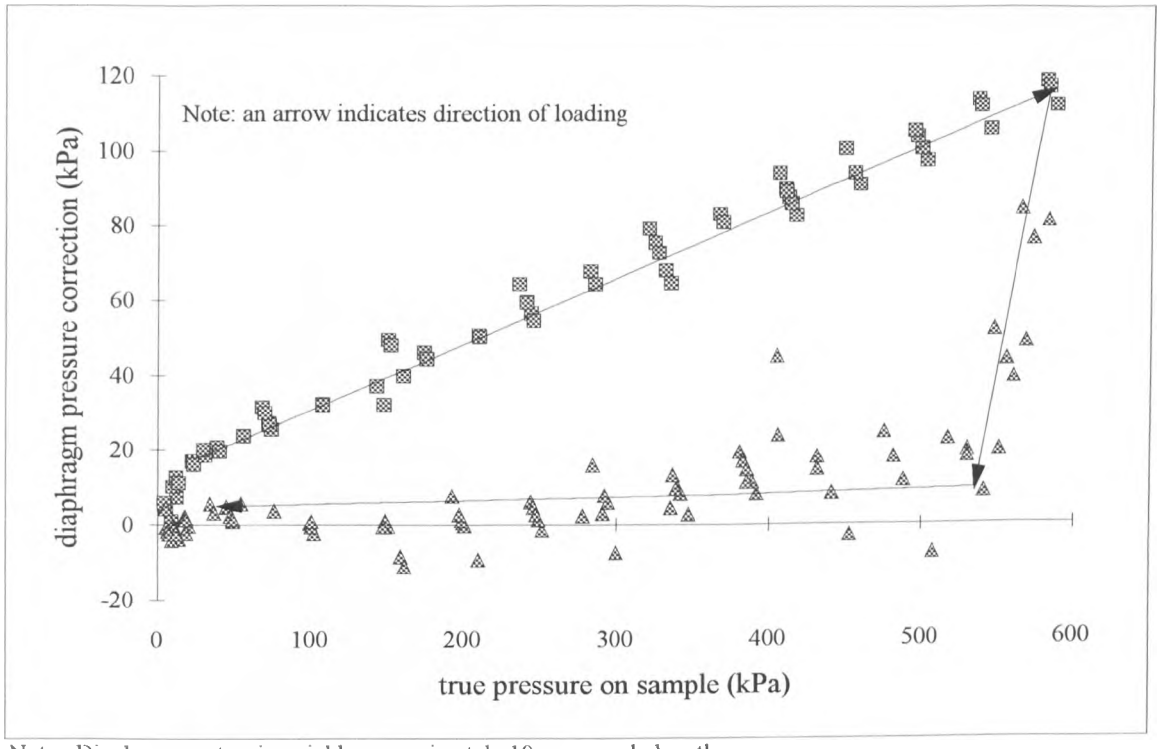

Note: Diaphragm extension yields approximately 10mm sample length.

Figure 3.5: 75mm Rowe cell calibration curve with the diaphragm unlubricated

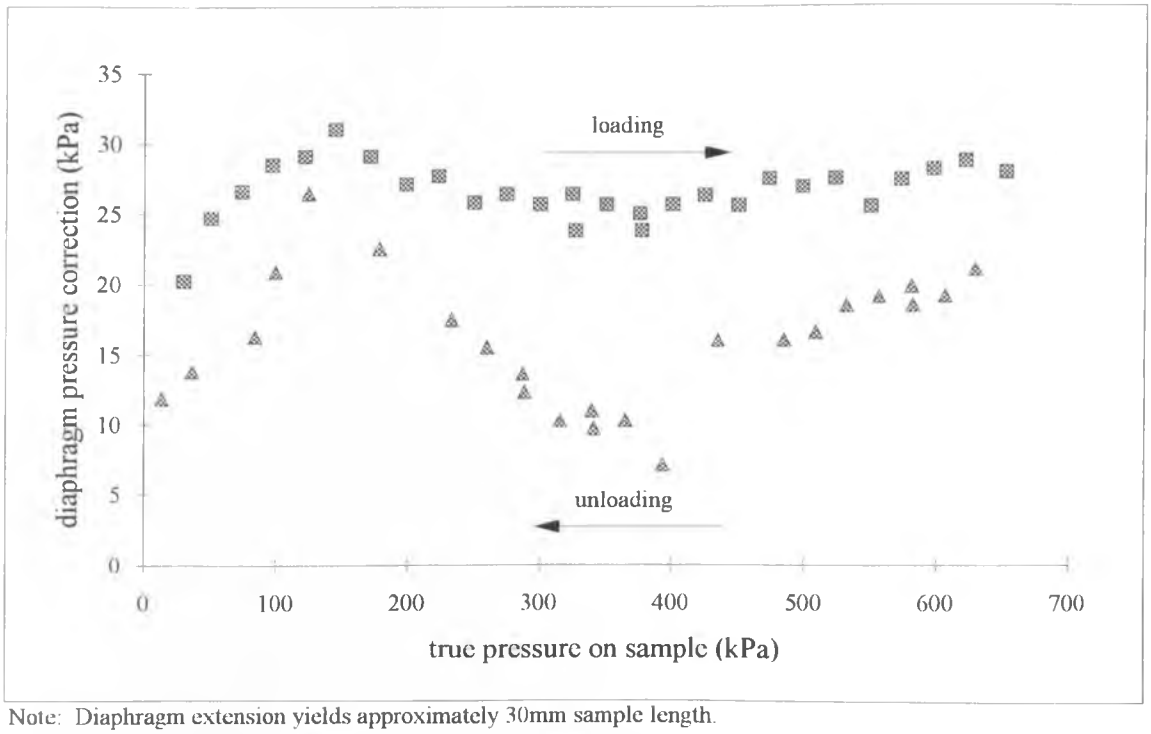

Note: Diaphragm extension yields approximately 30mm sample length.

Figure 3.6: 250mm Rowe cell calibration curve with the diaphragm unlubricated.

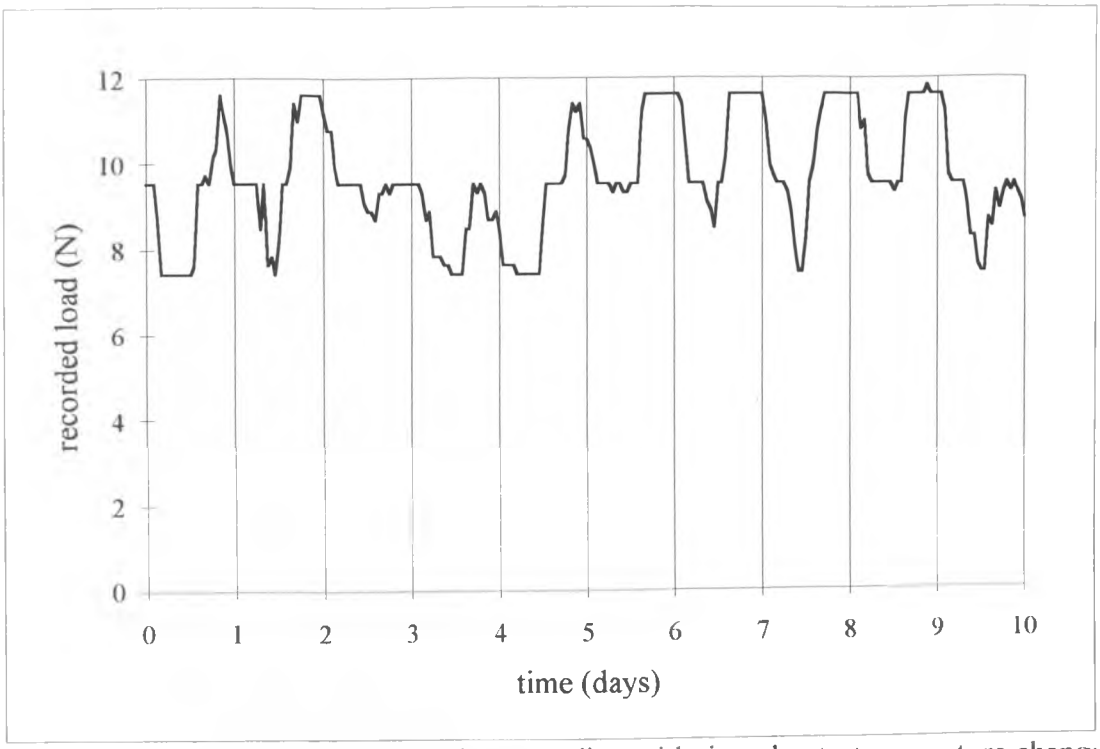

Figure 3.7a: Change in load transducer reading with time due to temperature change and electrical noise.

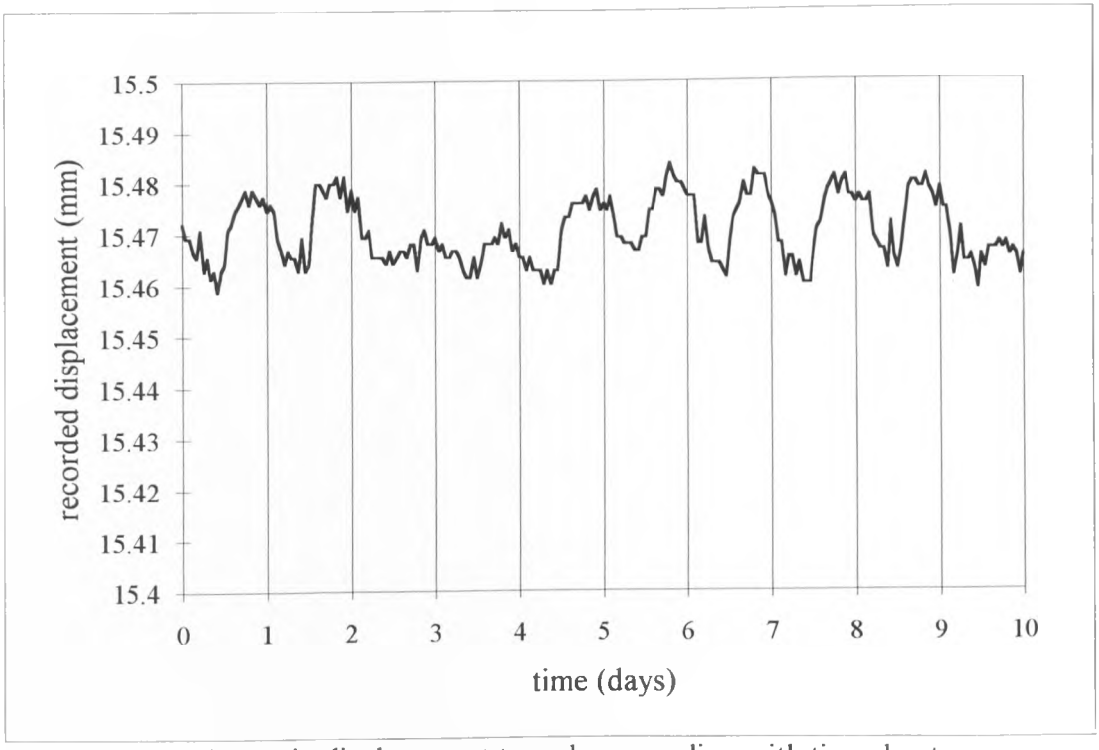

Figure 3.7b: Change in displacement transducer reading with time due to temperature change and electrical noise.

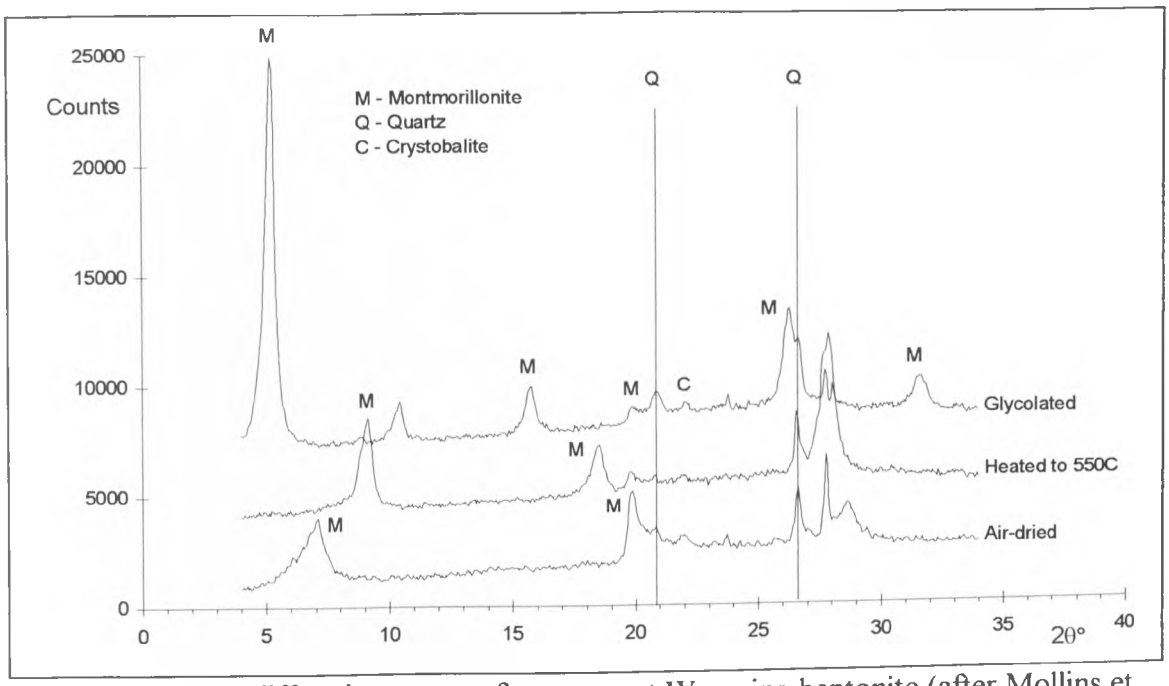

Figure 3.8: X-ray diffraction spectra for conquest Wyoming bentonite (after Mollins et al., in print).

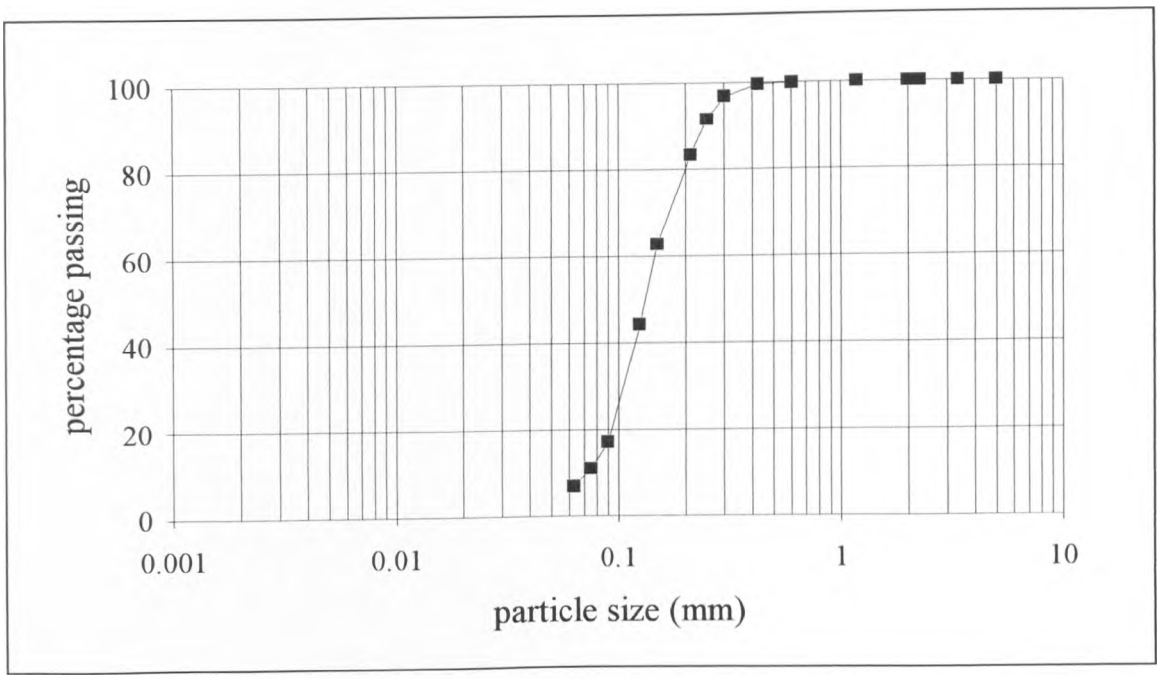

Note: Wet sieving method. B. S. 1377: Part 2: 1990.

Figure 3.9: Particle size distribution curve of Knapton Quarry sand.

CHAPTER 4
EXPERIMENTAL METHODS

4.1 Introduction

To investigate the mechanical behaviour of bentonite, sand, and bentonite-sand mixtures, three testing programmes were conducted:

1. Volume change tests (swelling, normal consolidation and rebound)[1]
2. Hydraulic conductivity tests
3. Strength tests

Mixtures of 5, 10 and 20% bentonite-sand (each constituent by dry weight) and 100% bentonite were used in all three programmes[2]. In addition, hydraulic conductivity and strength tests were conducted on the sand. Each mix was prepared immediately before placement into the test apparatus by using oven dry sand (passed through a 2mm sieve) and the bentonite in its as supplied state, as preliminary testing indicated that oven drying altered the swelling characteristics. The mix was then tested either as prepared, or dynamically compacted at optimum moisture content using the modified Proctor method. Distilled, de-aired water, and filter paper on either side of the sample (to prevent clogging of porous discs) were used throughout.

4.2 Volume change tests

A one-dimensional swelling test was developed to investigate the behaviour of bentonite powder and the bentonite-sand mixtures. The initial mass of the sample varied, because samples swelled by different amounts depending on the bentonite content and applied stress[3]. Dry samples were placed in a consolidometer ring (either 70mm or 100mm diameter), compacted by tamping and levelled. A vertical stress was applied by dead load and distilled water allowed to be drawn into the cell from a reservoir while the sample height was monitored until swelling ceased (typically 2-4 weeks). Tests were ended when the settlement dial gauge maintained a constant reading over a 24 hour period. The range of vertical effective stress was 1 to 450kPa. For stresses up to 10kPa weights were placed on the top cap: lever arm oedometers were used for higher stresses.

A multi-stage test was conducted on 100% bentonite to determine the effect of "swelling back" from a high to low stress. An initial vertical stress of 450kPa was applied and the sample allowed to swell to equilibrium. Once swelling had ceased, the vertical stress was

---

[1]Throughout the remainder of the text, swelling is used in reference to the volume increase of initially dry samples whilst consolidation and rebound refer to the volume change of samples which are initially saturated.

[2]The same batches of sand and clay were used throughout.

[3]For 100% bentonite @ 1kPa in a 70mm consolidometer ring, the initial mass was approximately 10g. For a 5% bentonite-sand mixture @ 450kPa in a 100mm consolidometer ring, the initial mass was 150g. The final sample heights for both these tests was approximately 10mm.

reduced and the sample allowed to swell to equilibrium under the new applied stress. This was repeated 4 times to a final stress of 2.7kPa.

Comparative tests were performed on dry 100% bentonite specimens using different initial compaction methods (static and vibratory) to determine what difference this would have on the swelling behaviour. Statically compacted samples were initially compressed to 1MPa on a hydraulic loading apparatus and then allowed to swell under vertical stresses of 240, 29.1 and 2.6kPa. Compaction by vibration was achieved by placing the assembled cell, sample and top cap on a vibrating table for 5 minutes, after which swell tests were conducted at vertical stresses of 240 and 29.6kPa. A low frequency of vibration ensured that bentonite powder did not escape from the consolidometer ring during compaction.

Standard consolidation tests on bentonite slurry (prepared at the liquid limit) and bentonite swollen from a dry state (under a vertical stress of 1.4kPa) were conducted for comparison. These two samples had approximately the same initial moisture content (~ 480%). The time required to complete a consolidation or rebound stage was typically 1-2 weeks.

4.3 Back pressure saturation

Rowe cell, triaxial permeameter and triaxial compression testing all incorporated back pressure application to saturate samples. Therefore, it is pertinent to describe briefly the process by which samples are saturated.

An elevated back pressure applies a sufficient back pressure of water on the pore fluid in the sample to cause the pore air to dissolve completely into the surrounding pore water. The time delays in achieving complete saturation depend on the hydraulic conductivity of the soil, and the time required for the bubbles of pore air to dissolve into the surrounding pore water after they have been compressed. Black and Lee (1973) applied consolidation theory to triaxial test specimens. They considered a 35mm x 70mm sample, initially 90% saturated, with a hydraulic conductivity of 1×10^{-10}m/s, and calculated that sufficient water can enter to produce complete saturation in less than 1 min. Their data showed times required for full saturation ranged from a minimum of 6 days to a maximum of over 40 days, indicating that diffusion of pore air into the pore water is the governing process. Lee and Black (1972) showed that the rate of diffusion of a particular sized bubble is independent of the applied pressure. However, for a given quantity of air, an increase in pressure will cause a decrease in volume of the bubble, and thus reduce the time necessary to dissolve it.

Hence, the time required for full saturation decreases with increasing back pressure. The standard recommended back pressure of 300kPa (e.g. Dunn, 1985) was applied in all tests, except for consolidated-drained triaxial tests on 5% bentonite-sand mixtures at effective cell pressures of 200kPa and 100kPa (see appendix 1).

4.4 Hydraulic conductivity tests

4.4.1 Introduction

Four methods of hydraulic conductivity measurement were used: Rowe cell, triaxial permeameter, compaction permeameter and hydraulic conductivity from consolidation data. This produced a large data set enabling comparison between test type and sample preparation technique. The Rowe cell and triaxial permeameter are believed to be the most accurate because vertical stresses (Rowe cell) and cell pressures (triaxial) are measured and can be controlled, full saturation is possible, and inflow and outflow are measurable (e.g. Daniel et al., 1985). Another advantage is that the sample can be allowed to swell to equilibrium before the hydraulic conductivity is measured[4].

4.4.2 Rowe cell tests

Bentonite specimens were compacted by tamping into the Rowe cell as dry powder, whereas mixtures (with one exception) were compacted into the cell at optimum moisture content. One mixture was prepared in the manner of the bentonite powder to investigate the influence of sample preparation technique. Initially dry samples were tested in a 75mm diameter cell. The initial mass was chosen to give a sample height of approximately 10mm after swelling (20 - 50g for a stress range of 25 to 200kPa). A 250mm diameter cell was necessary to produce dynamically compacted samples, the number of blows per layer was increased accordingly such that the compaction energy was commensurate with the modified Proctor method (see appendix 2). The initial mass of material varied between 2 and 3kg to produce specimen thicknesses in the range 20-30mm reducing swelling and/or saturation time.

All samples were confined by a vertical stress, vacuum de-aired for approximately 5 minutes, and allowed access to distilled water[5]. Back pressure saturation of 300kPa was used in all the tests. Dunn (1985) found vacuum application followed by 300kPa back pressure to be the optimum technique to achieve full saturation. Hydraulic conductivity was calculated from inflow and outflow measurements under constant head conditions (see chapter 5) once equilibrium was reached, indicated by constant volume conditions of

---

[4]In the compaction permeameter, for example, it is thought that at bentonite contents greater than 5%, swelling (which occurs at the onset of the falling head test) masks the flow data. This is due to incomplete saturation and the absence of a confining stress.

[5]This technique was performed at both sides of the sample.

the sample[6]. The time required to reach swelling equilibrium and/or full saturation was proportional to the hydraulic conductivity of the particular sample. For example, samples with hydraulic conductivities of approximately 10^{-12} m/s required between 1 and 2 months to reach equilibrium, however, sand ($k \sim 10^{-5}$m/s) was saturated within an hour.

Three independent pressure lines provided confining stress and inflow and outflow back pressures. This enabled hydraulic gradients to be applied either using a head or pressure difference between the inflow and outflow lines, or a combination of both. This was essential for feasible testing periods on low hydraulic conductivity samples. A hydraulic gradient caused by a pressure difference involved increasing the back pressure at the inflow end and decreasing the outflow back pressure by an equal amount. This decreases the stress at the inflow side and increases the stress at the outflow side, however, the average effective stress remains unchanged. The act of imposing a flow rate through and hence pore pressure gradient across the sample will tend to produce swelling at the inflow boundary and consolidation at the outflow boundary. Due to this a minimum vertical effective stress of 25kPa was chosen; the maximum vertical effective stress used in the tests was 200kPa. Little et al. (1992) state that the assumption of uniform hydraulic conductivity is reasonable, provided the void ratio does not vary significantly across the sample. They used pressure differences below 10-15% of the vertical effective stress to minimise this error. The same range was used in the hydraulic conductivity tests with the exception of the first Rowe cell test (described below).

The first Rowe cell test was quite sophisticated and was used to investigate the possibility of non-Darcian flow (chapter 2). Hydraulic conductivity was calculated at an initial hydraulic gradient of approximately 14. Hydraulic gradients were incrementally increased up to approximately 340[7] and hydraulic conductivity was always remeasured at the initial gradient before continuing to the next increment, to investigate particle migration effects. Darcy's law was found to be valid over this hydraulic gradient range (see chapters 5 and 6), therefore, hydraulic gradients for subsequent tests were chosen based on completing each in a reasonable time.

Large scatter in flow volume data was evident at a hydraulic gradient of 14 for the first Rowe cell test. Initially this was attributed to the small flow rate (approximately 1.5ml in

[6]No change in settlement dial gauge and inflow and outflow volume units over a 24hr period.
[7]For this test the sample height was approximately 30mm, therefore, a hydraulic gradient of 340 corresponds to a pressure difference of approximately 100kPa across the sample. This pressure difference is 50% of the vertical effective stress (200kPa). However, because the hydraulic conductivity of this sample was so low (10^{-12} m/s) it is likely that if any consolidation and swelling occurred over the test period, it would be restricted to the outer 1-2mm of the sample.

10days). However, similar scatter was observed at the following hydraulic gradient (approximately 45). The observed scatter was thought to be due to temperature changes causing thermal expansion and contraction, and the cell was insulated midway through the test. Figure 4.1 shows that after insulation the scatter is significantly reduced. Temperature was monitored and found to vary slightly (±2°) throughout the hydraulic conductivity stage which accounts for the slight deviations from the best fit lines in figure 4.1. All further hydraulic conductivity tests were thermally insulated, and temperature was monitored throughout by a thermocouple attached to the cell body. The thermocouple was connected to a Beckman Industrial temperature/voltage converter combined with digital voltmeter.

At swelling equilibrium, the salt concentration in the pore fluid is determined by the hydration of sodium cations. Measurement of hydraulic conductivity, involves gradual replacement of pore fluid, and therefore, possibly dilution in salt concentration. There are considerable data showing the effects of pore fluid concentration on the swelling behaviour and hydraulic conductivity of bentonite (e.g. Sridharan and Jayadeva, 1982, on swelling, Mesri and Olson, 1971, on hydraulic conductivity). To minimise these effects, all tests were ended when 20% of the sample pore volume had been replaced. The time required to measure hydraulic conductivity ranged from 5 mins. for sand ($k \sim 10^{-5}$ m/s) to 2 weeks on samples with $k \sim 10^{-12}$ m/s.

4.4.3 Triaxial permeameter tests

Preliminary tests on sand and 5% bentonite-sand mixtures in the Rowe cell showed large variation in the measured hydraulic conductivity (up to 5 orders of magnitude for mixtures). This was taken as indicating that 5% bentonite-sand mixes may possess non homogeneity when only a small thickness is used with the additional possibility of sidewall leakage. The scatter in hydraulic conductivity tests on sand was also attributed to sidewall leakage. Therefore, for these materials constant head hydraulic conductivity tests were conducted using a triaxial permeameter in addition to a Rowe cell.

Constant head tests on sand and 5% bentonite-sand mixes were conducted in a large triaxial permeameter (100mm sample diameter). For sand, the membrane was stretched over a mould and the sand tamped inside using a tamping rod. With the mould still surrounding the sample, a vacuum was applied to the volume change lines which provided the sample with strength, enabling removal of the mould and cell assembly. The cell pressure was applied and the valve to the vacuum closed, and water was allowed to be drawn into the sample from a header tank. A back pressure of 300kPa to the

inflow and outflow lines was used to achieve full saturation. Hydraulic conductivity was measured according to 4.4.2.

5% bentonite-sand samples were dynamically compacted into a Proctor mould at optimum moisture content, trimmed, extruded and set up in the triaxial cell. De-airing and sample saturation techniques, and hydraulic conductivity measurement were as described for Rowe cell tests. Saturation and test periods were in the range 3-8 days and 5mins to 1hr respectively.

A sample height of approximately 100mm was used for all tests.

4.4.4 Compaction permeameter tests

Due to long test periods, the data set was increased by conducting falling head tests in a compaction permeameter on 5% bentonite-sand mixtures. Samples with higher clay contents were excluded as it was thought excessive sample swelling would mask the flow data. The soil was dynamically compacted into the mould at optimum moisture content and de-aired in a vacuum dessicator. After 24hrs water was allowed to be drawn into the dessicator to saturate the sample. The falling head test was continued until a constant value of hydraulic conductivity was found.

4.4.5 Indirect measurement of hydraulic conductivity

Hydraulic conductivity values were calculated from consolidation test data (Terzaghi, 1943) utilising the logarithmic time method (Casagrande and Fadum, 1940) or square root time method (Taylor, 1942). Both methods are discussed in chapter 5. Tests were performed on 100% bentonite and 10 and 20% bentonite-sand mixtures. Samples were allowed to swell under various vertical stresses in the same manner as the swelling tests. The quantity of mix initially placed ensured a minimum height of 8mm at swelling equilibrium[8], when an additional stress was applied. Terzaghi's derivation is based on a small stress increment. However, it was found that this produced unmeasurable amounts of consolidation. A settlement large enough to produce a well defined laboratory curve required an applied stress increment up to four times greater than the initial stress.

Hydraulic conductivity is calculated by determining the coefficients of consolidation and volume compressibility, c_v and m_v, from consolidation data (see chapter 5). The

[8]The percentage settlement caused by consolidation was small, therefore, the error in measurement increases with decreasing sample height due to the resolution of the dial gauge (0.002mm) and the laboratory curves, become poorly defined. The height specification prior to consolidation was chosen as a compromise, so that the swelling and consolidation stages could be conducted in a reasonable time period.

coefficient of volume compressibility is inversely proportional to stiffness. An erroneous value of m_v would therefore result in differences between then calculated and actual hydraulic conductivities. This may occur when the sand content is high; such that particle interaction affects the accuracy of laboratory curves. In addition, if the voids between sand particles are not completely filled with swollen bentonite (at swelling equilibrium), settlement corresponds to compression of the sand matrix and not consolidation of the clay, which may further increase the error. Due to these reasons, 5% bentonite-sand mixtures were excluded from hydraulic conductivity measurement by this method[9].

Consolidation tests were ended when a distinct change in curvature from primary to secondary consolidation was observed on the settlement-time curve (for both methods). Test periods were typically 2-4 weeks to reach swelling equilibrium, and a further 1-2 weeks for the consolidation stage.

4.5 Strength tests

4.5.1 Introduction

Consolidated[10] drained triaxial compression tests were performed on sand and 5, 10 and 20% bentonite-sand mixtures, and drained shear box tests were used to determine the strength of bentonite. Drained tests were conducted so that strength could be measured in effective stress terms. It was also thought that full saturation may be difficult to achieve, therefore, for undrained testing, pore pressure measurement would be affected by compression of air within the sample. For each test the sample was allowed to reach swelling equilibrium indicated by a no volume change condition before shearing commenced. The chosen effective cell pressures or vertical effective stresses were 25, 50, 100 and 200kPa except for bentonite strength tests, where application of the lowest stress was beyond the limits of accuracy of the proving ring. At the end of the test programme, a further test to determine the strength of a 10% bentonite mix was desired. Due to time restrictions, a consolidated-undrained triaxial compression test with pore water pressure measurement was performed; this test can be conducted much faster than a drained test.

Triaxial samples were deformed to failure by applying a constant rate of strain in standard triaxial cells and constant rate of stress in a Bishop-Wesley cell. A limitation of

---

[9]The effect of stiffness may affect 10% bentonite mixes. This is discussed in chapter 5.

[10]This does not mean consolidation in the conventional sense, it is in reference to the standard test. All samples were prepared in a relatively dry state and swollen to equilibrium under the applied stress. Therefore, the stress path for samples was in the same direction as a conventional rebound line. This is discussed in chapter 6.

drained constant rate of stress testing is collapse of the sample at failure[11] with no relief of deviator stress. For samples of low hydraulic conductivity, excess pore water pressures cannot fully dissipate at the increased rate of straining, and the test may become partially undrained. Due to lengthy test periods (up to 10 weeks) it was necessary to use all available equipment. Therefore, to minimise the effects of unwanted pore pressures, 5% bentonite-sand mixtures[12] only were tested in the Bishop-Wesley cell.

4.5.2 Triaxial sample preparation

Due to the low hydraulic conductivity of the bentonite-sand mixtures, 38mm diameter x 76mm height samples were tested[13]. Compaction was performed into a Proctor mould, using the modified Proctor method, and 38mm cores taken. The ends of the sample were trimmed flush until a length of approximately 76mm was achieved. Whatman filter paper drains were attached to the periphery to promote saturation, and also decrease the testing time. Samples were placed in a large Wykeham Farrance triaxial cell which was modified to enable simultaneous saturation of 4 samples as shown in figure 4.2. This was necessary because of an anticipated long saturation period. A constant back pressure of 300kPa was applied together with the required cell pressure. In the saturation cell, each sample could be individually isolated, removal of one, therefore, should not alter the effective stress on the other three.

4.5.3 Saturation of test samples and B-values

Samples remained in the saturation cell (up to 4 months), until it was considered that the maximum possible saturation was achieved[14]. Saturation was verified by determining the B-value of the sample. This is the standard method of investigating if a test specimen and associated pore pressure measuring equipment are completely saturated prior to shear. The pore pressure increase, Δu, caused by an increase in cell pressure, $\Delta\sigma_3$, is measured (where $B = \Delta u/\Delta\sigma_3$). For samples having a compressibility greater than 10^{-4} m^2/kN the system is completely saturated if $B = 1$ (Black and Lee, 1973). At compressibilities less than this, B-values are significantly below 1.0 at full saturation and drop off rapidly with decreasing saturation (see appendix 3).

---

[11]For strain softening soils, the strain rate increases rapidly as failure is approached.

[12]5% bentonite mixes had hydraulic conductivities up to 4 orders of magnitude higher than other mixtures (see chapter 5).

[13]Head (1986) recommends the minimum dimension should be 10 times larger than the maximum particle size. Over 99% of the sand passed a 2mm sieve, and over 98% passed a 1.18mm sieve, therefore, particles larger than 2mm were removed to keep the sizes within the recommended limits.

[14]For an initial degree of saturation of 90%, Black and Lee (1973) show an increase in final degree of saturation from 99% to 99.5% for an order of magnitude increase on a logarithmic time scale (1 day to 1 week). Since saturation changes with the logarithm of time, a compromise was necessary such that all tests could be performed at the best achievable degree of saturation in the available time.

For stiff soils it is theoretically impossible to obtain B = 1.0 even at 100% saturation, because the pore pressure response is strongly dependent on the soil stiffness. At 99% saturation medium to soft soils have B values from 0.93-0.99. The corresponding values for a stiff or very stiff soil may be less than 0.5 (Black and Lee, 1973). A large range of stiffnesses was anticipated for the test samples and therefore conditions of full saturation were determined as described by Wissa (1969), and Black and Lee (1973). Several increments of cell pressure were applied without allowing sample drainage and the corresponding increase in pore water pressure was observed. The same pore pressure response for each increment of cell pressure or a slight decrease indicates full saturation. If the system is not saturated, the pore pressure response increases with each additional increment of cell pressure.

4.5.4 Rates of strain and stress used in the strength tests

Owing to the low hydraulic conductivity, drained tests were carried out slowly for the condition of negligible pore pressure to be satisfied. Using the theory of consolidation Gibson and Henkel (1953) and Bishop and Gibson (1963) found that the average degree of consolidation at failure, U_f, may be expressed in the form

$$U_f = 1 - \frac{h^2}{\eta c_v t_f} \qquad 4.1$$

where $2h$ = height of sample

c_v = coefficient of consolidation

t_f = time to failure

η = a factor depending upon drainage conditions at the sample boundaries = 40.4 for drainage from both ends and radial boundary.

A comparison between theory and results of drained tests shows that a theoretical degree of dissipation of 95% is sufficient to ensure a negligible error in the measured strength. Bishop and Henkel (1962) propose that in drained tests 95% pore pressure dissipation will occur if

$$t_f = \frac{20h^2}{\eta c_v} \qquad 4.2$$

Since the three dimensional coefficients of consolidation of the samples were unknown and limited results were available at the time, c_v was calculated from Rowe cell data on a 20% bentonite-sand mix using the relationship

$$k = c_v m_v \gamma_w \qquad 4.3$$

The hydraulic conductivity, k, was calculated at 200kPa vertical effective stress, and the coefficient of volume compressibility, m_v, for a stress increment of 200-100kPa, hence

c_v, which gave the required time to failure as 76 days. To choose a suitable rate of deformation the failure strain must be approximately known. It was thought the 20% bentonite-sand mix would behave essentially as a remoulded normally consolidated clay. Bishop and Henkel (1962) suggest failure at 20% axial strain with clays of this type. Thus, for 38mm diameter samples a strain rate of 1.5×10^{-4} mm/min. was used (the back calculated theoretical pore pressure dissipations are given in appendix 4).

Undrained testing must be slow enough such that pore pressure equalisation is allowed, i.e. the measured pore pressure is commensurate with the entire sample. The required strain rate for the consolidated undrained test on a 10% bentonite mix was determined using data from Bishop and Henkel (1962). They present values of required time to failure for 95% equalisation of pore pressure within a sample, which increases with decreasing coefficient of consolidation. A time to failure was conservatively chosen based on the calculated one-dimensional coefficient of consolidation for a 10% bentonite mix. The test was conducted at a strain rate of 0.001mm/min, which was calculated assuming failure at 20% axial strain.

Rates of stress to be used for 5% bentonite-sand mixtures were determined as follows. Preliminary tests were conducted on sand[15] in the Bishop-Wesley cell to establish the variation in rate of straining at a given constant rate of stress. The sample was compressed to failure by transmitting pulses to the loading ram stepper motor controller via a computer link (one pulse is equivalent to a deviator stress increment of 0.25kPa). As the material was strain softening, the stiffness decreased as the test proceeded with a corresponding increase in rate of strain. The rate of straining (for a constant frequency of pulses) was calculated for three compressive stages; 0-1.25mm, 1.25-3mm and from 3mm to failure. The pulse rate (rate of stress) was altered accordingly to produce an approximate constant strain rate throughout deformation. For rates of strain comparable to standard triaxial tests on other mixtures, pulse rates were input into Labtech Notebook (see chapter 3) corresponding to deviator stress increments of 0.67kPa/min., 0.067kPa/min. and 0.02kPa/min. for the three compressive stages[16]. This was done to minimise excess pore water pressure development (see 4.5.1).

4.5.5 Consolidated drained (CD) triaxial test

Consolidated drained triaxial tests were performed in accordance with B.S. 1377: Part 2: 1990 (Methods of test for soils for civil engineering purposes) with the exception of the

[15]Comparative tests were conducted on sand because it was thought 5% mixtures would exhibit behaviour characteristic of dense sand during shear.

[16]The software permitted the use of three pulse rates only. Variations in strain rate were found to be most pronounced at the end of each stated compression range, and reasonably linear over this range.

system saturation process. Sand samples were set up as described for the triaxial permeameter test (see 4.4.3). Bentonite-sand samples were transferred from the sample saturation cell to the triaxial cell, and the membrane and top cap assembled. After release of the vacuum, water was allowed to be drawn into the sample from the back pressure air/water cylinder via the volume change unit. The back pressure and cell pressure were incrementally increased to the required effective stress. Volume change was monitored until equilibrium, and a B-value determined. Standard drained tests were conducted until either peak strength or 20% axial strain was reached. The range of test durations was 7.5 days (5% bentonite mix @ 25kPa cell pressure) to 75 days (20% bentonite mix @ 50kPa cell pressure). All sand samples were tested in approximately 1hr at a strain rate of 0.3mm/min. Top and bottom drainage was provided at all times.

4.5.6 Consolidated undrained (CU) triaxial test

For the consolidated undrained test the sample was set up as described above. The volume change was monitored and when equilibrium was reached the drainage lines were closed. The sample was then compressed over a 10 day period to 20% axial strain at 0.001mm/min.

4.5.7 Measurement of stiffness of triaxial samples

When measuring stiffness of triaxial samples, it is necessary to consider the overall deflection in a triaxial test. This is given by Jardine et al. (1984) as

$$\Delta = \Delta_L + \Delta_T + \Delta_{BT} + \Delta_S + \Delta_{BB} + \Delta_{ram} \qquad 4.4$$

where Δ_L = load cell deflection
Δ_T = top cap sample reorientation
Δ_{BT} = top bedding
Δ_S = sample compression
Δ_{BB} = base bedding
Δ_{ram} = loading system deflection

Both triaxial systems had submersible low compliance load cells such that the load cell deflection can be considered negligible as can the loading system deflection. However, bedding of the end platens and tilting of the sample can lead to an underestimation of soil stiffness. These end effects can be minimised by conducting an unload-reload loop[17], after which the calculated stiffness is more representative of the sample as a whole. For 5, 10 and 20% bentonite-sand mixtures unload-reload loops were conducted shortly after the start of the test. Each sample was compressed to 1% axial strain at which point the direction of loading was reversed until a value of zero load was approached. The loading

[17]This is similar to anisotropic consolidation, which has been found to significantly reduce end effects (e.g., Jardine et al., 1984).

direction was again reversed and the sample was compressed to failure or 20% axial strain.

4.5.8 Consolidated drained shear box test

Due to time restrictions, one multi-stage consolidated drained shear box test was conducted to determine the effective stress characteristics of bentonite. Dry bentonite powder was tamped into a 60 x 60 x 40mm shear box packed out with porous stones at the top and bottom for drainage. The amount of bentonite placed was enough for an initial height of approximately 20mm (to reduce saturation time). A vertical stress of 200kPa was applied and water allowed to be drawn in until equilibrium was achieved (as in the swell tests). The sample was sheared at 0.00064mm/min.[18] until failure was reached. After shearing, the top half of the box was returned quickly to its original position, pore pressures were allowed to equalise, and the sample was swelled back to 100kPa. At swelling equilibrium, the sample was again sheared to failure. The procedure was repeated to determine the strength at a vertical effective stress of 50kPa. Shear force, change in height and horizontal displacement were monitored throughout the test (using a calibrated proving ring and dial gauges).

Approximately 10 weeks were required for the sample to reach swelling equilibrium at the initial vertical effective stress of 200kPa. This is due to an initial dry sample thickness of approximately 20mm, because the time for consolidation, and presumably swelling, is proportional to the square of the maximum drainage path (Terzaghi and Peck, 1948). With the exception of this swelling and saturation period, swelling and shearing stages were in the range 2.5 to 3.5 weeks, and 3.5 to 7 days respectively.

4.5.9 Possible errors in triaxial testing and corrections to test results

In addition to the restriction that two out of the three principal stresses must be equal, the results obtained from triaxial tests are affected by the end loading plates, their smoothness and size, by the flexible membrane surrounding the specimen, by the filter paper used and by the measuring system. This section discusses possible errors and corrections that were applied to triaxial test results.

Non uniformities of stress distribution within the sample are primarily due to friction on the end plates. Rowe (1962) found that even slight end friction prevents dilation at the ends of a granular sample during triaxial shear. However, dilation (with a resulting decrease in strength) occurs at the centre of the sample after which the load carried by

[18]The strain rate was calculated in a similar manner as for triaxial tests using consolidation data (Bowles, 1986).

the assembly is insufficient to start end dilation. Shockley and Ahlvin (1960) found that in tests on dry sand there was a volume increase in the middle third (or failure zone) of specimens and that a volume decrease occurs at the ends of the test specimens. For clays, based on moisture content changes, they found a volume decrease in the zone of shear and a volume increase at the ends of the specimens. All strength testing was conducted on samples with a length to diameter ratio approximately equal to 2 to minimise the effects of non-uniform stress distribution. Taylor (1948) showed that reliable results were obtained between normal platens, provided the length to diameter ratio was in the range 1.5-3.0. Barden and McDermott (1965) found that barrelling was minimised by using lubricated platens but the effective strength parameters were unaltered when the results were compared to specimens with a length to diameter ratio of 2 tested between ordinary platens.

Filter paper drains allowed radial drainage of triaxial samples during swelling and shear testing. This may cause local consolidation which gives rise to increased stiffness near the boundary, resulting in non-uniform stresses, strengths and water contents across the diameter of the sample. Atkinson et al. (1985) found that variation in water content across samples of kaolin increased with loading rate and concluded that non-uniformities in water content occur in samples with radial drainage when subjected to undrained loading followed by consolidation or when subjected to rapid drained loading. As these conditions were not imposed, the use of filter paper drains was considered satisfactory.

Poulos (1964) investigated the leakage problem associated with triaxial tests. He found the hydraulic conductivity of natural rubber membranes to water to be about 4.8×10^{-18} m/s, and leakage at the O-ring seals is about 10^{-4} ml/day and independent of the effective confining stress. For the worst pressure-time combination in the test programme (i.e., an effective confining stress of 200kPa and a 36 day test period) the total leakage amounts to about 0.02ml for a 0.2mm thick membrane. This value is less than the accuracy of volume change measurement ($\pm$0.05ml) and is therefore considered insignificant.

Filter paper drains and the rubber membrane, which both surround the sample, act to increase the strength of the soil, so it was necessary to apply the strength corrections detailed by Bishop and Henkel (1962) for 38mm diameter samples. At axial strains greater than 2%, a total correction of 14kPa was applied to the compressive strength to allow for both rubber membrane and drains. Corrections from 0-2% strain were interpolated, assuming no correction at the start of the test and a correction of 14kPa at 2% strain.

The error associated with measuring pore pressure was minimised by rigidly connecting the pressure transducer directly to the drainage lines in the base of the triaxial cell, without the use of flexible tubing. Thus the lines can be considered incompressible and the volume of water was kept to a minimum. The use of a small triaxial sample also minimises pore pressure errors (Wissa, 1969). Care was taken in fully de-airing drainage lines because small air bubbles contribute to a reduction in the overall stiffness of the system and can lead to errors in the measured pore pressures (Lee and Black, 1972). Therefore, any error associated with pore water pressure measurement was ignored.

4.6 Other tests

The wet sieving method was used to determine the particle size distribution of Knapton Quarry sand, the specific gravity was determined by the gas jar method. The small pycnometer method was employed for determination of specific gravity of Wyoming bentonite and the liquid limit was determined by the cone penetrometer method. Modified Proctor compaction tests were conducted on the mixtures to determine the optimum moisture content, and similar tests were conducted on sand by use of a vibrating hammer. All tests were conducted in accordance with B.S. 1377: Part 2: 1990 (Methods of test for soils for civil engineering purposes).

4.7 Test programme and numbering system

TEST TYPE	0-6 MONTHS	6-12 MONTHS	12-18 MONTHS	18-24 MONTHS	24-30 MONTHS	30-36 MONTHS
Compaction, index tests, particle size distribution, specific gravity etc.						
Swell tests on dry bentonite powder.						
Normal consolidation of bentonite.						
Swell tests on dry bentonite-sand mixtures.						
Rowe cell tests for hydraulic conductivity of bentonite and bentonite-sand mixtures.						
Swelling and consolidation tests on bentonite-sand mixtures to determine hydraulic conductivity.						
Compaction permeameter tests for hydraulic conductivity of 5% bentonite-sand mixtures.						
Triaxial permeameter tests for hydraulic conductivity of sand and 5% bentonite-sand mixtures.						
Strength of sand (consolidated-drained triaxial tests).						
Strength of bentonite-sand mixtures (consolidated-drained and consolidated-undrained triaxial tests).						
Strength of bentonite (consolidated-drained direct shear tests).						

Table 4.1. Test programme.

Table 4.1 lists the test types performed in the test programme, the shaded areas represent the time periods over which tests were conducted. Hydraulic conductivity and strength of samples were thought to be dependent on the clay content. Therefore it was necessary to characterise the swelling behaviour of 100% bentonite and bentonite-sand mixtures before the remainder of the test programme could logically proceed. Preliminary tests and swelling behaviour indicated a change in material properties as the bentonite content increased. At bentonite contents greater than 20%, swelling of the clay within the mixture was similar to 100% bentonite (see chapters 5 & 6). In addition, a designed barrier usually has a clay content less than 20% (e.g., Chapuis, 1990) and therefore a maximum clay content of 20% was selected for the test programme. It was thought that the behaviour of three mixtures only could be sufficiently investigated in the available time. Therefore, 10% and 5% bentonite-sand mixtures were chosen to investigate intermediate behaviour.

An applied effective stress range of 25-200kPa was chosen for hydraulic conductivity and strength tests, with one exception[19]. The maximum stress of 200kPa was chosen because changes in the swelling behaviour for all mixtures occurred below this value (see chapters 5 & 6). Additionally, the maximum available stress was limited by the airline and the application of back pressure. An applied stress less than 25kPa was considered to be outside the accuracy of the measurement systems.

For hydraulic conductivity and strength testing, the majority of the test equipment had to be set up in the laboratory. Hydraulic conductivity test apparatus was set up first because preliminary hydraulic conductivity data was required before strength testing could proceed. This allowed time for manufacture of data acquisition units, and for calibration and control of triaxial test systems. When sufficient data from swelling and hydraulic conductivity tests was acquired, strength tests were then conducted. Therefore, although the programme follows in a logical manner it was dictated to some extent by the manufacture and availability of equipment.

Swell tests are identified according to bentonite content, test number and vertical stress. The first number gives the bentonite content (100, 20, 10 or 5). This is followed by a letter from A to S which represents the 19 individual samples tested (for 100% bentonite samples, for example). Finally, vertical stresses are numbered in chronological order from 1 to 11 in bands of decreasing stress from approximately 450kPa to approximately 1kPa respectively. For example, tests 100B3 and 100C3 are swell tests on two different

[19]A consolidated-undrained triaxial test on a 10% bentonite-sand sample was conducted at 15kPa effective cell pressure.

100% bentonite samples both at a vertical effective stress of 240kPa, tests 100A1 and 100A8 are swell tests on the same 100% bentonite specimen at vertical effective stresses of 453kPa and 21kPa respectively[20]. Samples which were consolidated at swelling equilibrium to determine the hydraulic conductivity are preceded by the letter C (e.g., C20C3).

Rowe cell and triaxial cell hydraulic conductivity tests are labelled according to chronological order of test sample (B to Q for 16 different samples), stage (referring to a reduction in effective stress or increase in hydraulic gradient for a particular sample), and an indication of how many times the particular hydraulic gradient had been applied. For example, B3D is a stage of the first test on a 20% bentonite-sand mixture, at the third hydraulic gradient increment (increasing in magnitude from 1st to 5th), which has been applied to the sample on three previous occasions. Two compaction permeameter falling head tests were conducted and these are denoted by FH1 and FH2.

The identification of triaxial compression tests consists of the type of drainage conditions (CD or CU), the sample type, where S, 20, 10 and 5 denote sand, and 20, 10 and 5% bentonite-sand mixtures respectively, and the test number. The ninth consolidated-drained test on sand would therefore be labelled as CDS9.

4.8 General discussion on sample preparation and end of test parameters

The batch of clay was regularly checked to detect any changes in moisture content. Over the course of the test programme the moisture content was found to vary between 13.5% and 14.6%. However, the moisture content was determined prior to mixing and the mix proportions were measured by dry weight to account for any variation. Since the sand was oven dried prior to mixing, any effects of moisture content variation were eliminated.

Initially dry samples were mixed either in a beaker (using a spatula) or Hobart mechanical mixer depending on the volume of material required for the test. Mixing was continued until the sample was considered to be homogeneous by observation. Moisture contents were determined prior to testing by oven drying over a 24hr period at 105°C[21].

---

[20]In chapter 5, some tests in the swelling results section are labelled differently to described in this section. These are the swelling stage test results from hydraulic conductivity tests.

[21]All moisture contents were determined in this manner.

Compacted samples were initially mixed dry in a Hobart mechanical mixer for approximately 5 mins.[22], after which the extra water required to achieve optimum moisture content was gradually poured whilst the sample was still mixing. Mixing continued for a further 5 mins. until the soil was considered to be homogeneous by observation. Samples for moisture content determination were taken before and after compaction to investigate drying of the mixture during sample preparation. The maximum variation in moisture content was found to be no more than 0.2%, therefore the average value was taken.

At the end of testing, moisture contents were determined for all samples and the degree of saturation calculated. For volume change and hydraulic conductivity tests, moisture contents were generally found to be higher at sample drainage boundaries (typically a factor of 1.04 larger than the overall moisture content), this is consistent with a small amount of water being drawn into the sample on unloading. Triaxial specimens generally had moisture contents higher at the centre than at vertical drainage boundaries (typically 4%), this is attributed to dilation at the centre of the sample as described in 4.5.9.

The degree of saturation, S_r, is given by

$$S_r e = wG_S \qquad 4.5$$

where e is the sample void ratio, w the moisture content and G_S the specific gravity. Values of S_r calculated from overall moisture content for swelling tests are as follows[23]

100% bentonite: all samples $S_r > 0.95$, 93% of samples $S_r > 0.99$.
20% bentonite: all samples $S_r > 0.97$, 88% of samples $S_r > 0.99$.
10% bentonite: all samples $S_r > 0.97$, 88% of samples $S_r > 0.99$.
5% bentonite: all samples $S_r > 0.90$, 46% of samples $S_r > 0.95$.

Rowe cell specimens all had final degrees of saturation greater than 0.96. Degrees of saturation greater than 0.99, 0.98 and 0.95 were calculated for 20, 10 and 5% bentonite-sand triaxial specimens respectively.

The uniformity of triaxial samples (indicated by moisture content variation) was not verified prior to shear testing because the sample would have to be destroyed after the long saturation period. However, results of swelling tests had shown that moisture content variation throughout the sample was relatively small, which implies even distribution of bentonite throughout samples. Since sample preparation, cell assembly

[22]This was the time required such that no bentonite powder was visible in the mixture, i.e., the mix looked as uniform as is detectable by eye.
[23]$S_r = 1.0$ indicates full saturation

and test procedure were all conducted in the same manner (for a particular type of test), it is not unreasonable to assume that triaxial test specimens were also uniform[24].

4.9 Summary

The procedures have been outlined for swelling, hydraulic conductivity and strength testing, with detailed description of non-standard methods. It is usual practice in soils testing to consolidate to the required effective stress from an initially saturated sample. Therefore, modification to standard test methods was generally to account for samples being initially in a relatively dry state, from which saturation and swelling under the required effective stress was allowed until equilibrium conditions were reached. Saturation, rates of stress and strain, measurement of stiffness and possible errors and applied corrections for triaxial compression tests have been considered at length. Finally, the test programme, sample preparation and final sample parameters have been outlined. Results are presented in chapter 5.

[24]This does not apply to 5% mixtures because pore volumes containing 'free' water may mask moisture content data (see chapter 5).

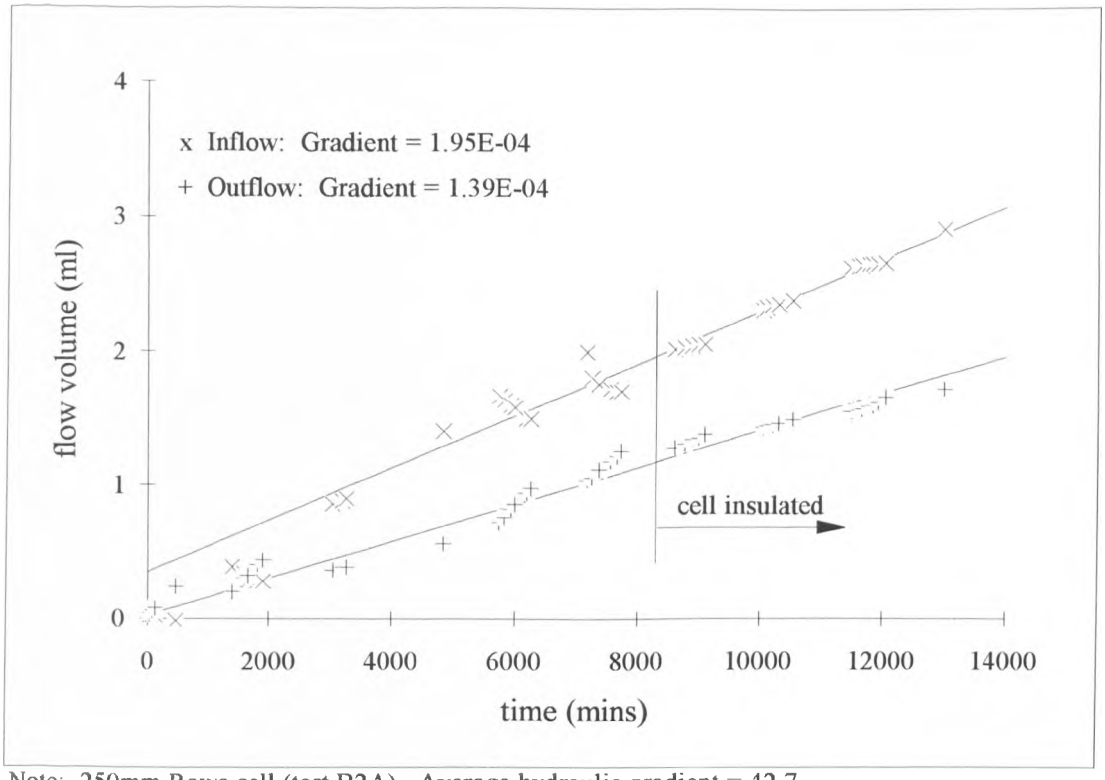

Note: 250mm Rowe cell (test B2A). Average hydraulic gradient = 42.7.

Figure 4.1: Inflow and outflow volumes against time for a 20% bentonite mixture at 200kPa vertical effective stress.

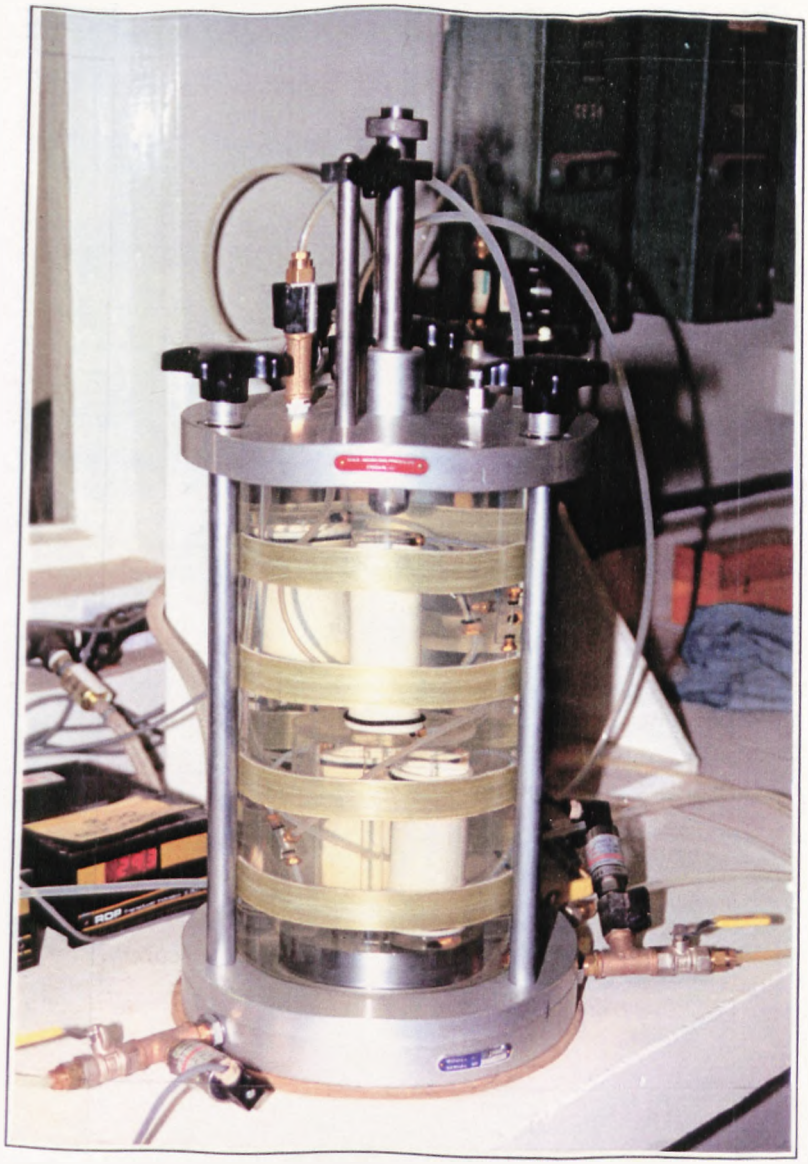

Figure 4.2: Large triaxial cell modified for saturation of multiple triaxial samples

CHAPTER 5
RESULTS AND DISCUSSION

5.1 Introduction

This chapter presents compaction, volume change (swelling, normal consolidation and rebound), hydraulic conductivity and strength data on bentonite-sand mixtures. The hydraulic conductivity and strength of sand and bentonite individually are also presented. General discussion on basic trends and scatter and some data analysis is included. The main discussion of results is given in chapter 6.

A sample referred to as initially dry consists of clay at a moisture content of approximately 14% (i.e., as supplied), plus oven dried sand. A wet sample has moisture added prior to any experimental technique. Wet samples are generally used for compaction, where the sample is mixed at optimum moisture content.

5.2 Compaction

Figure 5.1 shows the dry densities (ρ_d) achieved by modified Proctor compaction at different moisture contents (w) for various bentonite-sand mixtures. The shape and position of the compaction curves are typical of soils containing varying quantities of clay (e.g., Seed and Chan, 1959, Dixon et al., 1985). Therefore, no discussion is necessary. Table 5.1 summarises the results of all compaction tests. To investigate any possible changes in compaction properties with time, one 20% bentonite-sand mixture was cured[1] for 24hr prior to testing as indicated in the table. In addition, the first compaction stage of two tests was repeated at the end of the test period such that any moisture variations could be detected. These tests are indicated in figure 5.1

% Bentonite	0	5+	5	5	10	15	20	20	20+	20 24hr	25
w_{opt} (%)	11.3	11.5	11.3	12.4	11.3	11.3	11.2	11.7	11.3	11.7	11.8
ρ_{dmax} (Mg/m^3)	1.84	1.91	1.83	1.85	1.93	1.96	1.99	1.99	1.99	1.98	1.97
ρ_{max} (Mg/m^3)	2.05	2.20	2.07	2.29	2.18	2.21	2.23	2.33	2.25	2.32	2.32
e at ρ_{max}	0.45	0.40	0.46	0.44	0.39	0.37	0.35	0.35	0.35	0.36	0.37
% air voids	10.2	6.5	10.8	7.8	6.2	4.7	3.7	2.7	3.5	3.2	3.5

+ Note: the compaction curve of the indicated sample is shown in figure 5.1.

Table 5.1. Compaction Results.

[1]The sample was mixed at an initial moisture content of approximately 8% and left in a sealed container for 24hr prior to compaction. This is the standard recommended technique. However, it was more convenient to prepare samples immediately for other tests. Therefore, it was necessary to confirm that immediate preparation had no effect on the achievable density.

Table 5.1 shows that for all mixtures the optimum moisture content is between 11 and 12% (with the exception of one 5% mixture) and that the achievable dry density increases with increasing bentonite content (up to 20%). The results suggest that the sand pores are gradually filled with increasingly dense bentonite as the clay content increases, and up to 25% bentonite content the increasing clay dry density must outweigh the decreasing sand dry density.

For 5% bentonite mixes, there is a relatively large variation in void ratio at approximately the same moisture content (0.40 to 0.46). However, four tests performed on 20% bentonite mixes all had the same maximum achievable dry densities (hence void ratios). This difference in behaviour may be explained by the clay being unevenly distributed within the voids at low bentonite contents, resulting in variable compaction characteristics. As the bentonite content increases, the soil mixture becomes more homogeneous and the scatter reduces because local variations in bentonite content become less significant.

The repeat stages (shown in figure 5.1) have similar dry densities to the initial values, and the cured sample behaved in essentially the same way as a sample tested immediately. It appears, therefore, that there are no significant changes in the compaction characteristics of bentonite-sand mixtures over a 24hr period

5.3 Swelling, normal consolidation and rebound

5.3.1 Calculation of test parameters

To aid interpretation of the data of volume change, hydraulic conductivity and strength tests, it is useful to separate the two soil phases of a mixture to determine which is more significant in contributing to the overall characteristics. A way of modifying conventional soil parameters was achieved by use of a phase diagram. Figure 5.2 is a representation of the three phases of a fully saturated bentonite-sand mixture where

V_V = volume of water (voids)

V_C = volume of clay

V_S = volume of sand

The conventional void ratio is given as

$$e = \frac{V_v}{V_{solids}} \qquad 5.1$$

where $V_{solids} = V_C + V_S$, as shown on the left hand side of the figure. Using a similar approach to Chapuis (1990) and Wu and Khera (1990) the mixtures will be conceptualised as a two phase sand-bentonite gel system (see 2.3.10), and for

interpretation of swelling and hydraulic conductivity data will be described in terms of the clay void ratio, e_c:

$$e_c = \frac{V_v}{V_c} \qquad 5.2$$

This is shown on the right hand side of the figure. This parameter assumes that the water is associated solely with the bentonite. For 100% bentonite, e_c is the same as the conventional void ratio of the sample.

Considering the phase diagram, the clay void ratio can be calculated if the overall void ratio is known. This is given by the relationship:

$$e_c = \frac{e}{x} \qquad 5.3$$

Similarly, the void ratio of the sand (or sand void ratio), e_s, is given by

$$e_s = \frac{e + x}{(1 - x)} \qquad 5.4$$

where x is the volumetric fraction of dry solids occupied by the bentonite in a mixture[2]. The sand void ratio is useful for interpreting swelling data, and is essential to understanding the strength and dilatancy behaviour of bentonite-sand mixtures, and will be discussed further in chapter 6.

The proportion of the total volume occupied by the bentonite gel can be represented by the sand porosity, n_s:

$$n_s = \frac{(V_v + V_c)}{V_T} = \frac{e + x}{(1 + e)} \qquad 5.5$$

where $V_T = V_W + V_C + V_S$ is the total volume. The sand porosity is important when considering the hydraulic conductivity of bentonite-sand mixtures.

Many previous authors have recognised the importance of the clay-water phase (see 2.3.10), and have derived similar parameters to those given by equations 5.1-5.5. Kenney (1977) defines a volume ratio r_{VC}, identical to n_S in equation 5.5, and related this parameter to strength. Lupini et al. (1981) utilised the void ratio of the granular phase of the soil, e_g (equal to $(V_C+V_V)/V_S$), to discuss changes in residual shearing mechanisms. This parameter is the same as the sand void ratio given by equation 5.4. The clay specific volume, v_c, used by Graham et al. (1986) is given by $v_c = 1 + e_c$.

---

[2]Samples were produced by mixing dry weights of bentonite and sand. Therefore, an error in the value of x occurs, when weights are used, due to the different specific gravities of the bentonite and sand. The errors are 0.5, 0.3 and 0.2% for 20, 10 and 5% bentonite contents respectively (i.e., a 20% bentonite sand mixture by dry weight contains 19.5% bentonite and 80.5% sand by dry volume).

The void ratio, specific gravity[3], G_S, and dry density, ρ_d are related by the following equation:

$$1 + e = \frac{G_s \rho_w}{\rho_d} \qquad 5.6$$

where ρ_W is the density of water. In the swelling test programme, the initial void ratio, e_i, was calculated using equation 5.6. In a one-dimensional swelling test, the one-dimensional vertical strain is identical to the volumetric strain because the consolidometer ring prevents any lateral straining of the sample. Hence

$$\frac{\Delta h}{h_i} = \frac{\Delta v}{v_i} \qquad 5.7$$

where h_i and v_i are the initial sample height and specific volume respectively. Alternatively, equation 5.7 can be written as

$$\frac{\Delta h}{h_i} = \frac{\Delta e}{1 + e_i} \qquad 5.8$$

This relationship was used to calculate the void ratio throughout swelling and at equilibrium conditions, giving the final void ratio from pre-test conditions. In addition, the final void ratio was calculated from post test parameters (using equation 5.6), which enabled comparison of void ratios calculated from pre- and post test parameters (designated as methods 1 and 2 in the tables of results). The final clay void ratio from pre- and post test parameters was determined using equation 5.3 and the average of the two values taken as the final clay void ratio when swelling ceased. For all swelling tests, the difference between the two values was on average 1.2% and in all cases less than 4.2% (of the mean value).

5.3.2 Swelling: dry bentonite powder

Table 5.2 summarises the results of swelling tests on dry bentonite powder. Tests preceded by a letter C are swelling stages of consolidation tests to determine hydraulic conductivity. Two values for final clay void ratio are reported, corresponding to the methods described in 5.3.1. The percentage mean error was calculated from the average clay void ratio and the value calculated from post test parameters (method 2). A negative value indicates a sample height after unloading which is greater than the height measured at swelling equilibrium using equation 5.8. It can be seen that the differences are small and tend to increase with applied stress. This is attributed to a small amount of pore fluid being drawn into the specimens upon unloading. As the osmotic gradient is greater on removal of a higher stress, this causes a larger intake of water. However, the mean errors are small and are considered to have no significant effect on the measured behaviour.

[3]Overall specific gravities were calculated on relative percentages of each constituent.

The data show a large change in void ratio from approximately 1.3 to 13.5 for a corresponding vertical effective stress range of 453kPa to 1.4kPa. This demonstrates the high affinity for water which bentonite possesses and indicates that in a bentonite-sand mixture the pore water is likely to be associated entirely with the clay. Another indication of the water adsorption capacity of the bentonite is the final sample moisture content. Table 5.2 shows the final moisture contents at swelling equilibrium. At stresses of 2kPa and less, the water content is greater than the liquid limit (407%).

Volume change of a clay during consolidation or rebound can be idealised on a straight line plot of void ratio (or specific volume) against the logarithm of effective stress (e.g. Atkinson and Bransby, 1978). Figure 5.3 shows the relationship between final void ratio of initially dry bentonite, e_c, and vertical effective stress, σ'_v, on such a plot, for samples compacted by tamping, vibration and static loading. The similarity of data points for the three different types of compaction show the swelling of initially dry bentonite to be insensitive to sample preparation technique. This is discussed in chapter 6.

Scatter in the data is largest at low vertical effective stresses which may be due to a non uniform sample thickness prior to testing. If a dry specimen is not initially exactly level, for example the height is greatest in the centre, an arching effect may occur where the highest zones (e.g., the centre of the specimen) swell under the applied stress, and the lower zones (e.g., the peripheral bentonite) swell to a higher clay void ratio than the initially higher zones. A further error is introduced because if the sample is not level the initial calculated clay void ratio will be larger than the actual value and further void ratios will be consistently overestimated throughout the test. As the applied stress increases, compression of the sample occurs before and/or during swelling and also the smaller overall increase in height throughout the test will tend to reduce the effects of non-uniformity. Scatter of data from the swelling stages in Rowe cell hydraulic conductivity tests may be due to an error in the applied effective stress due to the pressure loss across the diaphragm (see chapter 3).

Differences in clay void ratio between the data and the straight line plot of figure 5.3 are greatest at the upper and lower limits of the applied stress range. Test C100R11 has a void ratio value of approximately 2 above that given by the fitted line. However, this may be due to the general scatter exhibited at applied stresses below 3kPa. At stresses above 3kPa, the repeatability of data is shown to be quite good, and therefore the deviations above 200kPa vertical effective stress are thought to be due to a cause other than experimental scatter. This is discussed in chapter 6. Generally, the tests are repeatable for a given applied stress.

Test	Surcharge kPa	e_c method 1	e_c method 2	e_c average	mean % error	w %
100A1*#	453	1.316	-	1.316	-	49
100A2*#	313	1.533	-	1.533	-	60
100B3	240	1.651	1.707	1.679	-1.67	85
100C3	240	1.423	1.466	1.445	-1.49	68
100D3'	240	1.488	1.532	1.510	-1.46	90
100E3x	240	1.796	1.848	1.822	-1.43	75
100A4*#	171	2.052	-	2.052	-	76
100F4	155	2.221	2.277	2.249	-1.24	93
100G5	100	2.520	2.582	2.551	-1.22	103
100H6	57.6	2.900	2.958	2.929	-0.99	126
100I6	52.2	3.517	3.595	3.556	-1.10	140
100J7'	29.6	4.971	-	4.971	-	184
100K7x	29.1	5.007	5.116	5.062	-1.08	173
100A8*#	21.0	5.254	5.363	5.309	-1.03	200
100L8	20.1	5.302	5.412	5.357	-1.03	213
100M9	7.72	7.068	7.209	7.139	-0.99	276
100N9	6.47	7.48	7.628	7.554	-0.98	274
100A10#	2.66	11.474	11.704	11.589	-0.99	417
100O10	2.62	9.769	9.957	9.863	-0.95	354
100P10x	2.57	9.323	9.514	9.419	-1.01	329
100Q10	2.02	11.404	11.621	11.513	-0.94	415
C100R11*	1.44	13.344	13.594	13.469	-0.93	483
100S11	1.25	12.032	12.260	12.146	-0.94	435
C1A''	200	1.470	-	1.470	-	79
I1A''	200	1.809	-	1.809	-	80
D1A''	100	2.966	-	2.966	-	107
E1A''	50	3.426	-	3.426	-	138
G1A''	25	5.401	-	5.401	-	204
K1A''	25	4.889	-	4.889	-	188

* Full saturation assumed.
# Multi-stage test.
' Compacted by vibration.
x Statically compacted.
'' Swelling stage of Rowe cell hydraulic conductivity test on dry bentonite powder.

Table 5.2. Results of swelling tests on initially dry bentonite.

In table 5.2, an asterisk denotes that full saturation was assumed when swelling equilibrium was reached at the quoted effective stress value. For these tests, the swelling stage was followed either by a consolidation stage (test C100R), a hydraulic conductivity stage (e.g., test C1A), or the sample was swelled back incrementally to a lower stress (tests 100A and D1A)[4]. Since samples were found to be fully saturated in tests that were ended after swelling had ceased (see 4.8), it was reasonable to assume that the same conditions were achieved at the end of swelling in all other tests.

A typical swelling curve for pure bentonite under 20.1kPa vertical effective stress is shown in figure 5.4a (test 100L8). A standard consolidation curve relates settlement to the logarithm of time as shown in figure 5.4b (after Craig, 1987). In figure 5.4a the clay void ratio replaces the settlement, but the plot is essentially the same, enabling comparison between consolidation and swelling. Adopting a similar approach to the description of laboratory consolidation curves, primary and secondary swelling stages can be identified as shown in figure 5.4a. In the primary swelling stage, the rate of volume increase is relatively large (a clay void ratio increase of 2.5 in approximately 2000min). In the secondary swelling stage (after 2000mins.), the rate of volume increase tends to zero. The sample is shown to reach swelling equilibrium after approximately 30000 min (21 days)[5].

5.3.3 Swelling: dry mixtures

Tables 5.3-5.5 summarise the results of swelling tests on 20, 10 and 5% dry bentonite-sand mixtures respectively. Tests preceded by a letter C are swelling stages of consolidation tests to determine hydraulic conductivity, and an asterix denotes assumed full saturation at swelling equilibrium, which was proceeded by a consolidation increment for indirect hydraulic conductivity testing (as for 100% bentonite in 5.3.2). Quoted moisture contents for all bentonite-sand mixtures are based on overall sample masses unless otherwise indicated.

For a vertical effective stress range of approximately 453kPa to 1.5kPa, the results of swelling tests show that the differences between clay void ratios at the highest and lowest stress decrease with decreasing bentonite content. The values are as follows:

100% bentonite: 1.32 - 13.47
20% bentonite: 2.72 - 11.41
10% bentonite: 5.74 - 11.74

---

[4]The clay void ratios at swelling equilibrium only are presented in table 5.2 and figure 5.3. This also applies to all bentonite-sand mixtures. Results from consolidation stages are presented in 5.4.
[5]A constant settlement dial gauge reading over a 24hr period was considered a sufficient indication of swelling equilibrium.

5% bentonite: 10.97 - 15.92

where the lower of the two values is the clay void ratio at approximately 453kPa. Therefore, although the overall range of final clay void ratios is less, as sand is added to the bentonite the clay swells more for a given vertical effective stress than if allowed to swell alone. In addition, the swelling of bentonite in 5% mixes under any applied stress is of the same order of magnitude as the largest swelling of 100% bentonite specimens. This effect is reduced at higher sand contents.

Figure 5.5 shows data from swelling tests on initially dry bentonite-sand mixtures on a graph of final clay void ratio against the logarithm of vertical effective stress. The solid line indicates the best fit through the 100% bentonite swelling data. It can be seen that the final clay void ratios of 20 and 10% mixes lie very close to the data for 100% bentonite when the applied stress is small. A different trend of swelling behaviour is exhibited by these mixtures at a higher stress (the value of which depends on the bentonite content). Although the data for 100% bentonite shows a similar trend, the cause is thought to be different (see chapter 6). Similar behaviour is shown for 5% bentonite mixes. However, swelling is consistently larger than for pure bentonite and is shown to lie well above the 100% best fit line at vertical effective stresses less than 4kPa.

One possible explanation of the much higher clay void ratios of 5% mixtures at applied stresses less than 4kPa is general scatter due to non uniform sample thickness. Or, since the calculation of clay void ratio assumes all the water is associated with the clay, free water within the sample, if present, is included in the calculation because void ratios are determined from external measurements. The latter is unlikely because external volume increase was measured for 5% mixes at effective stresses below 4kPa. This implies that water was drawn into the sample by the presence of the clay and is therefore adsorbed and associated with it. Therefore, the most likely explanation for the scatter of 5% bentonite-sand data is non homogeneity of the mix. Compaction results support this proposal (see 5.2).

Repeat tests were conducted at several applied stresses. The maximum differences in final clay void ratio between repeat tests are approximately 1.5 (20N10 and 20O10), 0.2 (10D4 and 10E4) and 1.0 (5F8 and 5G8) for 20, 10 and 5% bentonite-sand mixtures respectively. However, since the clay void ratio of these samples was relatively high, the differences are all less than 13% of the average values. As general experimental scatter increases with decreasing stress, this is considered a sufficient indication of test repeatability. Scatter is of the same order as for pure bentonite.

Test	Surcharge kPa	e_c method 1	e_c method 2	e_c average	mean % error	w %
20A1	453	2.714	2.720	2.717	-0.11	22.1
20B2	241	2.945	2.950	2.948	-0.08	24.6
M1A	200	2.820	-	2.820	-	25.1
C20C3*	199	3.206	3.213	3.210	-0.11	23.9
20D4	100	3.429	3.431	3.430	-0.03	26.8
20E5	54.5	3.830	3.834	3.832	-0.05	28.9
C20F6*	33.5	4.640	4.647	4.644	-0.08	34.5
C20G6*	32.1	5.238	5.393	5.316	-1.46	39.0
20I7	20.2	4.884	4.891	4.888	-0.07	36.9
C20J7*	20.2	5.683	5.691	5.687	-0.07	42.3
20K8	12.06	6.515	6.521	6.518	-0.05	49.9
C20L8*	10.02	7.055	7.063	7.059	-0.06	52.5
20M9	6.46	8.235	8.242	8.239	-0.04	59.9
20N10	2.31	10.845	10.855	10.850	-0.05	79.6
20O10	2.00	12.391	12.403	12.397	-0.05	98.0
20P11	1.67	11.405	11.419	11.412	-0.06	82.5

* Full saturation assumed.

Table 5.3. Results of swelling tests on initially dry 20% bentonite-sand mixtures.

Test	Surcharge kPa	e_c method 1	e_c method 2	e_c average	mean % error	w %
10A1	453	5.502	5.978	5.740	-4.15	20.8
10B2	240	6.504	6.507	6.506	-0.02	26.9
C10C3*	199	5.390	-	5.390	-	20.1
C10D4*	150	5.722	5.726	5.724	-0.03	21.3
C10E4*	150	5.555	5.558	5.557	-0.03	20.7
10F5	100	6.235	6.238	6.237	-0.02	23.7
C10G6*	60.1	5.889	5.893	5.891	-0.03	21.9
C10H6*	60.0	5.973	5.976	5.975	-0.03	22.2
10I6	54.4	6.340	6.343	6.342	-0.02	24.5
C10J7*	31.9	6.611	6.615	6.613	-0.03	24.7
C10K8*	17.7	7.551	7.554	7.553	-0.02	28.2
10L9	12.06	7.375	7.378	7.377	-0.02	28.7
C10M9*	10.20	7.380	7.390	7.385	-0.07	27.5
10N9	7.41	8.604	8.608	8.606	-0.02	32.0
10O10	3.50	9.889	9.893	9.891	-0.02	36.7
10P10	2.31	11.116	11.120	11.118	-0.02	40.6
10Q11	1.25	11.741	11.745	11.743	-0.02	42.5

* Full saturation assumed.

Table 5.4. Results of swelling tests on initially dry 10% bentonite-sand mixtures.

Test	Surcharge kPa	e_c method 1	e_c method 2	e_c average	mean % error	w %
5A1	453	10.971	10.973	10.972	-0.01	19.3
5B2	241	11.443	11.444	11.444	0.00	20.0
5C4	100.6	12.138	12.140	12.139	-0.01	22.8
5E5	54.4	12.221	11.799	12.010	1.76	22.5
5F8	12.06	13.134	13.135	13.135	0.00	22.7
5G8	11.58	12.096	12.119	12.108	-0.09	21.7
5H9	7.57	13.115	13.117	13.116	-0.01	24.8
5H10	3.19	12.908	12.931	12.920	-0.09	22.4
5J10	2.31	14.560	14.562	14.561	-0.01	24.8
5K10	2.31	14.179	14.181	14.180	-0.01	24.3
5L11	1.25	15.570	15.571	15.571	0.00	26.3
5M11	1.25	15.060	15.062	15.061	-0.01	25.8
5N11	1.25	15.920	15.921	15.921	0.00	28.7

Table 5.5. Results of swelling tests on initially dry 5% bentonite-sand mixtures.

Examples of typical swelling curves (clay void ratio against logarithm of time) for 20, 10 and 5% bentonite-sand mixtures are plotted in figures 5.6-5.8 respectively. Three different vertical effective stresses were chosen to illustrate the effects of bentonite content and applied stress on swelling, and the same magnitude of range of clay void ratio is used on the y-axes for comparison. Generally, the laboratory curves are less well defined as the clay content decreases, and it is harder to differentiate between primary and secondary swelling stages. At low clay contents and/or large applied stresses, access to water caused compression of certain samples and their corresponding swelling curves showed no noticeable trend. This behaviour is attributed to mechanical compression of the sand skeleton (due to shearing between and rolling of the particles) as the clay swells within the voids. Poorly defined laboratory curves are therefore probably a combination of the effect of the sand and a consequence of the relative decrease in overall volume change with decreasing clay content.

The time required for the dry mixtures to reach swelling equilibrium are all of the same order of magnitude as for 100% bentonite. However, this is affected by the initial sample height in addition to the bentonite content and surcharge. Therefore, no comparison between times for equilibrium is possible.

The swelling of dry mixtures is discussed further in chapter 6.

5.3.4 Analysis of swelling data

Logarithmic regression analysis was conducted on swelling data of 100% bentonite, to produce a straight line plot in e_c - log σ'_v space. The equation of the line is:

$$e_c = 12.08 - 4.57 \log \sigma'_v \qquad 5.9$$

The coefficient of correlation for the data (r^2) is 0.954, which indicates that the scatter in the data is relatively small. This idealised representation of swelling behaviour will be termed the bentonite swelling line.

To determine if the swelling of bentonite-sand mixtures was commensurate with swelling of 100% bentonite, logarithmic regression analysis was conducted on data from mixtures whose clay void ratios lay close to the bentonite swelling line combined with the 100% bentonite data. The corresponding stress ranges for 10 and 20% bentonite mixes were 1.25-10.2kPa and 1.67-100kPa respectively. 5% mixtures were omitted as all the data points were well above the bentonite swelling line. The equation of the line is:

$$e_c = 12.26 - 4.69 \log \sigma'_v \qquad 5.10$$

with a coefficient of correlation of 0.961. For clay void ratios of 1 and 12 the estimated stresses are 1.0kPa and 1.1kPa ($e_c = 1$) and 265kPa and 256kPa ($e_c = 12$) for equations

5.9 and 5.10 respectively. Since clay void ratios greater than 12 are unlikely in engineering applications, and none of the test samples had clay void ratios less than one, the chosen limits are satisfactory to show that the two equations are essentially equal. Therefore, swelling of mixtures is the same as swelling of clay alone for the given vertical effective stress ranges. Equation 5.9 will be taken as the bentonite swelling line as it was determined purely from the behaviour of the clay.

Logarithmic regression analysis was also performed on the remaining bentonite-sand mixtures whose final clay void ratios lay above the bentonite swelling line, i.e., 10% bentonite mixtures with a vertical effective stress range of 12.06-453kPa inclusive, 20% bentonite mixtures with a vertical effective stress range of 100-453kPa inclusive, and all 5% bentonite mixtures.

The equations of the calculated straight line plots in semi-logarithmic space are:

20%: $e_c = 5.54 - 1.08 \log \sigma'_v$ $(r^2 = 0.756)$ 5.11

10%: $e_c = 8.43 - 1.15 \log \sigma'_v$ $(r^2 = 0.627)$ 5.12

5%: $e_c = 14.98 - 1.63 \log \sigma'_v$ $(r^2 = 0.828)$ 5.13

The correlation coefficients are lower than for the bentonite swelling line (calculated as 0.954). However, the gradients of equations 5.11-5.13 are fairly similar to each other. Low correlation is attributed to the fewer number of data points available for analysis. Therefore, even though the scatter is comparable to the 100% bentonite data, the correlation is reduced because the ranges of clay void ratio and corresponding vertical effective stress are less. For 5% bentonite mixtures the scatter at stresses below 4kPa is responsible for the decreased correlation coefficient and the higher gradient than 20% and 10% mixes.

As an approximation all three gradients were assumed to be equal, and therefore a weighted average was taken to give a gradient of 1.34 in semi-logarithmic space. This assumes that the stiffness of all three mixtures will be equal for a given vertical effective stress range. The justification for this assumption is given in chapter 6. All data points for 5% mixtures were included.

The constant in each equation, equal to the clay void ratio at a vertical effective stress of 1kPa, was adjusted to minimise the error caused by altering the gradients of the best fit lines. Clay void ratios for each mix were calculated at a vertical effective stress at the middle of the data range for which equations 5.11-5.13 were determined. These values were re-substituted into the equations using 1.34 as the gradient to give the adjusted

constant. An example of the line fitting procedure is given in appendix 5. The idealised swelling equations for the mixtures above the bentonite swelling line are as follows:

20%: $e_c = 6.15 - 1.34 \log \sigma'_v$ 5.14

10%: $e_c = 8.79 - 1.34 \log \sigma'_v$ 5.15

5%: $e_c = 14.60 - 1.34 \log \sigma'_v$ 5.16

The threshold stresses above which the swelling behaviour of mixtures deviates from clay swelling behaviour can be calculated by equating the idealised equations to the bentonite swelling line (equation 5.9), and are as follows:

20%: $\sigma'_v = 68.7$kPa

10%: $\sigma'_v = 10.5$kPa

5%: $\sigma'_v = 0.2$kPa

The consequence of altering the gradients for mixtures above the threshold stress is a slight under or overprediction of the final clay void ratio for vertical effective stresses at the extremes of the data ranges used for analysis. However, since the changes in gradient are slight it is proposed that this has no significant effect on the predicted behaviour. If the actual and estimated clay void ratios are compared, the maximum differences in clay void ratio from the idealised lines are -0.14 (4%), 0.9 (13%) and 1.45 (9%) for tests 20C3, 10B2 and 5N11 respectively. As this is within experimental scatter, adjusting the gradients of the swelling lines is considered to have no significant effect.

The idealised swelling behaviour of the bentonite and bentonite-sand mixtures is shown in figure 5.9.

5.3.5 Swelling: modified Proctor compacted mixtures

In figure 5.10 data from swelling tests on bentonite-sand mixtures initially compacted into the Rowe cell using the modified Proctor method are superimposed on a plot of idealised swelling behaviour of initially dry mixtures (figure 5.9). Although the data points are consistently below the idealised behaviour of dry mixtures above the threshold stress, similar trends are apparent (i.e., the change in clay void ratio with vertical effective stress is similar). The scatter is greatest for 5% mixes and this can be attributed to non homogeneity of samples due to effects of mixing and/or compaction. Some errors may also be introduced by the diaphragm pressure correction, which increases as the applied stress decreases (see chapter 3). As a consequence clay void ratio data may be displaced horizontally in the figure. The effect has greater significance if the actual stress on the sample is less than the calculated stress because of the logarithmic scale. Since the data set is relatively small, the repeatability is unknown.

The two sample types had different initial moisture contents prior to swelling. Initially dry samples had moisture contents in the range 0.7-2.9% for 5% and 20% bentonite-sand mixtures respectively, whereas Proctor samples were compacted at optimum moisture content; this was approximately 12% for all mixtures (see table 5.1). It is thought that the different moisture contents affect the initial density of the sand, giving an apparently reduced amount of swelling for a particular vertical effective stress. This is discussed further in chapter 6.

Table 5.6 summarises the relevant parameters at swelling equilibrium. Also indicated are the estimated clay void ratios for dry mixtures using equations 5.9 and 5.14-5.16. The difference between the clay void ratios of compacted and the dry idealised theoretical samples is shown to increase with decreasing bentonite content (see chapter 6). Certain samples had final calculated degrees of saturation greater than 100%. This indicates that some water was drawn into the sample during dismantling[6].

Test	% bentonite	Surcharge kPa	e_c average	Estimated[7] e_c	w %
B1A	20	200	2.21	3.07	17.3
B3D	20	100	2.50	3.47	19.5
B3E	20	50	3.17	4.32	26.4
L1A	10	200	4.23	5.71	15.1
L2B	10	100	4.38	6.11	15.7
L3A	10	50	4.53	6.57	16.2
L4A	10	25	4.58	6.92	16.4
H1A	5	100	8.87	11.92	18.2
H1B	5	50	9.37	12.32	19.1
F1A	5	200	10.09	11.52	19.6
F1B	5	100	10.46	11.92	20.4
J1A	5	50	11.72	12.32	20.3

Table 5.6. Results of swelling tests on bentonite-sand mixtures compacted by the modified Proctor method (Rowe cell).

[6]Although volume change lines were closed, it is likely that water was drawn in from porous discs and any other free water in the cell after the vertical effective stress was removed.

[7]These are predicted clay void ratios for dry bentonite-sand mixtures calculated using equation 5.9 for vertical effective stresses less than the threshold values and equations 5.14-5.16 for vertical effective stresses greater than the threshold values.

5.3.6 One dimensional normal consolidation of bentonite

Tables 5.7 and 5.8 are results from one-dimensional normal consolidation tests on bentonite prepared by two different methods. One sample was initially mixed at approximately the liquid limit (LL = 407%) when the calculated degree of saturation was 99%. The other sample was initially swollen from a dry state under a surcharge of 1.44kPa (C100R11). This produced approximately the same initial moisture content as the reconstituted sample. Full saturation of the sample was assumed prior to consolidation which was considered reasonable since full saturation was calculated from other swelling tests (see 4.8).

Volume change tests tests were conducted to compare dry swelling, normal consolidation and rebound of bentonite in e_c - log σ'_v space. To further investigate the differences between an initially 'dry' and initially 'wet' sample, the hydraulic conductivity was determined for each consolidation stage by an indirect method (see 5.4.2). It was thought that comparison of hydraulic conductivities would give an indication of the differences in fabric of the two samples and also the change in clay fabric throughout normal consolidation. For example, for a specific void ratio a flocculated sample would be expected to have a higher hydraulic conductivity than a dispersed sample (see 2.4.4). This is discussed in chapter 6.

Hydraulic conductivity was calculated using the relationship

$$k = c_v m_v \rho_w g \qquad 5.17$$

where c_v = coefficient of consolidation

m_v = coefficient of volume compressibility

Coefficients of consolidation were found from the laboratory curve (settlement against logarithm of time) for each loading increment at 50% consolidation[8]. The coefficient of volume compressibility for each consolidation increment is given by

$$m_v = \frac{1}{1+e_0}\left(-\frac{de}{dp}\right) \qquad 5.18$$

where de = the change in void ratio over the consolidation period corresponding to a stress increment dp

e_0 = void ratio at 0% primary consolidation.

Changes in void ratio for all normal consolidation and rebound stages were determined using equation 5.8.

---

[8]The procedure for calculating the hydraulic conductivity from consolidation data is outlined in 5.4.2.

From a plot of void ratio against the logarithm of vertical effective stress, the virgin compression index, C_c, and the rebound index, C_r, can be determined. Values are given in tables 5.7 and 5.8 for individual normal consolidation and rebound stages, to indicate the behaviour of the bentonite as the applied stress is increased or decreased. The following equations were used to calculate the compression and rebound indices

$$C_c = \frac{de}{\log(\sigma'_1/\sigma'_0)} \qquad 5.19$$

$$C_r = \frac{de}{\log(\sigma'_1/\sigma'_0)} \qquad 5.20$$

where σ'_0 is the effective stress prior to the consolidation or rebound stage caused by a change in applied stress equal to σ'_1

Normal consolidation			Rebound	
Stage & surcharge (kPa)	**C_c**	**k x10^{-11} (m/s)**	**Stage & surcharge (kPa)**	**C_r**
1) 7.7	-	1.36	1) 111.0	1.73
2) 14.5	1.68	6.74	2) 55.4	2.92
3) 27.3	3.19	6.09	3) 27.3	3.17
4) 55.4	5.97	2.76	4) 14.8	2.43
5) 111.0	6.57	1.24	5) 7.7	3.47
6) 252.0	6.27	0.28	6) 2.7	2.89

Table 5.7. Normal consolidation and rebound of 100% bentonite mixed at the liquid limit.

Normal consolidation			Rebound	
Stage & surcharge (kPa)	**C_c**	**k x10^{-11} (m/s)**	**Stage & surcharge (kPa)**	**C_r**
1) 7.7	1.13	31.1	1) 110.8	2.03
2) 14.7	3.35	16.1	2) 55.3	3.02
3) 27.2	4.51	9.3	3) 27.2	3.16
4) 55.3	5.36	5.2	4) 14.7	3.06
5) 110.8	5.73	2.2	5) 7.70	3.93
6) 251.1	5.65	0.6	6) 2.54	5.28

Table 5.8. Normal consolidation and rebound of bentonite swollen from powder at 1.44kPa vertical effective stress.

5.3.7 Analysis of normal consolidation and rebound data

Figure 5.11 shows the bentonite swelling line, and the normal consolidation and rebound data for bentonite prepared from slurry (LL in figure 5.11), and bentonite swollen from a dry state at an effective stress of 1.44kPa (test C100R11). The initial void ratio at swelling equilibrium for test C100R11, as indicated on the figure, has the largest deviation from the bentonite swelling line of all the bentonite swelling tests, and therefore, is not a typical data point. However, it is assumed that this has no effect on the overall consolidation behaviour.

No significant difference is shown between the normal consolidation and rebound behaviour of the two sample types, and the only significant deviation of data points occurs at the end of the final unloading increment. At this effective stress, the samples have a clay void ratio difference of approximately 2. The higher of the two values is more typical of rebound behaviour[9]. Initial deviation from linearity on consolidating indicates either overconsolidation or a similar effect (see chapter 6).

For saturated normally consolidated clays the compression index ,C_c, is the slope of the straight line portion of the void ratio versus logarithm of vertical effective stress curve. Logarithmic regression analysis was performed on the combined data from both tests to give the normal consolidation line[10] (NCL) and any rebound line (assuming rebound lines have parallel orientation to each other in e_c - log σ'_v space) for bentonite consolidated from a slurry or swollen from its dry state:

NCL: $e_c = 19.67 - 6.55 \log \sigma'_v$ ($r^2 = 0.992$) 5.21

rebound: $e_c = C - 3.20 \log \sigma'_v$ ($r^2 = 0.965$) 5.22

Where C is the clay void ratio at 1kPa vertical effective stress. Therefore, the compression index is equal to 6.55 and the rebound index, C_r, 3.20.

The idealised swelling, normal consolidation and rebound lines are shown in figure 5.12. The data suggest that a straight line fit is justified over the applied stress range used. In addition, plots of this type conform with standard geotechnical representation of soil behaviour in one-dimensional compression tests. Clearly, the bentonite swelling line has a different gradient to the normal consolidation and rebound line, and has a value

---

[9]For conceptually describing soil volume change behaviour, a one dimensional rebound and associated recompression line are generally represented by a straight line in e (or v) - log σ'_v space, i.e., the behaviour is considered elastic. However, laboratory data will typically show some degree of hysteresis. Therefore the gradient tends to increase with decreasing applied stress on unloading (e.g., Atkinson and Bransby, 1978).

[10]Data on the initial curved portion of the normal consolidation line was excluded from the analysis.

between the compression and rebound indices. These differences are attributed to clay fabric effects and are discussed in chapter 6.

Although idealising the behaviour of the bentonite makes prediction of clay void ratios relatively simple, extrapolation beyond the stress range used in the testing programme may be inappropriate.

5.4 Hydraulic conductivity tests

5.4.1 Constant head analysis

Figures 5.13-5.16 are examples of typical inflow and outflow volumes against time plots for 100% bentonite and 20, 10 and 5% bentonite-sand mixtures respectively. Best fit gradients were calculated using linear regression analysis[11]. The applied head difference (either elevation, pressure or both combined) causes swelling and consolidation at the inflow and outflow ends of the sample respectively (see 4.4.2). Therefore an initial period was allowed for the sample to equilibrate under the applied stress difference before commencing the analysis[12]. Inset are inflow and outflow-time gradients for comparison.

After application of the head difference the inflow is generally greater than the outflow for an initial time period, as shown in the figures. However, after swelling and consolidation have occurred the changes in flow volumes with time are similar at both ends of the sample. The volume change of the sample is consistent with the behaviour described in section 5.3. Swelling at the inflow end will be described by the bentonite swelling line (since the sample has not been consolidated at any stage). It was shown in figure 5.11 that the volume change of a sample swollen from a dry state behaves in a similar way to an overconsolidated sample during compression, until it reaches the normal consolidation line. For small changes of effective stress, the volume change behaviour is likely to be described by a rebound line. Therefore, because the gradient of the bentonite swelling line is greater than the rebound index, swelling at the inflow side will be greater than the compression at the outflow side, with a subsequent overall increase in volume, i.e., the inflow is greater than the outflow.

Scatter of the data is attributed to general temperature changes which alter the viscosity of the pore fluid and causes expansion and contraction of the cell. It was shown in chapter 4 (figure 4.1) that insulation of the Rowe cells considerably reduced the effects of diurnal temperature change but this did not eliminate the effects of general temperature changes over long test periods (±2°). This accounts for the large amount of scatter in flow data in figure 5.15, where a significant change in the laboratory temperature is assumed (over a period between readings of approximately 27hr).

---

[11] In figure 5.15, the flow data after 4000mins. test duration was excluded from the analysis.

[12] Laboratory consolidation curves were used to determine the time required for 90% consolidation (t_{90}) of bentonite under the range of effective stresses used in hydraulic conductivity tests. This was then taken as the minimum time period for equilibration of the sample. However, for some 100% bentonite samples and all 5% bentonite-sand mixtures, where the pore fluid replacement criteria occurred before $t = t_{90}$, hydraulic conductivity was calculated over the most linear period of flow (e.g., tests G1A and Q4A in figures 5.13 and 5.16).

Despite experimental scatter, calculated inflow and outflow gradients in each test were approximately equal. This is a good indication that the sample is fully saturated[13].

Hydraulic conductivity was calculated using Darcy's law in the form:

$$Q = kAi \qquad 5.23$$

where Q = flow rate (m^3/s)

A = sample cross-sectional area

i = hydraulic gradient

An average of the inflow and outflow-time gradients gives the flow rate. Any error caused by evaporation of water from the burettes is virtually eliminated, because the resultant increase in inflow and decrease in outflow are the same. The hydraulic gradient was taken as the average value over the linear period of flow. Constant head conditions are not truly maintained because the hydraulic gradient decreases as the elevation head drops throughout the test period, i.e., the difference in water levels between inflow and outflow volume change units decreases. This accounts for the reduction in inflow and outflow gradients in figure 5.13 as the test proceeds. However, no noticeable difference is apparent in figure 5.14[14]. It was found that the assumption of constant head conditions has no effect on the calculated values of hydraulic conductivity (discussed below).

The maximum change in hydraulic gradients in the testing programme are 27% (test E1A), 14% (test B2B), 12% (test L3A) and 30% (test J1A) for 100% bentonite, 20, 10 and 5% bentonite-sand mixtures respectively, the corresponding averages for the complete data set are 14%, 5%, 5% and 16%. However, the decrease in flow rate is directly proportional to the decrease in hydraulic gradient (i.e., Darcy's law in the form $dQ/dt = kA.dh/L$). Therefore, when inflow equals outflow, the hydraulic conductivity has the same calculated value between any two adjacent data points on a flow volume versus time plot. The gradients of the best fit lines give the flow rate corresponding to the hydraulic gradient at the middle of the data range used for analysis, or, the average hydraulic gradient. Hence, this method of analysis is simply an averaging technique that minimises any errors caused by experimental scatter.

Hydraulic conductivity values were calculated using equation 5.23 and temperature corrected to 20°C using data from Bowles (1986), this allows for the change in viscosity

---

[13]If the soil was unsaturated, the inflow rate would be higher than the outflow rate whilst the pore air was replaced.

[14]The decrease in hydraulic gradient is dependent on the hydraulic conductivity of the sample and the chosen capacity of the volume change units, since the rate of head drop will be greater if the burettes only are used for measurement.

of the pore fluid. For example, at 15°C, the calculated hydraulic conductivity is multiplied by 1.135 to give the corresponding value at 20°C.

Tables 5.9-5.13 display the results from Rowe and triaxial permeameter tests. The reported hydraulic conductivity values are temperature corrected. All results were obtained from Rowe cell hydraulic conductivity tests with the exception of tests Q1A-Q4A (table 5.12), and P1A (table 5.13), which were conducted in the triaxial permeameter. The results show that the hydraulic conductivity of 20% bentonite-sand mixtures is the lowest ($k \sim 10^{-12}$ m/s) and increases by approximately 4 orders of magnitude for 5% mixes. The changes in hydraulic conductivity are most significant when the clay void ratio is relatively high. For example, there is a variation of 3 orders of magnitude for 5% mixes. At high clay void ratios, suggesting large distances between clay particles, the hydraulic conductivity tends towards the value of sand alone. For 100% bentonite the hydraulic conductivity is shown to increase by an order of magnitude over the stress range (hence clay void ratio range) used. This illustrates the dependence of the hydraulic conductivity on the clay void ratio and is discussed further in chapter 6. Given in the tables are the initial and final hydraulic gradients between which the analysis was conducted. The differences increase with increasing hydraulic conductivity because the flow rate, hence drop in head is greater. Any change of hydraulic gradient will alter the effective stresses at both ends of the sample causing swelling and consolidation and this may be the cause of some scatter in the data.

The first 20% bentonite-sand sample (B1A-B5A) was tested under various hydraulic gradients to check the validity of Darcy's law for bentonite-sand mixtures. The results for this sample on a plot of specific discharge, v, versus hydraulic gradient, i, are shown in figure 5.17. Hydraulic gradients were incrementally increased (described as a stage in figure 5.17) and the hydraulic conductivity calculated for each increment (see 4.4.2). No discernible trend is apparent for each stage of hydraulic gradient increments, indicating that effects on hydraulic conductivity such as particle migration and pore fluid replacement are insignificant, and Darcy's law can be considered valid for this sample over the range of hydraulic gradients used. Scatter in the data is small, and is possibly due to slight swelling and consolidation at the ends of the sample as described previously. Linear regression analysis of the data with the origin fixed at zero gives a coefficient of correlation of 0.966.

A. 100% bentonite

Test	Surcharge (kPa)	Clay void ratio	Sample height (mm)	Initial hydraulic gradient	Final hydraulic gradient	Average temp. (°C)	k (m/s)
C1A	200	1.47	7.08	62.7	46.0	17.3	2.34E-11
C2A	200	1.48	7.11	144.3	140.2	20.3	1.64E-11
I1A	200	1.81	8.56	54.1	48.5	17.4	1.50E-11
D2A	100	2.82	10.94	93.1	87.2	21.6	9.89E-11
D1A	100	2.97	11.36	43.2	38.7	22.3	2.77E-11
E1A	50	3.43	7.54	60.2	43.9	21.8	1.32E-10
K1A	25	4.89	7.46	53.7	45.2	18.4	1.01E-10
G1A	25	5.40	8.12	60.9	53.8	19.3	1.91E-10

Table 5.9. Hydraulic conductivity of bentonite (constant head analysis).

B. 20% bentonite-sand mixtures

Test	Surcharge (kPa)	Clay void ratio	Sample height (mm)	Initial hydraulic gradient	Final hydraulic gradient	Average temp. (°C)	k (m/s)
B1A	200	2.21	32.64	14.4	12.7	-	1.7E-12
B2A	200	2.21	32.63	45.6	39.7	19.5	1.3E-12
B2B	200	2.21	32.64	41.9	36.1	16.6	1.7E-12
B3A	200	2.21	32.64	109.6	109.1	18.0	1.1E-12
B2C	200	2.21	32.65	47.1	44.9	16.1	1.1E-12
B3B	200	2.21	32.64	109.2	108.8	16.1	1.1E-12
B4A	200	2.21	32.64	189.4	188.9	15.7	1.3E-12
B2D	200	2.21	32.65	44.9	38.7	16.2	0.9E-12
B3C	200	2.21	32.68	109.1	108.1	16.8	0.9E-12
B4B	200	2.23	32.87	188.8	188.5	16.0	1.0E-12
B4Br	200	2.23	32.87	187.4	185.8	16.8	1.0E-12
B5A	200	2.23	32.87	321.4	320.0	16.6	1.1E-12
B3D	100	2.50	35.53	87.0	85.1	19.4	1.5E-12
B3E	50	3.17	42.41	62.0	60.7	24.4	2.2E-12

Table 5.10. Hydraulic conductivity of 20% bentonite-sand mixtures (constant head analysis).

C. 10% bentonite-sand mixtures

Test	Surcharge (kPa)	Clay void ratio	Sample height (mm)	Initial hydraulic gradient	Final hydraulic gradient	Average temp. (°C)	k (m/s)
L1A	200	4.23	18.61	28.4	26.6	16.8	1.6E-12
L2A	200	4.23	24.30	80.8	80.0	17.1	4.5E-12
L3A	50	4.53	27.29	28.1	24.8	20.0	5.3E-12
L4A	25	4.58	27.52	27.6	27.2	18.6	4.2E-12

Table 5.11. Hydraulic conductivity of 10% bentonite-sand mixtures (constant head analysis).

D. 5% bentonite-sand mixtures

Test	Surcharge (kPa)	Clay void ratio	Sample height (mm)	Initial hydraulic gradient	Final hydraulic gradient	Average temp. (°C)	k (m/s)
Q1A	200	8.35	115.40	11.6	10.9	26.0	2.81E-11
Q2A	100	8.40	115.50	11.7	11.4	24.6	1.41E-09
Q3A	50	8.46	115.62	4.3	3.8	25.8	2.35E-08
Q4A	50	8.56	115.81	4.4	3.4	27.4	1.12E-07
H1A	100	8.87	24.42	19.9	15.9	19.7	5.04E-10
H1B	50	9.37	24.50	20.1	18.4	19.5	4.56E-10
F1A	200	10.10	18.40	24.4	19.6	22.3	3.44E-08
F1B	100	10.47	18.61	27.6	20.3	19.8	4.00E-08
J1A	50	11.73	28.29	16.0	11.2	19.3	1.42E-07

Table 5.12. Hydraulic conductivity of 5% bentonite-sand mixtures (constant head analysis).

E. Sand

Test	Surcharge (kPa)	Void ratio	Sample height (mm)	Initial hydraulic gradient	Final hydraulic gradient	Average temp. (°C)	k (m/s)
P1A	50	0.66	100.80	1.9	0.9	-	9.17E-06

Table 5.13. Hydraulic conductivity of sand (constant head analysis).

5.4.2 Indirect analysis

Coefficients of hydraulic conductivity were calculated from a consolidation increment at the end of one-dimensional swelling tests by using Terzaghi's theory of consolidation (Terzaghi, 1943). Laboratory consolidation data were compared to the theoretical curves by curve fitting which relates only to the primary consolidation phase and enables the coefficient of consolidation, c_v, to be determined. Two curve fitting procedures were used, one using the log time-settlement curve (Casagrande, 1936), the other using the square root time-settlement curve (Taylor, 1942). Casagrande and Fadum (1944) found satisfactory agreement between measured hydraulic conductivities and values calculated indirectly, provided the log time method was used, and provided a distinct change in curvature was observed where primary and secondary settlement curves merge. For the square root time method, Taylor (1942) found that calculated values are lower than measured values by 5-20% provided the clay is normally consolidated. The state of a sample swollen from dry is analogous to a normally consolidated sample and differs in direction of stress only; overconsolidation relates to unloading a normally consolidated sample or loading a swollen sample. Therefore, when laboratory log-time curves were poorly defined Taylor's method was considered satisfactory. Examples of both methods for indirect analysis are presented in figures 5.18 and 5.19 respectively.

Immediate settlement occurs on loading the sample, possibly due to compression of air. Therefore, a construction is necessary to determine the void ratio at which consolidation commences. In the log time method, the theoretical degree of consolidation of U = 0% is established as shown in figure 5.18. A time t_1 is selected and a time $t_2 = 4t_1$. The ordinate y is measured from t_1 to t_2 (distance ac) and the same value of y is marked off vertically above t_1 (distance ad). The procedure is repeated on three different portions of the initial curve and the best horizontal line fitted. The settlement (S_0) at the onset of consolidation is the intersection of the horizontal line on the settlement axis. This value is then used to calculate the initial height, void ratio etc. The intersection between the tangent to the linear portion of the curve and the backward extension of the secondary compression line defines the settlement (S_1) at U = 100%.

In the square-root-time method, shown in figure 5.19, the linear portion of the laboratory curve extrapolated backwards gives the settlement (S_0) at U = 0%. From an arbitrary square root time value such as B, an abscissa value 15% greater is marked (C), so that AC = 1.15 x AB. The intersection of a line drawn from S_0 to point C with the laboratory curve gives the intersection at U = 90%, hence, from interpolation, U = 100%.

The hydraulic conductivity is determined using equation 5.17. It is preferable to calculate c_v from t_{50} rather than t_{90} because the middle of the laboratory curve is the portion which agrees most closely with the theoretical curve. Mesri and Olson (1971) state the standard square root method (at 90% consolidation) usually yields higher hydraulic conductivity values than those calculated by either method when fitting is performed at 50% consolidation. The similarity between hydraulic conductivity values calculated by both methods at 50% consolidation is shown in figures 5.18 and 5.19. Since both these samples had similar clay void ratios it is not unreasonable to assume that their hydraulic conductivities (and consolidation periods) would also be similar[15]. The t_{50} values for both samples were approximately equal (41min and 36min for log time and square root time methods respectively. However, if t_{90} values are used the square root time method yields a value of approximately half the log time method which would consequently double the calculated hydraulic conductivity value.

Tables 5.14-5.16 present the data from indirect hydraulic conductivity tests. The void ratio change relates to the overall sample void ratio and the average of clay void ratios and sample heights relate to the values at 50% consolidation. Changes in hydraulic conductivity with bentonite content and clay void ratio show similar trends to those observed in the data from Rowe and triaxial permeameter tests. It is apparent that quite large stress increments were necessary to achieve reasonable amounts of settlement. Since Terzaghi's theory is based on small stress increments it is unknown how this affects the measured values of hydraulic conductivity. However, since the overall void ratio changes are quite small, i.e. the vertical strain is small, and values of hydraulic conductivity are of the same order of magnitude as determined for mixtures in Rowe cell tests, it is suggested that this did not have a significant effect on the values.

Also given in tables 5.14-5.16 are values of coefficient of volume compressibility, m_v, calculated from the consolidation increment. A stiff sample is indicated by a low m_v value. Therefore, it is seen that sample stiffness increases with sand content and/or vertical effective stress, implying greater interaction between sand particles. Since all the flow of water is assumed to be through the clay gel, it could be argued that determining the hydraulic conductivity in this way is not acceptable at high sand contents (see 4.4.5). The use of 10% mixtures was thought reasonable for indirect measurement because definite primary and secondary consolidation stages were identified on the laboratory curves. An indication of the sand preventing consolidation would be noticeable on the laboratory curve, i.e., the sand skeleton resisting the applied stress such that the settlement ceases. Also, because m_v is used in calculating the hydraulic conductivity and

[15]The 10% bentonite mix has a lower value of k. The reasons for this are discussed in chapter 6.

is purely a substitute for void ratio (equation 5.18), the use of 10% bentonite mixtures was judged to be satisfactory.

The hydraulic conductivity of 10% bentonite mixes was calculated by the Casagrande and Taylor methods (depending on the laboratory data) and these are indicated in table 5.16. The data show reasonable agreement in hydraulic conductivity values for both methods at similar clay void ratios (or overall void ratios), for example tests C10C3 and C10E4, and tests C10J7 and C10M9. However, the laboratory curves were less well defined at large stresses, suggesting sand interaction may affect the consolidation behaviour at bentonite contents less than 10% to such an extent that indirect measurement is unsatisfactory.

A. 100% bentonite

Test	Initial σ'_v (kPa)	Stress increment (kPa)	Void ratio change	Average clay void ratio	Average sample height (mm)	c_v (m^2/yr)	m_v (m^2/MN)	k (m/s)
C100R11	7.7	7.0	0.944	11.84	19.91	0.05	10.08	1.61E-10
C100R11	1.4	6.3	0.819	12.94	21.62	0.11	9.13	3.11E-10

Table 5.14. Hydraulic conductivity of bentonite calculated using the log time (Casagrande) method.

B. 20% bentonite-sand mixtures

Test	Initial σ'_v (kPa)	Stress increment (kPa)	Void ratio change	Average clay void ratio	Average sample height (mm)	c_v (m^2/yr)	m_v (m^2/MN)	k (m/s)
C20C3	199.2	141.6	0.004	3.18	9.16	0.31	0.02	1.7E-12
C20F6	33.5	7.0	0.003	4.63	9.07	0.09	0.22	6.3E-12
C20F7	40.5	28.2	0.022	4.55	8.98	0.05	0.41	6.3E-12
C20G6	32.1	13.8	0.009	5.21	10.04	0.11	0.32	1.12E-11
C20J7	20.2	12.5	0.015	5.64	10.23	0.06	0.56	9.8E-12
C20L8	10.0	9.4	0.037	6.96	7.98	0.06	1.38	2.70E-11
C20A	1.4	3.2	0.043	8.32	12.79	0.08	5.07	1.22E-10

Table 5.15. Hydraulic conductivity of 20% bentonite-sand mixtures calculated using the log time (Casagrande) method.

C. 10% bentonite-sand mixtures

Test	Initial σ'_v (kPa)	Stress increment (kPa)	Void ratio change	Average clay void ratio	Average sample height (mm)	c_v (m^2/yr)	m_v (m^2/MN)	k (m/s)
C10C3[I]	199.2	141.6	0.014	5.26	7.71	0.10	0.06	2.1E-12
C10E4[X]	150.1	98.0	0.004	5.49	7.45	0.14	0.03	1.2E-12
C10D4[X]	150.2	97.9	0.004	5.68	14.77	0.17	0.03	1.4E-12
C10G6[X]	60.1	41.8	0.002	5.83	7.33	0.45	0.03	4.2E-12
C10H6[X]	60.0	41.6	0.002	5.94	14.06	0.29	0.03	2.7E-12
C10J7[X]	31.9	13.8	0.001	6.59	8.43	1.12	0.04	1.51E-11
C10M9[I]	10.2	9.4	0.020	7.26	8.30	0.04	1.22	1.33E-11
C10K8[I]	17.7	12.5	0.009	7.49	10.01	0.08	0.41	1.07E-11
C10A[X]	1.4	3.5	0.008	9.37	13.72	2.08	1.18	8.60E-11

[I] Hydraulic conductivity determined by the log time (Casagrande) method.
[X] Hydraulic conductivity determined by the square root time (Taylor) method.

Table 5.16 Hydraulic conductivity of 10% bentonite-sand mixtures (indirect methods).

5.4.3 Falling head analysis

Hydraulic conductivity was calculated using the standard expression

$$k = \frac{aL}{At} \ln \frac{h_1}{h_2} \qquad 5.24$$

where a = cross-sectional area of burette or standpipe

A = cross-sectional area of soil sample

h_1 = hydraulic head across sample at $t = t_n$

h_2 = hydraulic head across sample at $t = t_{n+1}$ (where n = 0, 1, 2, 3...)

L = length of sample

t = elapsed time

This assumes Darcy's law to be valid, which was considered reasonable from Rowe cell test results (see 5.4.1).

Figure 5.20 presents hydraulic conductivity against time for two 5% bentonite-sand mixtures. Tests were ended when the calculated value was constant, and an average value was taken after the initial large decrease to minimise the scatter in results exhibited over the test period. The results are displayed in table 5.17. A final degree of saturation greater than 100% indicates excess water on the sample on removal from the mould.

Similar behaviour is exhibited by both samples. The hydraulic conductivity decreases with time and reaches an approximately steady value after 130000min (90 days). This is attributed to partial saturation[16] and swelling of the bentonite. Swelling of the bentonite within the sand voids is indicated by the large decrease in hydraulic conductivity at the start of the test. Further decreases are attributed to gradual closure of flow paths. The large increases in hydraulic conductivity at 60000min and 100000min are unknown. However, since the same effect is shown for both samples this suggests either a drastic change in temperature or a fault with the apparatus or readings. The latter two are more likely because there is no significant change in values prior to, and after, the increase and this excludes temperature effects.

5% bentonite-sand mixtures

Test	Sample height (mm)	Clay void ratio	Average k (m/s)	Final S_r (%)
FH2	115.7	8.40	1.86E-10	100
FH1	115.7	8.56	2.39E-10	104

Table 5.17. Hydraulic conductivity of 5% bentonite-sand mixtures (falling head analysis).

5.4.4 Hydraulic conductivity of bentonite-sand mixtures

Terzaghi and Peck (1967) suggest a linear relationship between the logarithm of hydraulic conductivity and the logarithm of void ratio for a particular soil type. Mesri and Olson (1971) have shown such linearity for different clays with different pore fluids (figures 2.11 and 2.12). The Kozeny-Carmen equation (Bear and Verruijt, 1987) is a formula obtained from theoretical derivations of Darcy's law. The hydraulic conductivity is given by

$$k = C_0 \frac{n^3}{(1-n^2)M_s^2} \frac{g}{\upsilon} \qquad 5.25$$

where C_0 is the pore size term, n is the porosity, M_S is the specific surface area of the solid matrix (defined per unit volume of solid), g is the acceleration due to gravity and υ the kinematic viscosity of the pore fluid. Similarly, this equation indicates that the relationship between the logarithm of hydraulic conductivity and the logarithm of void ratio tends to linearity with increasing void ratio for soils of the same type. Figure 5.21 shows hydraulic conductivity data against void ratio on a logarithmic plot. The spatial arrangement of data is essentially reproduced on a logarithmic plot of hydraulic

[16]Since samples were prepared by using the modified Proctor compaction technique and back pressures were not used an initial degree of saturation of approximately 90% is likely.

conductivity against the Kozeny-Carmen porosity term ($n^3/(1 - n^2)$), and this plot is therefore not presented. The best fit line through the data for 100, 20 and 10% bentonite mixtures indicate that these samples are behaving as a single soil type (the pore size term in the Kozeny-Carmen equation is the same), however, the data for the 5% bentonite mixes and sand do not follow the same trend.

For 5% bentonite-sand mixtures, figure 5.21 shows a variation in hydraulic conductivity of 4 orders of magnitude for a void ratio range of 0.4-0.6. The trend in data suggests that the hydraulic conductivity tends to the hydraulic conductivity of the sand as the void ratio increases. Therefore, it can be concluded that non homogeneity exists in 5% mixes. In zones where the bentonite content is less than 5%, the sand voids are likely to contain either free water or very highly swollen bentonite; only slightly reducing the flow compared to flow through sand only. Zones within the sample where the bentonite content is effectively higher than 5% reduce the flow to a greater extent. Therefore, the hydraulic conductivity of a 5% mix overall is less than that of the sand.

The swelling results and the literature suggest the behaviour of bentonite-sand mixtures can be characterised by the clay void ratio. For mixtures having bentonite contents greater than 10%, it is unlikely the clay void ratio will be greater than 10 in practical engineering applications (this corresponds to a vertical effective stress $\leq$ 2kPa). Therefore, the data have been replotted in figure 5.22 on a logarithmic plot of hydraulic conductivity against clay void ratio ($e_c < 10$)[17]. This is justified on the assumption that all the water, hence flow, is associated solely with the bentonite. The 5% bentonite-sand data have been omitted due to the reasons stated above.

The equations of the best fit lines were determined using regression analysis and are as follows:

100%: $k = 10^{-11.07} . e_c^{1.77}$ $(r^2 = 0.76)$ 5.26

20%: $k = 10^{-13.26} . e_c^{3.26}$ $(r^2 = 0.93)$ 5.27

10%: $k = 10^{-14.06} . e_c^{3.65}$ $(r^2 = 0.54)$ 5.28

It is apparent that at a particular clay void ratio the hydraulic conductivity decreases with increasing sand content, and as the clay void ratio increases the hydraulic conductivity of both mixtures tends towards that for bentonite alone. The reasons for this are discussed in chapter 6.

[17]The multi-stage test B1A-B5A is plotted as a single data point. The hydraulic conductivity was taken as the average of all data points.

For 100% bentonite, the largest difference in hydraulic conductivity values between samples with comparable clay void ratios is a factor of 3.5 (D1A and D2A in table 5.9, D2A is the larger of the two). It is possible that test D2A has a higher hydraulic conductivity due to the larger applied hydraulic gradient. However, the opposite behaviour is shown for samples C1A and C2A. It is also thought that any errors in analysis are small, as discussed in 5.4.1, and have no effect on the observed behaviour. A more likely explanation is small differences in fabric of samples which may be quite significant due to the small sample thicknesses (7.1mm to 11.4mm). Any relatively large pore volumes would significantly increase the flow rate as this is proportional to the square of the pore radius. The largest deviation from the best fit line is shown by test D1A. For this sample, the hydraulic conductivity is overestimated by a factor of 2.

20% bentonite mixture data show the best correlation. All the data points lie within a factor of 1.6 of the estimated hydraulic conductivity given by equation 5.27 with the exception of test C20A (the sample with the largest clay void ratio) which deviates from the best fit line by a factor of 2.2. However, this is only of the same order as data from 100% samples. The high coefficient of correlation indicates that reliable values of hydraulic conductivity can be determined by both direct and indirect measurement for 20% mixtures.

The largest amount of scatter is shown in the data from 10% bentonite-sand mixtures and the best fit line given by equation 5.28 has a relatively low coefficient of correlation. The largest deviations from the best fit line are shown for tests 10E4 and 10D4 (indirect method). For these samples the hydraulic conductivity is overestimated by a factor of 3.5. Test C10A (indirect method) lies above the best fit line by a factor of 2.8. For similar clay void ratios, differences in calculated hydraulic conductivity are all less than one order of magnitude. Since data from 20% samples showed that the indirect method is suitable for calculating hydraulic conductivity, it is thought that effects associated with the sample (and not the method) cause the scatter in the 10% mix data.

Laboratory settlement curves for 10% mixtures were not as well defined as for 20% mixtures (as discussed in 5.4.2). An error in construction of such a curve (for example, figures 5.18 and 5.19) not only alters the t_{50} value but also the settlement (hence sample height and void ratio) corresponding to the beginning and end of consolidation, which, in turn affects the calculated c_v and m_v values and ultimately the hydraulic conductivity. Errors of this nature are difficult to quantify because curve fitting by the log-time method or square root-time method is a matter of judgement, and for poorly defined curves the error is likely to increase. Poor definition indicates that interaction between sand

particles is relatively high and therefore the scatter would be expected to increase with increasing applied stress (or decreasing clay void ratio). The results tend to support this. In figure 5.22, differences between measured and estimated hydraulic conductivities decrease as the clay void ratio increases. Therefore, although indirect determination of hydraulic conductivity is believed to be satisfactory for 10% bentonite-sand mixtures, it is thought that scatter in data is increased due to the stiffness of the interacting sand matrix.

The three data points grouped above the best fit line at a clay void ratio of approximately 4.5 were determined from a multi-stage hydraulic conductivity test in the Rowe cell. The data are all within a factor of 2.5 of the anticipated values. Clay void ratio values are calculated by dividing the overall void ratio by the volumetric fraction of dry solids (equation 5.3). Therefore, an error in overall void ratio gives a corresponding error in clay void ratio, which increases with decreasing bentonite content. Another, more likely, cause of scatter is non homogeneity of the sample. Since the measured hydraulic conductivities are higher than the estimated values this assumption is reasonable, because zones within the sample with bentonite contents less than 10% will allow larger flow rates.

The validity of fitting a line to the 10% mix data may seem questionable. However, the analysis conducted on 20% mixtures gave a good correlation over a large clay void ratio and hydraulic conductivity range. The change in hydraulic conductivity with clay void ratio for 10% mixtures showed a similar trend over a similar range, and therefore, conceptually, it is justified to represent this behaviour in the same manner. Further, for engineering approximations the scatter is relatively small (most hydraulic conductivity values are quoted to 1 order of magnitude only). However, use of equations 5.26 to 5.28 may not be appropriate for predictive purposes at clay void ratios outside the limits of the data shown in figure 5.22, because at high clay void ratios the behaviour of mixtures appears to be similar that of bentonite alone (tests 20A and 10A). This is discussed further in chapter 6.

5.5 Strength tests

5.5.1 Introduction and test parameters

This section presents the results of shear tests on sand, bentonite and bentonite-sand mixtures from drained triaxial compression tests and drained shear box tests[18]. Swelling of triaxial samples is also considered and is compared to the one-dimensional swelling of dry mixtures. Finally, the stiffness of bentonite-sand mixtures at small strains is reported. Stiffnesses were calculated from the reload portion of an unload-reload loop during triaxial compression (see 4.5.7).

Peak shear strengths of all samples are represented by the angle of shearing resistance, ϕ'_{max}, at the deviator stress at failure or at 20% axial strain (whichever has the greater value). Assuming no cohesion between particles[19], the Mohr's circle of stress can be used to derive the following expression relating the angle of friction to the principal stresses:

$$\sin\phi' = \frac{\sigma'_1 - \sigma'_3}{\sigma'_1 + \sigma'_3} \qquad 5.29$$

Equation 5.29 was used to calculate the maximum angle of shearing resistance, ϕ'_{max}, in all triaxial compression tests.

For triaxial tests on sand only, Rowe's stress-dilatancy theory was used to determine the constant volume angle of shearing resistance, ϕ'_{cv} (see 2.5.6). Dividing the numerator and denominator of equation 5.29 by σ_3' gives

$$\sin\phi' = \frac{(\sigma'_1/\sigma'_3) - 1}{(\sigma'_1/\sigma'_3) + 1} \qquad 5.30$$

Equation 2.12 (Rowe's stress-dilatancy relation) was used to obtain $(\sigma'_1/\sigma'_3)_{cv}$, this value was substituted into equation 5.30 to give ϕ'_{cv}.

The relative density, I_D, is given by the expression

$$I_D = \frac{e_{max} - e}{e_{max} - e_{min}} \qquad 5.31$$

Values of relative density are presented for tests on sand and discussed further in chapter 6.

---

[18]The bentonite only was tested in the shear box. Production of uniform bentonite triaxial samples was considered impracticable, due to the anticipated large swelling.

[19]The view is taken throughout the text that no cohesion exists between particles and shear strength is determined purely by friction. Apparent cohesion intercepts for clay soils are believed to be caused either by variable dilatancy due to overconsolidation or from pore water pressures which are not accounted for (see chapter 2). Apparent cohesion intercepts for sand are also a result of variable dilatancy. Therefore, linear fitting of failure envelopes on effective stress plots has been conducted with the origin fixed at zero to determine the strength parameter ϕ'.

5.5.2 Strength of sand

Table 5.18 summarises the results of drained (CD) triaxial compression tests on Knapton Quarry sand, and the type of triaxial apparatus used for each test is indicated. Values of the maximum rate of dilation $(-d\varepsilon_V/d\varepsilon_1)_{max}$ are also included. These will be discussed in chapter 6. The peak angle of shearing resistance is shown to vary between 36.5° (test CDS8) and 40.9° (test CDS4), with a general trend of decreasing strength with increasing effective cell pressure, σ'_3. Constant volume angles of shearing resistance (determined by stress-dilatancy theory) have values between 28.9° and 31.8°, and no noticeable trend is evident. Figure 5.23 plots the peak and constant volume strength data from table 5.18 in modified stress space[20]. The strength envelopes were fitted by linear regression analysis (with the origin fixed at zero), and equation 5.29 was used to calculate a peak angle of shearing resistance of 37.5° ($r^2 = 0.998$) and constant volume angle of shearing resistance of 30.4° ($r^2 = 0.998$). Because the constant volume strength cannot be measured, the difference in individual values in table 5.18 is attributed to variable accuracy of stress-dilatancy curves which were used for the analysis.

Observation of figure 5.23 shows that scatter is small, and tests are repeatable for samples at comparable effective cell pressures. In addition, the data indicate that the test type, i.e., constant rate of stress or constant rate of strain, has no effect on the measured peak strength and the calculated constant volume strength. This is important for comparison of bentonite-sand mixtures where 5% mixes where all tested in the Bishop-Wesley stress path cell and all other mixtures in the standard triaxial cell (see chapters 3 and 4). The constant volume angle of shearing resistance is within typical ranges for a quartz sand (e.g., Bolton, 1986). However, the peak strength is lower than is typically found for dense sands. This is discussed further in chapter 6.

Typical plots of deviator stress versus axial strain, volumetric strain versus axial strain, and stress ratio versus dilatancy, for test number CDS8, are displayed in figures 5.24a-5.24c respectively. The gradient of the stress-dilatancy plot, m, is equal to (σ'_1/σ'_3) in Rowe's stress-dilatancy relation (equation 2.12).

Secant stiffnesses, E' (equal to $\Delta\sigma'_D/\Delta\varepsilon_A$), were calculated from the onset of reloading for an axial strain increment of 5E-03. This axial strain increment was selected because the stress-strain curve significantly deviated from linearity at strains greater than this, and there were insufficient data points to calculate stiffness for smaller strains. Generally, stiffness is shown to increase with increasing effective cell pressure, and at comparable

[20]Plotting in modified stress space enables peak and constant volume strength data to be represented by a single data point instead of a Mohr's circle.

cell pressures it appears that stiffnesses measured by constant rate of stress testing are greater than for constant rate of strain testing. It is proposed that in constant rate of stress testing the sand skeleton compresses (rather than individual particles shearing) at small strains because the sample is held under constant stress conditions for relatively long time periods when the frequency of loading pulses is low. This is analogous to the hardening of clay samples in compression tests after primary consolidation has occurred. Unload-reload loops were not conducted for tests CDS8 and CDS12 (both at 200kPa effective cell pressure). The stiffness of sample CDS8 is shown to be significantly lower than other samples at the same cell pressure. This indicates that stiffness increases for a previously unloaded sample at small strains on reloading. However, the stiffness of sample CDS12 has the largest value, which is consistent with the behaviour of other samples tested under a constant rate of stress.

Test	σ'_3 (kPa)	$\sigma'_1-\sigma'_3$ max. (kPa)	e_0	I_D	ϕ'_{max} (°)	ϕ'_{cv} (°)	$\left(-\frac{d\varepsilon_v}{d\varepsilon_1}\right)_{max}$	E' (MPa)
CDS1[+]	51	169	0.74	0.46	38.6	28.9	0.404	30.9
CDS2[x]	51	170	0.68	0.56	38.7	-	0.359	15.3
CDS3[x]	51	176	0.68	0.56	39.3	30.9	0.446	18.1
CDS4[+]	52	197	0.74	0.46	40.9	-	0.576	32.2
CDS5[x]	87	264	0.66	0.60	37.1	29.0	0.495	39.1
CDS6[+]	101	343	0.73	0.47	39.0	29.6	0.425	56.9
CDS7[+]	101	350	0.71	0.52	39.4	29.5	0.516	66.9
CDS8[x]	200	588	0.66	0.60	36.5	31.8	0.347	22.7
CDS9[x]	200	602	0.65	0.62	36.9	30.3	0.374	76.3
CDS10[x]	201	602	0.66	0.60	36.8	29.7	0.392	71.3
CDS11[x]	201	617	0.67	0.59	37.3	30.2	0.426	60.0
CDS12[+]	203	697	0.72	0.49	39.2	30.0	0.407	114.8
CDS13[x]	300	900	0.68	0.56	36.9	30.4	-	82.4

[x] Standard triaxial cell.
[+] Stress path triaxial cell.

Table 5.18. Consolidated drained triaxial compression test results for sand.

5.5.3 Strength of bentonite

Figure 5.25 shows the failure envelope for a multi-stage consolidated drained shear box test (strain rate = 0.00064mm/min.) on bentonite swollen from its dry state. The measured shear force causing failure, at each vertical effective stress, was corrected for ram friction which was found to have a constant value of 11N. A best fit envelope was produced by linear regression analysis (with the origin fixed at zero), giving a maximum angle of shearing resistance of 9.8° ($r^2 = 0.874$).

Corrected results of individual shearing stages are given in table 5.19. At an applied stress of 50kPa, the measured shear strength is significantly higher than at the two previous stresses and the angle of shearing resistance is shown to increase by approximately 6°. A best fit line through the data (without fixing the origin) gives a maximum angle of shearing resistance of 8° and an apparent cohesion value of 5kPa. The method of parabolic isochrones (Bolton, 1979) was used to determine the maximum pore pressure throughout the test, u_{max}, which corresponds to the maximum rate of volume change. The values given in table 5.19 do not account for the apparent cohesion intercept. In fact, since pore water pressures are positive, data points will be shifted to the left in figure 5.25 which gives a higher value of vertical effective stress and increases the differences in strength. As it is believed that any contribution from 'true' cohesion is minor, the increased strength is attributed to an effect similar to overconsolidation. This is discussed further in chapter 6.

Table 5.19 shows that there is relatively little increase in height (or clay void ratio) of the sample after successive swelling stages. This implies that the behaviour of the sample during incremental unloading is not described by the bentonite swelling line, and there is no significant movement of the shear plane from the centre of the shear box.
Throughout the test period, a loss of material from the shear box was observed. From the end of test parameters a loss in dry solids of 15g was calculated and the final clay void ratio was calculated as 2.58[21]. Therefore, the actual clay void ratios of the samples at swelling equilibrium under vertical effective stresses of 100kPa and 50kPa are likely to be much higher than reported. The final clay void ratio calculated from the end of test parameters lies within the scatter of the data from 100% bentonite swelling tests. In addition, it was shown in 5.3.2 that the swelling of an incrementally unloaded sample is given by the bentonite swelling line (test 100A in table 5.2). If the shear plane was effectively located at the centre of the shear box it is reasonable to assume that the measured strength would decrease with consecutive shearing stages due to alignment of clay particles. This is contrary to the behaviour. Therefore, it is likely that the shear

[21]This is the void ratio after shearing, not at swelling equilibrium.

plane moved far enough up the box during swelling to have a relatively small effect on the subsequent shearing stage.

The final degree of saturation of the sample was calculated as 107%, this is consistent with moisture being drawn into the sample on unloading.

Stage No.	σ'_v (kPa)	τ_{max} (kPa)	h_0 (mm)	e_0	e_1	u_{max} (kPa)	ϕ'_{max} (°)
1	200	34	21.1	1.681	1.668	0.6	9.6
2	100	16	22.6	1.871	1.857	1.0	9.1
3	50	14	23.6	1.994	1.968	1.1	15.7

Table 5.19. Consolidated drained direct shear test results for bentonite.

For stress-dilatancy analysis of shear box data, Taylor's flow rule (see 2.5.6) can be expressed in the form

$$(\tau/\sigma'_v) = \mu + \tan\psi \qquad 5.32$$

where $\mu = \tan\phi'_{cv}$

$\tan\psi = (dy/dx) =$ (vertical displacement/horizontal displacement)

Figure 5.26 shows a plot of stress ratio, (τ/σ'_v), versus dilatancy, ψ, using data from direct shear tests on bentonite. Although the scatter is very large, two distinct trends are shown between data at 50kPa vertical effective stress and the data from stages 1&2 combined. For stages 1 and 2 the best fit line yields a μ value of 0.168 at zero dilatancy, corresponding to a constant volume angle of shearing resistance of 9.5°. For stage 3, ϕ'_{cv} is calculated as 15.4°. These values correspond with data presented in table 5.19 and give further indication of the different shear behaviour at 50kPa vertical effective stress.

Equation 5.32 is derived by considering an element of soil in simple shear and therefore its application to direct shear data may be questionable due to the mechanism of failure imposed on the sample. However, according to Jewell (1989) the relations of Rowe (1969) and Taylor's flow rule are very similar, and since Rowe's stress-dilatancy relation accounts for positive and negative dilatancies, it was thought reasonable to apply a stress-dilatancy analysis to direct shear tests on bentonite. The agreement between strengths measured both directly and indirectly also show that the use of Taylor's flow rule is reasonable.

5.5.4 Strength of bentonite - sand mixtures

Presented in tables 5.20-5.22 are the relevant parameters for the analysis[22] of consolidated drained triaxial compression tests on bentonite-sand mixtures and one consolidated undrained test with pore water pressure measurement (CU101) on a 10% bentonite-sand mixture. All 5% bentonite-sand samples were tested in the Bishop-Wesley cell, and the remaining tests were conducted in the standard triaxial cell (see 4.5.1). Comparison of strength data was considered reasonable, since the maximum angles of shearing resistance of sand in triaxial compression in both cell types were approximately equal (see 5.5.2).

Generally, the maximum angle of shearing resistance is shown to increase with decreasing clay content, suggesting greater interaction between sand particles. Values of ϕ'_{max} for 20% mixtures are typical of loose sands (or stiff clays) and 5% mixtures have strengths typical of dense sands, and the strength of 10% mixtures is intermediate. The axial strain required to mobilise the peak strength is shown to increase with decreasing effective cell pressure for 20% and 10% mixtures. This is consistent with the swelling behaviour of mixtures which implies a more clay type behaviour at low stresses. Axial strains at peak strength for 5% mixes are all similar indicating that the material behaves essentially as sand during shear. This is confirmed by the range of sand void ratio values, e_S. As the sand void ratio decreases the strength increases, and for all mixtures the strength behaviour appears to become more characteristic of sand as the clay void ratio increases[23]. Further indication of changes in material behaviour with clay content and effective stress is provided by the volumetric strains at peak strength, which are shown to alter from negative values (dilation) to positive values (compression) with decreasing effective cell pressure for 20% and 10% mixtures.

Final degrees of saturation and B-values prior to shearing indicate that samples were at or near to full saturation during the tests. The lowest values for all three mixes were calculated at the highest confining stress. This is consistent with data from Black and Lee (1973) who showed that for stiff soils a B-value of 1.0 is theoretically impossible to obtain. In undrained testing, the presence of air in the sample or drainage lines can have a serious effect on the pore pressure response and as a consequence an analysis of data in effective stress terms may lead to large inaccuracies. However, full saturation is not as critical in drained testing because the excess pore water pressure is equal to zero and small air bubbles trapped within the sample are unlikely to escape due to the confinement imposed by the soil particles and the applied back pressure. Within the expected

[22] Analysis of strength data for mixtures is conducted in chapter 6.

[23] This may not be true for mixtures containing higher percentages of bentonite, where there is relatively little interaction between sand particles.

accuracy of pressure measuring instrumentation, B-values may be ±0.04 of the values quoted.

Figures 5.27-5.30 are examples of typical deviator stress versus axial strain curves and volumetric strain versus axial strain curves for 20%, 10% and 5% bentonite-sand mixtures (tests CD201, CD104 and CD55). Figure 5.29b shows the pore pressure versus axial strain curve for the consolidated undrained test (CU101) on a 10% bentonite-sand mixture. In figure 5.27, the stress-strain behaviour of a 20% mix at 200kPa effective cell pressure has characteristics generally associated with the behaviour of sand, i.e., the sample dilates during shear to until the peak strength is mobilised, after which the rate of dilation and strength decreases. In figure 5.28, the initial behaviour is more characteristic of clay, indicated by a positive volumetric strain and shallower stress-strain curve. Therefore, although the sand content is greater, its effects on the shear behaviour are less. At an effective cell pressure of 25kPa, the swelling of the 10% mix is such that there is less interaction between the sand particles than the 20% mix at 200kPa cell pressure, thus accounting for the different shearing characteristics. This further illustrates the effects of bentonite content and effective cell pressure on the shear behaviour of bentonite-sand mixtures. Further discussion and analysis of triaxial strength data is given in chapter 6.

Test periods were extensive (up to 10 weeks), therefore the amount of raw data was reduced by stripping the data files of a number of data points in every ten (dependent on the initial file size). The remaining data was smoothed by a running average to minimise the scatter caused by changes in temperature and electrical noise of the transducers and data acquisition unit[24]. The smoothed data was used to plot the laboratory curves and to calculate values of maximum deviator stress (hence peak strength).

For a conservative interpretation of results the expected accuracy of transducers quoted in chapter 3 (table 3.1) is assumed; not the apparent increased accuracy given by smoothing of data. Because the accuracy has a fixed value, the error in measured deviator stress increases as its value decreases. This is evident in figures 5.27-5.30. The scatter is more noticeable for weaker samples and lower cell pressures and is most pronounced in figure 5.28a. In figure 5.29a, the variation in deviator stress is less because the test was conducted over a much shorter time period, and therefore, changes in transducer readings with temperature are not as large. Despite these variations, the

[24]In chapter 3, diurnal changes in temperature were shown have a greater effect on the stability of transducers than electrical noise (see figures 3.7a and 3.7b)

errors in the calculated angle of shearing resistance associated with drift of transducers are small, and are expected to be within ±1° (this is discussed further in chapter 6).

A. 20% bentonite - sand mixtures

Test	σ'_3 (kPa) eqm.	e_c	e_s	B value	σ'_3 (kPa) peak	σ'_D max. (kPa)	ε_A peak (%)	ε_V peak (%)	ϕ'_{max} (°)	S_r (%)
CD201	200	2.222	0.727	0.59	195	373	8.8	-4.3	29.3	101
CD202	100	2.439	0.860	0.92	99	208	10.1	-3.0	30.8	99
CD203	50	3.034	1.009	0.98	47	80	19.0	2.9	27.4	99
CD204	25	3.903	1.226	0.98	21	46	15.4	3.8	31.5	101

Table 5.20. Consolidated drained triaxial compression tests results for 20% bentonite-sand mixtures.

B. 10% bentonite - sand mixtures

Test	σ'_3 (kPa) eqm.	e_c	e_s	B value	σ'_3 (kPa) peak	σ'_D max. (kPa)	ε_A peak (%)	ε_V peak (%)	ϕ'_{max} (°)	S_r (%)
CD101	200	3.678	0.520	0.69	197	807	4.7	-0.8	42.2	98
CD102	100	4.105	0.567	0.98	98	460	2.3	-0.9	44.5	99
CD103	50	3.957	0.551	1.00	50	269	4.8	-2.9	46.8	101
CD104	25	5.002	0.667	0.98	24	89	8.8	1.9	40.5	100
CU101	15CU	5.266	0.696	1.00	15	49	8.3	-	38.3	97

Table 5.21. Consolidated drained and consolidated undrained triaxial compression test results for 10% bentonite-sand mixtures.

C. 5% bentonite - sand mixtures

Test	σ'_3 (kPa) eqm.	e_c	e_s	B value	σ'_3 (kPa) peak	σ'_D max. (kPa)	ε_A peak (%)	ε_V peak (%)	ϕ'_{max} (°)	S_r (%)
CD51	200	8.348	0.492	0.12	187	983	4.2	-1.9	46.4	95
CD52	100	8.166	0.482	0.96	103	473	4.0	-1.8	44.2	94
CD53	100	8.458	0.498	0.93	103	558	4.0	-2.5	46.9	101
CD54	50	7.606	0.452	1.00	51	253	5.4	-3.0	45.5	96
CD55	25	8.058	0.476	1.00	25	156	4.6	-3.1	49.2	94
CD56	25	7.650	0.455	0.98	25	143	3.8	-2.6	47.8	100

Table 5.22. Consolidated drained triaxial compression tests results for 5% bentonite-sand mixtures.

5.5.5 Analysis of triaxial swelling data

The initial clay void ratios (e_c initial) at equilibrium conditions immediately prior to shearing are given in tables 5.20-5.22. These values are plotted against the logarithm of effective cell pressure (σ'_3) in figure 5.31, superimposed on the idealised swelling behaviour of 100% bentonite from one-dimensional swelling tests[25]. Included in the figure are equilibrium clay void ratios from triaxial permeameter tests (Q1A-Q4A, from table 5.12). Since the cell pressure is the only stress acting on the samples at this stage, the plot would be identical in e_c - log p' space, where p' is the mean effective stress.

In one-dimensional consolidation, and therefore swelling, the horizontal effective stress (σ'_h) will vary with the vertical effective stress (σ'_v) such that the horizontal strain, ε_h, is zero. The relationship between σ'_h and σ'_v is written

$$\sigma'_h = K\sigma'_v \qquad 5.33$$

where K is an earth pressure coefficient dependent on the state of straining of the soil. Hence, if K were known for one-dimensional swelling of 100% bentonite, the stress invariant p' could be calculated using the following relationship

$$p' = 1/3\sigma'_v(1+2K) \qquad 5.34$$

thus enabling representation of bentonite swelling in e_c - log p' space.

It is reasonable to assume that the normal consolidation lines for one-dimensional and isotropic compression (and all one-dimensional and isotropic rebound lines) are parallel in semi-logarithmic space (e.g. Atkinson and Bransby, 1978). Therefore, it seems reasonable to assume that one-dimensional and isotropic swelling lines for 100% bentonite will also be parallel on a plot of void ratio against the logarithm of mean effective stress, provided there is no previous consolidation stage[26]. None of the triaxial samples were subject to consolidation at any stage in their stress history. The final state of triaxial samples is therefore assumed to be described by an isotropic swelling line.

Because the one-dimensional and isotropic bentonite swelling lines are assumed parallel, the gradient of either swelling line is constant whichever value K is assigned[27]. Therefore, evaluation of K is unnecessary. To position the 100% bentonite isotropic swelling line, data are required from the swelling stages of triaxial samples which have no

---

[25]It is incorrect to superimpose one dimensional swelling behaviour on a plot of this type, because the vertical effective stress cannot be directly substituted for the effective cell pressure. However, for differentiating between one-dimensional and isotropic swelling data this error is ignored.

[26]The volume change behaviour of bentonite showed that initially dry samples swell to reach a point on the bentonite swelling line, depending on the applied vertical effective stress. A subsequent reduction in stress results in further swelling along the bentonite swelling line. However, loading a sample after a previous swelling stage causes volume change behaviour which is described by a rebound line.

[27]The analysis assumes K is constant during swelling.

sand in contact at equilibrium. Samples of this nature achieve the same final clay void ratio as bentonite alone, hence, will lie on the 100% bentonite isotropic swelling line. This assumption is justified by the behaviour exhibited in one-dimensional swelling of initially dry samples. Below the respective threshold stress, these mixtures swell to the same final clay void ratio as 100% bentonite (see 5.3.4).

Considering the phase model described in 5.3.1 and by use of equation 5.4, the initial void ratio of the sand, e_S, can be calculated. The maximum void ratio of the sand alone was found to be 0.978 (see chapter 3). A value greater than 0.978 will be assumed to indicate no interaction between sand particles, and swelling in the same manner as 100% bentonite. Sand void ratios of triaxial samples prior to shear testing are given in tables 5.20-5.22. It is apparent that only 20% bentonite-sand mixtures at cell pressures of 50kPa and 25kPa (CD203 and CD204) have no sand particles in contact prior to shear testing.

It is assumed, albeit from two data points, that the 20% bentonite-sand mixtures at low effective stresses lie on a bentonite isotropic swelling line parallel to the one-dimensional line drawn in figure 5.31. Since the gradient of the one-dimensional swelling line is known (see 5.3.4), a line with the same gradient was fitted as described in section 5.3.4, and appendix 5, to give the equation of the bentonite isotropic swelling line as

$$e_C = 10.55 - 4.57 \log p' \qquad 5.35$$

this is illustrated in figure 5.32. Also shown in the figure are the final clay void ratios of all triaxial samples at swelling equilibrium.

Figures 5.32 and 5.5 show that isotropic and one-dimensional swelling of bentonite-sand mixtures is similar both in data trends and spatial arrangement in semi-logarithmic space. Deviations from the bentonite isotropic swelling line are shown to increase with decreasing bentonite content and, for 20% and 10% mixtures, the clay void ratio increases with decreasing mean effective stress. The data for 5% mixes shows the opposite trend to the expected behaviour, i.e., the clay void ratio decreases with decreasing mean effective stress. As before, this is attributed to non homogeneity of this mixture.

The isotropic swelling line indicates a clay void ratio of zero at approximately 200kPa mean effective stress for 100% bentonite. Therefore, its use in predicting void ratios for pure bentonite samples at cell pressures greater than 100kPa may be highly inappropriate. However, conceptually it is very useful for interpreting the isotropic swelling behaviour of bentonite-sand mixtures, in that an indication of the proposed

change from sand to clay behaviour is given. This is of fundamental importance when considering the strength of mixtures. Further discussion is given in chapter 6.

5.5.6 Stiffness of bentonite - sand mixtures

Secant stiffnesses were determined from the onset of reloading for axial strain increments of 0.1%, 0.2%, 0.5% and 1%. The drained stiffness ,E', or the undrained stiffness, E_u, is equal to $\Delta\sigma_D'/\Delta\varepsilon_A$. Results are presented in table 5.23. For a particular mix, stiffness is shown to increase with increasing cell pressure, for each axial strain increment. The change in the stress-strain behaviour from clay to sand (discussed in 5.5.4) is implied by the general decrease in stiffness with increasing bentonite content, and for most samples, E' decreases as the axial strain increases.

The calculated values at 0.5% axial strain can be compared with sand data to give an indication of the behaviour of the mix. Data for 20% mixes are all approximately four times lower than that calculated for sand alone at comparable effective cell pressures, indicating a more clay type behaviour, whereas 10% and 5% mixtures[28] (with three exceptions) have approximately the same stiffness values as calculated for sand. Tests CD104 and CU101 have stiffness values similar to 20% mixtures. This is interpreted as meaning that the shear behaviour is more characteristic of clay for the two lowest effective cell pressures. Values of E' calculated for test CD54 significantly deviate from other 5% mixtures at all axial strains. The most likely explanation is softening at the ends of the sample either during removal from the saturation cell or during assembly of the test apparatus. In figures 5.33a to 5.33d the stiffnesses for the mixtures at the four axial strains are individually presented. More clearly defined trends (as discussed above) are apparent as the axial strain increases. This is attributed to the accuracy of both the displacement transducers and load cells. Displacement measurement is believed to be accurate to within ±0.01mm, and load measurement to within ±2N (which is approximately equal to a deviator stress of ±2kPa). Therefore, as the axial strain and deviator stress increments decrease the error increases. Using these values, the expected accuracy of stiffness measurement is ±2MPa. This value is seen to be higher than some of the reported stiffnesses in table 5.23. Therefore, at small strains, it appears that only a qualitative interpretation of data is valid.

[28] 10% mixtures were tested in a standard triaxial cell, and are therefore compared to sand tested in the same cell. The same applies for 5% mixtures and sand tested in the Bishop-Wesley cell.

Test	% bentonite	σ'_3 (kPa)	E' (MPa) $\varepsilon_A = 0.1\%$	E' (MPa) $\varepsilon_A = 0.2\%$	E' (MPa) $\varepsilon_A = 0.5\%$	E' (MPa) $\varepsilon_A = 1\%$
CD201	20	200	33.1	38.4	22.8	14.2
CD202	20	100	21.1	14.1	12.4	7.7
CD203	20	50	13.1	9.9	5.4	2.7
CD204	20	25	-	1.6	1.1	1.1
CD101	10	200	39.9	36.4	88.9	60.2
CD102	10	100	12.4	9.5	32.9	37.5
CD103	10	50	7.4	16.5	27.8	19.4
CD104	10	25	9.6	7.0	4.5	2.5
CU101	10	15	$E_u = 3.2$	$E_u = 2.4$	$E_u = 1.3$	$E_u = 1.4$
CD51	5	200	274.8	167.4	115.3	59.4
CD52	5	100	141.0	113.3	66.1	28.6
CD53	5	100	95.7	107.7	72.7	36.9
CD54	5	50	18.3	19.8	17.8	14.4
CD55	5	25	29.9	25.5	19.1	10.6
CD56	5	25	10.4	14.8	14.2	8.1

Table 5.23. Stiffness of bentonite-sand mixtures in triaxial compression.

5.6 Summary and conclusions

One-dimensional and isotropic swelling data of bentonite and bentonite-sand mixtures has been presented. It appears that the data is best characterised by plotting the clay void ratio against the vertical effective stress (or mean effective stress) in semi-logarithmic space. One-dimensional and isotropic bentonite swelling lines have been proposed. Above a threshold stress, the swelling of mixtures has been shown to be of a different nature than for bentonite alone. This is believed to indicate a change in material properties from clay type behaviour to a behaviour more characteristic of sand. The importance of stress path and stress history has been described.

The clay void ratio has been shown to be useful in describing the hydraulic conductivity data. Hydraulic conductivity decreases with decreasing clay void ratio (for all mixtures) and increasing sand content for 20% and 10% mixtures. Large changes in hydraulic conductivity of 5% mixes for relatively small changes in clay void ratio are attributed to non homogeneity of the mix. Predictive equations for 100% bentonite, and 20% and 10% mixes have been presented.

Strength and stiffness of bentonite-sand mixtures decreases with increasing clay content. This is believed to be dependent on the swelling behaviour which determines the packing of the sand, hence, the interaction of particles during shearing. As the angle of shearing resistance of bentonite alone is small, the effect of the bentonite on the shear behaviour of mixtures is also expected to be small when sand particles are in contact.

A further discussion and analysis of data is given in chapter 6.

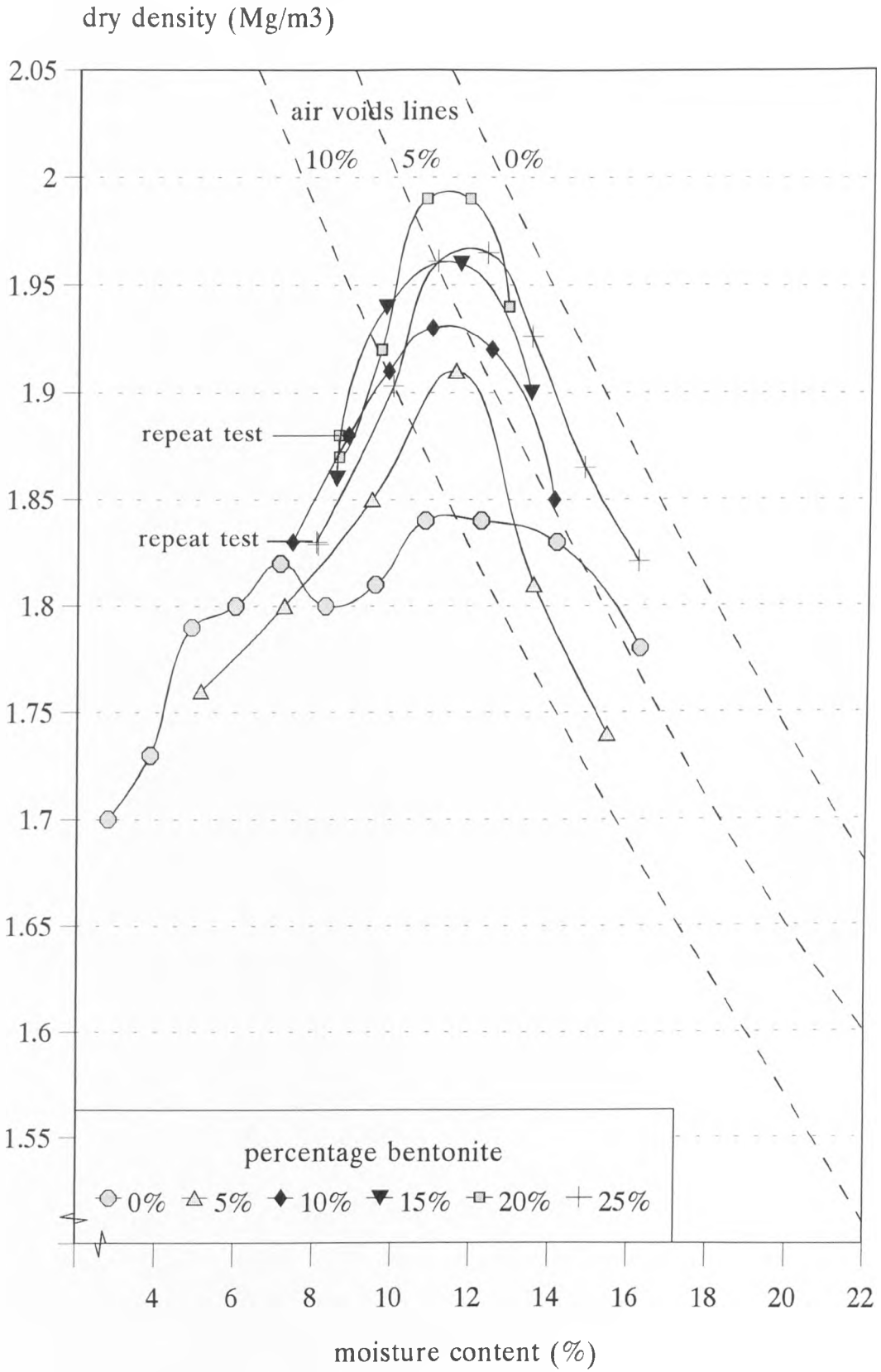

Figure 5.1: Modified Proctor compaction curves for bentonite-sand mixtures.

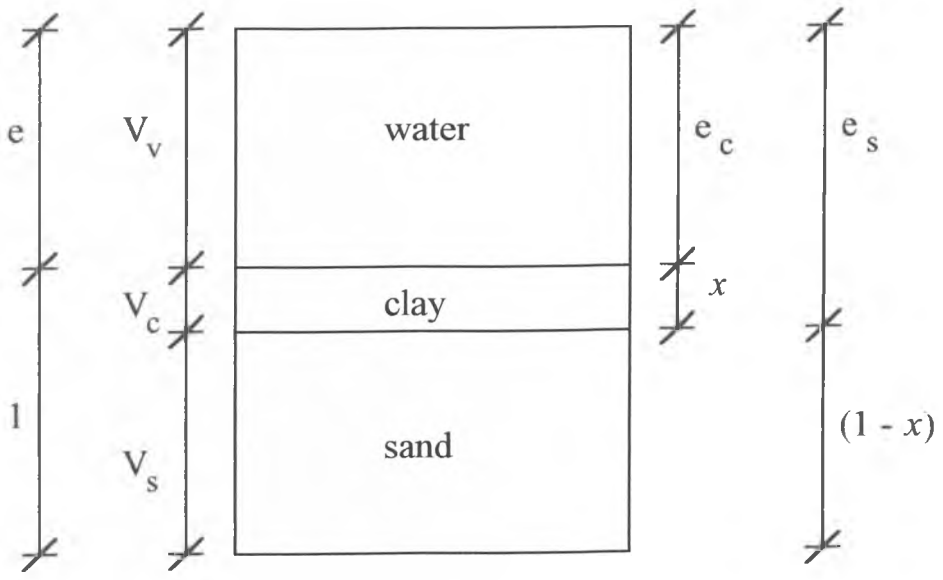

Figure 5.2: Phase diagram of a bentonite-sand mixture.

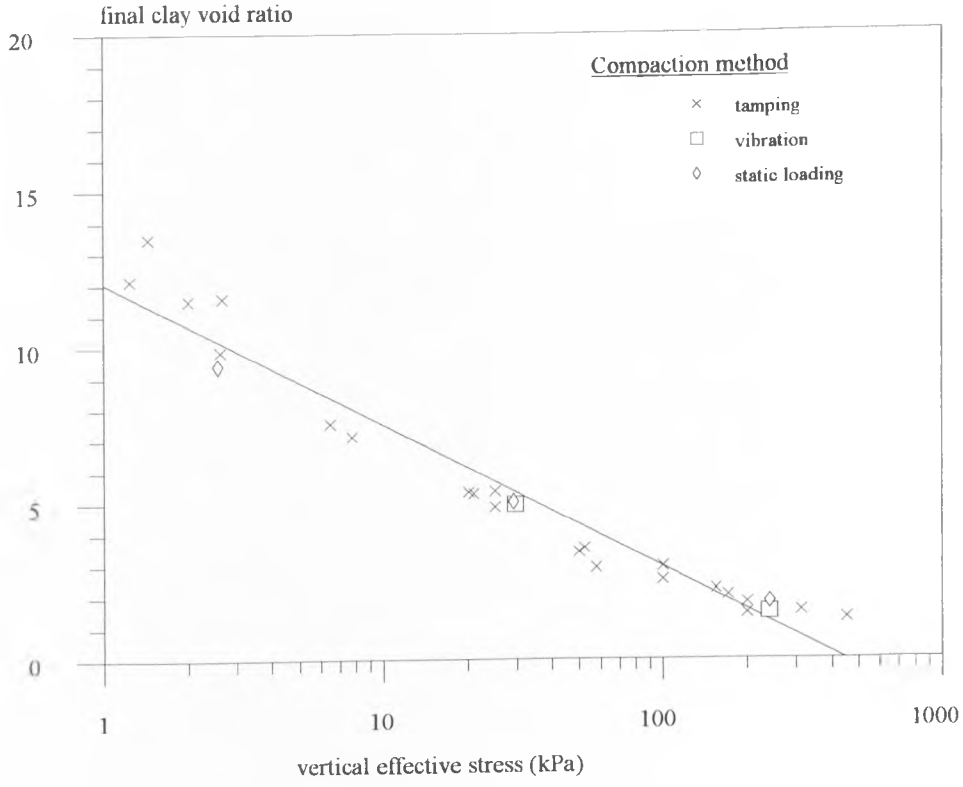

Figure 5.3: Swelling of bentonite powder.

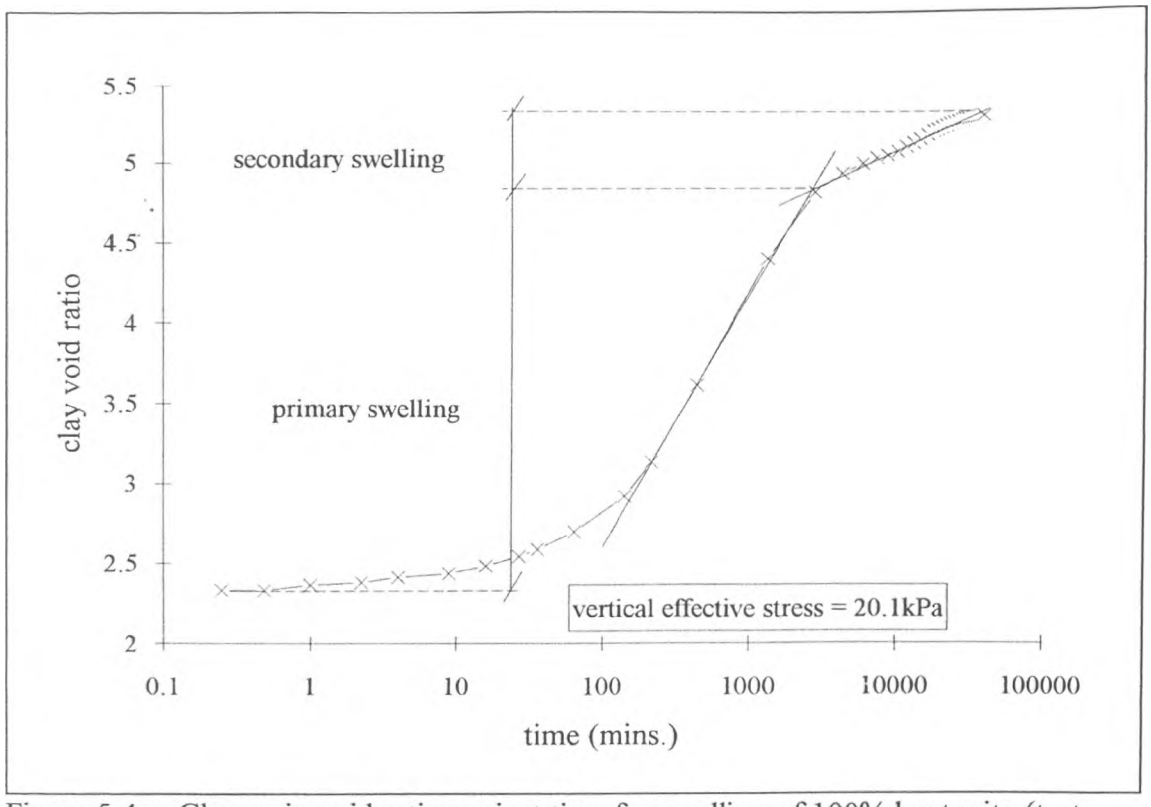

Figure 5.4a: Change in void ratio against time for swelling of 100% bentonite (test 100L8).

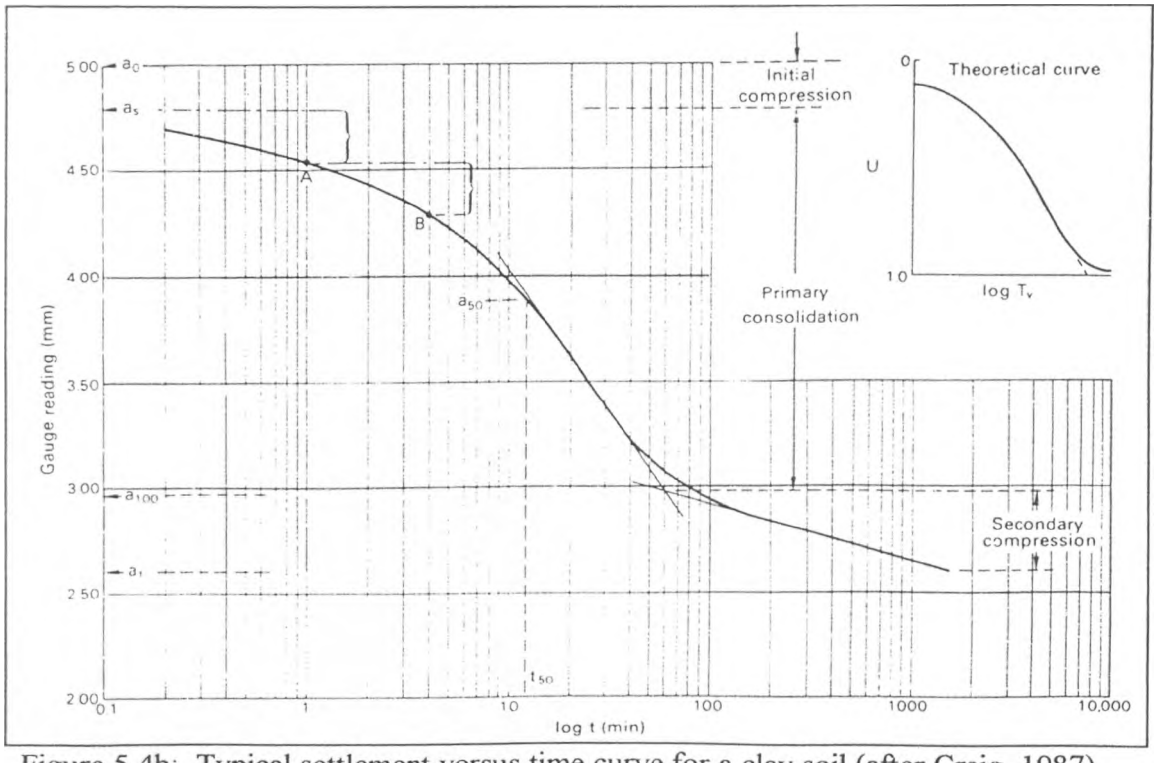

Figure 5.4b: Typical settlement versus time curve for a clay soil (after Craig, 1987).

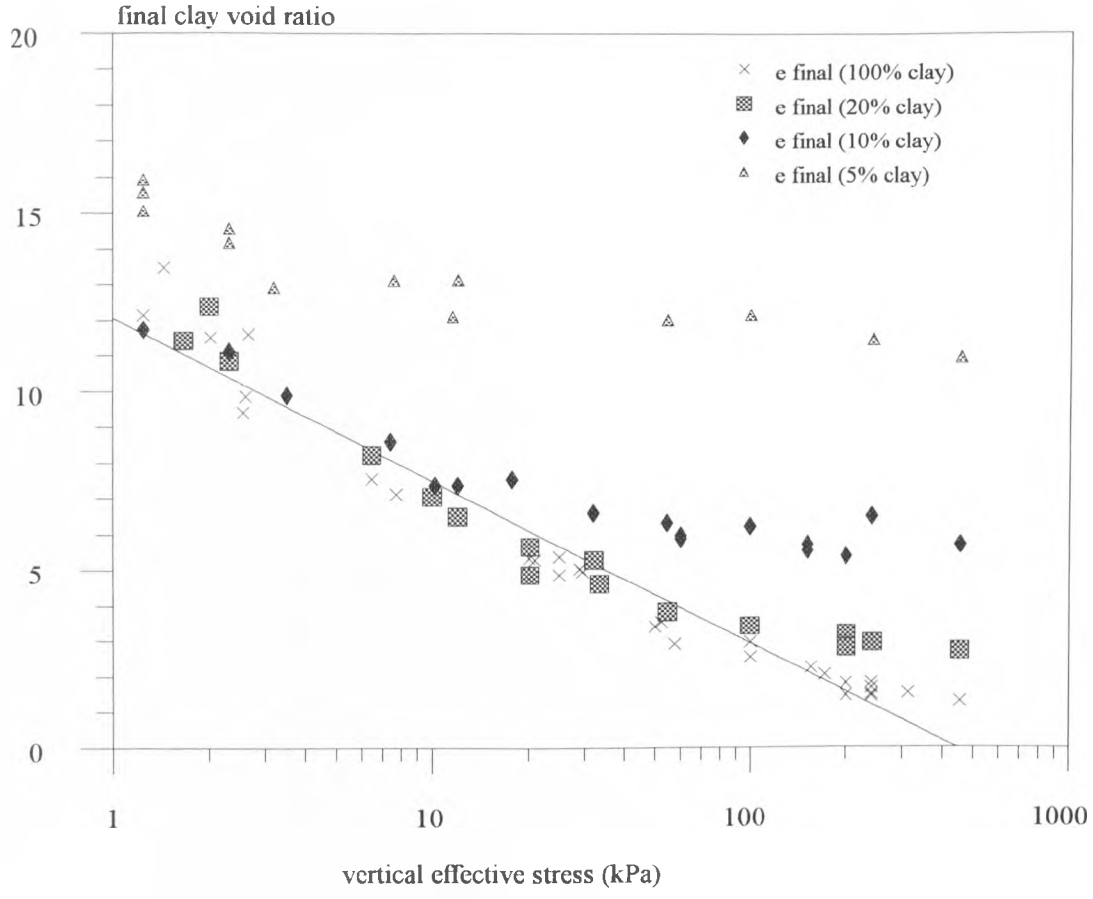

Figure 5.5: Swelling of bentonite-sand mixtures

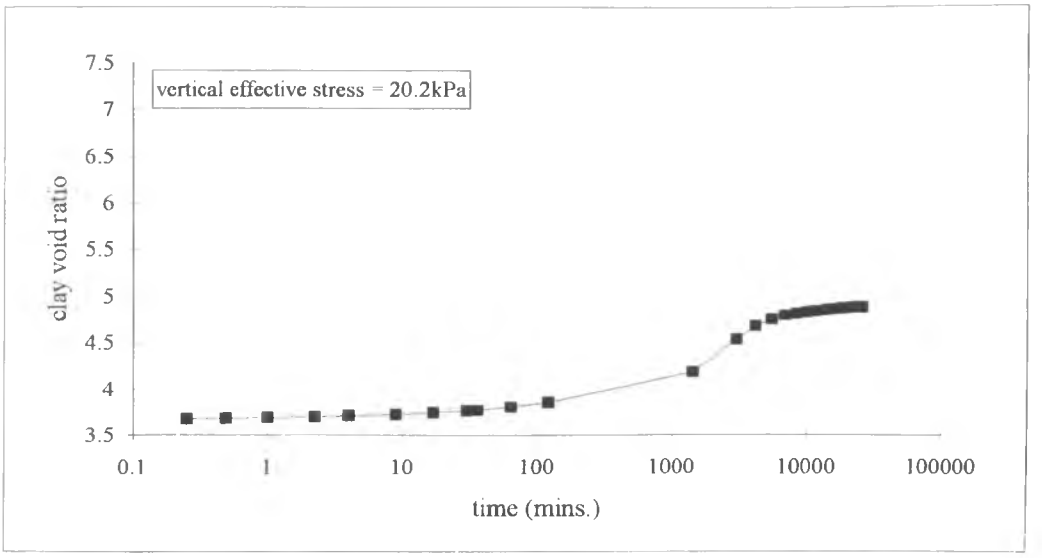

Figure 5.6: Change in clay void ratio against time for swelling of a 20% bentonite-sand mixture.

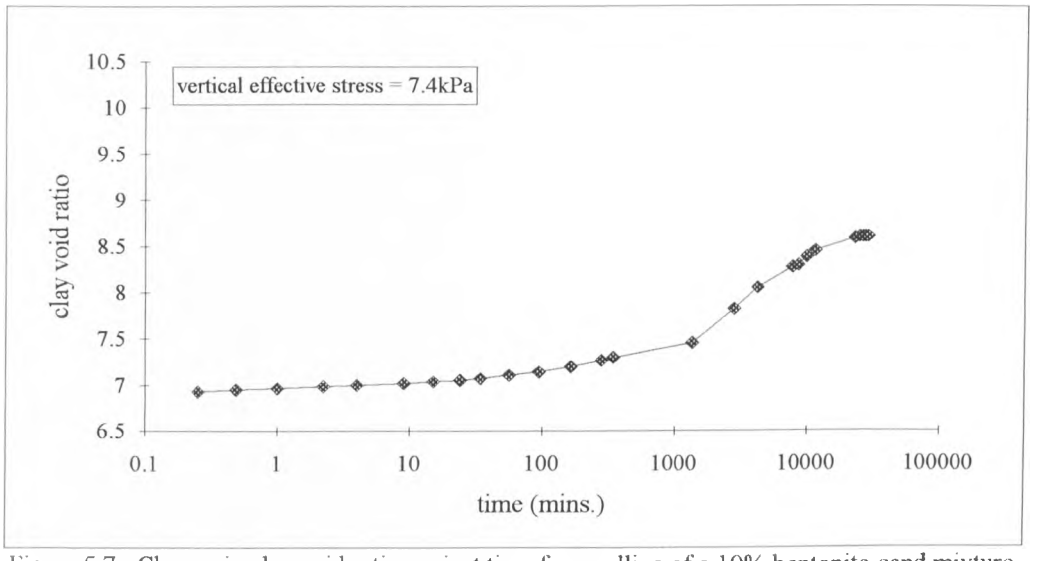

Figure 5.7: Change in clay void ratio against time for swelling of a 10% bentonite-sand mixture.

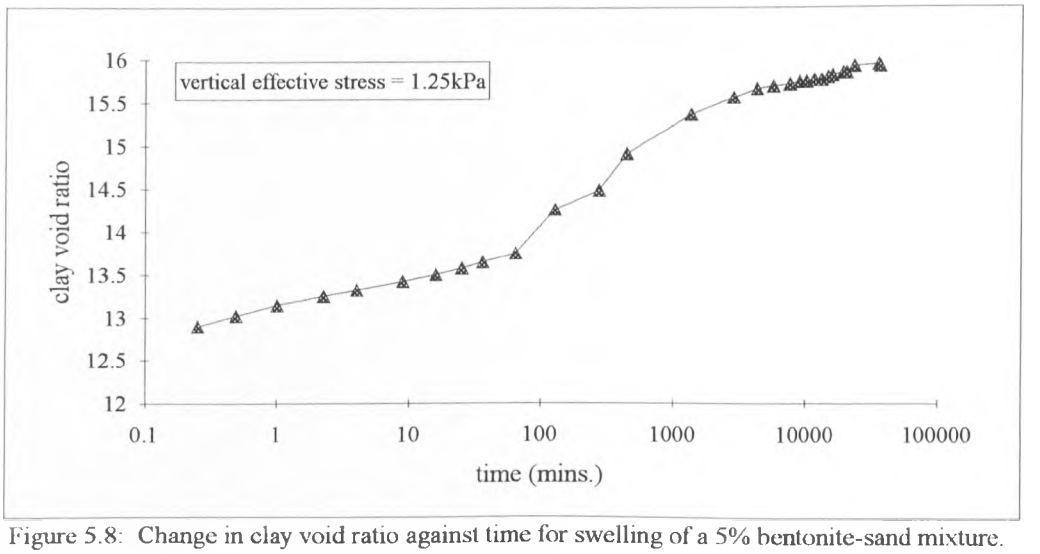

Figure 5.8: Change in clay void ratio against time for swelling of a 5% bentonite-sand mixture.

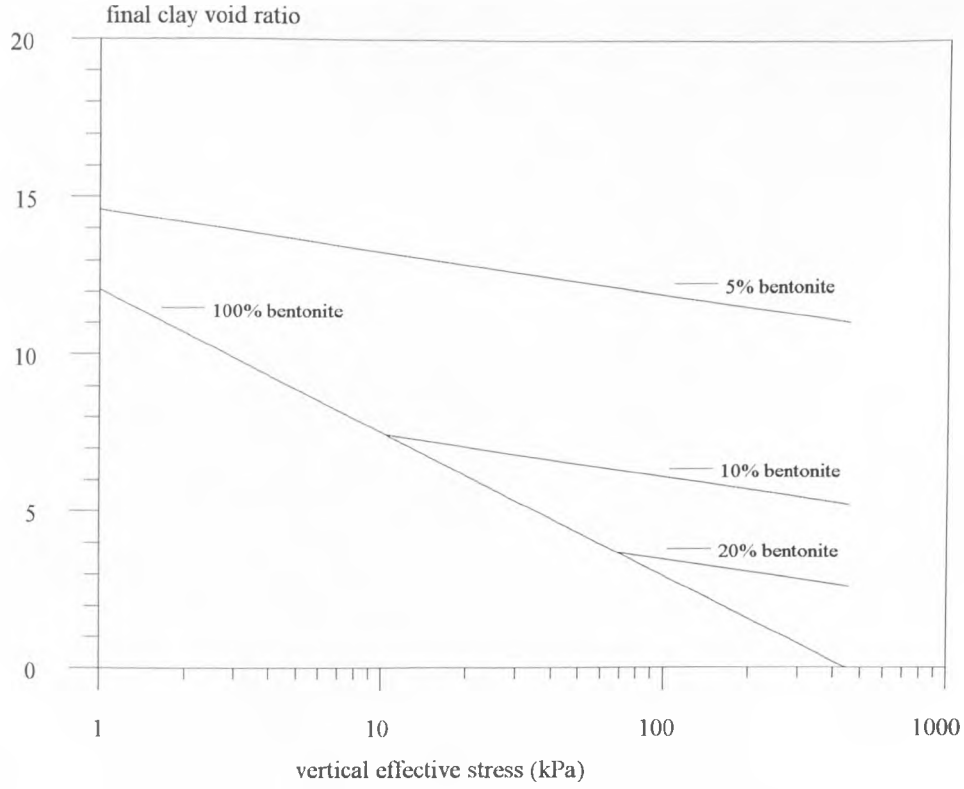

Figure 5.9: Idealised swelling behaviour of bentonite-sand mixtures.

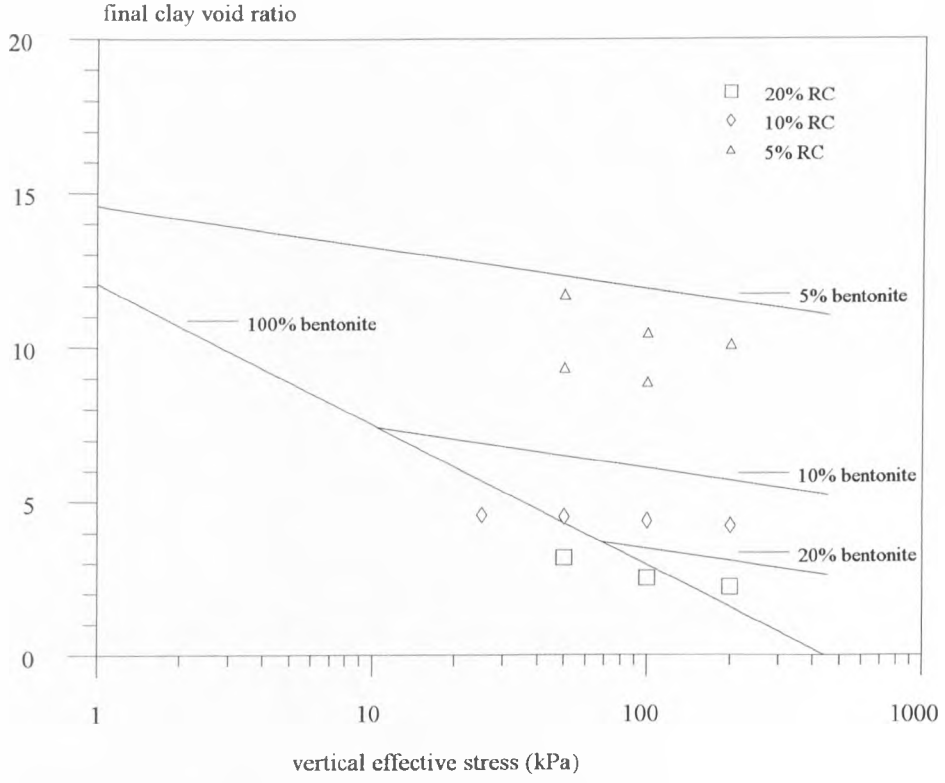

Figure 5.10: Swelling of bentonite-sand mixtures compacted by the modified Proctor method into the Rowe cell (RC).

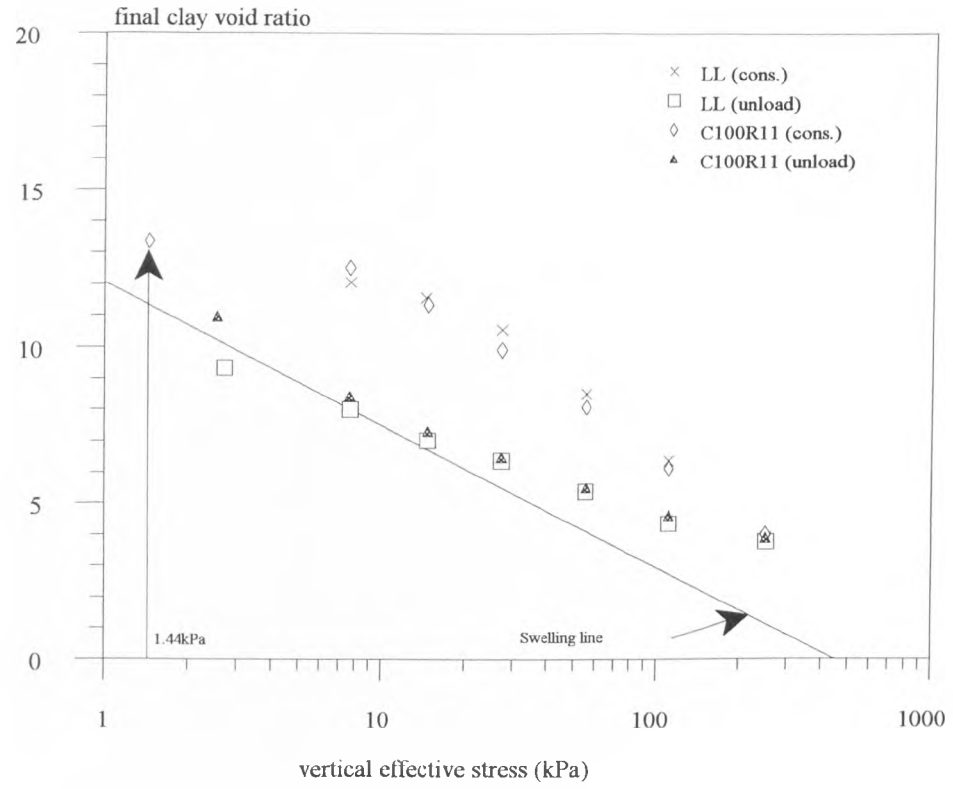

Figure 5.11: Normal consolidation and rebound of bentonite mixed at the liquid limit and bentonite swollen under 1.44kPa vertical effective stress.

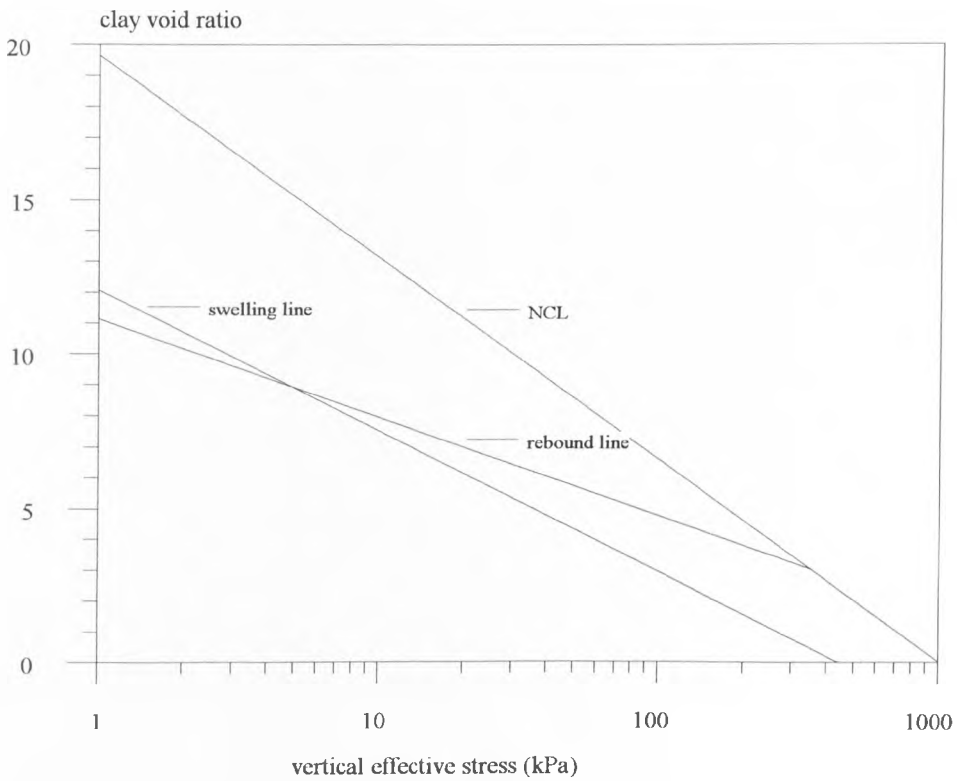

Figure 5.12: Idealised swelling, normal consolidation and rebound lines (100% bentonite).

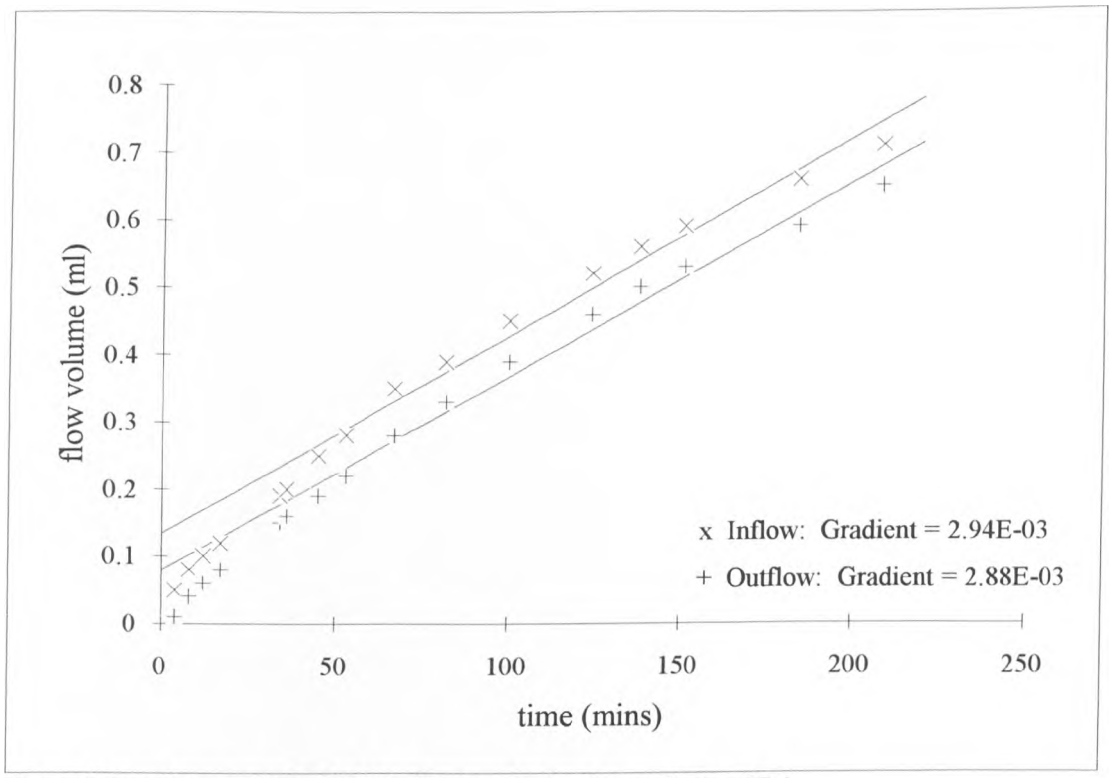

Note: 75mm Rowe cell (test G1A). Average hydraulic gradient = 57.4.

Figure 5.13: Inflow and outflow volumes against time for a 100% bentonite mixture at 25kPa vertical effective stress.

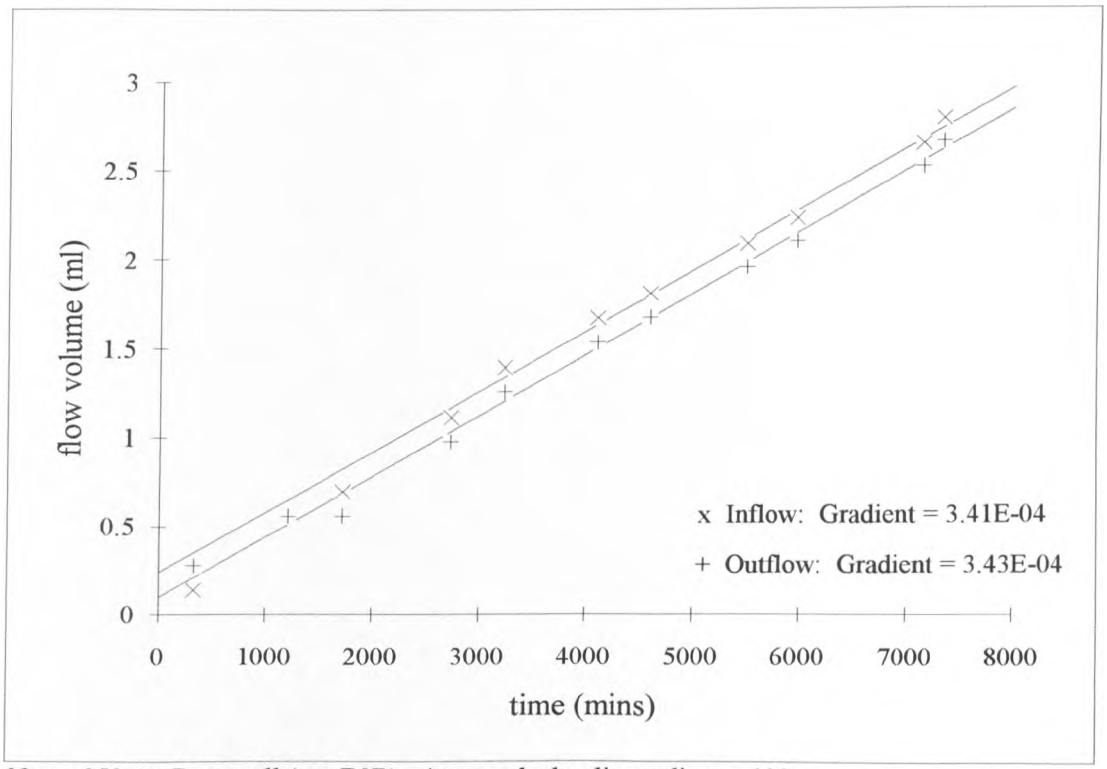

Note: 250mm Rowe cell (test B3B). Average hydraulic gradient = 109.

Figure 5.14: Inflow and outflow volumes against time for a 20% bentonite mixture at 200kPa vertical effective stress.

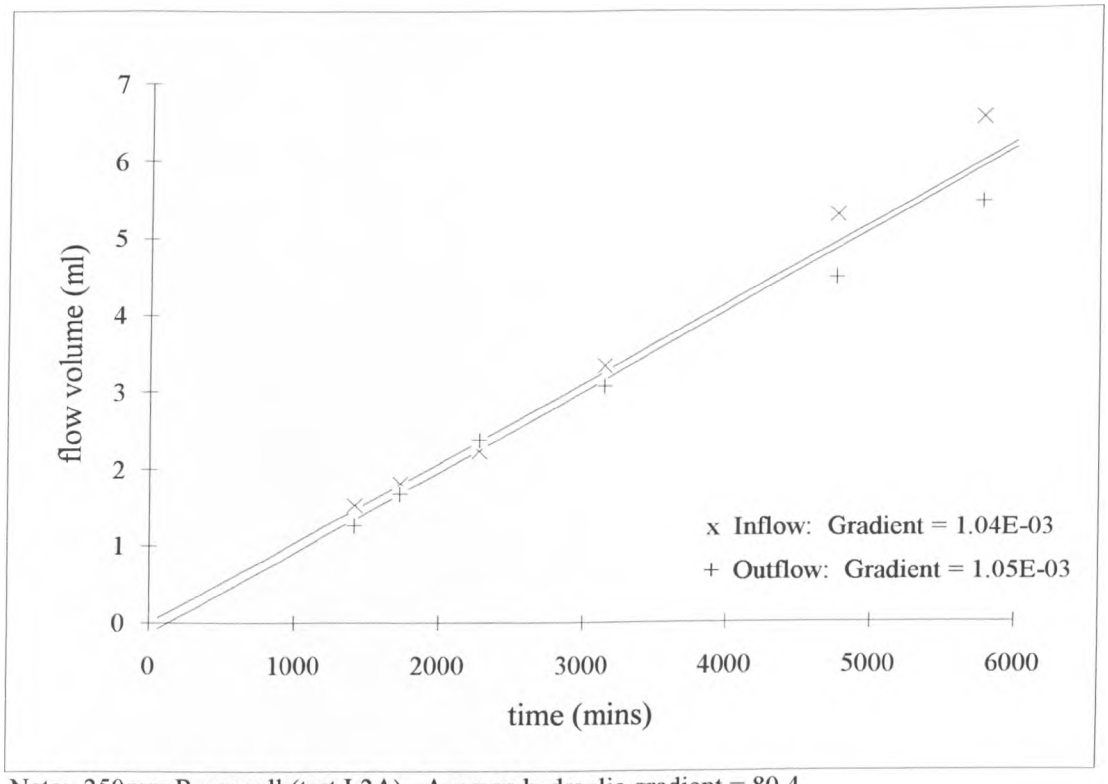

Note: 250mm Rowe cell (test L2A). Average hydraulic gradient = 80.4.

Figure 5.15: Inflow and outflow volumes against time for a 10% bentonite mixture at 200kPa vertical effective stress.

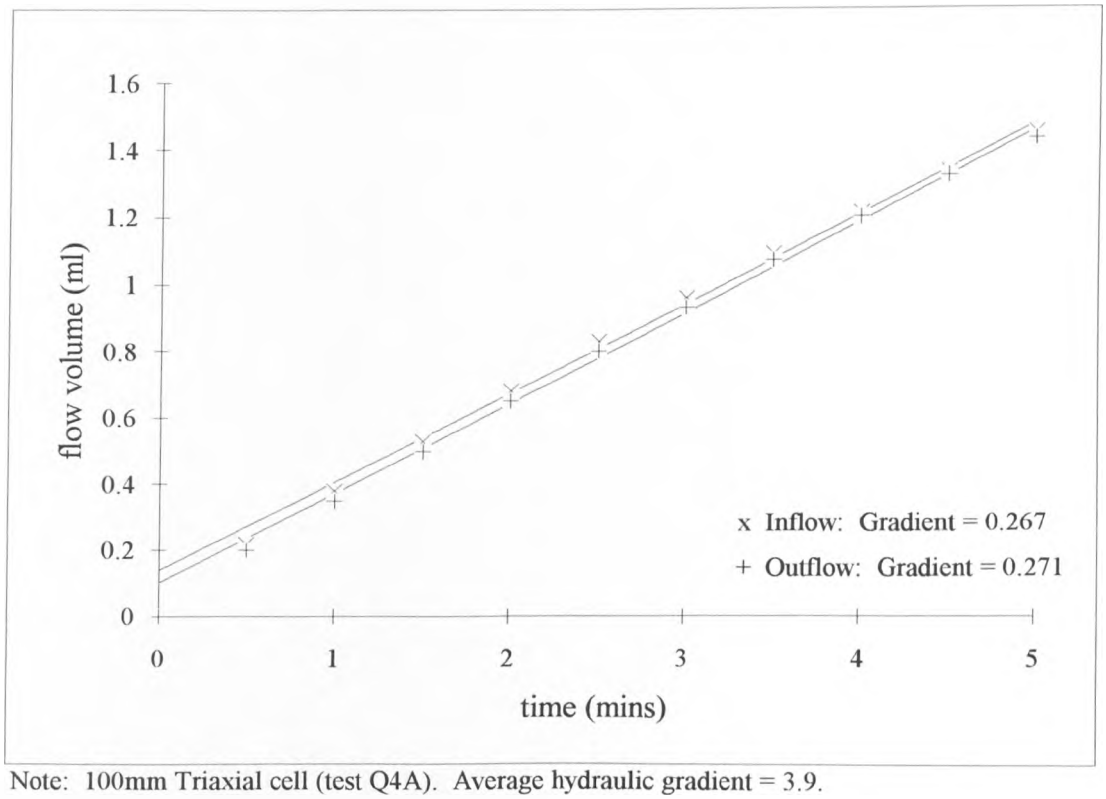

Note: 100mm Triaxial cell (test Q4A). Average hydraulic gradient = 3.9.

Figure 5.16: Inflow and outflow volumes against time for a 5% bentonite mixture at 25kPa effective cell pressure.

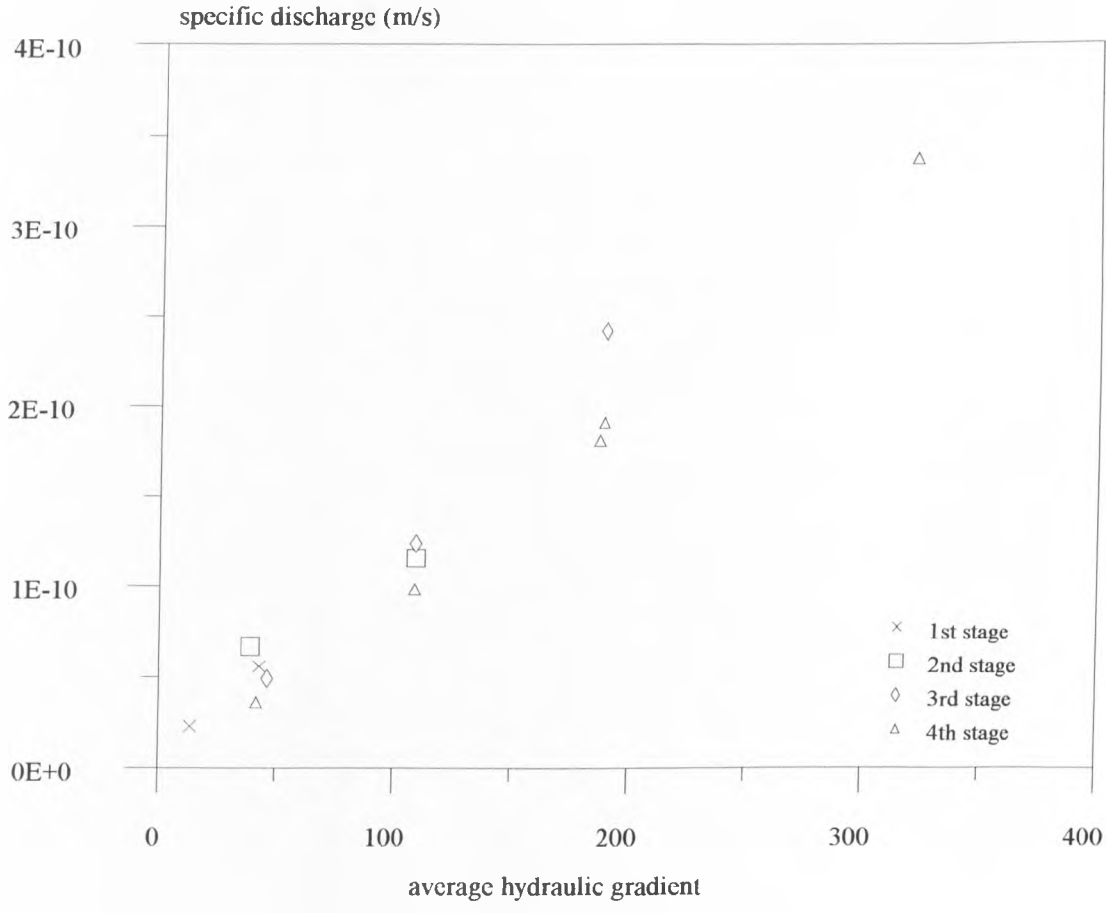

Figure 5.17: Specific discharge (v) versus hydraulic gradient (i) for a multi-stage test on a 20% bentonite-sand mixture to verify the validity of Darcy's law.

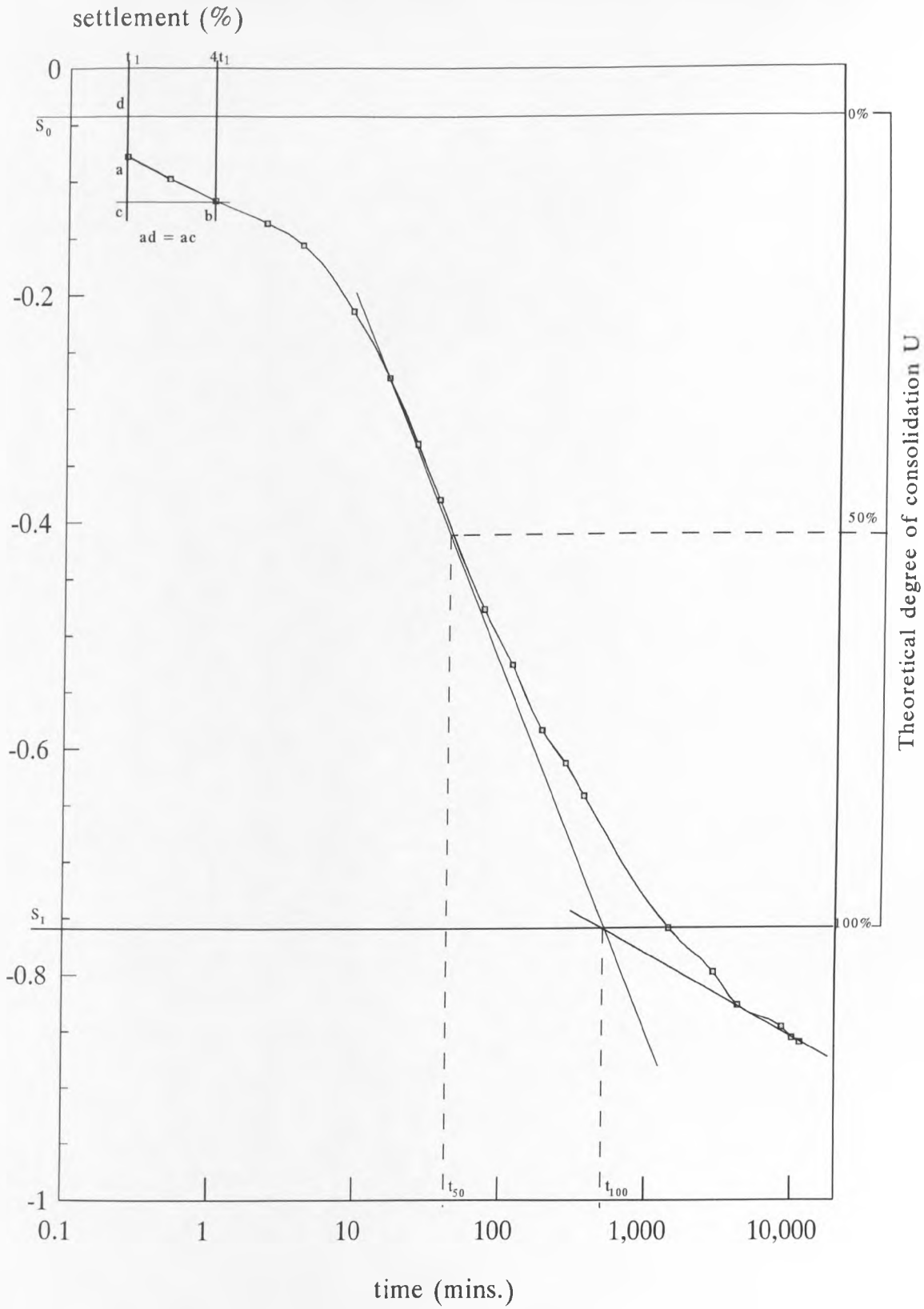

Figure 5.18: Percent settlement vs time 20% bentonite - sand mix.
Test number 20J7, log-time (Casagrande) method.

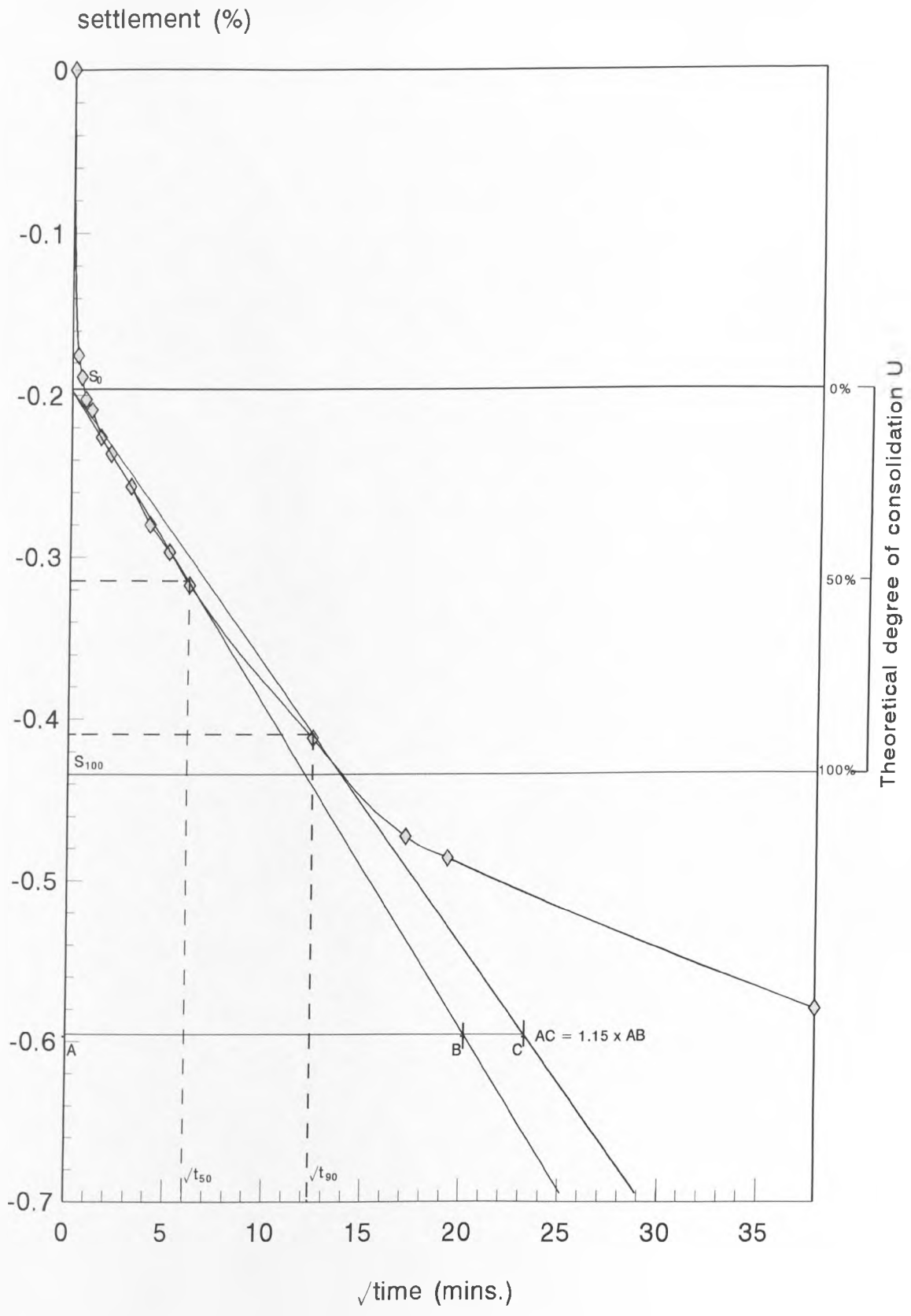

Figure 5.19: Percent settlement versus square-root-time for a 10% bentonite - sand mix. Test number 10d4, square-root-time (Taylor) method.

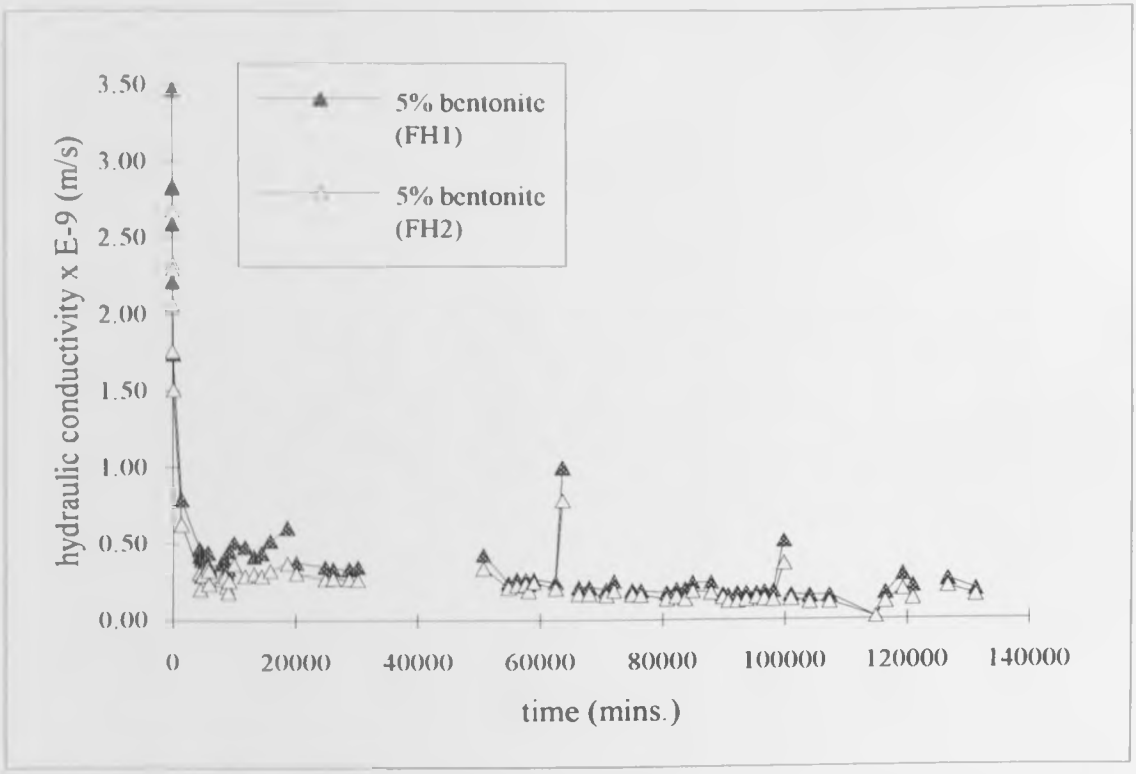

Figure 5.20: Hydraulic conductivity versus time. Falling head tests on 5% bentonite-sand mixtures.

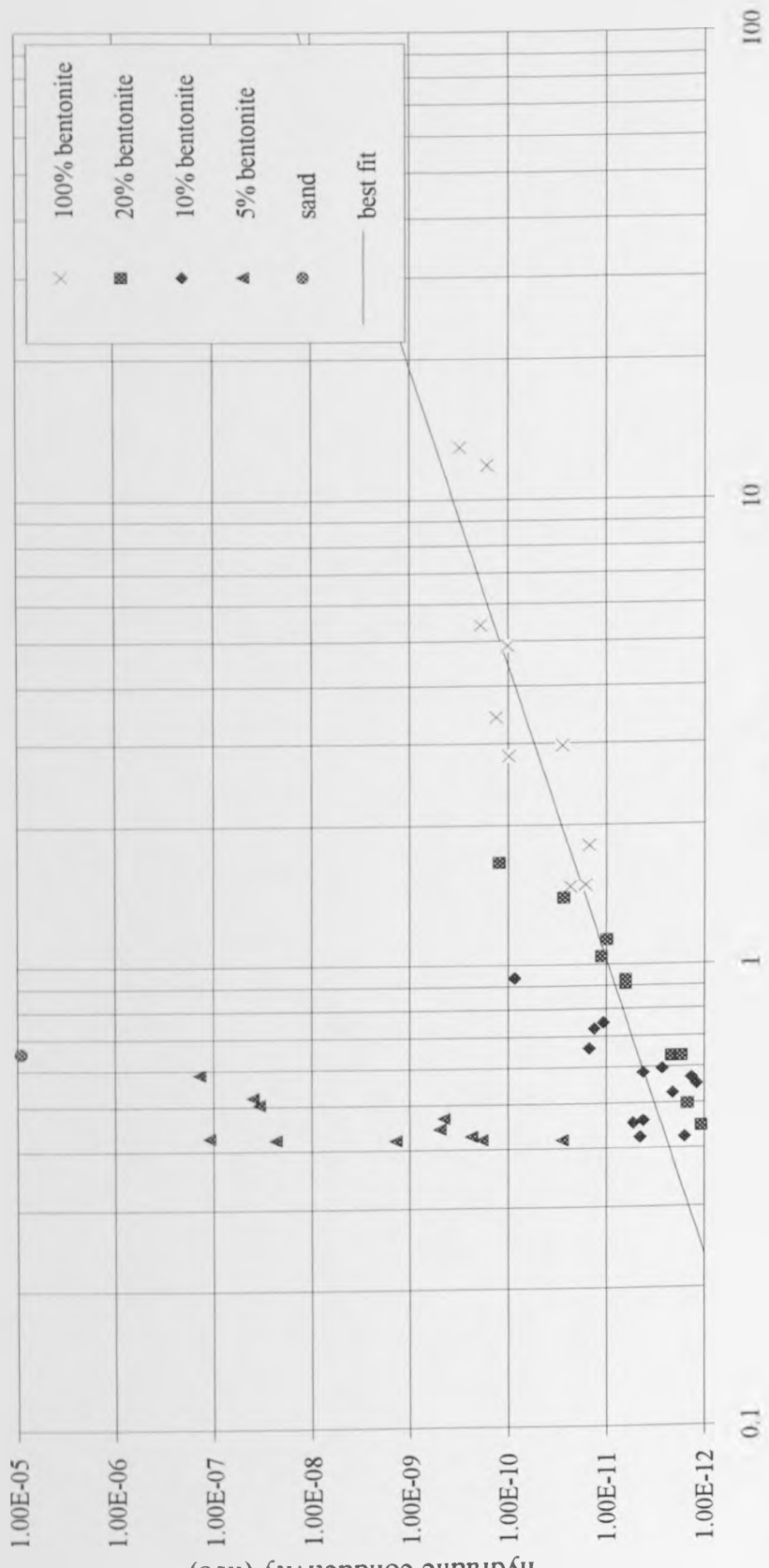

Figure 5.21: Hydraulic conductivity related to overall void ratio.

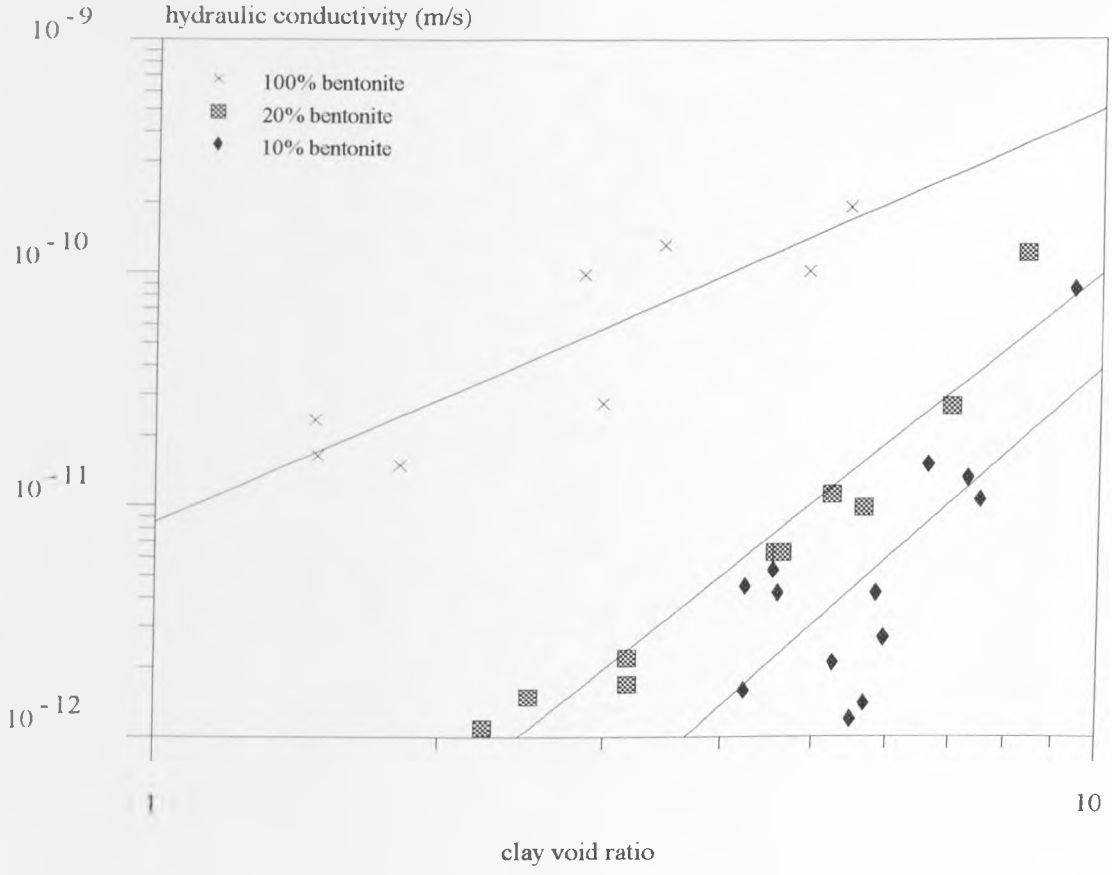

Figure 5.22: Hydraulic conductivity of bentonite-sand mixtures (5% data omitted).

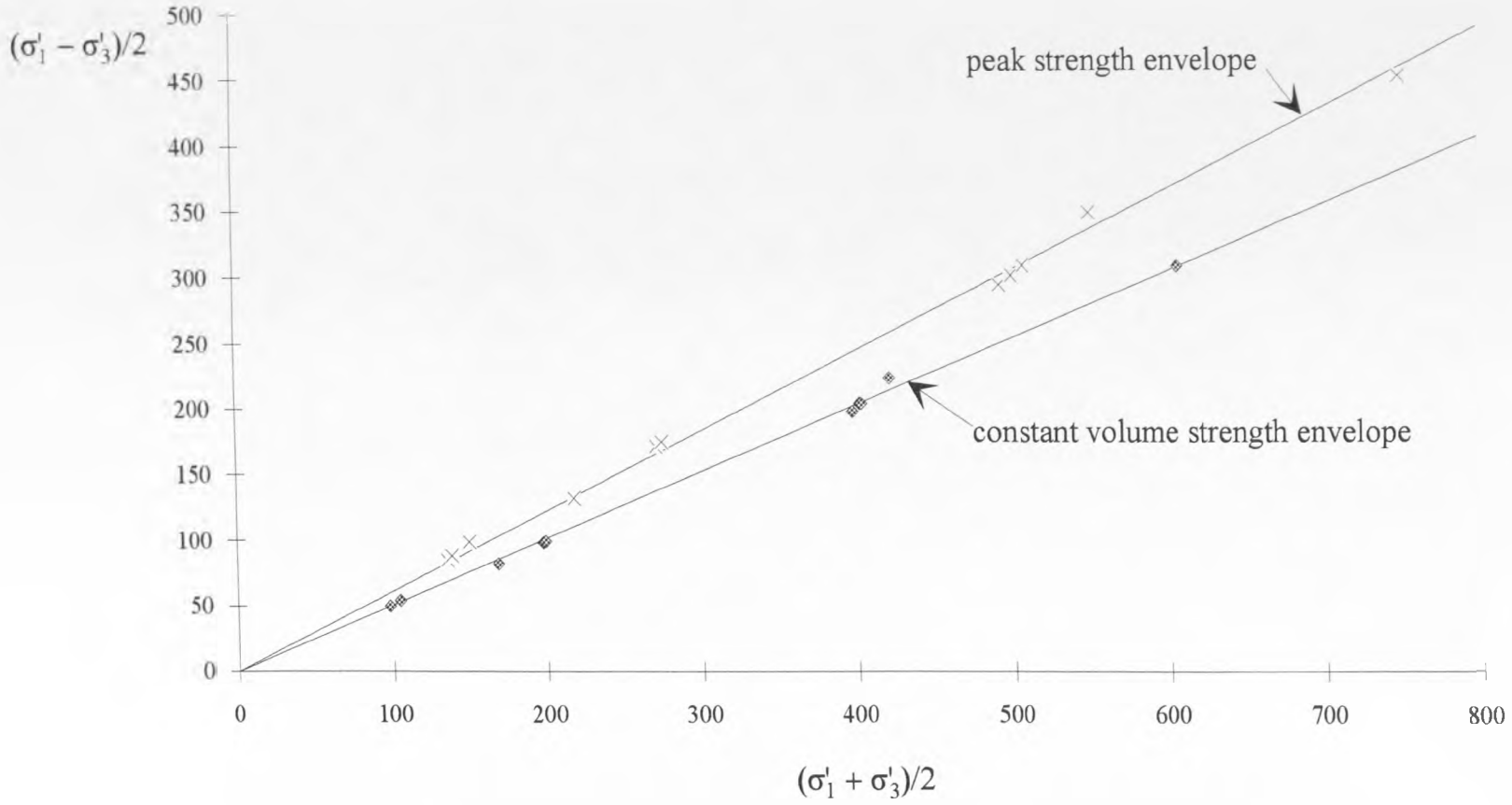

Figure 5.23: Modified failure envelope for medium dense Knapton Quarry sand.
CD triaxial compression test, strain rate = 0.5mm/min.

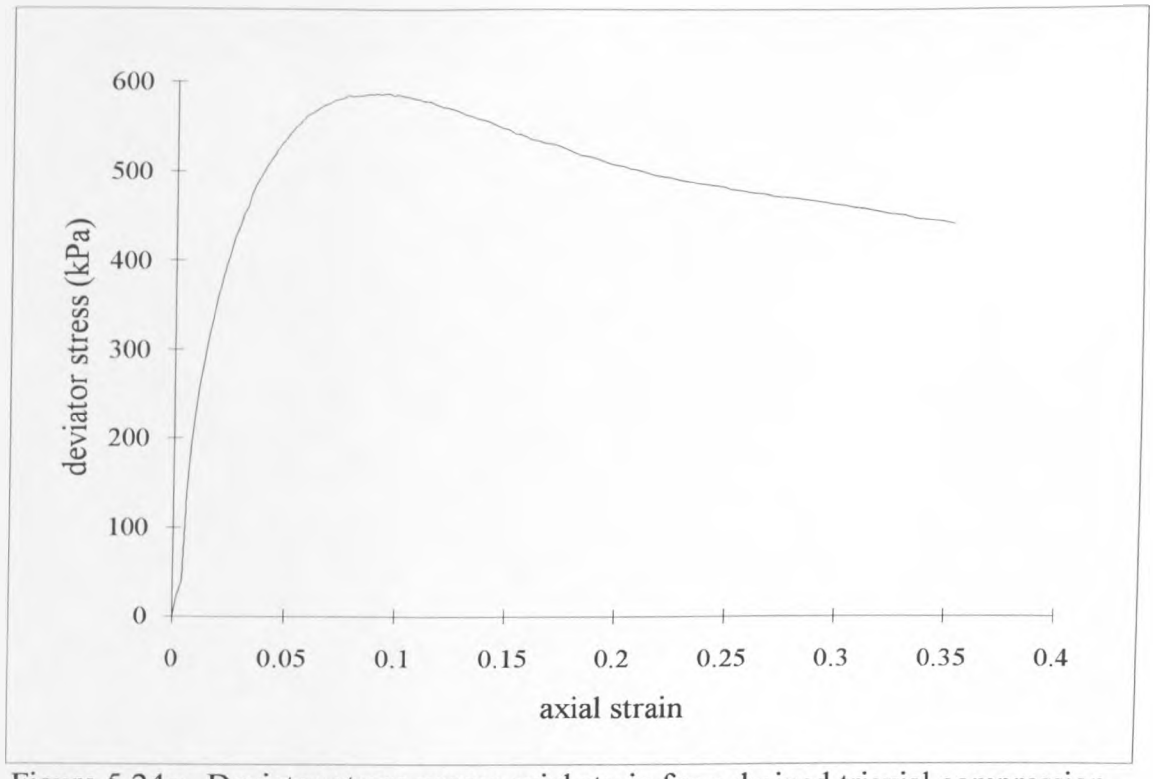

Figure 5.24a: Deviator stress versus axial strain for a drained triaxial compression test on sand at 200kPa effective cell pressure.

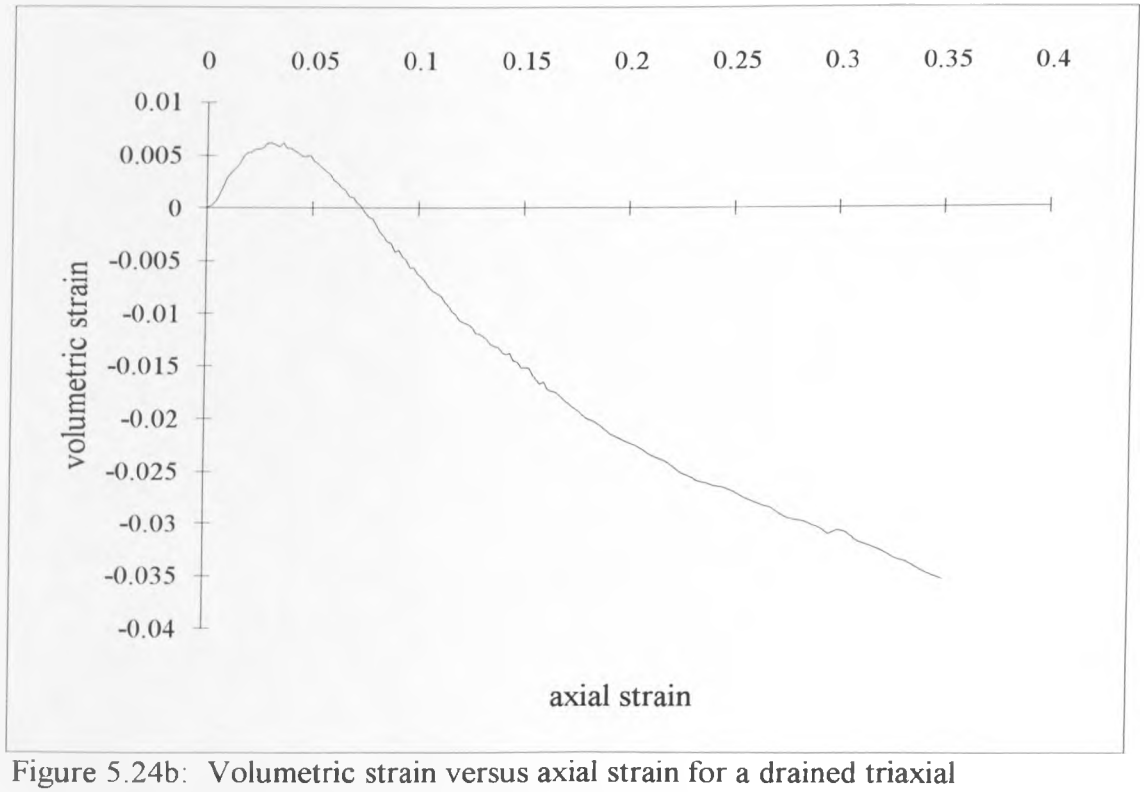

Figure 5.24b: Volumetric strain versus axial strain for a drained triaxial compression test on sand at 200kPa effective cell pressure.

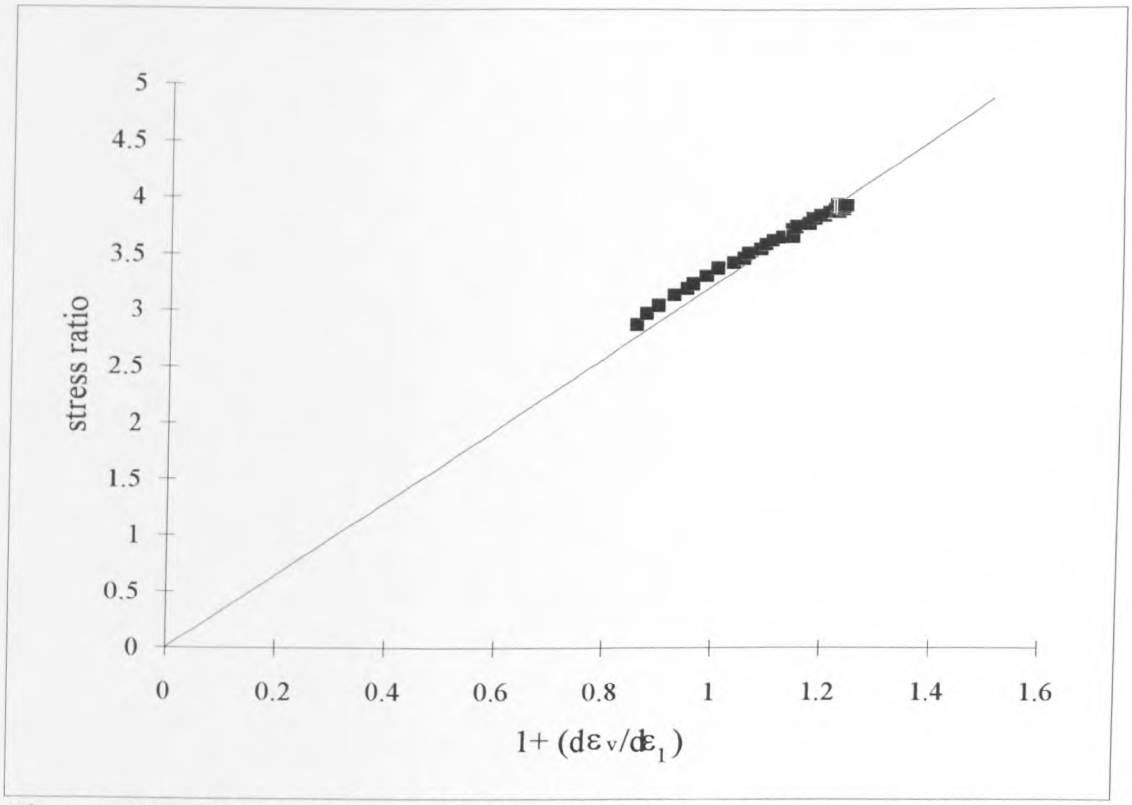

Figure 5.24c: Stress-dilatancy plot for a drained triaxial compression test on sand at 200kPa effective cell pressure.

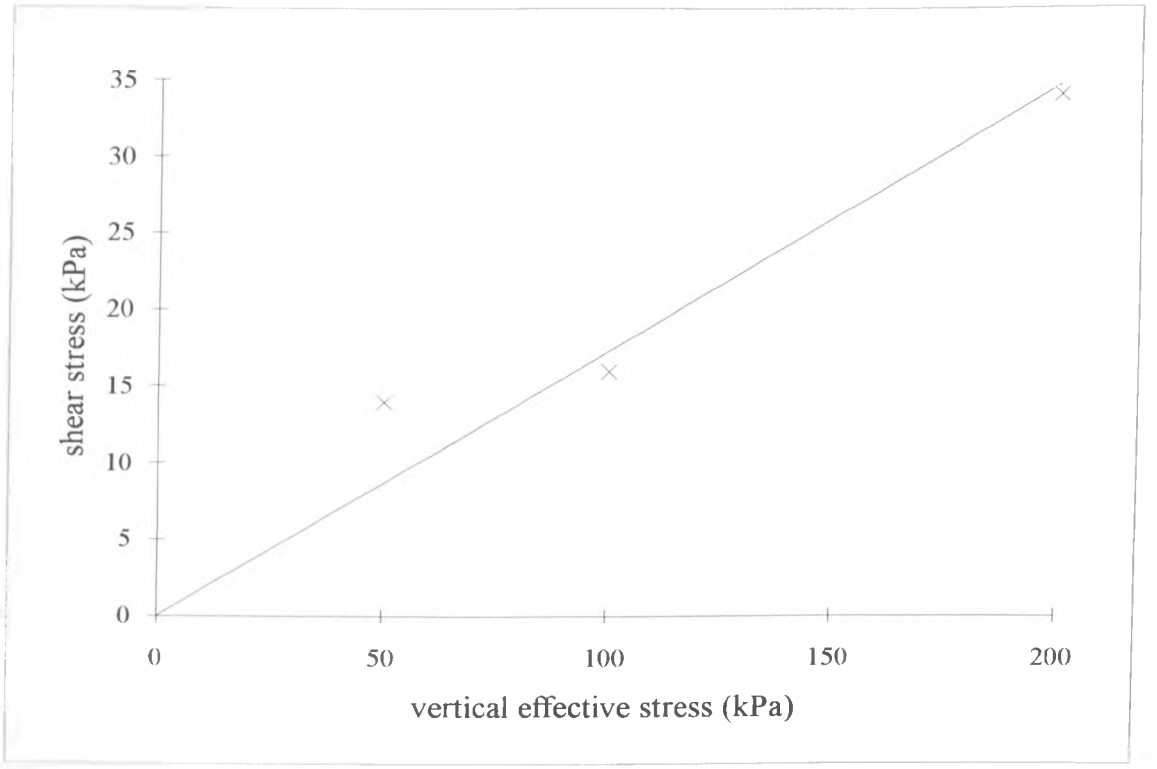

Figure 5.25: Bentonite failure envelope.
Consolidated drained direct shear test. Strain rate = 0.00064mm/min.

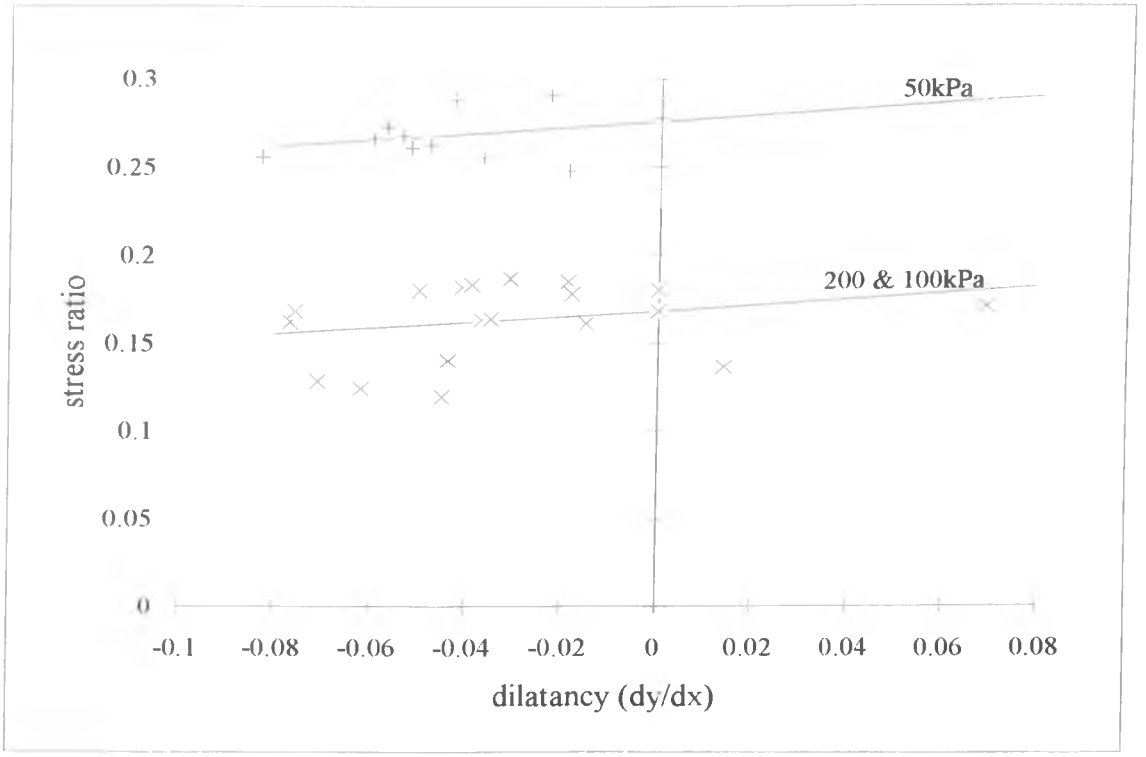

Figure 5.26: Taylor's flow rule for calculation of constant volume friction angle.
Direct shear tests on bentonite

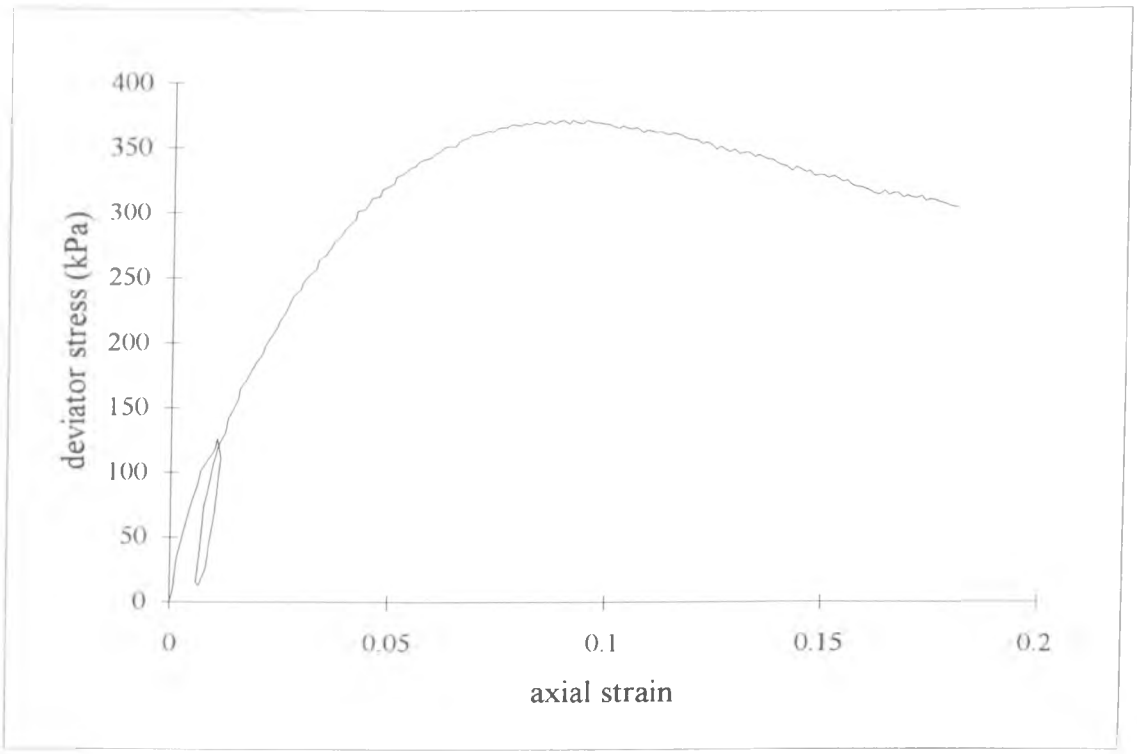

Figure 5.27a: Deviator stress versus axial strain for a consolidated drained triaxial compression test on a 20% bentonite-sand mixture at 200kPa effective cell pressure.

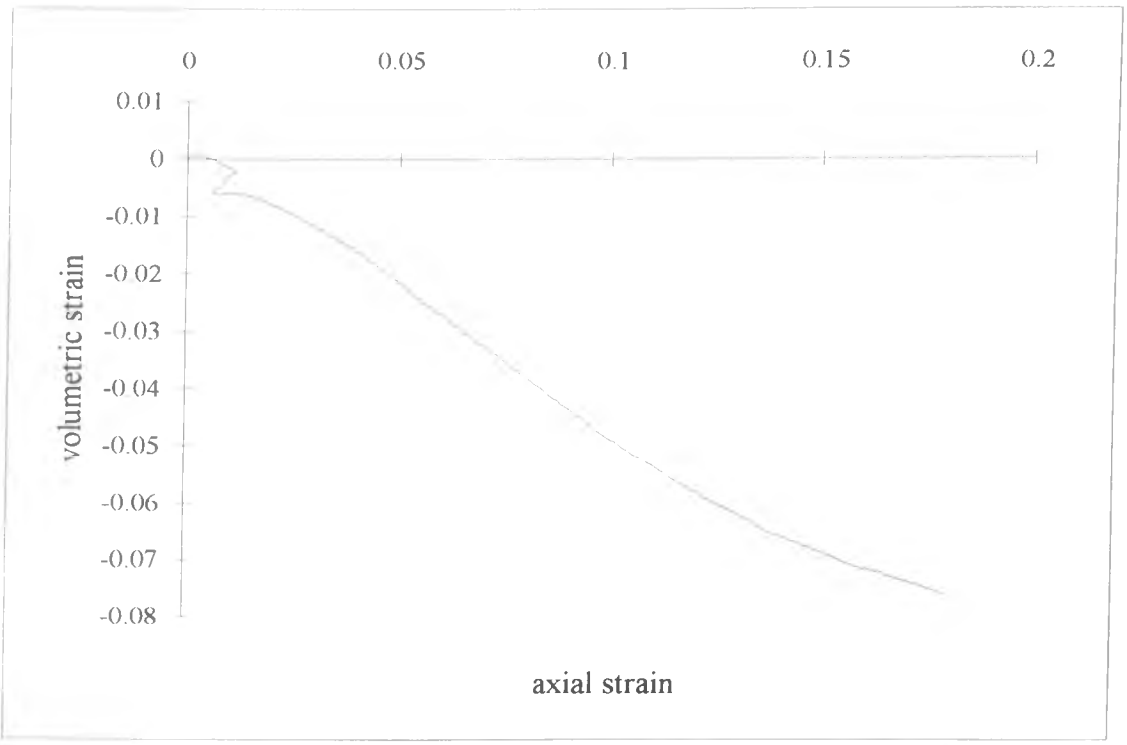

Figure 5.27b: Volumetric strain versus axial strain for a consolidated drained triaxial compression test on a 20% bentonite-sand mixture at 200kPa effective cell pressure.

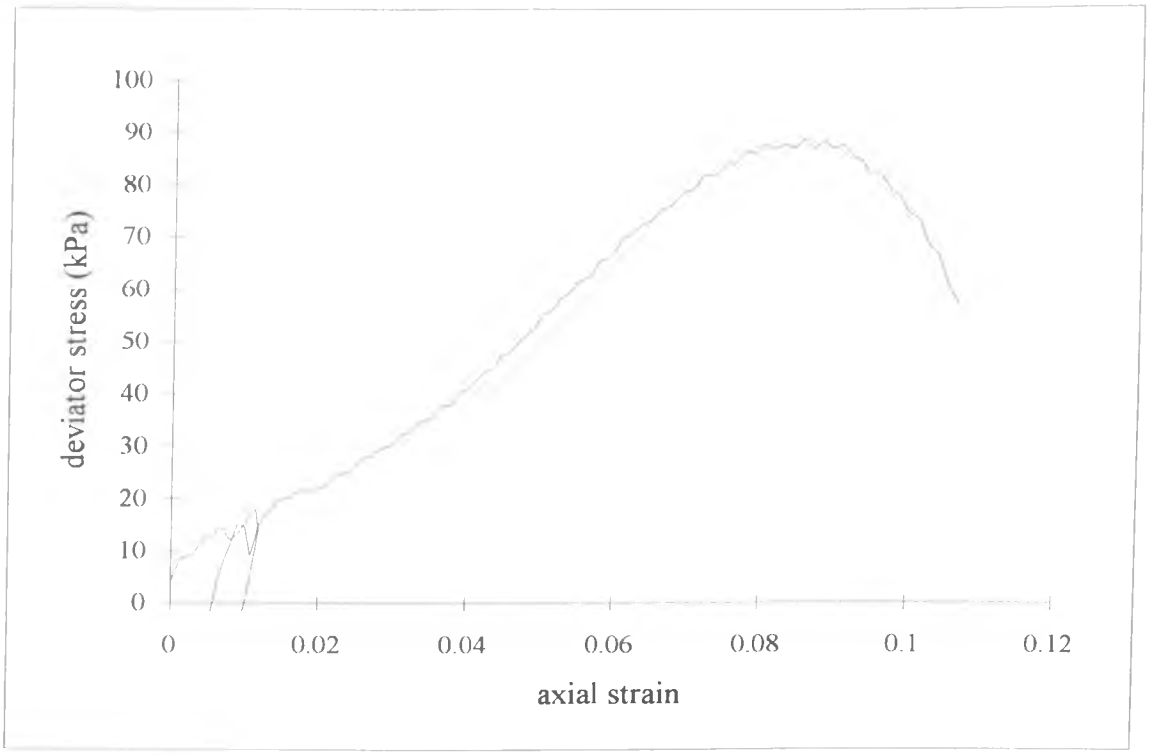

Figure 5.28a: Deviator stress versus axial strain for a consolidated drained triaxial compression test on a 10% bentonite-sand mixture at 25kPa effective cell pressure.

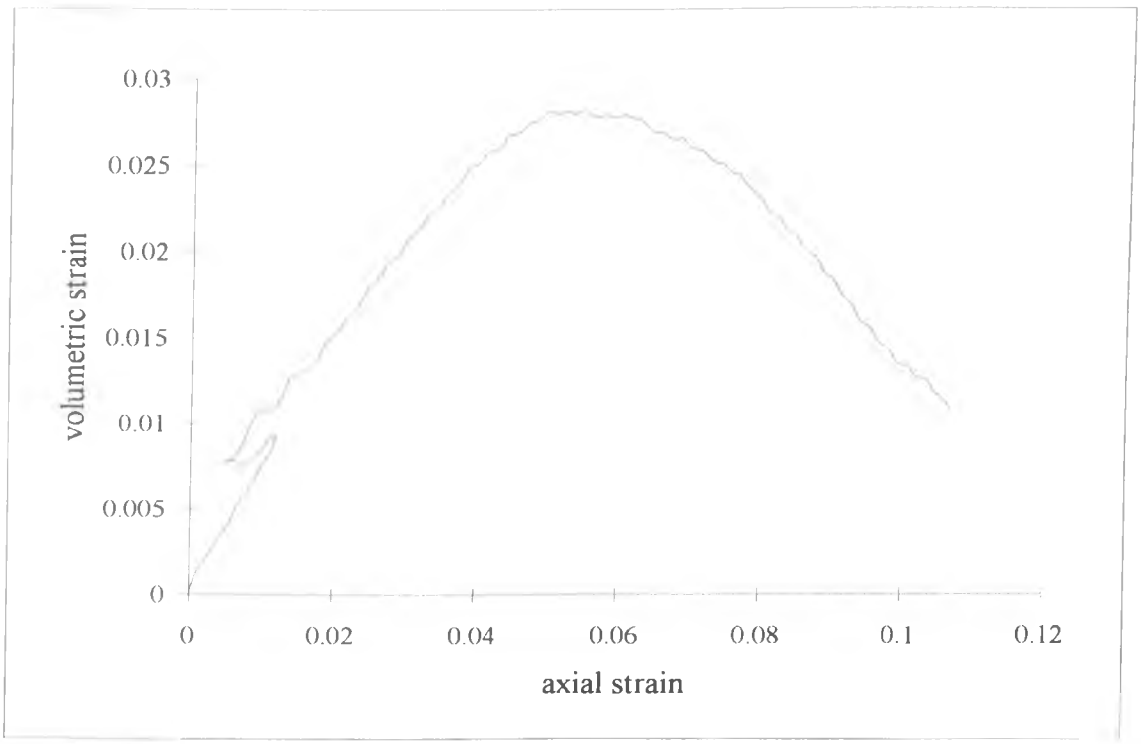

Figure 5.28b: Volumetric strain versus axial strain for a consolidated drained triaxial compression test on a 10% bentonite-sand mixture at 25kPa effective cell pressure.

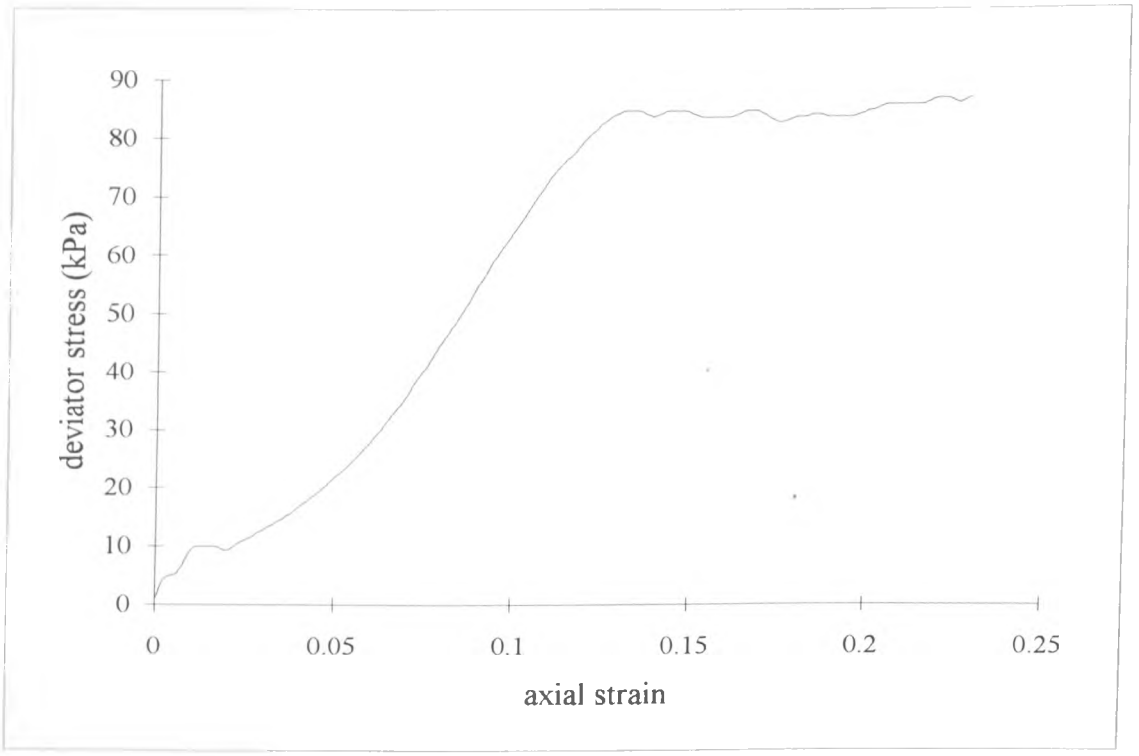

Figure 5.29a: Deviator stress versus axial strain for a consolidated undrained triaxial compression test with pore water pressure measurement on a 10% bentonite-sand mixture at 15kPa effective cell pressure.

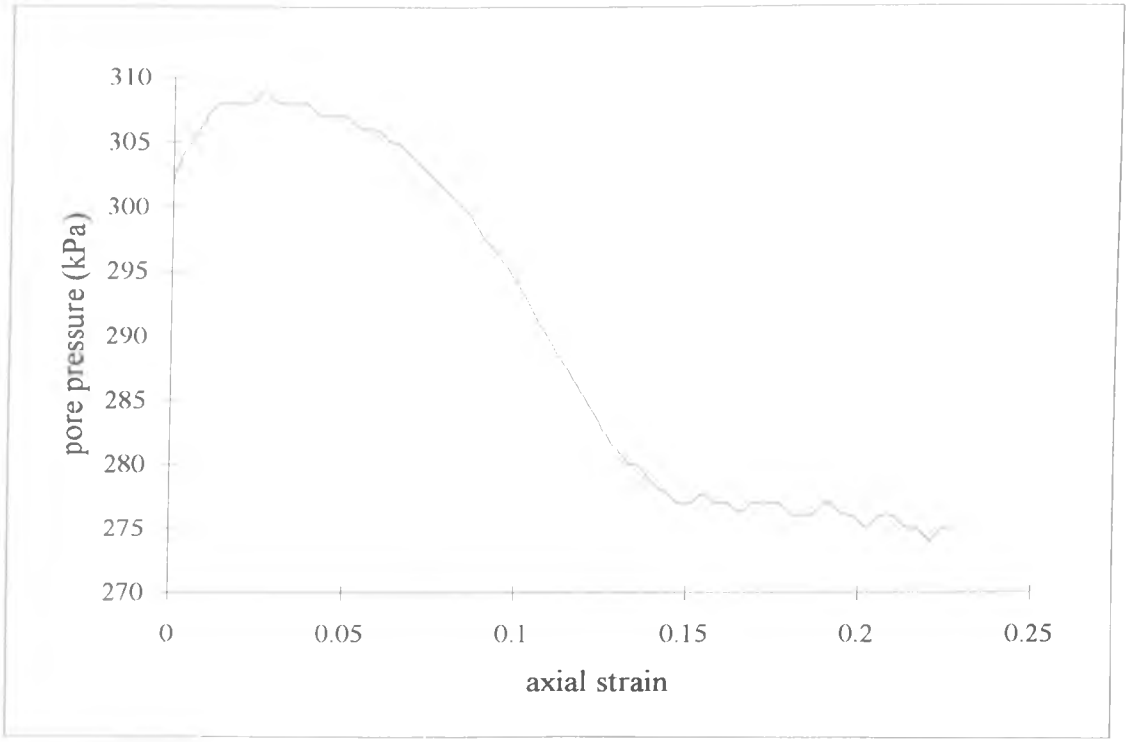

Figure 5.29b: Pore water pressure versus axial strain for a consolidated undrained triaxial compression test with pore water pressure measurement on a 10% bentonite-sand mixture at 15kPa effective cell pressure

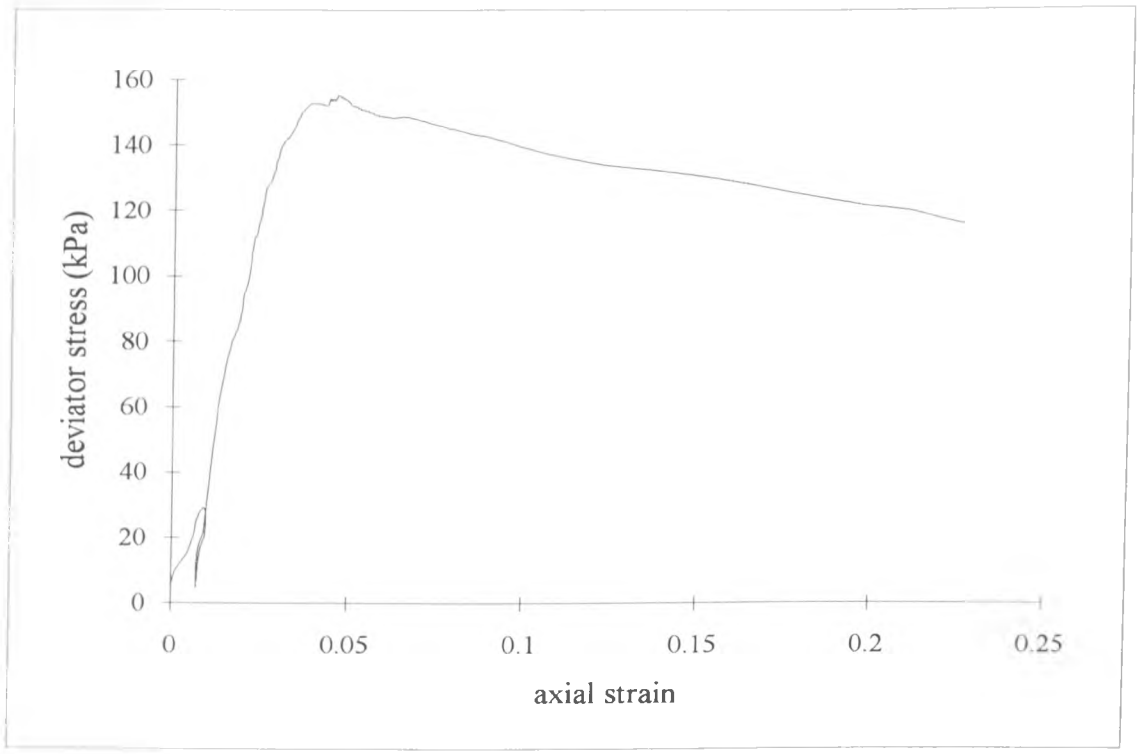

Figure 5.30a: Deviator stress versus axial strain for a consolidated drained triaxial compression test on a 5% bentonite-sand mixture at 25kPa effective cell pressure.

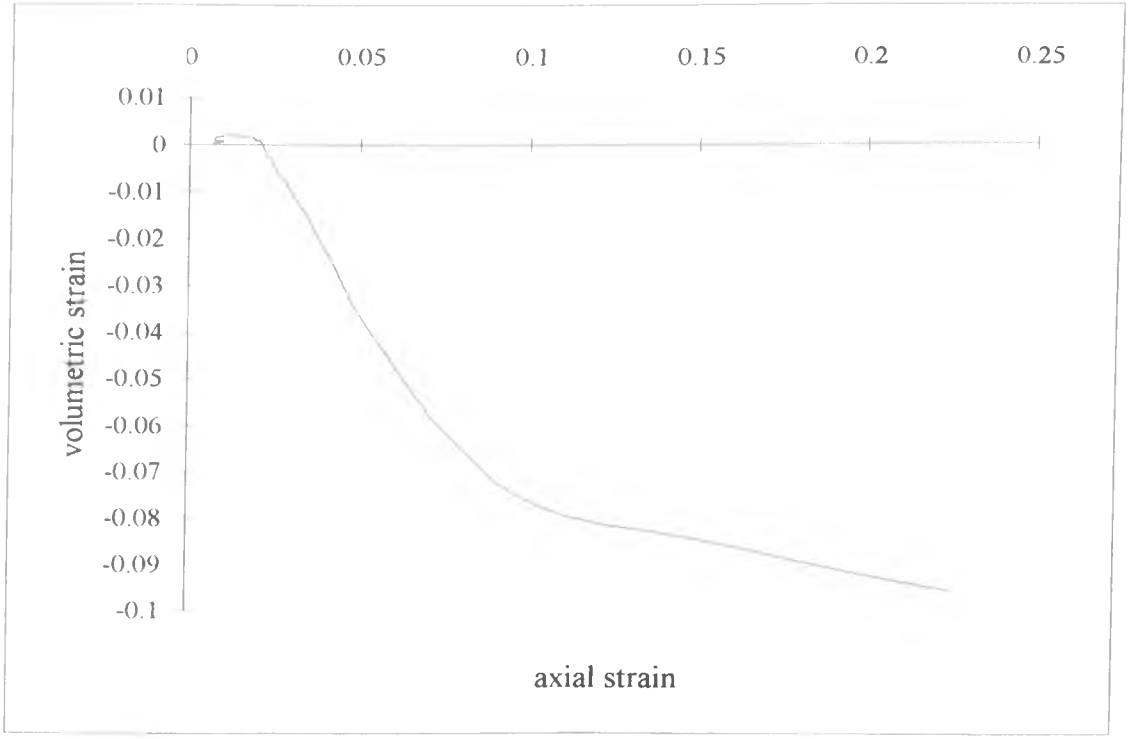

Figure 5.30b: Volumetric strain versus axial strain for a consolidated drained triaxial compression test on a 5% bentonite-sand mixture at 25kPa effective cell pressure.

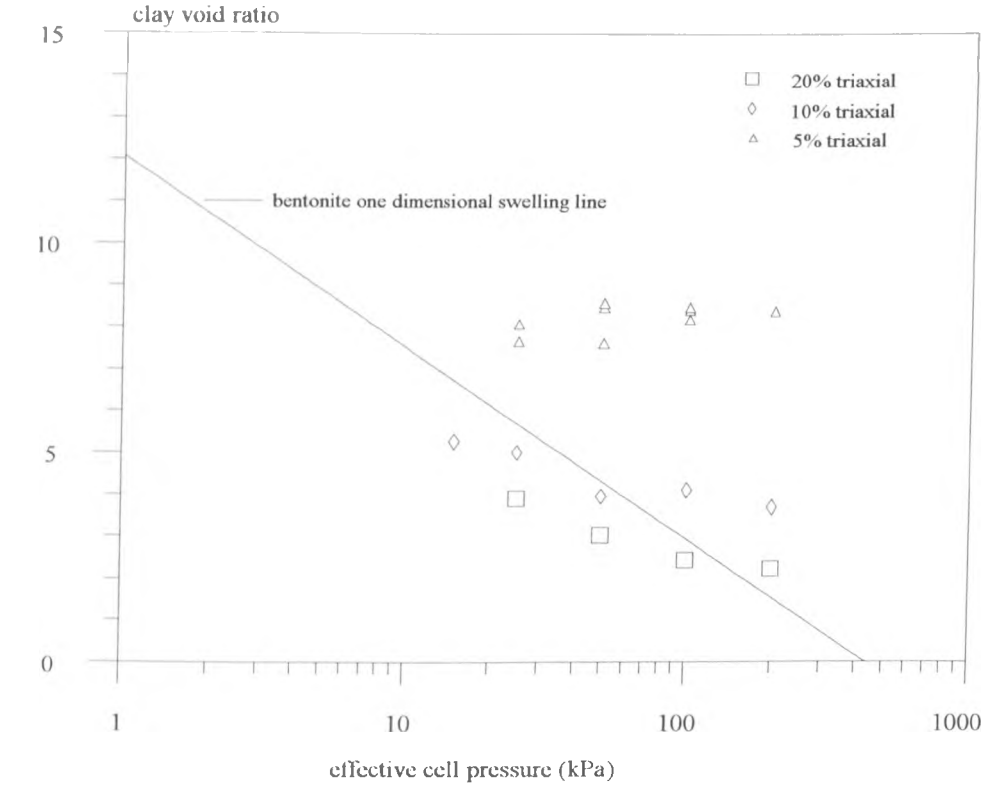

Figure 5.31: Isotropic swelling of compacted bentonite-sand mixtures related to idealised swelling behaviour.

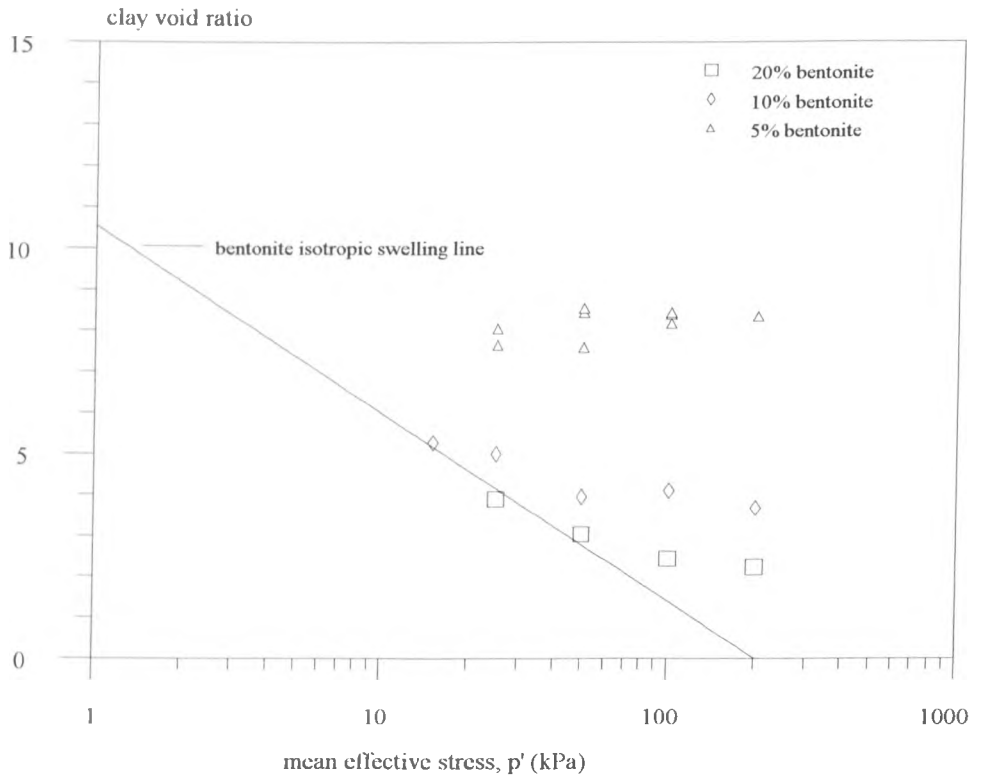

Figure 5.32: Isotropic swelling of compacted bentonite-sand mixtures.

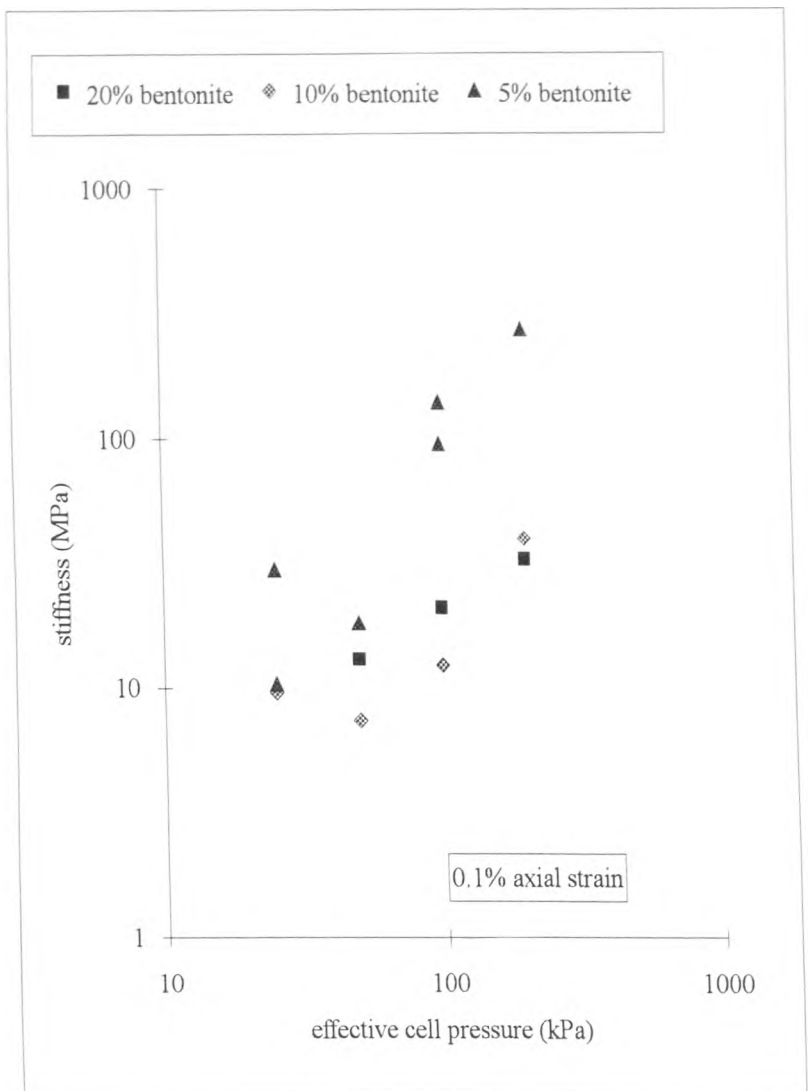

Figure 5.33a: Stiffness of bentonite-sand mixtures in triaxial compression at 0.1% axial strain.

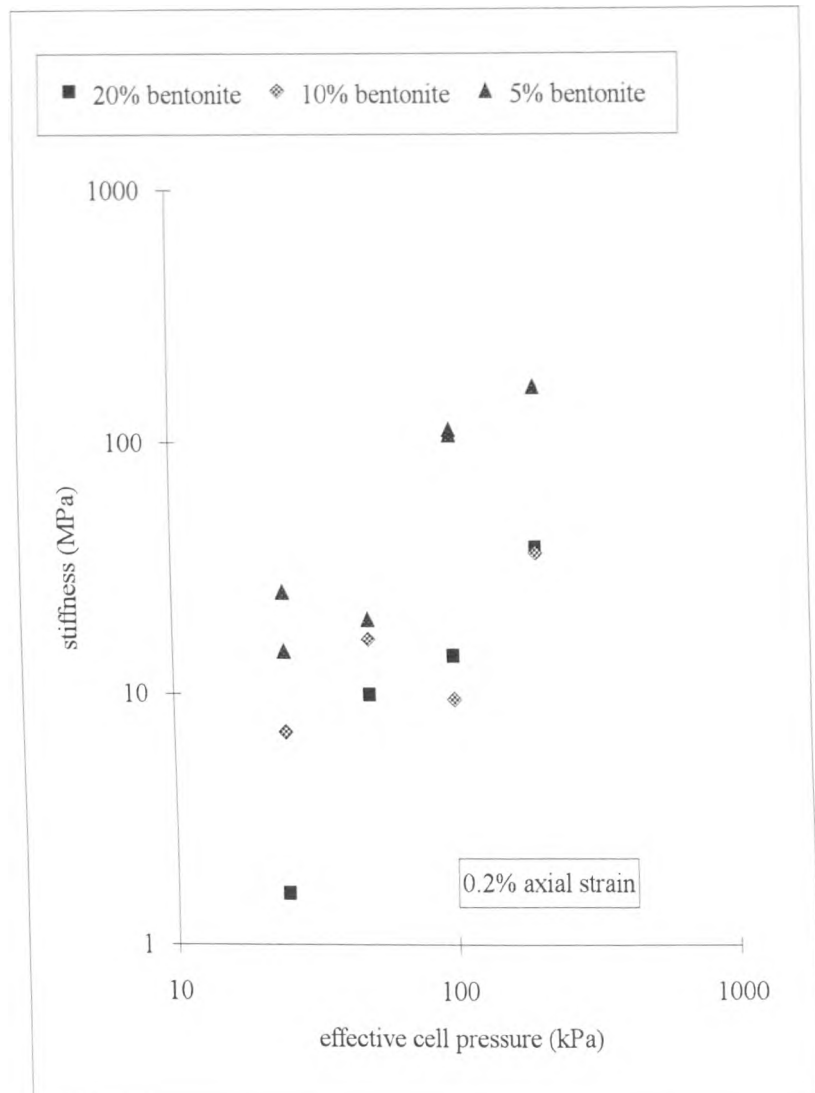

Figure 5.33b: Stiffness of bentonite-sand mixtures in triaxial compression at 0.2% axial strain

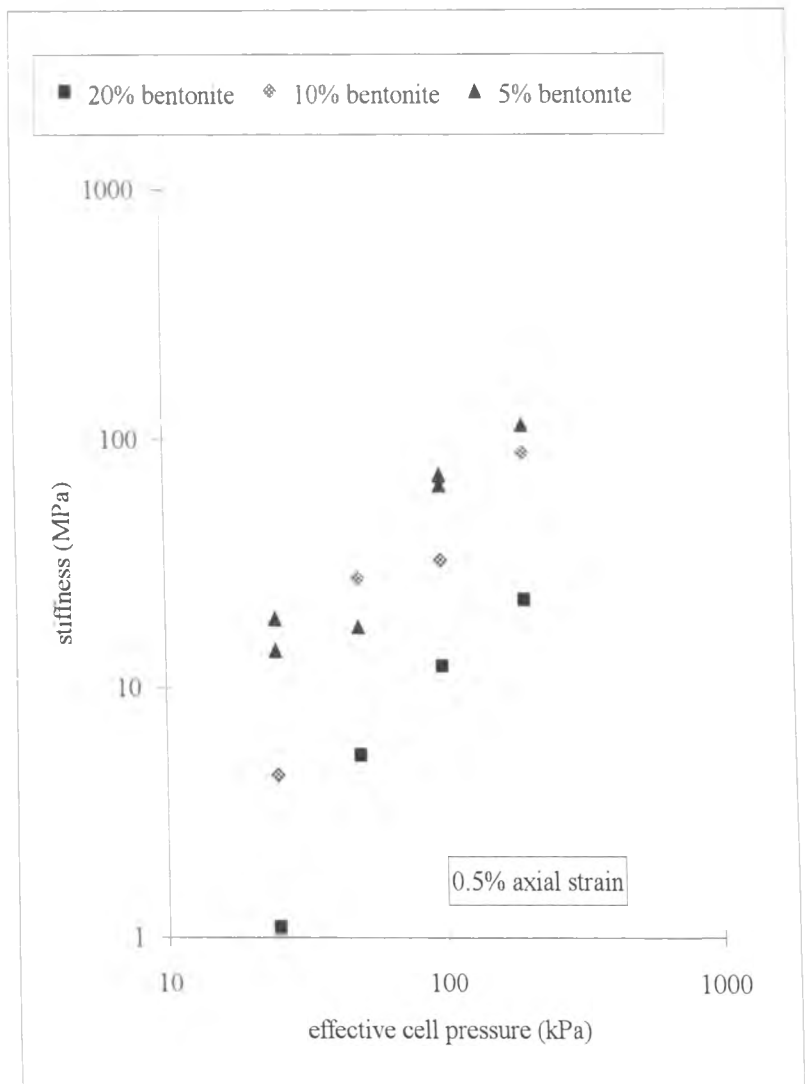

Figure 5.33c: Stiffness of bentonite-sand mixtures in triaxial compression at 0.5% axial strain.

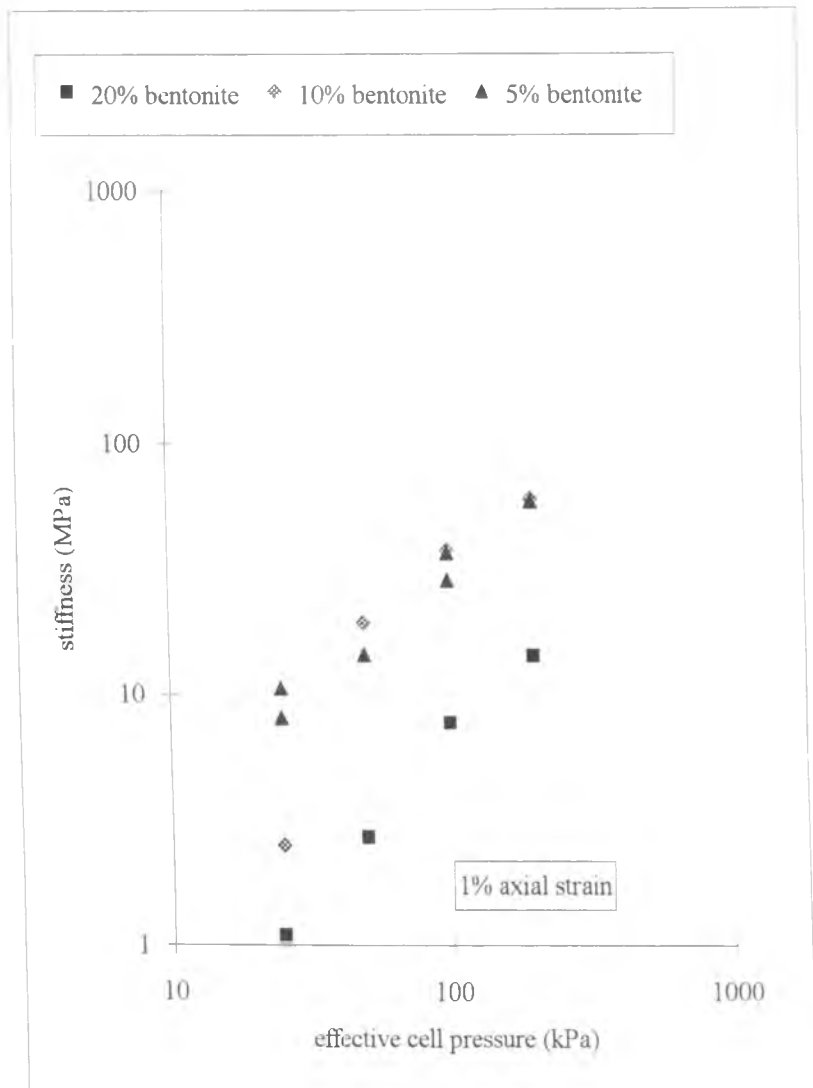

Figure 5.33d: Stiffness of bentonite-sand mixtures in triaxial compression at 1% axial strain.

CHAPTER 6
FURTHER DISCUSSION

6.1 Introduction

In chapter 5, a general discussion of the basic data trends was presented and the behaviour of bentonite-sand mixtures was shown to be usefully characterised by considering the individual phases of the material. This approach will be developed in this chapter in an attempt to quantify the individual contributions of the phases to the overall behaviour of the mix. Following this, the design of these mixtures will be discussed in chapter 7. The discussion of results from the various test series is in the same order as chapter 5.

6.2 Compaction

Figure 5.1 and table 5.1 indicate an increasing maximum achievable dry density of bentonite-sand mixtures with increasing bentonite content up to 20%. It appears that the maximum dry density decreases with bentonite contents greater than 20%. This observation is consistent with results of Dixon et al. (1985), who found the maximum attainable dry density of bentonite-sand mixtures increased at sand contents up to 75%, and decreased beyond this percentage. As implied in chapter 5, the decrease in clay void ratio is greater than the increase in sand void ratio with increasing bentonite content up to 20%, and therefore the overall void ratio decreases because the specific gravity of the bentonite is higher than that of the sand.

With optimum moisture contents in the range 11-12% for all mixtures, it is likely that the water within the sample is associated entirely with the bentonite. It is suggested that this water/clay mixture (or gel) creates a lubricating effect which aids compaction, allowing a higher density to be achieved up to 20% bentonite content. At 25% bentonite content, the void ratio of the sand in the mixture is approaching the maximum value for sand alone (calculated as 0.978). At this stage an increase in the overall dry density can only occur if the increase in density of the bentonite is greater than the decrease in density of the sand. During compaction, it is unlikely that any water is expelled from the sample. Therefore, at high clay contents there is sufficient clay volume available to keep the sand particles widely spaced hence lowering the mixture dry density.

Three states of a mixture can be inferred from the results of compaction tests:

1. Sand particles wholly in contact at low bentonite contents with the clay-water phase partly or fully filling the voids.

2. Sand in contact with increasing amounts of clay (by dry volume) in the voids due to the decreasing ratio of water to clay, with an overall dry density increase (behaviour observed up to 20% bentonite content).

3. Sand particles dispersed as inclusions in the clay-water matrix, which cannot be compacted to equivalent sand dry densities due to adsorbed water. As the clay content is increased beyond this point, the overall dry density decreases. Throughout the remainder of this chapter, the swelling behaviour, hydraulic conductivity and strength of bentonite-sand mixtures will be shown to suggest the existence of these three proposed material states.

6.3 Swelling, normal consolidation and rebound

6.3.1 Swelling: dry bentonite powder

In chapter 5, a single bentonite swelling line was shown to be appropriate for initially dry bentonite regardless of sample preparation technique. It is proposed that different compaction techniques do not alter the fabric of the sample because of its initially dry state. Similar results were shown by Seed et al. (1962), who found that clay samples compacted dry of optimum maintained a flocculated structure which was independent of the compaction technique.

The bentonite swelling line predicts a clay void ratio of zero at approximately 440kPa vertical effective stress. However, it is standard geotechnical practice to idealise the volume change behaviour of clay soils on a plot of this type (i.e., normal consolidation lines), which always predict a void ratio of zero at a specific applied stress. This effect is more noticeable due to the large swelling at low vertical effective stresses and the different type of behaviour exhibited by an initially dry sample. These two effects lead to an intercept with the σ'_v axis at a lower effective stress than is typical of normal consolidation lines of other clays.

At vertical effective stresses in excess of 200kPa there appears to be a deviation in linearity from the best fit line plotted through the data (i.e., the gradient becomes flatter). Contrary to the behaviour at low stresses, this is not attributed to experimental scatter. Above approximately 200kPa, it is postulated that double layer swelling is significantly reduced and interlayer swelling predominantly controls particle spacing. At an applied stress exceeding that large enough to suppress the formation of appreciable double layers, the swelling line gradient will continually decrease and theoretically become flat when the absolute minimum of interlayer water is adsorbed[1]. Bolt (1956) and Mesri and

[1]It is thought that although double layer swelling is significantly suppressed by the application of high stresses, interlayer swelling continues due to the strong tendency of the first two water layers to penetrate between the clay sheets.

Olson (1971) have shown that the gradient of the one-dimensional consolidation line for bentonite with various pore fluids tends to zero at vertical effective stresses of approximately 5MPa. Consolidation data for montmorillonite from Low (1980) shows that the change in particle spacing considerably decreases with increasing applied stress, and tends to zero at approximately 700kPa. However, at the effective stresses likely to exist in a landfill the approximation of linearity is acceptable. Extrapolation beyond the stress range used in the experimental programme is, however, questionable.

The shape of the clay void ratio-log time plot for 100% bentonite reinforces the analogy between swelling and consolidation, as figures 5.4a and 5.4b are similar in shape. The change from primary to secondary swelling is attributed to the continually decreasing osmotic gradient as the clay swells with a corresponding decrease in the rate of swelling[2]. As the differences in ionic concentration between the interparticle void space and the external solution are high, water uptake (hence swelling) is initially relatively fast. However, when the concentration difference is such that the osmotic pressure tends to the same value as the applied stress, the swelling curve becomes much flatter. At applied stresses greater than 200kPa, laboratory curves were less well defined, and primary and secondary swelling (due to osmotic double layer effects) were not as easily identifiable. This is attributed to the decreasing significance of double layer swelling with increasing applied stress.

6.3.2 Swelling: dry mixtures

It is clear from figure 5.5 that above a boundary stress (see 5.3.4), which will be termed the threshold stress, the final clay void ratio of bentonite-sand mixtures is higher than that for clay alone. Below the threshold stress, the clay in the mixture swells to reach the same final void ratio as 100% bentonite and the overall behaviour can be considered the same as for bentonite only. Above the threshold stress, sand particles begin to interact and the overall sample stiffness increases as stress is transferred from the clay to the sand[3]. This behaviour is dependent on bentonite content in addition to effective stress. Threshold stresses for 20, 10 and 5% bentonite-sand mixtures are given in 5.3.4 as 68.7kPa, 10.5kPa and 0.2kPa respectively. Therefore, the value substantially reduces

---

[2]When describing the increase in volume of dry bentonite on exposure to water, osmotic swelling is not to be confused with mechanical swelling which is the result of a hydrostatic pressure deficiency. Traditionally, consolidation is regarded as positive pore water pressure dissipation, rebound negative pore water pressure dissipation and swelling osmotic pressure equalisation (see chapter 2).

[3]An increased sample stiffness is shown by the smaller gradient (compared to the bentonite swelling line) of the idealised swelling behaviour of mixtures above the threshold stress in c_c - log σ'_v space. Conventionally, stiffness is indicated by calculated m_v values from the loading stages of a consolidation test. However, in this test programme the stress path was always one of reducing stress. Therefore, the term stiffness should be thought of as qualitatively indicating the differences in clay void ratio between two vertical effective stresses.

with decreasing bentonite content. Since the threshold stress for 5% bentonite mixes was calculated as 0.2kPa, the mechanical properties of this mixture are expected to be essentially those of sand, whereas a more 'clay type' behaviour would be expected for 20% mixtures. This is consistent with the proposed material states described in 6.2.

Although the transition from a 'clay' to a more 'sand type' behaviour may be relatively smooth, for engineering purposes it is easier to idealise the behaviour to produce the plot shown in figure 5.9. It is assumed that each mixture has a linear relationship between clay void ratio and the logarithm of vertical effective stress (originating at the respective threshold stress), and all mixtures have the same gradient. This is discussed further in 6.3.3.

6.3.3 Modified principle of effective stress

Since the principle of effective stress states that any distortion, compression or expansion of a soil is accompanied by a change in effective stress, it follows that a sample not changing in volume, under drained conditions, has a constant effective stress. For a given vertical effective stress, bentonite reaches a unique clay void ratio when allowed to swell from a dry state with distilled water, the value of which is given by the bentonite swelling line (equation 5.9). Above the threshold stress, the final clay void ratio of a bentonite-sand mixture is higher than that reached by 100% bentonite when allowed to swell under the same conditions. Therefore, the effective stress supported by the clay must be less than the overall effective stress, and this lower effective stress is given by the bentonite swelling line by the substitution of the mixture clay void ratio into equation 5.9. At equilibrium, the sample has no further volume change, and the pore water pressure can be considered negligible under drained conditions. Hence, the effective stress in the sand is the difference between the applied stress and the effective stress in the clay. It can therefore be stated that the effective stress, σ' (calculated as applied normal load divided by sample area), is equal to the effective stress supported by the sand, σ'_S, plus the effective stress supported by the clay, σ'_C, and because the sample is at constant volume the pore water pressure, u, is zero, thus

$$\sigma' = \sigma'_S + \sigma'_C \qquad 6.1$$

Hence, Terzaghi's principle has been modified to account for the two soil phases of the mixture. In it's general form the modified principle can be written

$$\sigma = \sigma'_S + \sigma'_C + u \qquad 6.2$$

The effect of physico-chemical interactions are not accounted for in equation 6.2. However, it is postulated that a similar principle holds. For any applied stress, if the clay void ratio in a bentonite-sand mixture is higher than that for 100% bentonite, the

effective stress in the clay is less than the applied stress and the remainder is supported by the sand.

For bentonite-sand mixtures the gradients of the swelling lines might be expected to decrease with increasing sand content and/or applied stress, due to the greater interaction between sand particles and hence overall increasing sample stiffness (sand stiffness increases with sand effective stress). However, the data indicate that the gradients of the mixture swelling lines are approximately equal. Further, one-dimensional compression lines of sand with different initial void ratios are approximately parallel on a plot of void ratio against the logarithm of vertical effective stress (e.g., Atkinson and Bransby, 1978). Therefore, as an approximation, the assumption of equal gradients for the mixture swelling lines was considered satisfactory.

6.3.4 Swelling: modified Proctor compacted mixtures

Figure 5.10 shows that final clay void ratios are consistently lower for bentonite-sand mixtures compacted using the modified Proctor method than initially dry samples at the same effective stress. Figure 6.1 re-plots the 100% bentonite swelling data, the bentonite swelling line, and additional data points from the swelling of compacted 10 and 20% bentonite-sand mixtures at vertical effective stresses of 50-25kPa and 100-50kPa respectively (L3A, L4A, B3D and B3E from table 5.6). Although three of the data points are below the bentonite swelling line, the final clay void ratios achieved are within the experimental scatter of tests conducted on initially dry bentonite powder. Therefore, it is proposed that these mixtures exhibit swelling characteristic of 100% bentonite and lie on the bentonite swelling line. Results of Gray et. al (1984) support this hypothesis. They showed that initial water content had little, or no effect on the final swelling pressure developed by bentonite-sand mixtures (for bentonite contents of 25, 35 and 50%).

Compacted mixtures with final clay void ratios above the bentonite swelling line deviate from the idealised behaviour of dry 5, 10 and 20% bentonite-sand mixtures above their respective threshold stresses as shown in figure 5.10. Hence, for mixtures compacted at optimum moisture content, where the behaviour deviates from that exhibited by 100% bentonite, the swelling (indicated by the clay void ratio) is less than the corresponding 'dry' mixture.

These differences are attributed to the effects of clay water on remoulding during compaction, leading to a denser sand packing. All mixtures were compacted at 11-12% moisture content, and therefore, as the bentonite content reduces, the moisture content

of the clay significantly increases (assuming all the pore water is associated with the clay). Figure 5.10 illustrates that the largest deviation from the idealised dry swelling behaviour occurs when the initial clay water content is highest (i.e., 5% bentonite-sand mixtures). Therefore, as the clay water content increases, the sand can be compacted to a lower void ratio than the corresponding dry mixture, hence, a greater proportion of the effective stress is supported by the clay, or, the clay void ratio is lower

6.3.5 Consolidation characteristics of bentonite

The change in clay void ratio of saturated bentonite with increasing vertical effective stress follows the normal consolidation line shown in figure 5.11. Consolidation follows a similar line for both clay allowed to swell to equilibrium from a dry state and that mixed as a slurry. Test C100R11 initially reached equilibrium (prior to consolidation) close to the bentonite swelling line at a vertical effective stress of 1.44kPa. For this sample, the compression index, C_c, calculated from the first loading increment is initially quite low. However, as further consolidation stages are applied the calculated values of C_c are all similar indicating virgin compression along the normal consolidation line (see tables 5.7 and 5.8). The same behaviour is exhibited by the sample mixed at the liquid limit which initially had a clay void ratio only slightly below the normal consolidation line.

The initial deviation from linearity on the e_c - log σ'_v plot of the bentonite slurry is attributed to slight overconsolidation due to placement into the consolidation ring. Therefore, the bentonite initially compresses along an elastic rebound line until the applied stress is equivalent to the overconsolidation stress produced by sample preparation, after which compression is along the normal consolidation line. The initial clay void ratio of the sample which was allowed to swell initially is also below the normal consolidation line (see figures 5.11 and 5.12). However, it is suggested that a different clay fabric is manifested in swelling from the dry state, which, from a single datum point, appears as overconsolidation[4]. The data indicate that when subsequent consolidation occurs and the vertical effective stress exceeds an 'equivalent overconsolidation stress', the clay void ratio will be equivalent to that on the normal consolidation line.

Figures 5.11 and 5.12 illustrate that the bentonite swelling line is clearly different from the normal consolidation line or any associated rebound line, further suggesting

[4]Although the position of the datum point is similar to that of a fully saturated soil following a consolidation-rebound sequence, the state of the sample and the stress history are different. By definition, an overconsolidated soil has been consolidated in its previous stress history. This is not the case for swollen samples even though the stress path may be one of decreasing vertical effective stress. In addition, swollen samples are dry before swelling is allowed, whereas overconsolidated samples are saturated prior to volume increase along a rebound line.

differences in fabric for different sample states. This makes a knowledge of stress history critical if the equations of the lines are to be used for predictive purposes. For example, consolidation appears to remove the effects of any initial variation in fabric because the behaviour of both sample types converge on the normal consolidation line and the rebound characteristics are essentially identical. The difference arises from the bentonite being in an initially 'dry' state, meaning that a consolidation stage never occurs. If the clay powder is compressed by an applied stress whilst dry, it is postulated that the fabric does not change. When allowed access to water, the final clay void ratio of this type of sample will lie on the bentonite swelling line. In contrast, an initially saturated clay with a void ratio higher than is able to support an applied stress will consolidate, and its subsequent stress path on unloading will be along a rebound line.

Seed et al. (1962) found the subsequent swelling characteristics of compacted clay samples previously subjected to high stresses are less than those of identical samples subjected directly to low stresses because of the increased degree of particle orientation induced by the high stress application. A multistage test (test 100A in table 5.2) was performed to investigate this. The results show that provided the sample is initially dry it will follow a stress path on unloading corresponding to the bentonite swelling line. This confirms that dry samples will lie on the bentonite swelling line at equilibrium provided there is no consolidation at any stage.

6.3.6 Effect of initial moisture content on the swelling of bentonite-sand mixtures

Graham et al. (1989) performed isotropic swelling tests on bentonite-sand mixtures at bentonite contents greater than 50%[5]. They established a swelling equilibrium line by plotting clay specific volume, v_c, against the logarithm of effective confining stress (or cell pressure, σ'_3). The model developed suggested that if the effective confining pressure is lower than the swelling pressure, time-dependent swelling will occur as the bentonite moves towards its equilibrium water content. Similarly, the results of one-dimensional swelling tests on dry and compacted bentonite-sand mixtures show that this is reasonable provided the mixture is in a relatively dry state, and the effective stress is below the threshold value (i.e., mixtures of this type lie on the bentonite swelling line).

The increase in void ratio during the unloading of a bentonite specimen which has been swollen to equilibrium from a dry state is described by the bentonite swelling line. However, when such a sample is loaded, the volume change tends to the normal consolidation line. Therefore, it is proposed that, provided the initial moisture content is

[5]Since a sodium bentonite was used for these swelling tests it is assumed that the samples exhibited the same swelling behaviour as bentonite alone because any contact between sand particles at 50% bentonite content is unlikely.

less than the value at equilibrium, and also there has been no previous volume decrease, the clay will swell in the same manner as initially dry samples.

Above the threshold stress, the final clay void ratios of compacted mixtures are less than initially dry mixtures. This was attributed to the increased clay moisture content which enables the sand to be compacted to a lower sand void ratio (see 6.3.4). However, it is proposed that the swelling of the compacted clay is consistent with that of dry mixtures, provided the initial clay moisture content is less than the equilibrium value on the bentonite swelling line. If all the water is assumed to be associated with the bentonite, clay moisture contents can be evaluated by dividing the overall moisture content by the fraction of clay in the mix. If 12% is taken as the initial overall moisture content of all compacted samples (table 5.1), the corresponding clay moisture contents are 60, 120 and 240% for 20, 10 and 5% mixtures respectively, i.e., the bentonite becomes increasingly wet as the clay percentage reduces. Substitution of the final clay void ratios of compacted mixtures (table 5.6) into equation 5.9 gives the effective stress in the clay at swelling equilibrium. This is less than the overall effective stress because the final void ratios lie above the bentonite swelling line. Figure 6.2 compares the initial clay moisture contents of compacted mixtures to the final clay moisture contents of 100% dry bentonite specimens at swelling equilibrium in e_c - log σ'_c space. Although the clay in the mixtures may be relatively wet, figure 6.2 shows that initial clay moisture contents of compacted samples are less than the equilibrium values. Therefore, the swelling of the clay within the mixture should still be in the same manner as that for dry bentonite.

6.3.7 Effects of surcharge on bentonite fabric

The swelling behaviour is consistent with the swelling models presented in chapter 2. When the bentonite powder is allowed access to distilled water the osmotic concentration difference which exists between the interparticle void space and the pore fluid causes the water to flow between the particles, causing swelling. The osmotic pressure balances the externally applied stress, and therefore, the equilibrium void ratio decreases with increasing stress. At higher applied stresses it is likely that the effects of double layer are reduced but interlayer swelling remains, and the gradient of the swelling line decreases.

When bentonite is allowed to swell from an initially dry state it has a different fabric than if consolidated from a slurry. The cluster concept proposed by Olsen (1962) provides a satisfactory explanation for this behaviour. When the clay is mixed unconfined with water, is it likely that a uniformly flocculated fabric is developed without a tendency for the particles to form clusters, and the contribution to swelling is from individual particles.

When confined in an initially dry state, a more random fabric is likely consisting of clusters of particles. It is suggested that the swelling mechanism does not alter the fabric but merely increases the separation between particles within a cluster and between the clusters themselves, and due to the random orientation the void ratio is less than that of a normally consolidated sample. Hence, the normal consolidation line is higher than the bentonite swelling line in e_c-log σ'_v space. Consolidation removes the effect of initial fabric by compressing first the inter-aggregate voids then the intra-aggregate voids in swollen samples. Therefore, as the degree of particle alignment increases, the fabric of both samples becomes similar[6].

Consolidation data were used to indirectly calculate the hydraulic conductivity of the swollen dry bentonite sample and the sample mixed at the liquid limit for each loading stage (tables 5.7 and 5.8). At comparable void ratios, the swollen dry bentonite sample had an initial hydraulic conductivity more than one order of magnitude above that of the sample mixed at the liquid limit. For subsequent loading stages the hydraulic conductivity decreases to approximately twice that of the liquid limit sample. This supports the concept of inter and intra-aggregate groupings for samples lying on the bentonite swelling line. The effect of consolidation is to compress the larger inter-aggregate pores where the majority of the flow occurs, and therefore as the stress increases the two hydraulic conductivities are comparable. The initially 'wet' bentonite will still possess a lower hydraulic conductivity because the fabric is not as open, which makes the tortuosity of the flow path longer.

6.3.8 Effect of surcharge and bentonite content on swelling

For dry bentonite-sand mixtures, the degree of sand particle contact before swelling, and at swelling equilibrium, is dependent on both the bentonite content and applied stress. The amount of contact can be established by calculating the sand void ratio for each mixture using equation 5.4. The maximum sand void ratio for the sand alone was found to be 0.978. In developing a model of the behaviour of the mixtures, it will be assumed that at a value greater than this there is no contact between sand particles. Conversely, sand void ratios less than 0.978 will be interpreted as indicating variable degrees of particle contact. Table 6.1 presents sand void ratios before and after swelling of 20, 10 and 5% bentonite-sand mixtures. Not all data are included, but values corresponding to the full stress range used in the tests are shown.

[6]The existence of the proposed fabrics has been shown by various authors (e.g., Mitchell, 1993).

Test number	% bentonite	Surcharge kPa	Initial sand void ratio	Final sand void ratio	Final sand relative density
20A1	20	453	1.055	0.929	0.09
20B2	20	241	1.093	0.987	-0.02
20D4	20	100	1.166	1.108	-0.25
20E5	20	54.5	1.189	1.208	-0.44
20I7	20	20.2	1.167	1.472	-0.94
C20L8	20	10.02	1.303	2.015	-1.97
20N10	20	2.31	1.297	2.963	-3.77
20P11	20	1.67	1.262	3.103	-4.03
10A1	10	453	0.775	0.749	0.43
10B2	10	240	0.922	0.834	0.27
10F5	10	100	0.869	0.804	0.33
10I6	10	54.4	0.856	0.816	0.31
C10K8	10	17.7	0.909	0.950	0.05
C10M9	10	10.20	0.866	0.932	0.09
10O10	10	3.50	0.827	1.210	-0.44
10Q11	10	1.25	0.851	1.416	-0.83
5A1	5	453	0.663	0.630	0.66
5B2	5	241	0.687	0.655	0.61
5C4	5	101	0.737	0.692	0.54
5E5	5	54.4	0.727	0.685	0.56
5G5	5	11.58	0.689	0.690	0.55
5H10	5	3.19	0.678	0.733	0.47
5M11	5	1.23	0.722	0.845	0.25

Table 6.1. Sand void ratios of bentonite-sand mixtures.

The data presented illustrate that the initial sand void ratios are merely a function of bentonite content. There is a slight expected tendency to decrease with increasing effective stress which is attributed to particle rearrangements. The data suggest that sand particle contact is unlikely for any 20% bentonite-sand mixtures, and that sand interaction increases with decreasing bentonite content and/or increasing applied stress. The same behaviour is observed with final sand void ratios and is more exaggerated due to swelling of the bentonite.

From table 6.1, can be seen that the sand void ratios of certain samples decrease during testing. This implies that consolidation is occurring. However, the bentonite is initially dry and it is inappropriate to view this behaviour as consolidation in the conventional sense. It is proposed that as the clay swells, the mixture becomes wetter which disturbs the sand fabric allowing a lower sand void ratio to be reached (a similar phenomenon to that exhibited by compacted samples). The stress path is still one of stress reduction in the bentonite as the osmotic pressure deficiency between the clay particles is reducing when fluid enters the sample. Hence, the conclusions concerning stress path effect on fabric in 6.3.6 remain valid.

The state of packing of a sand can be represented by the relative density, I_D (equation 5.31); a value of 1 relates to the densest possible packing. In a bentonite-sand mixture, a relative density equal to zero corresponds to the sand being in the loosest possible packing on its own. A value less than zero indicates that sand particles are separated. Relative densities were calculated based on the final sand void ratios of bentonite-sand mixtures at swelling equilibrium, and are presented in table 6.1. The final state of interaction between the sand and clay becomes clear. Negative relative densities relate to the clay supporting all the applied stress (most 20% mixes), the lower the value, the more discrete the sand inclusions become in the clay matrix. Intermediate values indicate that the stress is shared between the sand and clay, and high relative densities (i.e. 5% mixes) indicate that the sand supports virtually all the applied stress. Theoretically, at a sand relative density of zero the sand particles are just in contact in their loosest possible packing with swollen bentonite completely filling the voids. It is likely that due to non homogeneity of the mixture this idealised structure will contain areas of higher sand relative density and areas where sand is contained as inclusions within the clay matrix. This reason is possibly what accounts for some scatter in the swelling data and, as a consequence, in the hydraulic conductivity results and behaviour during shear.

At high externally applied stresses, before swelling commences, the sand particles are interconnected to varying degrees depending on the bentonite content and must therefore

support some of the applied stress. The stress on the bentonite is the difference between the externally applied stress and that supported by the sand[7]. On access to water, the bentonite will swell towards the bentonite swelling line. If the osmotic pressure is greater than the stress supported by the clay, swelling will tend to force the sand particles apart, decreasing the sand stress and increasing the clay stress. This continues until equilibrium when the clay effective stress balances the osmotic pressure. At low applied stresses the sand particles are forced completely apart and the clay void ratio lies on the bentonite swelling line. If, however, the bentonite content is very low, most or all sand particles are initially in contact. The clay swells to fill the voids, but when full, the clay void ratio is so low that the osmotic pressure is not sufficient to force sand particles apart and the sand remains in contact. This is exhibited by 5% bentonite-sand mixtures, whose final clay void ratios all lie above the bentonite swelling line.

To conclude, if the osmotic pressure causing swelling is greater than the effective stress supported by the clay when the sand relative density is equal to zero, the bentonite will continue to swell and force the sand particles apart. The final clay void ratio will be given by the bentonite swelling line. Otherwise, the effective stress is shared between the bentonite and the sand to a degree depending on the vertical stress and bentonite content.

[7]At this stage the material is unsaturated, and the amount of stress supported by each soil phase should be regarded as a proportion of the externally applied (total) stress. An interpretation in terms of effective stresses is only possible at swelling equilibrium when the sample is fully saturated.

6.4 Hydraulic conductivity

6.4.1 Validity of Darcy's law

When the velocity head is small, and inertial effects are neglected, flow of water through soil can be described by Darcy's law, which can be written

$$v = ki \qquad 6.3$$

where v is the specific discharge or superficial flow velocity in m/s, k the hydraulic conductivity, and i the hydraulic gradient (e.g., Bear, 1972).

Clearly, when Darcy's law is valid the specific discharge will increase proportionally with hydraulic gradient, and have a value of zero when the applied total head difference is zero. Further, for accurate direct measurement, the volume of the sample must remain constant such that there is no additional contribution to the measured flow due to swelling or compression. Chapter 2 discussed the factors which influence hydraulic conductivity, k (i.e. mechanical and physico-chemical effects), and possible deviations from Darcy's law.

Figures 5.13-5.16 showed that inflows and outflows for each test on 100% bentonite and bentonite-sand mixtures are effectively equal after initial equalisation of samples following the applied head difference. Sample heights were monitored throughout the tests and it was found that no significant volume change occurred. Thus, there is no sample volume change and flow is due solely to steady state seepage. Figure 5.17 shows a linear variation of specific discharge with hydraulic gradient for a 20% bentonite-sand mixture (tests B1A-B5A). Linear regression analysis gives a coefficient of correlation, r^2, of 0.968. However, the line fitted for this predicts flow through the sample at a hydraulic gradient of zero. Linear regression analysis of the data with the origin fixed at zero yields a value of 0.966. For each test stage, measurements were made when the volume of the sample remained constant, but over the test as a whole, the change in sample volume was 0.7% of the initial volume which may account for the different correlation values. Therefore, for the range of hydraulic gradients used in the testing programme, Darcy's law appears to be valid. A 20% bentonite-sand mixture was used for verification of equation 6.3 because the relatively large volume of bentonite will be subject more adversely to physico-chemical effects than in other mixtures.

The falling head analysis assumes Darcy's law to be valid. Once this was established, falling head compaction permeameter tests were performed to increase the data set. Figure 5.20 shows that the hydraulic conductivity of 5% bentonite mixes initially decreases with time, apparently contradicting Darcy's law. However, the decrease in hydraulic conductivity is probably caused by the swelling of the clay. At the start of the

test the sample is not in a condition of swelling equilibrium. Therefore, as the amount of water permeating increases, the depth of sample where particle swelling occurs increases, reducing the pore space available for water flow hence causing the hydraulic conductivity to decrease with time.

All hydraulic conductivity tests were ended before 20% of the pore fluid was replaced. This minimised the potential to alter swelling characteristics and bentonite fabric caused by physico-chemical effects. For example, the applied head difference may cause cations to be washed out of the sample. The effects of this would be to decrease the net attraction between particles resulting in overall swelling of the sample. As a consequence the double layer thickness would increase with a reduction in the 'effective' area available for flow because of the greater quantity of adsorbed water[8]. The resultant effect would be a decrease in flow rate not caused by the decreasing hydraulic gradient, but by a decreasing hydraulic conductivity.

6.4.2 Hydraulic conductivity of bentonite and bentonite-sand mixtures

Figure 5.21 displays data of hydraulic conductivity of bentonite, sand and bentonite-sand mixtures against overall sample void ratio on a logarithmic plot. Included are all results from constant head tests, falling head tests and indirect measurement. As expected the hydraulic conductivity decreases with decreasing void ratio for all mixtures because of the reduced pore space available for flow.

Despite experimental scatter, data for 100, 20 and 10% bentonite mixtures all follow a similar trend and can be plotted on a straight line in logarithmic space (figure 5.21) given by

$$k = 10^{-11.016}\, e^{1.571} \qquad 6.4$$

with a coefficient of correlation of 0.768. As discussed in chapter 5, this is taken as indicating that these mixtures are behaving as the same soil type. Data for 5% bentonite-sand mixtures lie on a different trend, the path of which tends towards the hydraulic conductivity of sand alone.

The implication of the data for 5% bentonite-sand mixtures is that the low bentonite content leads to an uneven distribution of bentonite within the sand matrix. This may be due to the mixing method or an effect of compaction causing local variations. A relatively large variation in maximum achievable dry density after mixing and compaction of three different 5% bentonite-sand mixtures is shown in table 5.1, but relatively little change was found for 20% mixes, which shows that uneven distribution is more

[8]This is the effective porosity discussed by Oscarson and Cheung (1983); see chapter 2.

significant as the clay content decreases. Non homogeneity results in the existence of preferential flow-paths throughout the volume of the sample in areas with low bentonite contents. Chapuis (1990) found that variations in bentonite content throughout a mixture may be in the range 25-35%, when the overall clay content is very low. Cowland and Leung (1991) report non homogeneous mixtures at 5% bentonite content, and recommend a minimum bentonite content of 7% to avoid non homogeneity.

Figure 5.21 shows that the data for 20 and 10% mixes deviate from the best fit line at the highest void ratios (tests C20A and C10A in tables 5.15 and 5.16 respectively). The data trends are in accordance with the Kozeny-Carman equation which predicts a greater than proportional increase in hydraulic conductivity with void ratio (tending to linearity) on a logarithmic plot. The differences between mixtures are attributed to different pore size terms and specific surface areas (see 5.4.4). However, as an approximation, the linear relationship shown in figure 5.21 is considered reasonable.

6.4.3 Factors affecting the hydraulic conductivity of bentonite

As the effective stress is increased the swelling of bentonite powder is reduced with a corresponding lower void ratio which is given by the bentonite swelling line. As a consequence, it is proposed that there are three factors which contribute to the lower hydraulic conductivity:

1. The pore space available for flow decreases simply because of the lower void ratio. At higher void ratios it is more likely that relatively large inter-aggregate pores conduct most of the flow. At low void ratios it is likely that all the pores are of a comparable size.

2. The tortuosity of flow paths is longer due to greater interaction between clay particles. A more open fabric of a highly swollen sample presents less of a tortuous path for pore water to permeate.

3. As less water is adsorbed overall, the higher viscosity of water in close proximity to the bentonite particle surfaces further reduces the area available for flow.

A linear relationship between hydraulic conductivity and clay void ratio on a logarithmic plot (figure 5.22) appears to account for the above factors. Therefore, although the hydraulic conductivity of bentonite is dependent on the fabric of the sample and double layer interactions it can be sufficiently characterised by the clay void ratio.

6.4.4 Effect of sand on hydraulic conductivity of bentonite-sand mixtures

The literature highlights the uncertainties regarding the effects of sand (or bentonite) content on the hydraulic conductivity of bentonite-sand mixtures. The results of Daniel (1987) show that at bentonite contents greater than or equal to 8%, the measured

hydraulic conductivity was about 10^{-10} m/s. Cowland and Leung (1991) found no noticeable relationship, Garlanger et al. (1987) and Chapuis (1990) found that hydraulic conductivity decreases with increasing bentonite content, whereas Dixon and Gray (1985) found that adding up to 50% sand to bentonite decreases the hydraulic conductivity of the compacted material. Incorrect representation and/or characterisation of the mixture are thought to be the cause of these often contradictory findings. For example, unconfined hydraulic conductivity tests on samples with bentonite contents greater than 5% are likely to give erroneous values due to swelling at the sample boundaries. Samples must be at equilibrium conditions prior to testing and all relevant parameters are needed to interpret the data (i.e., inflow, outflow, void ratio, etc.). This is illustrated by the data in figure 5.21. At the lowest void ratio values the hydraulic conductivity of 5% mixtures is comparable to that for bentonite. However, at the highest void ratios the 5% mix is shown to have a hydraulic conductivity almost 3 orders of magnitude greater. A method of understanding and interpreting the data is presented in this section.

Figure 5.22 shows the data from 100, 20 and 10% bentonite-sand mixtures replotted on a logarithmic plot of hydraulic conductivity against clay void ratio. The data from 5% mixes have been omitted for the reasons discussed in 6.4.2. Three distinct trends are apparent, indicated with best-fit straight lines given by equations 5.26-5.28. The largest amount of experimental scatter occurs for 10% bentonite-sand mixtures (with a maximum factor of 4 difference in hydraulic conductivity at approximately the same clay void ratio). As discussed in chapter 5 this is attributed to the interaction between sand particles in 10% mixtures, which increases the sample stiffness. This reduces the accuracy of curve fitting when hydraulic conductivity is calculated indirectly.

An advantage of plotting the data in this way is that clay void ratios are easily determined from the swelling behaviour and can therefore be substituted into the equations to give hydraulic conductivity values. In addition, the consequences of assuming similar soil types are removed (see 6.4.2). Therefore, the effects of the sand on hydraulic conductivity of bentonite-sand mixtures can be identified and quantified as follows.

Solutes diffuse at slower rates in soil than in free solution because the pathways for migration are more tortuous in soil. Also, diffusive mass fluxes are less in soil than in free solution because solid particles occupy some of the cross-sectional area. Figure 6.3 is a schematic diagram of a bentonite-sand mixture, showing bentonite gel occupying a tortuous pore within a sand matrix. In bentonite-sand mixtures pore fluid flows through the bentonite gel within the tortuous pores of the sand matrix, and the impermeable sand

particles occupy some of the cross-sectional area. Adopting the approach taken by Porter et al (1960) to define the effective diffusion coefficient of an ion in saturated soil from its diffusion coefficient in dilute solution, Darcy's flow law can be written as:

$$Q = k_{mix} A \frac{\Delta h}{\Delta L} = k_{clay} A_e \frac{\Delta h}{\Delta L_e} \qquad 6.5$$

where Q is the flow volume, k_{mix} and k_{clay} are the hydraulic conductivities of the mixture and clay respectively, Δh is the head difference, ΔL is the macroscopic length over which flow takes place, ΔL_e is the average length of a flow tube through the sand, A is the cross-sectional area, and A_e is the effective cross-sectional area available for flow normal to the flow direction; the remaining area being occupied by the sand matrix and unavailable for flow.

The volume of voids, V_V, plus the volume of clay, V_C (i.e. the volume of swollen bentonite gel), is equal to $A_e.\Delta L_e$, and the total volume, V_T, is $A.\Delta L$. Therefore the sand porosity, n_S defined in 5.3.1, is equal to $(A_e.\Delta L_e/(A.\Delta L))$. The sand tortuosity factor, τ_S, is defined as $(\Delta L/\Delta L_e)^2$, and therefore, the relationship between the mixture and the clay hydraulic conductivity is;

$$\frac{k_{mix}}{k_{clay}} = \frac{A_e \Delta L}{A \Delta L_e} = n_s \tau_s \qquad 6.6$$

Therefore the separation of the lines in figure 5.22 will depend on the sand porosity and tortuosity.

Equations 5.26-5.28 can be used to determine the sand porosity and tortuosity factors at any clay void ratio. At a clay void ratio of 5, the combined sand porosity/tortuosity factors for the 20% and 10% bentonite-sand mixtures are 0.07 and 0.02 respectively. At this clay void ratio the sand porosities are 0.6 and 0.4 for the 20% and 10% clay mixtures, respectively, suggesting tortuosity values for the sand matrix of 0.12 and 0.05. These are discussed in 6.4.5.

6.4.5 Porosity and tortuosity factors

The tortuosity range found in 6.4.4 seems low for a saturated sand. Porter et al. (1960) found values of $(\Delta L/\Delta L_e)^2$ of 0.04 at low saturation levels. However, because the materials were partially saturated, pores become predominantly less interconnected with decreasing saturation, and therefore, the flow is not commensurate with flow through a fully saturated material. Shackleford and Daniel (1991) report tortuosity values in the range 0.08-0.22 for a saturated sandy loam. The calculated values for the sand are quite close to this range and are expected to be on the low side for sands because the effective particle size (D_{10}) is towards the lower limit of the sand range.

Shackleford and Daniel (1991) define an apparent tortuosity factor, τ_a, in which is included not only the actual, geometric tortuosity, τ, but also all other factors which may be inherent in its measurement. A mobility factor, α, after Kemper et al. (1964) accounts for the increased viscosity of water adjacent to clay mineral surfaces. This can have no effect on the measured values since sand tortuosity values are calculated at specific clay void ratios and any effects associated with the clay are therefore removed. Porter et al. (1960) and van Schaik and Kemper (1966) define a factor, γ, to account for exclusion of anions from the smaller pores of the soil. This may have some effect when the sand is at a very high density. Berner (1971) states that anion exclusion may occur in natural deposits when the average porosity of the soil is less than 0.3. However, anion exclusion is mainly due to double layer effects and is likely to have no significant effect on the calculated sand tortuosity values.

The most likely explanation for the low tortuosity values is an overestimation of the sand porosity at low clay void ratios. A low clay void ratio implies a corresponding low sand void ratio. Several authors (e.g. Bear, 1972) state that in materials not subject to physico-chemical effects, the available volume for flow is less than the calculated porosity when the overall porosity is low. This effect is attributed to 'dead end pores' in the sand matrix where the flow path is effectively terminated, and the hydraulic conductivity is related to the effective porosity. As the overall porosity of the sand increases the effect of dead end pores is removed and the volume available for flow is simply the porosity.

The consequence of a lower sand porosity than calculated would be to increase the tortuosity value, as the overall reduction factor remains the same. However, the value of this parameter is unknown and therefore its effect can only be considered qualitatively.

Figure 6.4 shows combined sand porosity-tortuosity values for 20 and 10% bentonite-sand mixtures against clay void ratio plotted on a logarithmic scale. Values were calculated from equations 5.26-5.28. At large clay void ratios the combined factor for both mixtures tends to unity. Provided the mixture remains homogeneous and the clay can swell enough to completely fill the sand voids, the hydraulic conductivity becomes equal to that of bentonite alone when the combined factor equals one. This corresponds to a clay matrix with sand particles as discrete inclusions. The mixture hydraulic conductivity cannot be greater than that of the bentonite because a sand porosity or tortuosity greater than one is impossible.

At low clay contents (i.e. 5% bentonite), for which a non homogeneous mixture is likely, the hydraulic conductivity is higher than for the bentonite alone, yielding a combined factor greater than one. Therefore, when the swelling of the bentonite is not sufficient to completely fill the sand voids the behaviour cannot be represented in this manner, and tortuosity-porosity factors become meaningless. In contrast, for higher bentonite contents (for example, greater than 50%) it is postulated that the mixture and bentonite hydraulic conductivities will be virtually identical because the reduction due to the sand porosity and tortuosity will be insignificant.

6.4.6 Effect of applied stress on the hydraulic conductivity of mixtures

In addition to bentonite content, the hydraulic conductivity is dependent on the applied stress. Although the hydraulic conductivity of 10% mixes are lower than for 20% mixes for a particular clay void ratio, the same is not necessarily true for a given effective stress. If the effective stress is high, i.e. above the threshold level (see 5.3.4), the sand particles will be in contact. In this state, the final clay void ratio at swelling equilibrium increases with decreasing bentonite content which will consequently increase the hydraulic conductivity (for a given effective stress). However, if the clay is supporting the surcharge, i.e., the applied stress is below the threshold value, a reduction in hydraulic conductivity will only occur if the sand porosity and tortuosity are reduced (equation 6.6). In this case, the hydraulic conductivity will decrease with decreasing bentonite content.

It is advantageous to represent the hydraulic conductivity in terms of the clay void ratio because this accounts for the swelling behaviour. This is important in the design of bentonite-sand mixtures (see chapter 7).

6.5 Strength

6.5.1 Strength of sand

The peak angles of shearing resistance given in 5.5.2 (table 5.18) are lower than is usually expected for a dense sand. The density, or void ratio, of sand affects the amount and rate of dilation during shear and consequently the additional dilatant component of strength above the constant volume value (ϕ'_{cv} was calculated as 30.4°). Cornforth, (1973) found that relative density offers a superior correlation compared with void ratio for the strength of sands, because it compensates for effects of particle grading and shape which influence the maximum and minimum achievable void ratios, e_{max} and e_{min} respectively.

The relative density values presented in table 5.18 account for the low measured peak strengths. The range of values are 0.46-0.62 for a strength range of 36.5°- 40.9°. The densities achieved are attributed to the sample preparation method in the triaxial apparatus. Due to the limitations of the particular triaxial systems used, the sand was tamped into the mould dry. To achieve high relative densities, it is generally recommended (e.g., Head, 1981) that the sand is compacted under saturated conditions. In addition, the effect of tamping will temporarily force the membrane against the mould. As the membrane pulls away from the mould on removal of the tamping rod, it is likely that the sand is sheared into a looser state.

Therefore, the results show that due to the sample preparation method the sand can be regarded as being in a medium dense state as described by the sand relative density. At higher relative densities the amount and rate of dilation would be greater than given in table 5.18 and, as a consequence, the maximum angle of shearing resistance more typical of a dense sand. This illustrates the importance of a stress-dilatancy approach for interpretation of laboratory test results and is discussed further in 6.5.4.

6.5.2 Strength of bentonite

Assuming no cohesion between clay particles, the calculated peak angles of shearing resistance (table 5.19) indicate a higher shear strength at a vertical effective stress of 50kPa than at vertical effective stresses of 200kPa and 100kPa. As discussed in chapter 2, apparent values of cohesion are usually due to either dilatancy in overconsolidated clays, or because pore water pressures have not been properly accounted for. Data from triaxial compression tests by Mesri and Olson (1970), show that the cohesion term is minor compared to the friction term on an effective stress failure diagram for calcium and sodium montmorillonite. Therefore, as an approximation, the contribution to measured shear strength from 'true cohesion' will be ignored.

In the multi-stage shear box test conducted on bentonite, the stress path was one of reducing stress with the clay initially swollen from a dry state to equilibrium at the highest vertical effective stress (200kPa). Following the arguments of section 6.3, the fabric of the sample should remain unchanged as there is no consolidation throughout the test. Pore water pressures were calculated as approximately 1kPa at peak strength for all shearing stages, and therefore the effect on the measured strength is assumed to be insignificant.

These considerations initially offer no explanation for the enhanced shear strength at the lowest vertical effective stress. One possibility is a change in the sample fabric due to the shearing - unloading sequence, such that the sample behaves in a similar manner to an overconsolidated clay as the vertical effective stress is decreased. Or, since montmorillonite exhibits time dependent strength characteristics (e.g., Mitchell, 1993), the increased strength may be due to thixotropic hardening. Studds (personal communication, 1996) performed ring-shear tests on a sodium bentonite under a vertical effective stress range of 20-500kPa. Each sample was swollen from dry powder in distilled water until equilibrium conditions were reached under the applied stress. Within experimental scatter, the results show no significant change in angle of shearing resistance with applied stress.

In conclusion, it is thought that the angle of shearing resistance of bentonite is approximately 10° when swollen from a dry state.

6.5.3 Isotropic swelling of bentonite-sand mixtures

Prior to triaxial shear testing the bentonite-sand mixtures are at swelling equilibrium under the mean effective stress, p', equal to the effective cell pressure, σ'_3. If sand particles are not in contact, the state of stress of the sample will be represented by a point lying on the bentonite isotropic swelling line, and the clay void ratio can be calculated using equation 5.35 for the relevant cell pressure. Figure 5.32 shows the 20% bentonite mixtures at cell pressures of 25 and 50kPa, and a 10% mixture at 15kPa, lie on or very close to the isotropic swelling line. It can be inferred that in these samples the clay supports all the applied effective stress. For samples above the swelling line, the effective stress is shared between the bentonite and sand depending on the clay content and cell pressure. The effective stress in the bentonite is given by substituting the measured clay void ratio into equation 5.35. The effective stress in the sand is simply the difference between the applied stress and the clay effective stress because the excess pore water pressure is zero at swelling equilibrium. Values are presented in table 6.2, where σ'_c is the clay effective stress, and σ'_s the sand effective stress.

Also included in table 6.2 are values of initial sand void ratio and sand relative density, the maximum angle of dilation during shear, $\phi'_{max} - \phi'_{cv}$, and the rate of dilation at peak strength $(-d\varepsilon_v/d\varepsilon_1)_{max}$, both ε_v and ε_1 are defined positive in compression[9]. These parameters are discussed further in 6.5.4.

Test	% bentonite	σ'_3 (kPa)	e_c	σ'_c (kPa)	σ'_s (kPa)	e_s	I_D (sand)	$\phi'_{max} - \phi'_{cv}$ (°)	$\left(-\frac{d\varepsilon_v}{d\varepsilon_1}\right)_{max}$
CD204	20	21	3.903	21	0	1.226	-0.47	1.1	0.01
CD203	20	47	3.034	47	0	1.009	-0.06	-3	-0.06
CD202	20	99	2.439	60	39	0.860	0.22	0.4	0.42
CD201	20	195	2.222	66	129	0.806	0.33	-1.1	0.54
CU101	10	15	5.266	15	0	0.696	0.53	7.9	-
CD104	10	24	5.002	16	8	0.667	0.59	10.1	0.49
CD103	10	50	3.957	28	22	0.551	0.81	16.4	1.02
CD102	10	98	4.105	26	72	0.567	0.78	14.1	0.90
CD101	10	197	3.678	32	165	0.520	0.87	11.8	0.71
CD55	5	25	8.058	4	21	0.477	0.95	18.8	1.22
CD56	5	25	7.650	4	21	0.455	0.99	17.4	1.24
CD54	5	51	7.606	4	47	0.453	1.00	15.1	1.07
CD53	5	103	8.458	3	100	0.498	0.91	16.5	0.94
CD52	5	103	8.166	3	100	0.482	0.94	13.8	0.90
CD51	5	187	8.348	3	184	0.492	0.92	16	1.17

Table 6.2. Initial and shear parameters of bentonite-sand mixtures.

[9] ϕ'_{max} is the maximum angle of shearing resistance of the mixture from tables 5.20-5.22. ϕ'_{cv} is the constant volume angle of shearing resistance of the sand, calculated as 30.4° (see 5.5.2). Maximum rates of dilation were calculated by linear regression analysis on the portion of the smoothed volumetric strain-axial strain curve at peak strength.

Table 6.2 and figure 5.32 show that experimental scatter is greatest for 5% bentonite mixes, and again this is attributed to non homogeneity of the mixture as an effect of mixing and/or compaction. Due to scatter and lack of data, idealised swelling lines have not been fitted for mixtures with clay void ratios above the bentonite isotropic swelling line, and therefore the threshold stresses are not computed. However, it is suggested that the conclusions from the swelling behaviour of compacted mixtures in 6.3.4 remain valid. Samples which are initially relatively dry with a large enough bentonite content or small enough applied stress will swell to a point on the bentonite isotropic swelling line. Samples lying above the line will have a final clay void ratio lower than the corresponding dry mixture for a particular applied stress, due to the decreased sand void ratio caused by compaction. As the clay moisture increases, so will the difference between the dry and compacted mixture clay void ratios.

The clay and sand effective stresses give an indication as to how the material will behave in shear. In 5% bentonite mixes almost all the effective stress is supported by the sand matrix, the shear behaviour would therefore be expected to be characteristic of sand. As the bentonite content increases and applied stress reduces, the clay supports an increasing proportion of the effective stress and shear behaviour similar to that exhibited by clays is expected.

6.5.4 Analysis of strength data and possible sources of error

Bolton (1986) derived a relative dilatancy index, I_R, which offered a unique set of correlations for the dilatancy related behaviour of 17 sands in laboratory shear tests (equations 2.13 and 2.14). He presents unique plots of maximum dilatant angle of shearing resistance, $\phi'_{max} - \phi'_{cv}$, and maximum rate of dilation, $(-d\varepsilon_v/d\varepsilon_1)_{max}$, against I_R. Evidence suggests that the strength of a clay-sand mix is largely dependent on the sand when the clay-water volume is small enough for interaction between sand particles to occur (e.g., Kenney, 1977, Lupini et al, 1981). Therefore, Bolton's approach will be adopted for the analysis of triaxial strength data. As the relative dilatancy index was derived empirically, the dilatancy behaviour of bentonite-sand mixtures will be related to the sand relative density, I_D, as this is a fundamental parameter which provides easier visualisation of the state of the sand particles. In addition, the sand relative density can be calculated from simple phase relationships. Therefore, for design purposes, simpler correlations between the swelling behaviour and strength of bentonite-sand mixtures are possible (see chapter 7).

Figures 6.5a and 6.5b are plots of maximum dilatant angle of shearing resistance and rate of dilation at peak strength against sand relative density respectively, for bentonite-sand

mixtures tested in triaxial compression[10]. Included in the figures are data for triaxial tests on sand (table 5.18). A strength and dilatancy analysis with the sand relative density as a parameter can only be valid when the sand particles are in contact. Sand void ratios greater than 0.978 (or $I_D < 0$) are interpreted as indicating no particle contact (see 6.3.8). Therefore, data from 20% bentonite-sand samples at the two lowest confining stresses (CD203 and CD204) were excluded from the analysis. These samples exhibited positive volumetric straining during shear and are indicated in figure 6.5, where c denotes that the samples compressed (volumetrically) on shearing. Linear regression analysis was conducted on samples with I_D values equal to or greater than zero (i.e., dilating at failure) to give

$$\phi'_{max} - \phi'_{cv} = 20.60 I_D - 3.40 \qquad (r^2 = 0.789) \qquad 6.7$$

$$\left(-\frac{d\varepsilon_v}{d\varepsilon_1}\right)_{max} = 1.18 I_D - 0.12 \qquad (r^2 = 0.712) \qquad 6.8$$

The behaviour of samples with negative relative densities is discussed in 6.5.5.

By relating the strength and dilatancy to the sand relative density, the significance of mean effective stress on the peak strength (i.e., for a given density, increasing stress decreases strength and dilatancy) is ignored. Bolton's dilatancy index accounts for these factors. This affects measured dilatant angles of shearing resistance by a maximum of 0.4° (avg. = 0.3°), 2.7° (avg. = 1.9°), 4.2° (avg. = 2.5°) and 2.5° (avg. = 1.2°) for 20, 10 and 5% bentonite mixtures and sand respectively, over a stress range of 25-200kPa. The effect is clearly visible in figure 6.5a, where four of the five sand data points grouped below the best fit line were tested at the highest stress (200kPa). This demonstrates the loss in dilatant strength with increasing confining stress. However, plotting in terms of relative dilatancy index provides no improvement for this experimental stress range. In addition, it may be inappropriate to report data of samples with negative sand relative densities on such a plot.

At constant volume there is no dilation, therefore, both $(\phi'_{max} - \phi'_{cv})$ and $(-d\varepsilon_v/d\varepsilon_1)_{max}$ are equal to zero. The corresponding values of sand relative density are 0.165 (equation 6.7) and 0.104 (equation 6.8). Fundamentally the I_D intercept on each plot must be identical. The differences between the calculated intercepts, and between the coefficients of correlation, are attributed to the rates of dilation of the two dilatant 20% bentonite-sand samples shown in figure 6.5b, which are not consistent with the measured peak strength. These data are clearly higher than the expected values and do not fit the broad trends exhibited by all other data points (of dilatant specimens) on both plots. However, the source of this error is unknown. Bolton's analysis suggests that no dilation occurs at

[10]Data from the consolidated-undrained test, CU101, is excluded from figure 6.5b.

sand relative densities of 0.147 and 0.213 for mean effective stresses of 25 and 200kPa respectively. Since this was the stress range used for the test programme, a sand relative density of 0.165 at constant volume is more likely of the two calculated values.

The maximum deviations from the best fit line given by equation 6.7 in figure 6.5a are as follows:
20% bentonite: -4.4° to -0.8°
10% bentonite: -2.7° to 3.1°
5% bentonite: -2.2° to 2.6°
sand: -2.9° to 4.4°
This results in the relatively low coefficient of correlation. Experimental scatter may result from ignoring the effect of confining stress (discussed above) which is accounted for in Bolton's relative dilatancy index. However, a lower coefficient of correlation ($r^2 = 0.772$) was found when linear regression analysis was conducted on the data with the relative dilatancy index replacing the sand relative density. It is suggested, therefore, that the experimental scatter is due to either the triaxial system instrumentation, or non homogeneity of the sample, or a combination of both. These are discussed below.

The angle of shearing resistance is proportional to the ratio of maximum deviator stress to the sum of the principal stresses (equation 5.29). At low effective cell pressures, or high bentonite contents, the measured deviator load is small compared to the maximum range of the load transducer, and the accuracy of the transducer becomes increasingly significant. Any errors in load or pressure measurement are therefore exaggerated when the deviator stresses are small. Smoothing was performed on the raw data of triaxial tests to account for electrical noise (see chapter 5), and a maximum error in load exceeding 2N is unlikely. This corresponds to a deviator stress of approximately 2kPa[11]. If a maximum drift of 2kPa is also assumed for cell and back pressure transducers, the worst combined error gives a strength estimation within ±4° at the smallest deviator stress (test CD204). As this scenario presents the worst case, the expected maximum error in the measured strength is 1-2°. The scatter in the majority of the data is within this error band.

Another cause of experimental scatter may be local variations across the shear plane, which lead to areas where the sand supports an effective stress different from that calculated by equation 6.1. The results from compaction, swelling and hydraulic

[11]The manufacturers specifications indicate an accuracy to 0.05% of full scale deflection. Using this value the accuracy should be to within ±1kPa. However, diurnal temperature changes were shown to have a significant effect on the response of transducers in chapter 3, and an accuracy of ±2kPa is believed to be more likely.

conductivity tests indicate that a homogeneous mix was produced for samples with 20% bentonite content. However, slight variations may have a significant effect on the shear behaviour when the clay content is high. The strength of mixtures appears to be largely dependent on the interaction between sand particles. Therefore, the scatter in data decreases with increasing sand content (for mixtures only) because local variations in bentonite content have a less significant effect on the degree of sand particle interaction[12].

6.5.5 Strength and dilatancy of bentonite-sand mixtures

The data indicate that when the sand relative density of a bentonite-sand mixture is greater than zero, the sand packing determines the strength, and the dilatancy-related behaviour is characteristic of sand alone. At relative densities in the range 0-0.17, stress-strain behaviour characteristic of loose sand is likely, i.e., tending towards constant volume conditions at an angle of shearing resistance of 30.4°. When the sand relative density is greater than 0.17, the material dilates during shear and the peak strength increases with increasing sand relative density. Peak strengths can be calculated by addition of the dilatant angle of shearing resistance given by equation 6.7 to the constant volume value of 30.4°.

When the initial sand relative density is zero or negative, no contact between sand particles is assumed. In this state, shearing will cause a positive volumetric strain (-ve dilation) bringing the sand particles into closer proximity. It is postulated that the material shears as clay until the volumetric strain is sufficiently large such that sand particle interaction occurs, when the strength will be equal to the constant volume angle of shearing resistance of sand[13]. If the initial clay void ratio is large enough, then a strength purely characteristic of clay is suggested. Swelling tests results have shown that the initial clay void ratio is dependent on the mean effective stress and bentonite content.

Figure 6.6 is an idealised plot of the peak angle of shearing resistance of bentonite-sand mixtures against the sand relative density. This plot is similar to figure 6.5a. The slope of the mixture peak strength line is given by equation 6.7. No dilation occurs when the strength is equal to 30.4°, this is indicated by the sand constant volume strength line. When the stress-strain behaviour is purely characteristic of clay, a peak strength of 10° is assumed (see 6.5.2). This is indicated by the bentonite peak strength line. Intermediate strengths of mixtures are bounded by the sand constant volume strength line and the bentonite peak strength line. In this area, strength estimation is impossible because it will

[12]Scatter in the test data for sand is attributed to the sample preparation method (see 6.5.1).
[13]This model assumes that the volume of sand is sufficiently large that significant sand particle contact occurs on compression of the clay-water phase.

be dependent on the bentonite content and volumetric strain. It is suggested that intermediate strengths will exist at bentonite contents greater than used in this study, or at very low effective confining stresses (both effects lead to lower sand relative densities).

A threshold sand relative density is postulated, below which the strength will be given by the bentonite peak strength line. However, suggesting a value is difficult, due to the dependency on the degree of strain (i.e., if the compression is sufficient to bring the sand particles into contact, when the sand volume is relatively large, the strength will be given by the sand constant volume strength line). Inherent in this proposal is the assumption of the sand having no significant effect on the shear behaviour, and angle of shearing resistance, when the bentonite content is high and/or the effective stress low and/or the compression on shearing is small. This is substantiated by the results of Graham et al. (1989). They performed drained and consolidated-undrained triaxial tests with pore water pressure measurement on 50% bentonite-50% sand mixtures (at a mean effective stress of 100kPa the sand relative density is likely to be approximately -2.5). They found the strength of the mixture to correspond to the mineralogy of the clay phase (ϕ'_{max} = 14°).

In summary of the idealised behaviour, a bentonite-sand mixture with an initial sand relative density less than a threshold value (dependent on bentonite content and/or mean effective stress and/or degree of strain during shear) will exhibit shear behaviour characteristic of bentonite, with an angle of shearing resistance of approximately 10°[14]. As the sand relative density increases, intermediate strengths are expected as some sand interaction occurs, and the sand relative density tends to a value of 0.17 (constant volume conditions) as the sample compresses. For sand relative densities higher than 0.17, dilation of the sample occurs and peak strengths are given by the mixture peak strength line. Strength increases with increasing sand relative densities greater than 0.17. The idealised plot calculates a maximum strength of 47.6° at a sand relative density of 1.

6.5.6 Behaviour during shear of bentonite-sand mixtures

The change in shearing behaviour of bentonite-sand mixtures with increasing clay content and/or decreasing mean effective stress (both causing a reduction in sand relative density), is analogous to the three modes of shearing proposed by Vaughan et al. (1976) and Lupini et al. (1981) described in chapter 2. At a sand relative density greater than

[14]As discussed in 6.5.2, this is the shear strength of swollen bentonite with a stress path of decreasing mean effective stress. For mixtures where the sand particles are separated the state of the bentonite will be described by the isotropic swelling line, the remainder will have clay void ratios above the line. However, for all samples consolidation has not occurred at any stage.

zero, shear behaviour will be of the turbulent type, involving rolling and translation of the sand particles. The sand dilates to achieve a constant volume strength at a sand relative density of 0.17. Below a threshold sand relative density, shearing behaviour of the sliding type occurs. As the sample shears, the platelike bentonite particles align and a low strength equivalent to bentonite alone is measured. Transitional shear behaviour is postulated at intermediate sand relative densities. Although there is initially no sand in contact, shearing causes a positive volumetric strain which, if continued, may cause interference between some sand particles, with a corresponding strength intermediate between that of bentonite and sand (at constant volume). Further shearing will cause the strength to tend towards the constant volume value; behaviour exhibited by samples CD203 and CD204 in figure 6.5.

Figure 6.7a shows an idealised state of packing for a 20% bentonite-sand mixture at 25kPa mean effective stress prior to shear (test CD204). Sand particles exist as inclusions within the clay matrix, and therefore all the effective stress is carried by the clay. Figure 6.7b is a possible packing at 20% axial strain. Shearing of the sample has produced a positive volumetric strain of the clay causing some interaction between sand particles along the shear plane. At this state the effective stress is carried by the bentonite and very loose sand skeleton. The sand density is still less than that at constant volume. However, the compression of the sample caused sufficient particle interaction for the sand constant volume strength to be mobilised (measured value = 31.5°), and the state of the sample is represented by the sand constant volume strength line in figure 6.6. It is postulated that the sand relative density tends to the constant volume value of 0.17 with further shearing with no change in strength. For this sample a plastic failure occurred, typical of a normally consolidated clay or a loose sand (figure 6.7c).

In figure 6.8a the initial packing yields a sand relative density greater than 0.17 prior to shear (test CD201). As the sand is denser than critical, shearing causes a negative volumetric strain, the sample dilates, and theoretically the peak strength is given by the mixture peak strength line[15]. As for all other samples, the sand relative density will tend towards 0.17 (i.e., constant volume conditions) during shear. Figure 6.8b shows the state of packing after shear. Sand particles shear against each other on a definite failure plane (as was observed in the test). The failure diagram at 20% axial strain is shown in figure 6.8c. The behaviour of the sample during shear is typical of a sand with a density higher than at the critical state.

[15]The measured peak strength was lower than that predicted by equation 6.7. Suggested reasons for this were given in 6.5.4.

The deviator stress versus axial strain curves further support the proposed behaviour of bentonite-sand mixtures during shear. Figure 5.27 shows that the stress-strain behaviour of a 20% mixture at 200kPa cell pressure (test CD201) is characteristic of sand with a density higher than critical. This is the mixture idealised in figure 6.8.

Figure 5.28 best illustrates the interaction between the two soil phases in a bentonite-sand mixture (test CD104 - 10% bentonite @ 25kPa). At swelling equilibrium the effective stresses are 16 and 8kPa in the clay and sand phases respectively. Since the clay supports the majority of the effective stress the initial behaviour during shear is characteristic of clay alone, i.e., a rather shallow stress-strain curve with a corresponding positive volumetric strain. At this stage it is envisaged that the clay alone is being compressed bringing the sand particles to a closer packing. As the clay matrix is further compressed the sand particles begin to interlock, and therefore, at approximately 5% axial strain, the direction of volumetric strain becomes negative, i.e. the sample dilates. Dilation should continue until the sand reaches its critical state at a sand relative density equal to 0.17. The same type of behaviour was exhibited for the consolidated-undrained test (CU101) in figure 5.29. Initially the pore water pressure increases, followed by a decrease in pore water pressure at approximately 3% axial strain. This is analogous to positive and negative volumetric straining respectively in drained testing.

Figure 5.30 illustrates the shear behaviour of a 5% bentonite-sand mixture at 25kPa cell pressure (CD55). In this sample the calculated effective stresses in the clay and sand phases are initially 4 and 21kPa respectively. The stress-strain response indicates that the sample is initially stiff, and there is a large amount of dilation as the sample shears to achieve constant volume conditions: this is typical of a dense sand.

6.5.7 Stiffness as an indication of material behaviour

Secant stiffnesses of bentonite-sand mixtures calculated at 0.1, 0.2, 0.5 and 1% axial strain increments from the onset of reloading are reported in table 5.23 and presented graphically in figures 5.33a to 5.33d. Generally, it can be seen that an increase in bentonite content and/or decrease in cell pressure yields a lower stiffness for a particular axial strain, with the exception of a few anomalous results (discussed in chapter 5). Further, for any given sample, E' decreases with axial strain. The reported data agree with the results of various other workers (e.g., Hardin and Drnevich, 1972, Anderson and Stokoe, 1978, Bolton and Wilson, 1989). Hardin and Drnevich (1972) state that the three parameters of most importance to soil stiffness are strain amplitude, mean effective

stress and void ratio[16]. Figure 6.9 (after Hardin and Drnevich, 1972) shows the effects of strain and mean effective stress on the stiffness of a clean sand. The stiffness decreases with decreasing confining stress and increasing strain, and is not constant at any strain level. The general shape of the stiffness-strain amplitude curve is similar for clay soils and other sands as shown in figure 6.10 (after Hardin and Drnevich, 1972).

Peak strength data suggest that when the initial sand relative density is greater than zero, the stress-strain behaviour is primarily dependent on the interaction between sand particles. Similarly, the stiffness of mixtures should also increase with sand relative density. Figure 6.10 (after Hardin and Drnevich, 1972) indicates that stiffness decreases with increasing void ratio for a given strain and confining stress. Since an increase in bentonite content and/or a decrease in effective stress cause an increase in both the sand and clay void ratios, the behaviour of bentonite-sand mixtures is consistent with the reported literature. When there is initially no sand in contact, the stiffness will be determined by the density of the clay phase until sand particle interaction occurs (dependent on the degree of strain). Figure 5.33 shows that 5% mixtures have E' values consistently higher than other mixtures (with a few exceptions). These samples have the highest sand relative densities; the clay has virtually no effect on the measured stiffness as the proportion of the effective stress supported by the clay is only small. At axial strains of 0.1 and 0.2%, 10 and 20% mixes have approximately equal values of E'. However, as the strain increases, the stiffness of 10% and 5% mixtures are comparable, and values for 20% mixtures are consistently lower. This is taken as indicating that at small strains the sand matrix controls the stiffness of 5% mixtures, and the clay matrix controls the stiffness of 10 and 20% mixtures. As the axial strain is increased there is greater interaction between sand particles in 10% mixes and therefore the stiffness increases. However, since the sand relative density of 20% mixtures is less than other mixtures at similar strains, the measured stiffness is lower. At higher strains it is thought that the stiffness of 20% mixes will increase, as compression causes an increase in the sand relative density.

Although there is a large amount of scatter in the data, the results broadly fit the concepts described in the previous sections. At 25kPa, the 10% bentonite-sand mixture (CD104) has values of E' which are generally lower than the trends shown at higher stresses. This is consistent with the stress-strain behaviour described in 6.5.6 where behaviour characteristic of clay was exhibited up to approximately 5% axial strain.

[16]For soils containing significant quantities of clay, the degree of saturation is also of great importance. However, all samples in this study are thought to be at, or very close to, full saturation. Therefore, this effect is considered insignificant.

6.6 Summary of results

Using classical fundamental theories of soil mechanics, a modified principle of effective stress has been proposed for bentonite-sand mixtures, which quantifies the amount of effective stress that is supported by each of the two soil phases of the mixture. Any contribution to the total stress from a pore water pressure is thought to be similar to the term in Terzaghi's equation. For initially dry specimens, the effective stress in the bentonite and the sand can be calculated using the modified principle (equation 6.1) and further equations derived from unique swelling lines in e_c-log σ'_v space, where e_c is the clay void ratio and σ'_v the vertical effective stress (external normal load/sample area).

The effect of initial clay moisture content has been shown to have an effect on the overall swelling behaviour of compacted mixtures. For a particular applied stress, an increase in moisture content allows the sand to be compacted to a lower void ratio than the corresponding dry mixture. Consequently, the final clay void ratio is lower as it supports a greater proportion of the effective stress.

Three material states are proposed, which describe the change from sand to clay behaviour with applied stress and bentonite content.

For a particular clay void ratio, the hydraulic conductivity of 10 and 20% bentonite-sand mixtures has been shown to be less than that of bentonite only. This is attributed to the sand porosity and sand tortuosity which reduce the available area for flow and increase the length of flow path (both through the bentonite gel) respectively. The hydraulic conductivity of 5% bentonite-sand mixtures was found to show a different trend to the other mixtures and this is attributed to non homogeneity. Scatter in data for 5% mixes was found to be the greatest of all the mixes tested.

It has been shown that a stress-dilatancy approach is sufficient to describe the behaviour during shear of bentonite-sand mixtures. The relative density of the sand, the value of which increases with increasing cell pressure and/or decreasing bentonite content, is the dominating factor and determines the measured peak strength. An initial sand relative density greater than approximately 0.17 will result in a peak strength greater than the constant volume strength of sand, and the mixture will dilate to achieve constant volume (or critical state) conditions. At initial sand relative densities less than zero, the sand particles are not in contact and shearing will cause a positive volumetric strain with a strength intermediate between sand and clay (depending on the amount of volumetric strain induced). Below a threshold sand relative density, the behaviour during shear will be characteristic of bentonite only (provided the volumetric strain does not bring the

sand into contact) and the sand particles will have no significant contribution to the strength

The stiffnesses of bentonite-sand mixtures are again thought to be related to the density of sand in the mix. As stated previously, sand density increases with increasing cell pressure and/or decreasing bentonite content. The stiffness of the material will change throughout shear as particle rearrangements occur within a sample. At 1% axial strain the stiffness of 5 and 10% bentonite mixtures are comparable and this is thought to be due to dilation of the sand (in 5% mixtures), and compression of the clay (in 10% mixtures), as both effects will tend to rearrange the sand particles into similar packings. Conversely, 20% mixtures have a considerably lower stiffness at 1% axial strain. This is attributed to less interaction between sand particles (at this strain) than in mixtures with lower bentonite contents

Separating the two soil phases of the mixture is an effective method for interpreting and understanding the mechanical behaviour, and predictive equations have been derived to quantify the effects of the bentonite and sand. In chapter 7, these equations will be exploited for the design of bentonite-sand mixtures.

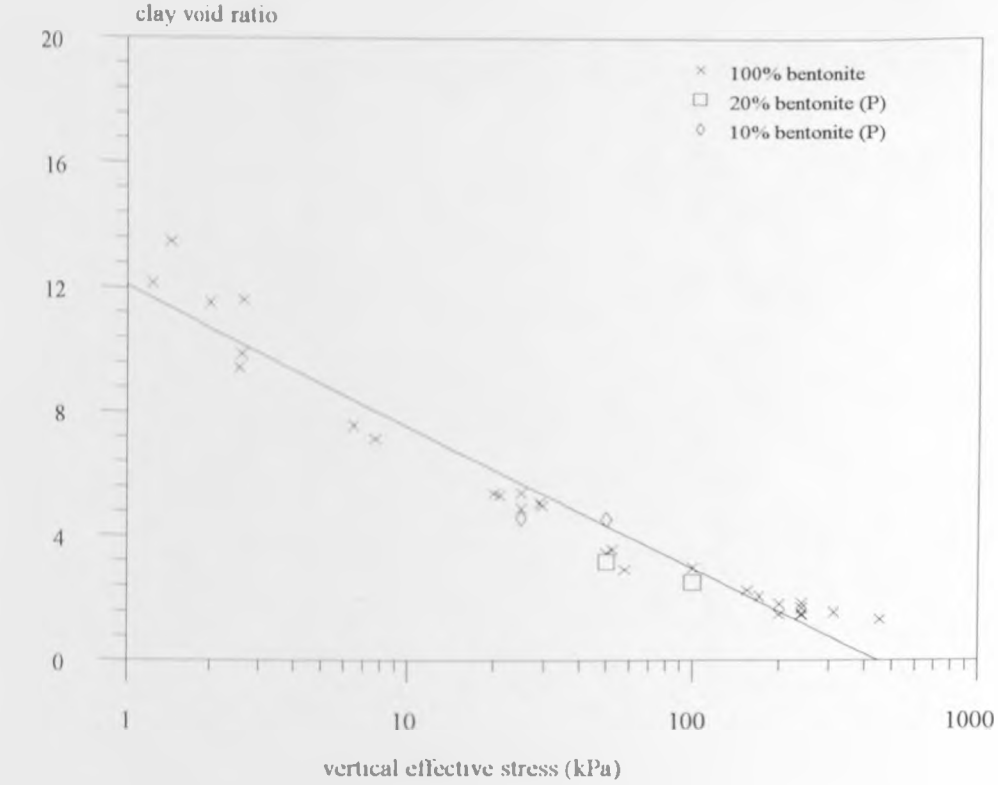

Note: P indicates Proctor compacted samples.

Figure 6.1 Swelling of modified Proctor compacted bentonite-sand mixtures exhibiting clay behaviour

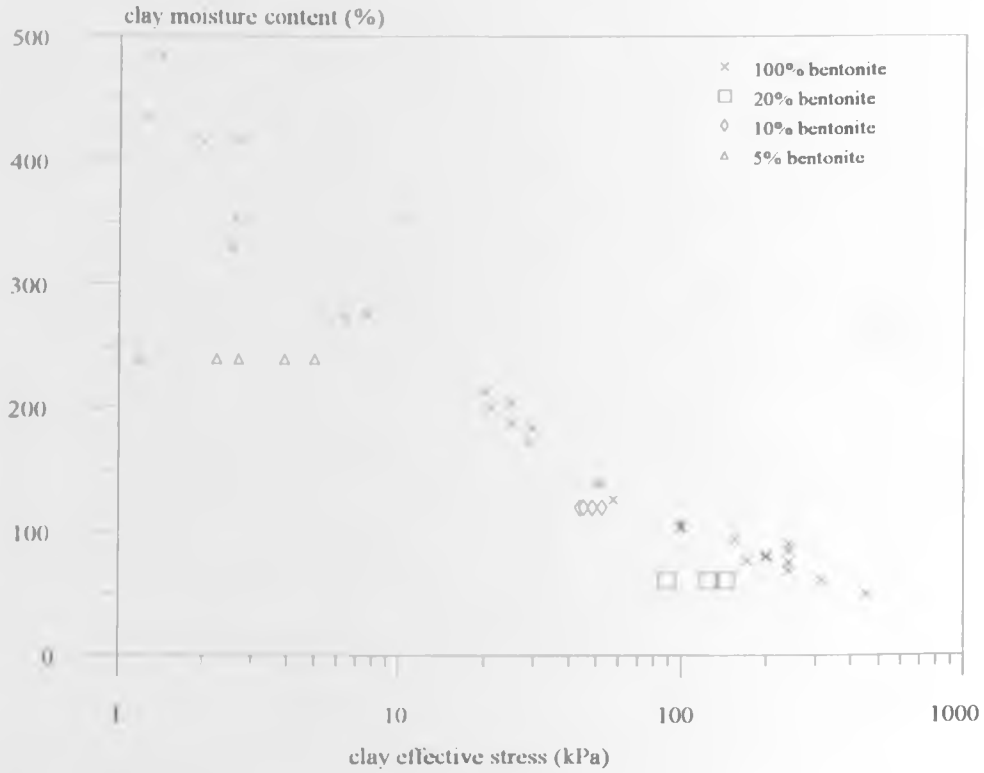

Figure 6.2 Relationship showing initial moisture content of compacted bentonite-sand mixtures and swelling equilibrium moisture content of initially dry bentonite to clay effective stress

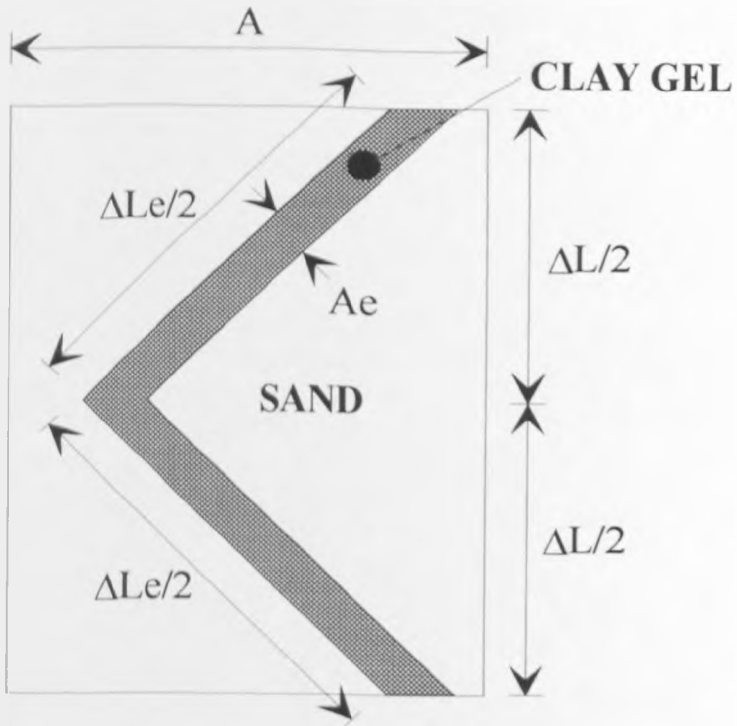

Figure 6.3 Simplified porous medium

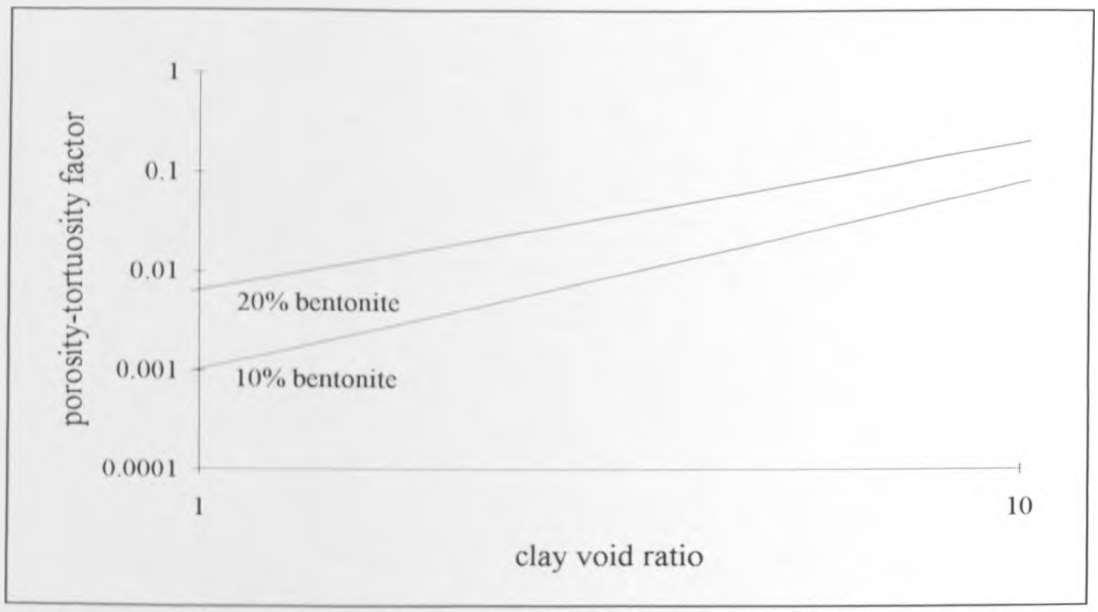

Figure 6.4: Combined porosity-tortuosity factors for bentonite-sand mixtures.

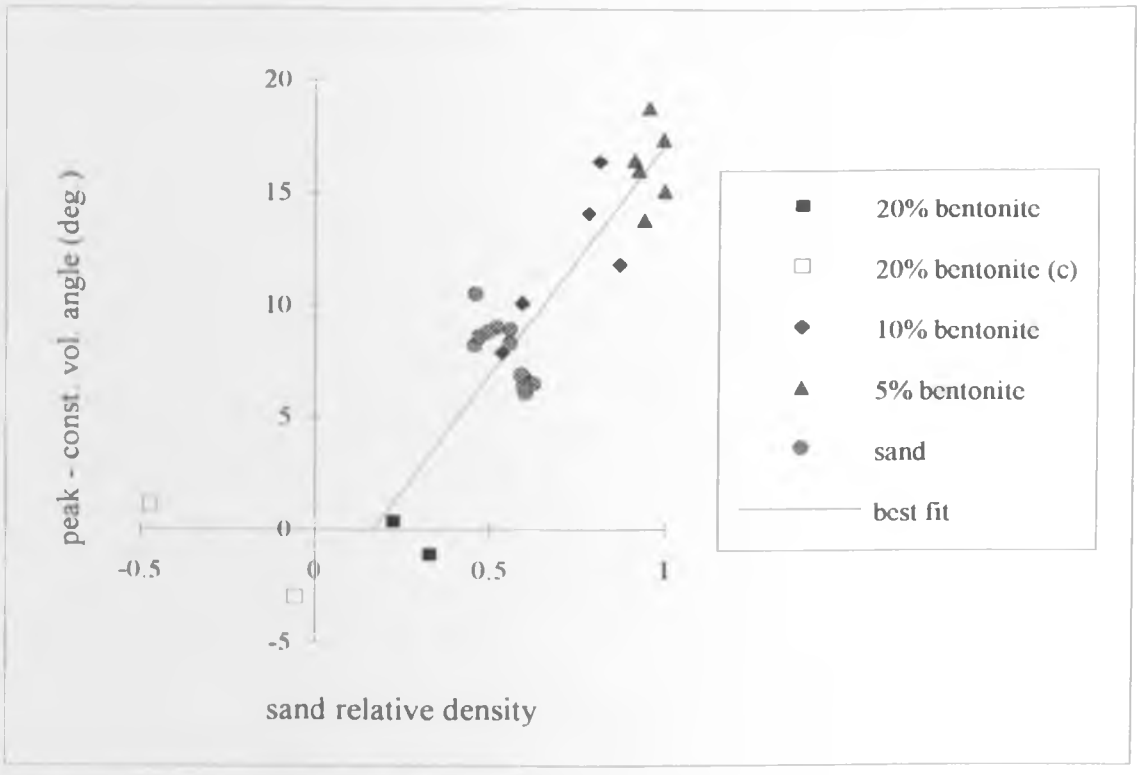

Note: c indicates samples compressed on shearing.

Figure 6.5a: Dilatant strength of sand and bentonite-sand mixtures.

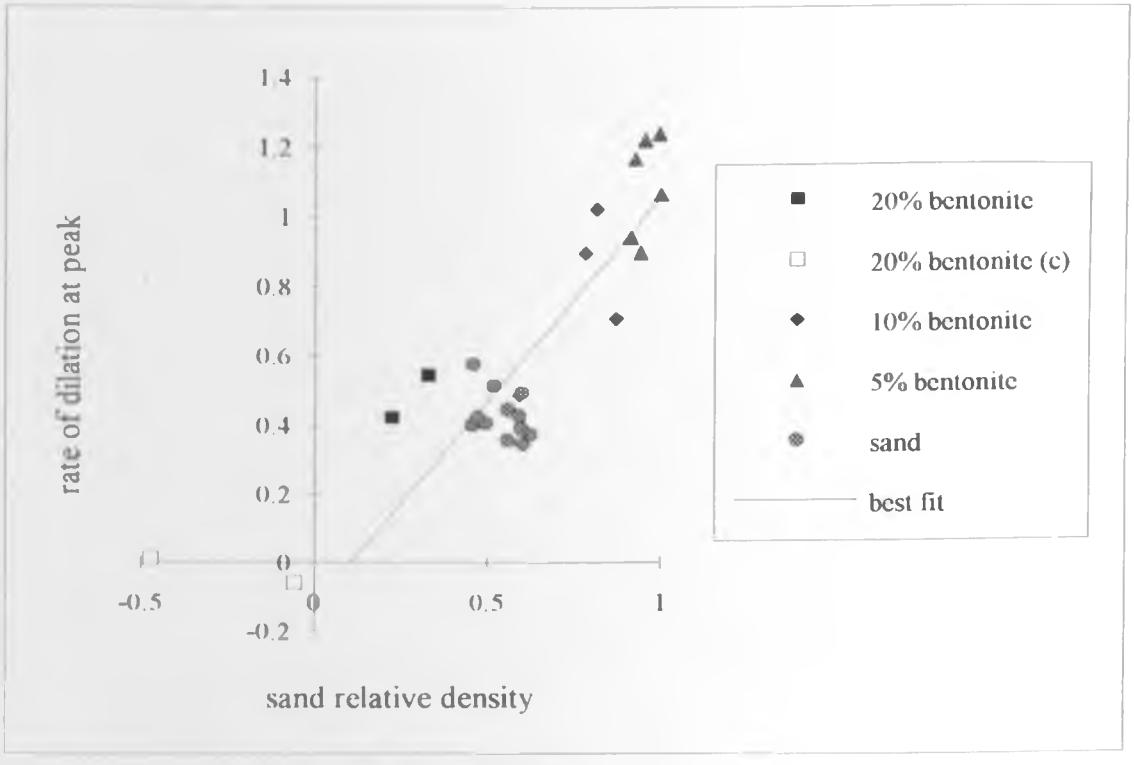

Note: c indicates samples compressed on shearing.

Figure 6.5b: Dilation of sand and bentonite-sand mixtures.

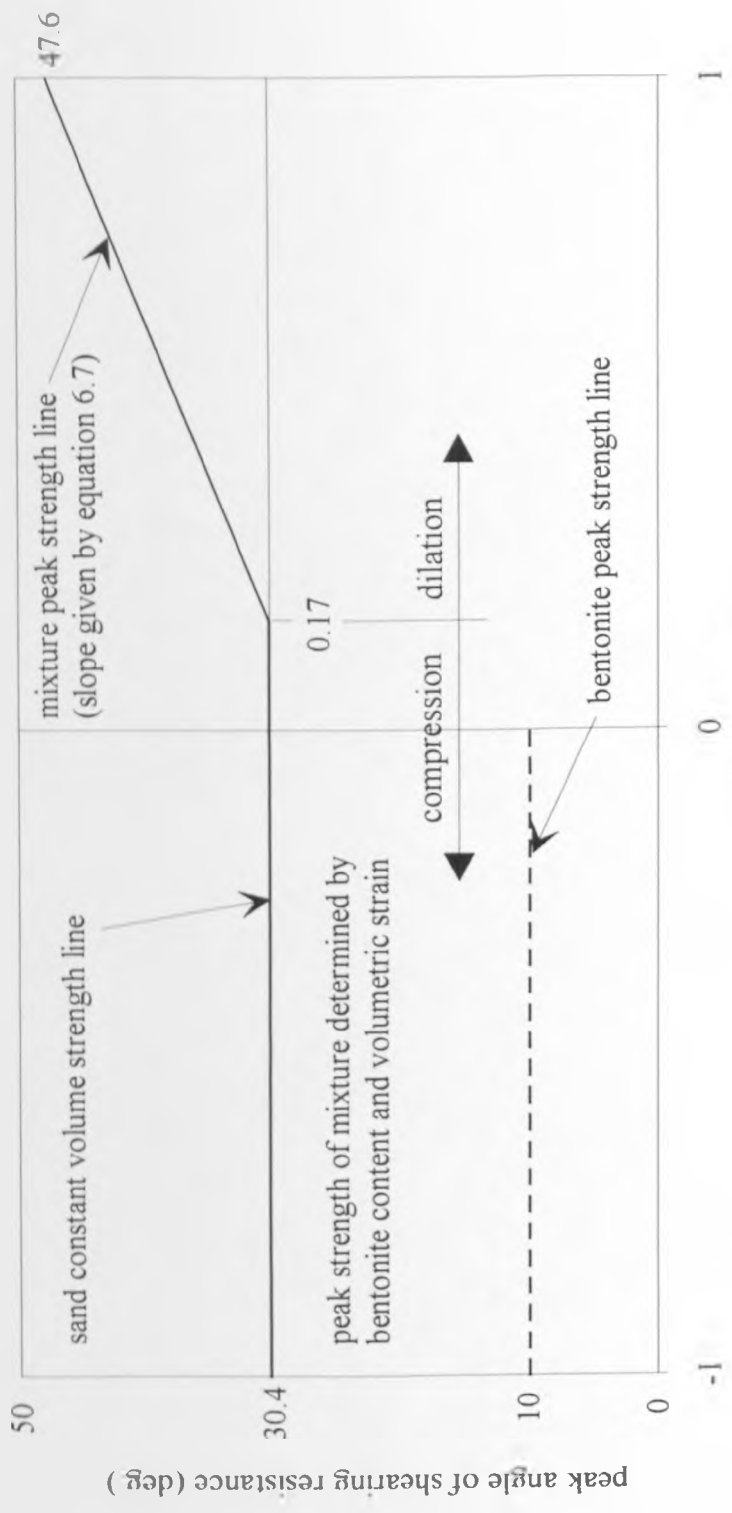

Figure 6.6. Idealised plot of peak strength against sand relative density for bentonite-sand mixtures.

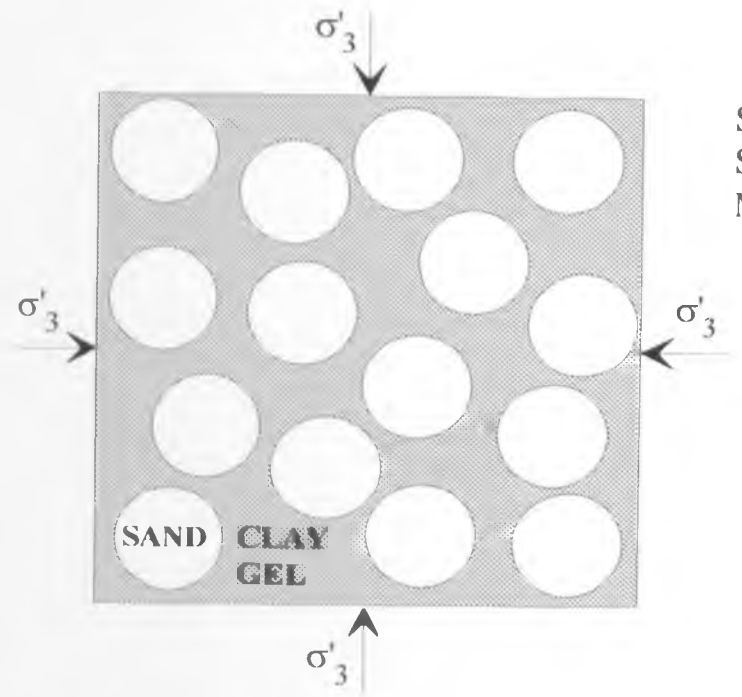

Sand void ratio = 1.226
Sand relative density = -0.47
Mean effective stress = 25kPa

Figure 6.7a. Packing of a 20% bentonite-sand mixture prior to shear.

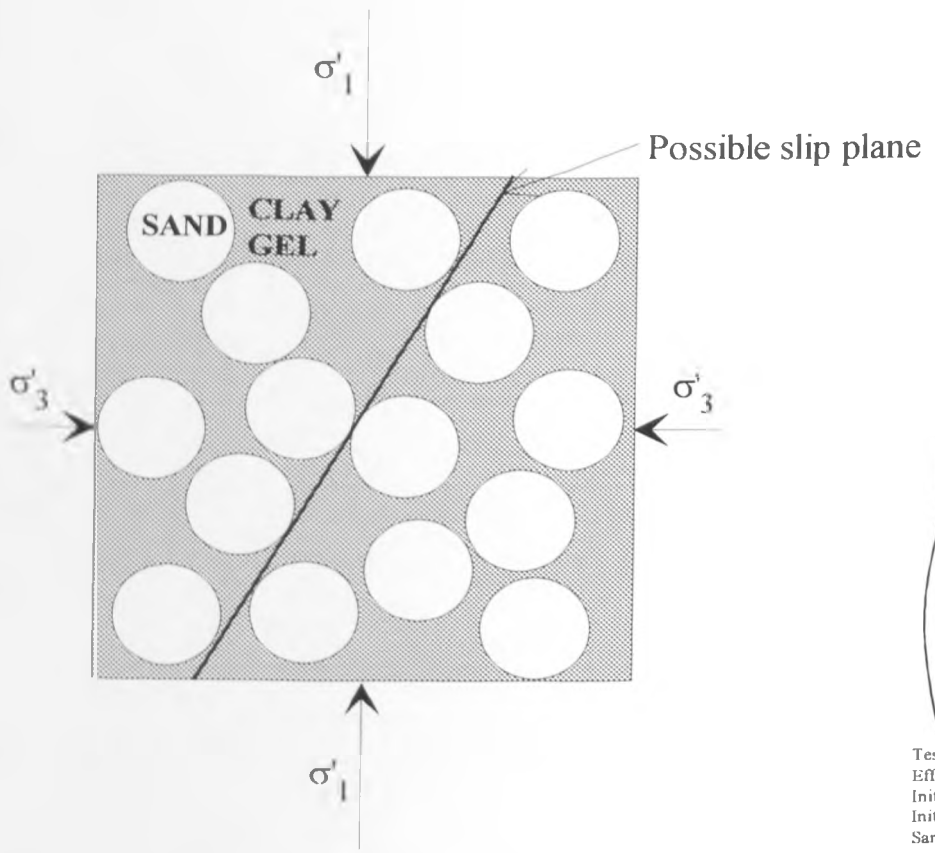

Figure 6.7b. Packing of a 20% bentonite-sand mixture after shear.

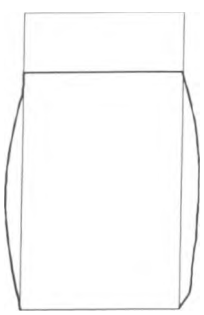

Test CD204 (20% bentonite)
Effective cell pressure = 25kPa
Initial height = 76mm (approx.)
Initial diameter = 38mm (approx.)
Sample at 20% axial strain

Figure 6.7c: Failure diagram.

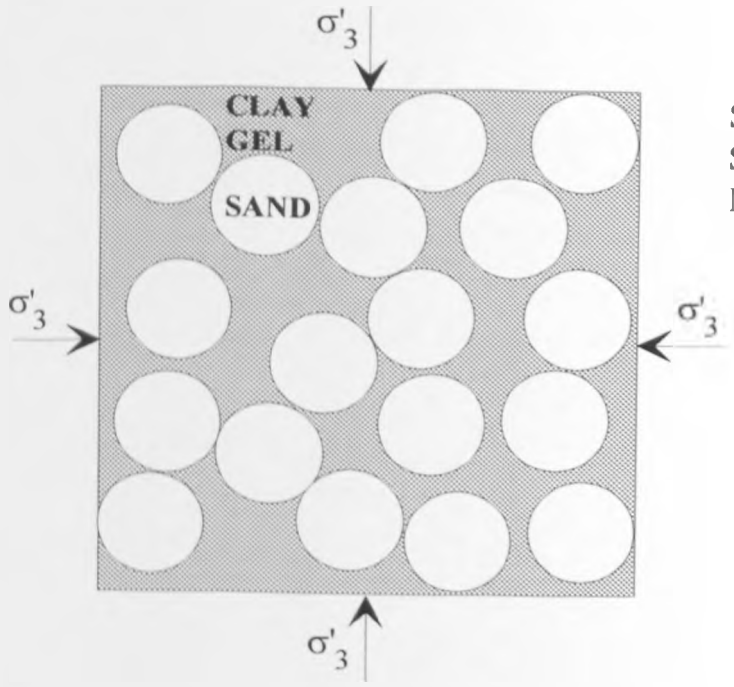

Sand void ratio = 0.806
Sand relative density = 0.33
Mean effective stress = 200kPa

Figure 6.8a Packing of a 20% bentonite-sand mixture prior to shear.

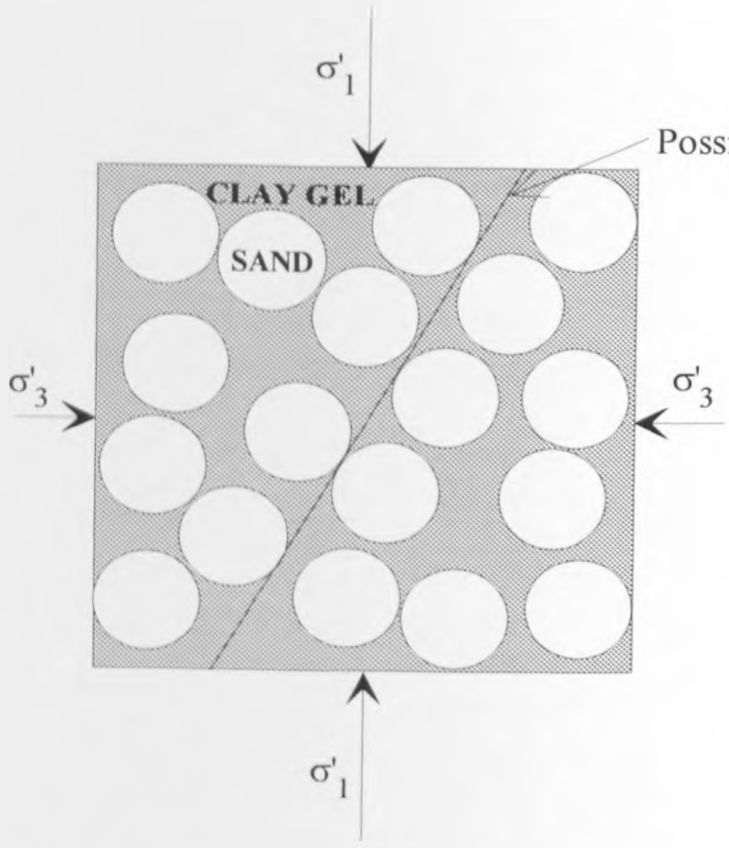

Figure 6.8b Packing of a 20% bentonite-sand mixture after shear.

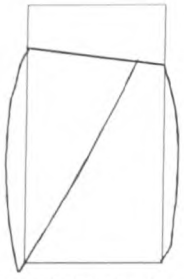

Test CD201 (20% bentonite)
Effective cell pressure = 200kPa
Initial height = 76mm (approx.)
Initial diameter = 38mm (approx.)
Sample at 20% axial strain

Figure 6.8c: Failure diagram.

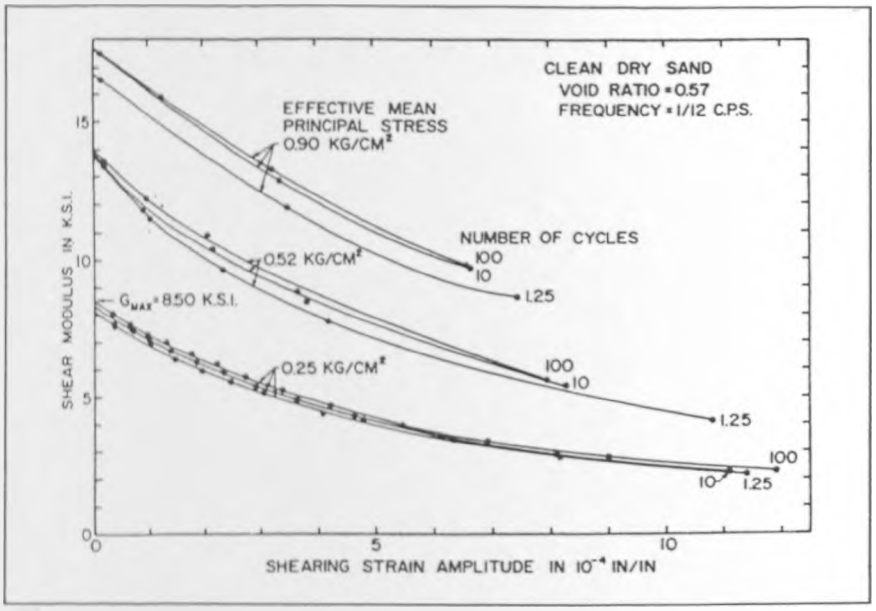

Figure 6.9: Effects of strain amplitude, effective mean principle stress, and numbers of cycles of loading on shear modulus of clean sand (after Hardin and Drnevich, 1972).

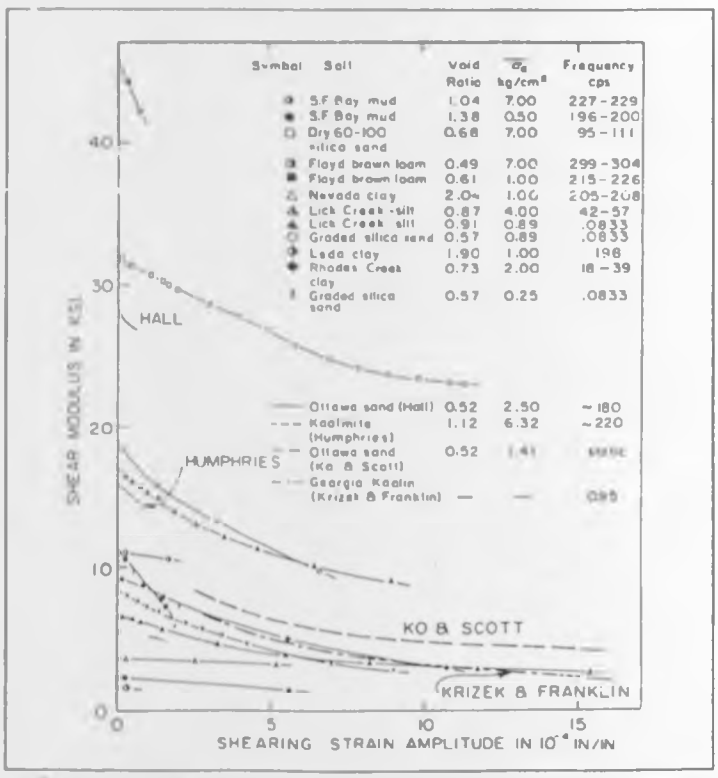

Figure 6.10: Shear modulus versus shearing strain amplitude for a variety of soils (after Hardin and Drnevich, 1972)

CHAPTER 7
THE DESIGN OF BENTONITE-SAND MIXTURES

7.1 Introduction

Based on the laboratory test data, predictive equations for the swelling behaviour, hydraulic conductivity and strength of bentonite-sand mixtures were proposed in chapters 5 and 6. It was shown that the swelling behaviour and hydraulic conductivity are effectively characterised by the clay void ratio. Further, the sand porosity and tortuosity determine the differences in hydraulic conductivity between 100% bentonite and the mixtures. Finally, the packing of the sand, indicated by the sand relative density, was shown to successfully characterise the stress-dilatancy behaviour of mixtures. The parameters used for analysis are easily determined from the phase relationships given in 5.3.1.

The reported data suggest that there are three main steps in the rational design of bentonite-sand mixtures to meet a landfill liner specification: i) measurement of the swelling behaviour and hydraulic conductivity of the selected bentonite under various surcharge stresses, ii) estimation of the sand porosity and tortuosity and iii) measurement of the stress-strain characteristics of the sand and bentonite. The maximum and minimum sand void ratios must also be determined for interpretation of the swelling behaviour of mixtures and to enable calculation of the sand relative density for analysis of strength data. In this chapter, a proposed design method for hydraulic conductivity and strength specifications of mixtures based on the predictive equations is presented and the relevant required laboratory testing outlined.

7.2 Designing for a hydraulic conductivity criteria

7.2.1 Characterisation of bentonite and mixture behaviour

The bentonite swelling behaviour can be established conveniently in an oedometer cell (without a loading frame for lower surcharge stresses). For each surcharge stress (or void ratio), a subsequent loading increment can be used to calculate the hydraulic conductivity (using Terzaghi's consolidation theory). Hence relationships such as equation 5.9 (the bentonite swelling line) and equation 5.26 (bentonite hydraulic conductivity-void ratio relationship) can be determined. The gradient of the swelling data in e_c - log σ'_v has been shown to be approximately linear over the range of engineering interest. However, it may be advisable to use a stress range which is comparable to the expected field values to improve accuracy.

Sand porosity (for an appropriate mixture and surcharge) can be calculated from oedometer swelling tests, by substitution of the clay content and final void ratio of the mixture into equation 5.5. This will also give an indication of the swelling behaviour of mixtures above the bentonite swelling line[1]. Sand tortuosity can then be calculated from the difference in mixture and bentonite hydraulic conductivities at the same clay void ratio using equation 6.6. If the final clay void ratio lies on the bentonite swelling line then clay swelling separates the sand particles and a consolidation increment in the oedometer cell is sufficient to calculate the hydraulic conductivity, otherwise a more sophisticated apparatus would be preferable[2].

7.2.2 Selection of clay content

The clay content required to satisfy any hydraulic conductivity criteria at a particular surcharge stress can be calculated as follows. The specified mixture hydraulic conductivity, and the sand porosity and tortuosity values are substituted into equation 6.6 to determine the required bentonite hydraulic conductivity. The maximum permissible clay void ratio is then determined from the hydraulic conductivity-void ratio relationship established for the bentonite (equation 5.26), and the clay swelling behaviour will indicate whether such a clay void ratio can be achieved under the applied surcharge, and the minimum clay content at which it will be achieved. An example of the proposed design method is given in appendix 6.

If the effective stress is high, i.e. above the threshold level (see 5.3.4), the sand particles will be in contact. In this state, the hydraulic conductivity can be further decreased by an increase in clay content. When the clay is supporting the surcharge, i.e. the applied stress is below the threshold value, a further decrease in hydraulic conductivity can only be achieved by reducing the sand porosity and value of tortuosity (equation 6.6), which means decreasing the bentonite content in the mixture.

---

[1]Full characterisation of the swelling of mixtures is unnecessary as the gradients in e_c - log σ'_v space above the bentonite swelling line are essentially equal. Therefore, once this relationship has been established for a particular mix, only a relatively small number of tests will be required for other mixtures.

[2]Use of oedometers to calculate the hydraulic conductivity of 10% mixtures indirectly is unlikely to yield a value greater than a factor of 2 different from the actual value (see chapter 5) but may require several tests and the average hydraulic conductivity taken. However, at clay contents less than this (or large applied stresses) it is suggested that hydraulic conductivity is measured directly either using a Rowe or triaxial cell.

7.3 Designing for a shear strength criteria

7.3.1 Required laboratory tests

If the strength is to be determined in the laboratory by triaxial compression tests then the bentonite isotropic swelling behaviour must first be established. This is not as simple as for one-dimensional swelling because triaxial samples are more difficult to prepare and the time required to reach swelling equilibrium may be much longer due to the relatively large sample height. However, only a few data points would be required because the isotropic swelling line is assumed parallel to the one-dimensional swelling line. The confidence in the accuracy of the calculated line would be proportional to the number of data points. Samples must have a high enough clay content that sand particles are not in contact at swelling equilibrium. Hence a relationship such as that given by equation 5.35 (the bentonite isotropic swelling line) can be determined. From further tests on mixtures, whose clay void ratios are higher than that given by the isotropic swelling line at equilibrium conditions, the idealised swelling behaviour can be determined[3].

When the mean effective stress (or clay content) is such that there is interaction between sand particles (i.e., the mixture has a clay void ratio above the bentonite isotropic swelling line), the strength is dependent on the sand relative density. This would require the stress-dilatancy behaviour of the sand only to be determined; a relatively quick and straightforward procedure. However, if the sand particles are expected to be fully separated, then the strength of the bentonite must also be determined.

It is proposed that consolidated-drained triaxial tests are necessary with the selected sand in its loosest and densest possible states and at an intermediate density. This will then enable stress-dilatancy relationships such as equations 6.7 and 6.8 to be determined. To account for the loss in dilatant strength with increasing confining stress the triaxial tests should be conducted at the largest anticipated field stress to give a conservative estimation of the strength. A direct shear test on bentonite swollen from a dry state would be satisfactory to calculate the maximum angle of shearing resistance. It is important that the sample is not subjected to a consolidation increment because of the change in fabric associated with stress history, i.e., the state of the bentonite should be comparable to that in a mixture. From these laboratory tests, an idealised plot of peak strength against sand relative density, such as figure 6.6, can be produced. As before, it is suggested that the largest anticipated field effective stress is used.

[3]Fitting of gradients to the data can be performed in a similar manner to that described in chapter 5.

7.3.2 Selection of clay content

If a ductile mixture is required, such that the clay supports all the effective stress throughout shearing, and a strength corresponding to the mineralogy of the clay phase only is preferred, then the clay content should be relatively high (or the effective stress low). For mixtures of this type the swelling behaviour will be described by the isotropic bentonite swelling line. It is suggested that the strength of such a mix will correspond to the mineralogy of the clay phase (the bentonite peak strength line) until the sand particles begin to interact[4], when the strength tends towards the sand constant volume strength. Therefore, it is necessary to estimate both a volumetric strain (based on anticipated field strains) and value of final sand relative density at which behaviour characteristic of clay alone occurs. From this, the change in sand void ratio (or relative density) during shear can be determined, hence the initial sand relative density. The required clay content for a particular effective stress can then be calculated using equations 5.3, 5.4 and 5.35.

The design of a landfill liner may often demand relatively steep side slopes, or a large bearing capacity may be required to accommodate a particular type of waste. In such situations, a strength higher than that of the clay alone is likely to be desired. If a higher strength is required, i.e., the effective stress is distributed between the bentonite and sand phases, then a choice between a ductile or brittle mixture is available. The stress-dilatancy relationship determined from laboratory shear tests will give the sand relative density corresponding to constant volume conditions (approximately 0.2 in this study). For ductile mixtures with sand strength (looser than critical), the chosen initial sand relative density should be greater than zero but less than the value at constant volume. For brittle mixtures, i.e., behaviour characteristic of dense sand, the difference between the required peak angle of shearing resistance and the constant volume angle of shearing resistance of the sand can be substituted into the stress-dilatancy relationship (equation 6.7) to give the sand relative density. As sand is in contact for both types of mixture, the final clay void ratio will lie above the isotropic swelling line. Therefore, the clay content (for a particular applied stress) must be selected using relationships similar to equation 5.9 and 5.14-5.16 (idealised swelling behaviour), and the phase relationships given in 5.3.1.

Examples of the proposed design methods are given in appendix 6.

---

[4]This assumes that the percentage volume of sand in the mixture is sufficient that compression of the clay on shearing allows significant interaction between sand particles.

7.4 Summary and conclusions

Economically, it is desirable to minimise the clay content of a bentonite-sand mixture. Other factors for a low clay content are that a mixture with the sand particles in contact is unlikely to exhibit macroscopic shrinkage cracks on drying (see 2.2) and the mechanical stability of the mixture is provided by the sand matrix. Therefore, it is desirable that some stress is carried by the sand after saturation. Factors against a low clay content are a decrease in mixture ductility as the amount of stress carried by the sand increases, inability of the bentonite to fill the sand voids due to reduced swelling of the bentonite as contaminants from the landfill permeate the mixture, and a higher than expected hydraulic conductivity at very low bentonite contents due to mixture non homogeneity.

A design compromise requires some stress to be carried by the sand matrix, whilst leaving the clay with reserve swelling capacity. Once the swelling behaviour has been characterised and idealised, the modified principle of effective stress (equation 6.1) can be used to determine how much stress is carried by the sand and clay respectively. This stress distribution allows an interpretation of how the material will respond to changes in applied stress or pore fluid by changing in volume, and indicates how the soil will behave during shear.

If a mixture is designed specifically for a hydraulic conductivity criteria, then the strength can be determined by substitution of the calculated sand relative density into equation 6.7. Conversely, if a strength criteria is used for design, substitution of the sand porosity and tortuosity and bentonite hydraulic conductivity into equation 6.6 (for the particular clay void ratio or effective stress) will give the mixture hydraulic conductivity. The latter approach may be preferable as the data imply that hydraulic conductivity decreases with increasing sand relative density provided a homogeneous mixture is produced. However, a compromise may be necessary to allow some reserve swelling potential of the clay within the mix and sufficient ductility of the liner, for example, to accommodate differential settlements.

In the reported tests, the vertical effective stress imposed on the specimens was in the range 1 to 450kPa, and the isotropic effective stress range 15 to 200kPa. Such stress ranges are sufficient for studying of the engineering behaviour of landfill liner materials, but extrapolation of the reported trends beyond the corresponding stress ranges may be inappropriate. Further, at low clay contents (5% or less), the proposed design methods may be untenable due to non homogeneity of the mixture.

CHAPTER 8
CONCLUSIONS AND RECOMMENDATIONS

8.1 Scope

In recent years, the technique of adding bentonite to a local soil to produce a low hydraulic conductivity material has been widely practised in application to the containment of waste in landfills. However, the properties of such a material are not fully understood and quantitative interpretations of the mechanical behaviour are rare. This also applies generally to the behaviour of systems containing two soil phases. Further, since materials of this type are likely to begin in a relatively dry state, the geotechnical properties may significantly differ to the well documented laboratory behaviour of initially fully saturated soils. The objective of this study was the investigation of the fundamental geotechnical properties of bentonite-sand mixtures whose initial conditions are relatively dry prior to equilibrium being established. The relevant literature has been reviewed, and a laboratory test programme conducted to determine the volume change behaviour (swelling, normal consolidation and rebound), hydraulic conductivity and strength of sand, bentonite, and 20, 10 and 5% bentonite-sand mixtures. The conclusions of the laboratory data have been summarised at the end of the relevant preceding chapters, and a design method proposed. In this chapter, the main conclusions drawn from the work, and recommendations for engineering practice and for further research, are summarised.

8.2 Conclusions

1. The geotechnical properties of bentonite-sand mixtures are best interpreted and characterised by the use of phase relationships to account for the individual phases of the mix. The clay void ratio sufficiently describes the swelling behaviour and indicates the change in material properties, from sand to a more clay type behaviour, with increasing clay content and/or decreasing applied stress. Interpretation of the hydraulic conductivity data of mixtures is simplified by relating the measured values to the clay void ratio and sand porosity, and strength data can be adequately interpreted by use of the sand void ratio (or sand relative density).

2. Dry sodium bentonite swells on access to distilled water to reach a unique void ratio under a particular confining stress, and this void ratio varies linearly with the logarithm of vertical effective stress. The relationship is termed the one-dimensional bentonite swelling line. The linear relationship given by the bentonite swelling line is intermediate between the one-dimensional normal consolidation and rebound lines for consolidated bentonite slurry, indicating a difference in fabric from an initially 'wet' clay. It is

proposed that initially dry samples have a structure consisting of aggregations of clay particles giving rise to intra- and inter-aggregate void spaces, whereas wet samples have a more uniform fabric with void spaces all of comparable size.

3 The swelling behaviour of dry bentonite-sand mixtures can be characterised by a threshold stress that is a function of the clay content. Below the threshold stress, the clay in the mixtures is able to swell against the surcharge and separate the sand particles to reach the same clay void ratio, for a given surcharge, as 100% bentonite. When the confining stress exceeds the threshold value, the clay void ratio upon filling the pores is greater than that of 100% bentonite at equilibrium with the confining stress and the sand particles remain either partially or fully in contact. In this state, the effective stress in the clay is lower than the applied stress and therefore the remainder of the effective stress is supported by the sand particles. A modified principle of effective stress is proposed, which, combined with the bentonite swelling line can be exploited to determine the magnitude of the effective stresses in each soil phase of the mixture.

4 Compacted mixtures swell in the same general manner as dry mixtures provided the initial clay moisture content is less than the swelling equilibrium value at the same clay effective stress. For a given moisture content, the clay becomes increasingly wet with increasing sand content, and swelling is less than the corresponding dry mixture at applied stresses greater than the threshold value. This is attributed to the effects of clay water on remoulding during compaction enabling the sand to be compacted to a lower void ratio than the corresponding dry mixture.

5 Darcy's law is valid for the range of applied hydraulic gradients used in the test programme. The relationship between hydraulic conductivity and void ratio for Wyoming bentonite and 20% and 10% bentonite sand mixtures can be represented by a power law. 5% mixtures show a different trend to other mixtures which is attributed to non homogeneity. For a particular clay void ratio, the hydraulic conductivity decreases with increasing sand content. This is due to the sand porosity and tortuosity which decrease the available area for flow and increase the length of the flow path respectively. Once the properties of the bentonite are known, the hydraulic conductivity of bentonite-sand mixtures can be predicted from the bentonite content, sand porosity and tortuosity, and vertical effective stress.

6 Swelling of triaxial samples of bentonite-sand mixtures can be characterised in a similar manner to the one-dimensional swelling by relating the clay void ratio to the logarithm of the mean effective stress. An isotropic bentonite swelling line, which is

parallel to the one-dimensional line is proposed. The two soil phases of mixtures whose final clay void ratios lie above the isotropic swelling line share the effective stress depending on the bentonite content and/or mean effective stress. This gives an indication of how the material will behave during shear.

7. Peak strengths and stress-strain behaviour of bentonite-sand mixtures tend towards those of bentonite alone with increasing clay content and/or decreasing mean effective stress, i.e., as the clay void ratio at swelling equilibrium approaches the bentonite isotropic swelling line. A stress-dilatancy analysis of laboratory data shows that the shear behaviour is characterised by the sand relative density. For mixtures with sand relative densities greater than 0.17, the stress-strain behaviour is similar to that typical of sands at densities greater than the critical state. Dilation of samples occurs as the mix shears to reach constant volume conditions. The peak strength increases with increasing sand relative density. The analysis suggests that behaviour typical of sands looser than critical occurs for sand relative densities between zero and 0.17. At sand relative densities less than zero the shear behaviour is more characteristic of clay. However, this depends on the sand relative density and the magnitude of the strain applied to the sample. It is proposed that the peak strength of mixtures is intermediate between that of sand and clay when the sand relative density is above a threshold value (dependent on volumetric strain). Below the threshold value, strength and stress-strain behaviour is characteristic of bentonite alone. Once the stress-strain behaviour of the bentonite and sand alone are known, the peak strength of bentonite-sand mixtures can be predicted from the sand relative density obtained from the swelling behaviour.

8. The stiffness of bentonite-sand mixtures decreases with increasing bentonite content and/or decreasing mean effective normal stress, indicating a smaller interaction between sand particles. The stiffness of mixtures is consistent with the stress-strain behaviour.

9. A low bentonite content can lead to an uneven bentonite distribution within the mixture as a result of mixing and/or compaction. This can result in a higher hydraulic conductivity than would be estimated for a uniform mixture due to areas of relatively large flow where the bentonite content is very low. The largest amount of variation in swelling and hydraulic conductivity data was found for 5% bentonite-sand mixtures. Conversely, when the bentonite content is relatively high (but not so high as to completely prevent interaction between sand particles), an uneven distribution within the mix may result in an overestimation or underestimation of the strength, depending on the distribution of the bentonite across the shear plane. The largest variation in strength data was found for 20% bentonite-sand mixtures.

8.3 Practical recommendations

8.3.1 Production of homogeneous mixes

At very low bentonite contents it may be practically impossible to produce a homogeneous mixture Based on the results of this study, a minimum bentonite content of approximately 10% is recommended to account for variations in clay content within the sand pores (highly aggressive pore fluids may require larger bentonite contents). However, this value may vary depending on the grading of the sand. Thorough mixing in a Hobart mechanical mixer with both soil phases initially dry, followed by further mixing after the required compaction moisture has been added, appears to achieve a reasonably homogeneous mixture It will be necessary to achieve a similar level of mixing in the field if low bentonite contents are to be used.

8.3.2 Hydraulic conductivity testing

If the hydraulic conductivity of clay-sand mixtures, whose engineering properties are expected to be controlled by the clay fraction, are to be determined in the laboratory, then a consolidation increment in an oedometer has been shown to be sufficient. The hydraulic conductivity can be calculated using Terzaghi's consolidation theory using the laboratory log time-settlement or square root time-settlement curves, provided the analysis is conducted using data from the laboratory curve at 50% primary consolidation. If however, the content of coarse grained particles or applied stress is such that significant interaction between these particles occurs, then a more sophisticated apparatus such as a Rowe or triaxial cell should be used For low hydraulic conductivity materials, a small sample thickness and back pressure are recommended to reduce saturation and testing times

For bentonite-soil liner materials, it is economically preferable to use a relatively small bentonite content Also, the swelling of pure bentonite may be less in contaminated pore fluids than in distilled water This may exclude indirect measurement of hydraulic conductivity when the bentonite swelling is not sufficient to separate the sand particles in these situations For such conditions, determining realistic hydraulic conductivity values may only be possible by the use of other apparatus.

8.3.3 Shear testing

Black and Lee (1973) suggest that samples with initial degrees of saturation greater than 75% can be brought to 99% saturation in less than 1 week provided an elevated back pressure is applied to the sample However, achieving complete saturation may require up to 200 days Accepting 99% saturation is reasonable for drained testing because small amounts of air, if present, are likely to remain within the sample due to the

confinement imposed by the soil particles. Since excess pore water pressures will be negligible, the analysis can be conducted in effective stress terms with reasonable confidence. In contrast, accepting 99% saturation for undrained testing may lead to a large discrepancy between the actual and measured pore water pressure response, especially for stiff samples. Therefore, to minimise the effects of incomplete saturation, any laboratory shear testing programme to determine the strength would be best conducted under drained conditions.

If multiple samples are required for an extensive laboratory test programme then a saturation cell, as used in this study, is recommended to reduce the time required for equilibration of samples and to ensure high degrees of saturation prior to testing. A large triaxial cell can be modified to enable simultaneous saturation of 4 samples. This could be further increased if necessary. Tests times can be decreased further by the use of filter paper drains. However, these may have a significant effect on the measured strength when the deviator stress required to cause failure is small.

8.3.4 Laboratory effective stress range for design of mixtures

If a laboratory test programme is conducted to provide data on hydraulic conductivity or strength (such as described in chapter 7), then an applied stress range comparable to the anticipated field values should be used. Hydraulic conductivity and strength are dependent on the swelling of the mixture. Therefore, equations derived from laboratory swelling tests can be used to predict the behaviour with greater accuracy if determined over the field stress range, thus making the model more effective for design purposes.

8.4 Recommendations for further research

A coherent framework for the interpretation of the geotechnical properties of bentonite-sand mixtures has been presented. However, it is unknown if similar types of data analysis are possible, or similar behaviour occurs, when a relatively inactive clay (such as kaolinite) is mixed with sand, or when permeants other than distilled water are used as the sample pore fluid. Further, the properties of clay-sand mixtures that begin in an initially fully saturated state (i.e., reconstituted from a slurry), and are consolidated to a particular effective stress, or unloaded to an overconsolidated state, are likely to differ from that of initially dry samples.

For relatively inactive clays (i.e., clays which swell only slightly), it is likely that the properties will be more characteristic of sand at the clay contents used for this study However, evidence suggests that behavioural thresholds do exist when the clay content is such that sand particle interaction ceases (e.g., Lupini et al. (1981) on changes in residual

shearing mechanism with clay content (see 2.5.5)). Therefore, similar idealised swelling behaviour, differences in hydraulic conductivity and strength may be valid, but significantly greater ranges of clay content may be required to distinguish easily between different mixtures. It is also of fundamental importance to the study of geotechnics to understand the behaviour of such materials with various pore fluids and under different states of stress and stress history. Further, quantifying the behaviour of different clay-sand mixtures may be of use in predicting the performance of existing landfill liners containing clays other than bentonite.

References

Anderson, D. G. and Stokoe, K. H. 1978. Shear modulus: a time dependent soil property. Dynamic Geotechnical Testing, ASTM STP 654. American Society for Testing and Materials, pp.66-90.

ASTM. 1974. Standard test method for permeability of granular soils (constant head). ASTM-D2434-68. *In* Annual book of ASTM standards. Vol. 04.08. American Society for Testing and Materials, Philadelphia, PA.

Atkinson, J. H. 1973. Elasticity and plasticity in soils. Geotechnique. Vol. 23, pp.565-571.

Atkinson, J. H. and Bransby, P. L. 1978. The mechanics of soils. McGraw-Hill, London.

Atkinson, J. H., Evans, J. S. and Ho, E. W. L. 1985. Non-uniformity of triaxial samples due to consolidation with radial drainage. Geotechnique. Vol. 35, pp.353-355.

Atkinson, J. H. and Richardson, D. 1985. Elasticity and normality in soil - experimental examinations. Geotechnique. Vol. 35, No. 4, pp.443-449.

Atkinson, J. H., Richardson, D. and Stallebrass, S. E. 1990. Effects of recent stress history on the stiffness of overconsolidated soil. Geotechnique. Vol. 40, No. 4, pp.531-540.

British Standards Institution 1990. Methods of test for soils for civil engineering purposes: BS1377: Part 2.

Barden, L. and McDermott, J. W. 1965. The use of free ends in triaxial testing of clays. Proceedings of the American Society of Civil Engineers. Vol. 91, SM6, pp 1-23.

Bear, J. 1972. Dynamics of fluids in porous media. American Elsevier publishing Company inc., New York, London, Amsterdam.

Bear, J. and Verruijt, A. 1987. Theory and application of transport in porous media Modelling groundwater flow and pollution. D. Reidel Publishing Company

Berner, R. A. 1971. Principles of chemical sedimentology. McGraw-Hill, Inc., New York.

Bishop, A. W. 1966. The strength of soils as engineering materials. Sixth Rankine Lecture. Geotechnique. Vol. 16, pp.89-131.

Bishop, A. W. and Gibson, R. E. 1963. The influence of the provisions for boundary drainage on strength and consolidation characteristics of soils measured in the triaxial apparatus. ASTM STP 361 (Laboratory Shear Testing of Soils), pp.435-451.

Bishop, A. W. and Henkel, D. J. 1962. The measurement of soil properties in the triaxial test. 2nd Edition. Edward Arnold, Publishers, Ltd. London.

Black, D. K. and Lee, K. L. 1973. Saturating laboratory samples by back pressure. Journal of the Soil Mechanics and Foundations Division. ASCE. Vol. 99, No. SM1, Proc. Paper 9484, pp.75-93.

Bolt, G. H. 1956. Physico-chemical analysis of the compressibility of pure clays. Geotechnique. Vol. 6, No. 2, pp.86-93.

Bolton, M. 1979. A Guide to Soil Mechanics. Macmillan Press Ltd.

Bolton, M. D. 1986. The strength and dilatancy of sands. Geotechnique. Vol. 36, No. 1, pp.65-78.

Bolton, M. D. and Wilson, J. M. R. 1989. An experimental and theoretical comparison between static and dynamic torsional soil tests. Geotechnique. Vol. 39, No. 4, pp.585-599.

Borowicka, H. 1965. The influence of colloidal content on the shear strength of clays. Proceedings of the 6th International Conference on Soil Mechanics and Foundation Engineering. Vol. 1, pp.175-178.

Bowden, F. P. and Tabor, D. 1954. The Friction and Lubrication of Solids. Oxford, Clarendon Press.

Bowles, J. E. 1986. Engineering properties of soils and their measurement. McGraw-Hill.

Boynton, S. S. and Daniel, D. E. 1985. Hydraulic conductivity tests on compacted clay. Journal of Geotechnical Engineering. Vol. 111, No. 4, pp.465-478.

Casagrande, A. 1936. The determination of the pre-consolidation load and its practical significance. Proceedings of the 1st International Conference on Soil Mechanics and Foundation Engineering, Harvard, Vol. 3, pp.60-64.

Casagrande, A. and Fadum, R. E. 1944. Notes on soil testing for engineering purposes. Soil Mechanics Series No. 8. Harvard Graduate School of Engineering.

Chapuis, R. P. 1981. Permeability testing of soil-bentonite mixtures. Proceedings of the 10th International Conference on Soil Mechanics and Foundation Engineering. Vol. 4, pp.744-745. Stockholm.

Chapuis, R. P. 1990a. Sand-bentonite liners: predicting permeability from laboratory tests. Canadian Geotechnical Journal. Vol. 27, No. 2, pp.47-57.

Chapuis, R. P. 1990b. Sand-bentonite liners: field control methods. Canadian Geotechnical Journal. Vol. 27, No. 2, pp.216-223.

Chatterji, P. K. and Morgenstern, N. R. 1990. A modified shear strength formulation for swelling clay soils. Physico-Chemical Aspects of Soil and Related Materials. ASTM 1095. American Society for Testing and Materials, pp.118-135.

Cheung, S. C. H., Gray, M. N. and Dixon, D. A. 1987. Hydraulic and ionic diffusion properties of bentonite-sand buffer materials. Atomic Energy of Canada Limited Whiteshell Nuclear Research Establishment, pp.393-407.

Cornforth, D. H. 1973. Prediction of drained strength of sands from relative density measurements. In Evaluation of relative density and its role in geotechnical projects involving cohesionless soils. ASTM Special Technical Publication 523, pp.281-301.

Cowland, J. W. and Leung, B. N. 1991. A field trial of a bentonite landfill liner. Waste Management and Research. Vol. 9, pp.277-291.

Craig, R. F. 1987. Soil Mechanics. Van Nostrand Reinhold.

Daniel, D. E. 1984. Predicting hydraulic conductivity of clay liners. Journal of Geotechnical Engineering. Vol. 110, No. 2, pp.285-300.

Daniel, D. E. 1987. Earthen liners for land disposal facilities: Geotechnical Practice for Waste Disposal. Proceedings of the American Society of Civil Engineers Specialty Conference, pp.21-39. Ann Arbor, Michigan.

Daniel, D. E. 1990. Summary review of construction quality control for compacted soil liners. Waste containment systems: construction, regulation, and performance. ASCE pp.175-189.

Daniel, D. E., Anderson, D. C. and Boynton, S. S. 1985. Fixed-wall versus flexible-wall permeameters. Hydraulic Barriers in Soil and Rock. ASTM 874, pp.107-126.

Darcy, H. 1856. Les Fontaines Publique de la Ville de Dijon. Dalmont, Paris.

Davidtz, J. C. and Low, P. F. 1970. Relation between crystal-lattice configuration and swelling of montmorillonites. Clays and Clay Minerals. Vol. 18, pp.325-332.

Day, S. R. and Daniel, D. E. 1985. Hydraulic conductivity of two prototype clay liners Journal of Geotechnical Engineering. Vol. 111, No. 8, pp.957-970.

Delage, P. and Lefebvre, G. 1984. Study of the structure of a sensitive Champlain clay and its evolution during consolidation. Canadian Geotechnical Journal. Vol. 21, pp.21-35.

Dixon, D. A. and Gray, M. N. 1985. The engineering properties of buffer material research at Whiteshell Nuclear Research Establishment. Proceedings of the 19th Information Meeting of The Nuclear Waste Management Program. Atomic Energy of Canada Limited Technical Report. TR-350, pp.513-530. Toronto.

Dixon, D. A., Gray, M. N. and Thomas, A. W. 1985. A study of the compaction properties of potential clay-sand buffer mixtures for use in nuclear fuel waste disposal. Engineering Geology. Vol. 21, pp.247-255.

Dixon, D. A., Gray, M. N., Baumgarter, P. and Rigby, G. L. 1986. Pressures acting on waste containers in bentonite based materials. Proceedings of the 2nd International Conference on Radioactive Waste Management, pp.221-227.

Dunn, R. J. 1985. Laboratory measurement of a fine-grained soil fluid conductivity. Engineering Geology. Vol. 21, pp.215-223.

Elton, G. A. H. 1948. Electroviscosity. Proceedings of the Royal Society. Vol. 194A, pp.41-61.

Fernandez, F. and Quigley, R. M. 1988. Viscosity and dielectric constant controls on the hydraulic conductivity of clayey soils permeated with simple liquid hydrocarbons. Canadian Geotechnical Journal. Vol. 22, pp.582-589.

Garlanger, J. E., Cheung, F. K. and Tannous, B. S. 1987. Quality control testing of a sand-bentonite liner. Geotechnical Practice for Waste Disposal, pp.488-499.

Georgiannou, V. N. 1988. The behaviour of clayey sands under monotonic and cyclic loading. PhD. thesis, University of London.

Georgiannou, V. N., Burland, J. B. and Hight, D. W. 1990. The undrained behaviour of clayey sands in triaxial compression and extension. Geotechnique. Vol. 40, No. 3, pp.431-449.

Gibson, R. E. and Henkel, D. J. 1953. Influence of duration of tests at constant rate of strain on measured drained strength. Geotechnique. Vol. 1, No. 1, pp.6-15.

Goodhall, D. C. and Quigley, R. M. 1977. Pollutant migration from two sanitary landfill sites near Sarnia, Ontario. Canadian Geotechnical Journal. Vol. 14, No. 2, pp.223-236.

Gouy, G. 1910. Charge électrique à la surface d'un electrolyte. Journal of Physics. Vol. 4, No. 9, pp.457-468.

Graham, J., Gray, M. N., Sun, B. C. C. and Dixon, D. A. 1986. Strength and volume change characteristics of a sand-bentonite buffer. Proceedings of the 2nd International Conference on Radioactive Waste Management, pp.188-194.

Graham, J., Saadat, F., Gray, M. N., Dixon, D. A. and Zhang, Q. Y. 1989. Strength and volume change behaviour of a sand-bentonite mixture. Canadian Geotechnical Journal. Vol. 26, No. 2, pp.292-305.

Gray, M. N., Cheung, S. C. H. and Dixon, D. A. 1984. The influence of sand content on swelling pressures and structure developed in a statically compacted Na-bentonite. Atomic Energy of Canada Limited Report. AECL-7825.

Gray, M. N., Cheung, S. C. H. and Dixon, D. A. 1985. Swelling pressures of compacted bentonite-sand mixtures. Proceedings of the 44th Materials Research Society Symposium on Scientific Basis for Nuclear Waste Management. Vol. 44, pp.523-530. Boston.

Griffiths, F. J. and Joshi, R. C. 1989. Change in pore size distribution due to consolidation of clays. Geotechnique. Vol. 39, No. 1, pp.159-167.

Haefeli, R. 1951. Investigation and measurements of the shear strength of saturated cohesive soils. Geotechnique. Vol. 2, No. 3, pp.186-207.

Hansbo, S. 1960. Consolidation of clay, with special reference to influence of vertical sand drains. Swedish Geotechnical Institute Proceedings. No. 18, pp.41-61.

Hardin, B. O. and Drnevich, A. M. 1972. Shear modulus and damping in soils: Measurement and parameter effects. ASCE Journal of the Soil Mechanics and Foundations Division. Vol. 98, No. SM6, pp.603-624.

Haxo, H. E. 1990. Determining the transport through geomembranes of various permeants in different applications. American Society for Testing and Materials Symposium on Geosynthetic Testing for Waste Containment Applications, Las Vegas, Nevada.

Head, K. H. 1980. Manual of soil laboratory testing. Vol. 1. Pentech Press.

Head, K. H. 1981. Manual of soil laboratory testing. Vol. 2. Pentech Press.

Head, K. H. 1986. Manual of soil laboratory testing. Vol. 3. Pentech Press.

Helferrich, F. 1962. Ion-exchange. London. McGraw-Hill.

Hoeks, J., Glas, H., Hofkamp, J. and Ryhiner, A. H. 1987. Bentonite liners for isolation of waste disposal sites. Waste Management and Research. Vol. 5, pp.93-105.

Holopainen, P. 1985. Crushed aggregate-bentonite mixtures as backfill material for repositories of low and intermediate level radioactive wastes. Engineering Geology. Vol. 21, pp.239-245.

Holtz, W. G. 1985. Predicting hydraulic conductivity of clay liners: Discussion. ASCE Journal of Geotechnical Engineering. Vol. 111, pp.1457-1459.

Holtz, W. G. and Lowitz, C. W. 1957. Compaction characteristics of gravelly soils. Special Technical Publication No. 232. ASTM, Philadelphia, pp.70-83.

Jardine, R. J., Symes, N. J. and Burland, J. B. 1984. The measurement of soil stiffness in the triaxial apparatus. Geotechnique. Vol. 34, No. 3, pp.323-340.

Jessberger, H. L. and Beine, R. A. 1981. Impermeabilisation of disposal sites by impervious blankets consisting of mine refuse. Proceedings of the 10th International Conference on Soil Mechanics and Foundation Engineering. Vol. 4, pp.745-746. Stockholm.

Jones, C. W. 1954. The permeability and settlement of laboratory specimens of sand and sand-gravel mixtures. Special Technical Publication No. 163. ASTM, Philadelphia, pp.68-78.

Kemper, W. D., Maasland, D. E. L. and Porter, L. K. 1964. Mobility of water adjacent to mineral surfaces. Proceedings of the Soil Science Society of America. Vol. 28, No. 2, pp.164-167.

Kenney, T. C. 1977. Residual strength of mineral mixtures. Proceedings of the 9th International Conference on Soil Mechanics. Vol. 1, pp.155-160.

Klausner, Y. and Shainberg, I. 1971. Consolidation properties of adsorbed montmorillonites. Proceedings of the 4th Asian Conference on Soil Mechanics and Foundation Engineering. Vol. 1, pp.371-378. Bangkok.

Lamb, H. 1932. Hydrodynamics 6th Edition. Cambridge University Press, London.

Lambe, T. W. 1958. The engineering behaviour of compacted clay. Proceedings of the American Society of Civil Engineering. Vol. 84, No. SM2.

Lambe, T. W. 1960. A mechanistic picture of shear strength in clay. Conference on the Shear Strength of Soils, pp.503-532. Colorado.

Lambe, T. W. and Whitman R. V. 1979. Soil Mechanics. SI Version. J. Wiley and Sons, Toronto.

Lee, K. L. and Black, D. K. 1972. Time to dissolve an air bubble in a drain line. Journal of the Soil Mechanics and Foundations Division. ASCE. Vol. 98, No. SM2, Proc. paper 8728, pp.181-194.

Little, J. A., Muir Wood, D., Paul, M. A. and Bouzza, A. 1992. Some laboratory measurements of permeability of Bothkennar clay in relation to soil fabric. Geotechnique Vol. 42, No. 2, pp.355-361.

Low, P. F. 1960. Viscosity of water in clay systems. Proceedings of the National Conference on Clays and Clay Minerals. Vol. 8, pp.170-182. New York.

Low, P. F. 1961. Physical chemistry of clay-water interaction. Advances in Agronomy. Vol. 13, pp.269-327.

Low, P. F. 1980. The swelling of clay: II. Montmorillonites. Journal of the Soil Science Society of America. Vol. 44, pp.667-676.

Low, P. F. and Margheim, J. F. 1979. The swelling of clay: I. Basic concepts and empirical equations. Journal of the Soil Science Society of America. Vol. 43, pp.473-481.

Lundgren, T. A. 1981. Some bentonite sealants in soil mixed blankets. Proceedings of the 10th International Conference on Soil Mechanics and Foundation Engineering. Vol. 4, pp.745-746. Stockholm.

Lundgren, T. A. and Söderblom, R. 1985. Clay barriers - a not fully examined possibility. Engineering Geology. Vol. 21, pp.201-208.

Lupini, J. F., Skinner, A. E. and Vaughan, P. R. 1981. The drained residual strength of cohesive soils. Geotechnique. Vol. 31, No. 2, pp.181-213.

Lutz, J. F. and Kemper. W. D. 1959. Intrinsic permeability of clay as affected by clay-water interaction. Soil Science. Vol. 88, pp.83-90.

Macey, H. H. 1942. Clay on dash water relationships and the internal mechanism of drying. Transactions of the British Ceramic Society. Vol. 41, pp.73-121.

McEnroe, B. M. 1992. Maximum saturated depth over landfill liner. ASCE Journal of Environmental Engineering. Vol. 119, No. 2. pp.262-270.

Mesri, G. and Olson, R. E. 1971. Mechanisms controlling the permeability of clays. Clays and Clay Minerals. Vol. 19, pp.151-158.

Mesri, G. and Olson, R. E. 1971. Consolidation characteristics of montmorillonite. Geotechnique. Vol. 21, No. 4, pp.341-352.

Mitchell, J. K. 1956. The importance of structure to the engineering behaviour of clay. Sc. D. Thesis, M.I.T.

Mitchell, J. E. 1960. The application colloidal theory to the compressibility of clays. Interparticle forces in clay-water-electrolyte systems. Melbourne, CSIRO, 2.92-2.98.

Mitchell, J. K. 1976. Fundamentals of Soil Behaviour. 1st edition. J. Wiley and Sons Publishers, Toronto.

Mitchell, J. K. 1991. The 31st Rankine Lecture. Conduction phenomena: from theory to geotechnical practice. Geotechnique. Vol. 41, No. 3, pp.299-340.

Mitchell, J. K. 1993. Fundamentals of Soil Behaviour. 2nd edition. J. Wiley and Sons Publishers, Toronto.

Mitchell, J. K., Singh, A. and Campanella, R. G. 1969. Bonding, effective stresses, and strength of soil. Journal of the Soil Mechanics and Foundations Division Proceedings of the American Society of Civil Engineers. Vol. 95, No. SM5, pp.1219-1246.

Mollins, L. H., Stewart, D. I. and Cousens, T. W. Predicting the properties of bentonite-sand mixtures. In print.

Moore, R. 1991. The chemical and mineralogical controls upon the residual strength of pure and natural clays. Geotechnique. Vol. 41, No. 1, pp.35-47.

Nagaraj, T. S. and Murthy, B. R. 1983. Rationalization of Skempton's compressibility equation. Geotechnique. Vol. 33, No. 4, pp.433-443.

Nagaraj, T. S. and Murthy B. R. 1986. Prediction of compressibility of overconsolidated uncemented soils. ASCE Journal of Geotechnical Engineering Vol 112, No. 4, pp.484-488.

Nagaraj, T. S. and Murthy B. R. 1986. A critical reappraisal of compression index equations. Geotechnique. Vol. 36, No. 1, pp.27-32.

Nagaraj, T. S. and Murthy, B. R. 1990. Change in pore size distribution due to consolidation of clays: Discussion. Geotechnique, Vol. 40, No. 2, pp.303-309.

O'Sadnick, D. L., Simpson, B. E. and Kasel, G. K. 1995. Evaluation and performance of a sand-bentonite liner. Geoenvironment 2000. ASCE Geotechnical Special Publication. No. 46, pp.688-701.

Oakley, R. E. 1987. Design and performance of earth-lined containment systems. Geotechnical practice for waste disposal. Proceedings of the American Society of Civil Engineers Specialty Conference, pp.117-136. Ann Arbor, Michigan.

Olsen, H. W. 1962. Hydraulic flow through saturated clays. Proceedings of the 9th National Conference on Clays and Clay Minerals, pp.131-161.

Olson, R. E. and Mesri, G. 1970. Mechanisms controlling the compressibility of clays. Journal of the American Society of Civil Engineers. Vol. 96, No. SM6, 1853-1878.

Oscarson, D. W. and Cheung, S. C. H. 1983. Evaluation of phyllo-silicates as a buffer component in the disposal of nuclear fuel waste. Atomic Energy of Canada Limited Report, AECL-7812.

Oscarson, D. W., Dixon, D. A. and Gray, M. N. 1990. Swelling capacity of an unprocessed and processed bentonite clay. Engineering Geology. Vol. 28, pp.281-289.

Parry, R. H. G. 1960. The role of interparticle forces in the behaviour of clay. Seminar on Interparticle Forces in Clay-Water-Electrolyte Systems, pp.29-34. Melbourne.

Pellissier, J. P. and Maree, L. 1991. A hypothetical clay model to describe free swell in active clays. The Civil Engineer in South Africa, pp.419-424.

Porter, L. K., Kemper, W. D., Jackson, R. D. and Stewart, B. A. 1960. Chloride diffusion in soils as influenced by moisture content. Proceedings of the Soil Science Society of America. Vol. 24, No. 6, pp.460-463.

Poulos, S. J. 1964. Report on control of leakage in the triaxial test. Harvard University Soil Mechanics Series, No. 71, Cambridge, Massachusetts.

Pusch, R. 1970. Microstructural changes in soft quick clay at failure. Canadian Geotechnical Journal. Vol. 7, pp.1-6.

Pusch, R. 1973. Influence of salinity and organic matter on the formation of clay microstructure. Proceedings of International Symposium on Soil Structure, pp.161-173. Gothenburg: Swedish Geotechnical Society.

Pusch, R. 1980. Swelling pressure of highly compacted bentonite. SKBF/KBS Teknisk Rapport, 80-13.

Pusch, R. 1982. Mineral-water interactions and their influence on the physical behaviour of highly compacted Na-bentonite. Canadian Geotechnical Journal. Vol. 19, pp.381-387.

Pusch, R. and Carlsson, T. 1985. The physical state of pore water of Na-smectite used as a barrier component. Engineering Geology. Vol. 21, pp.257-265.

Pusch, R. 1983. Isolation of toxic waste products from the biosphere by the use of clay barriers. Luleå University of Technology, Sweden, Division of Soil Mechanics.

Quigley, R. M. and Rowe, R. K. 1986. Leachate migration through clay below a domestic waste landfill, Sarnia, Ontario, Canada: chemical interpretation and modelling philosophies. Hazardous and industrial solid waste testing and disposal. ASTM STP 933, pp.93-103. Philadelphia.

Quigley, R. M., Yanful, E. K. and Fernandez, F. 1987. Ion transfer by diffusion through clayey barriers. Geotechnical Practice for Waste Disposal, Special Publication No. 13, ASCE, pp.137-158. New York.

Roscoe, K. H. 1970. The influence of strains in soil mechanics. Geotechnique. Vol. 20, No. 2, pp.129-170.

Roscoe, K. H., Schofield, A. N. and Wroth, C. P. 1958. On the yielding of soils. Geotechnique. Vol. 8, No. 1, pp.22-53.

Rowe, P. W. 1962. The stress-dilatancy relation static equilibrium of an assembly of particles in contact. Proceedings of the Royal Society of London. A269, 1336-1339, pp.500-527.

Rowe, P. W., Oates, D. B. and Skermer, N. A. 1963. The stress-dilatancy performance of two clays. ASTM STP 361, pp.134-146.

Sällfors, G. B. and Peirce, J. 1985. Determination of the permeability of a clay liner. Engineering Geology. Vol. 21, pp.225-228.

Schofield, R. K. 1946. Ionic forces in thick films of liquid between charged particles. Transactions of the Faraday Society, 42B, 219.

Seed, H. B. and Chan, C. K. 1959. Structure and strength characteristics of compacted clays. ASCE Journal of the Soil Mechanics and Foundations Division. Vol. 85, No. SM5, pp.87-128.

Seed, H. B., Mitchell, J. K. and Chan, C. K. 1962. Studies of swell and swell pressure characteristics of compacted clays. Highway Research Bulletin Board 313, pp 12-39.

Shackleford, C. D. and Daniel, D. E. 1991. Diffusion in saturated soil. I: Background. Journal of Geotechnical Engineering. ASCE. Vol. 117, No. 3, pp.467-484.

Shakoor, A. and Cook, B. D. 1990. The effect of stone content, size, and shape on the engineering properties of a compacted silty clay. Bulletin of the Association of Engineering Geologists. Vol. 27, No. 2, pp.245-253.

Shelley, T. L. and Daniel, D. E. 1993. Effect of gravel on hydraulic conductivity of compacted soil liners. Journal of Geotechnical Engineering. ASCE. Vol. 119, No. 1, pp.54-68.

Skempton, A. W. 1985. Residual strength of clays in landslides, folded strata and the laboratory. Geotechnique. Vol. 35, pp. 3-18.

Skempton, A. W. and Bishop. A. W. 1950. Measurement of shear strength of soils Discussion. Geotechnique. Vol. 4, No. 4, pp.90-113.

Skinner, A. E. 1969. A note on the influence of interparticle friction on the shearing strength of a random assembly of spherical particles. Geotechnique. Vol. 19, No. 1, pp.150-157.

Sridharan, A. 1968. Some studies of the strength of partly saturated clays. PhD thesis, Purdue University, Indiana.

Sridharan, A. 1990. Strength and volume change of a sand-bentonite mixture: Discussion. Canadian Geotechnical Journal. Vol. 27, pp.404.

Sridharan, A. and Jayadeva, M. S. 1982. Double layer theory and compressibility of clays. Geotechnique. Vol. 32, No. 2, pp.133-144.

Sridharan, A. and Venkatappa Rao, G. 1973. Mechanisms controlling volume change of saturated clays and the role of the effective stress concept. Geotechnique. Vol. 23, No. 2, pp.359-382.

Sridharan, A. and Venkatappa Rao, G. 1979. Shear strength behaviour of clays and the role of the effective stress concept. Geotechnique. Vol. 29, No. 2, pp.177-193.

Sridharan, A., Rao, S. M. and Gajarajan, V. S. 1990. Effect of sulfate contamination on the volume change behaviour of bentonite. Physico-Chemical Aspects of Soil and Related Materials, ASTM STP1095. American Society for Testing and Materials, pp 60-68. Philadelphia.

Stearns, N. D. 1927. Laboratory tests on physical properties of water-bearing materials U. S. Geological Survey Water Supply Paper 596, pp.121-176.

Stokoe, K. H., Anderson, A. M., Hoar, R. J. and Isenhower, A. M 1978. In-situ laboratory shear velocity and modulus. Discussion. Eighth Pasadena Conference, pp.1498-1502.

Storr, T. 1992. The geotechnical properties of bentonite enhanced soil to be used as a load bearing cap for landfill. Department of Earth Sciences. University of Leeds.

Swarzendruber, D. 1962. Non-Darcy flow behaviour in liquid saturated porous media. Journal of Geophysical Research. Vol. 67, No. 13, pp.5205-5213.

Taylor, D. W. 1942. Research on consolidation of clays. Serial 82. Massachusetts Institute of Technology, Department of Civil Engineering, Cambridge.

Taylor, D. W. 1948. Fundamentals of soil mechanics. J. Wiley and Sons, New York

Terzaghi, K. 1923. Die Berechnung der Durchlassigkeitsziffer des Tons aus dem Verlauf der hydrodynamischen Spannungserscheinungen. Mathematischnaturwissenschaftliche Klasse-IIa, 132, pp.125-138.

Terzaghi, K. 1925. Determination of the permeabililty of clay. Engineering News Record. Vol. 95, pp.832-836.

Terzaghi, K. 1943. Theoretical Soil Mechanics. Wiley. New York

Terzaghi, K. and Peck, R. B. 1967. Soil mechanics in engineering practice J Wiley and Sons, New York.

van Olphen, H. 1977. An introduction to clay colloid chemistry. For clay technologists, geologists and soil scientists. 2nd edition. A Wiley - Interscience Publication.

van Schaik, J. C. and Kemper, W. D. 1966. Chloride diffusion in clay-water systems Proceedings of the Soil Science Society of America. Vol. 30, No. 1, pp.22-25.

Vaughan, P. R., Davachi, M. M., El Ghamrawy, M. K., Hamza, M. M. and Hight, D. W. 1976. Stability analysis of large gravity structures. Proceedings of the 1st International Conference on the Behaviour of Off-Shore Structures Vol 1, pp 467-480

Vaughan, P. R., Hight, D. W., Sodha, V. G. and Walbancke, H. J. 1978. Factors controlling the stability of clay fills in Britain. Clay fills, pp.203-217. London Institution of Civil Engineers.

Verwey, E. J. W. and Overbeek, J. Th. G. 1948. Theory of the stability of lyophobic colloids. Elsevier Publishing Company, Amsterdam.

Von Englehardt, W. and Tunn, W. L. M. 1955. The flow of fluid through sandstones Illinois State Geological Survey Circular 194.

Wissa, A. E. Z. 1969. Pore pressure measurement in saturated stiff soils. ASCE Journal of the Soil Mechanics and Foundations Division. Vol. 95, No. SM4, Proc. Paper 6670, pp.1063-1073.

Wu, J. Y. and Khera, R. P. 1990. Properties of a treated bentonite/sand mix in contaminant environment. Physico-Chemical Aspects of Soil and Related Materials, ASTM STP1095. American Society for Testing and Materials, pp.47-59. Philadelphia.

Yong, R. N. A. and McKyes, E. 1971. Failure and yield of a clay under triaxial stresses. ASCE Journal of the Soil Mechanics and Foundations Division. Vol. 97, No. SM1, pp.159-176.

Yong, R. N. and Sheeran, D. E. 1973. Fabric unit interaction and soil behaviour. Proceedings of the International Symposium on Soil Structure, Gothenburg, Sweden, pp.176-183.

Yong, R. N. and Warkentin, B. P. 1975. Soil properties and behaviour. Elsevier Scientific Publishing Company, Amsterdam.

APPENDIX 1

Pressure limitations of the Bishop-Wesley stress path triaxial cell

The stress which can be applied to the sample in a Bishop-Wesley triaxial cell is limited by the maximum available airline pressure (approximately 600kPa), because the pressure forcing the ram upwards is opposed by the cell pressure. In the bearing housing of the apparatus the effective area of the Bellofram's seals is 2940mm^2. If the area of a standard triaxial sample is assumed to be approximately 1134mm^2, then the excess pressure available to fail the sample is (2940/1134) ~ 2.6 times the difference between the airline pressure and the total cell pressure. Therefore, the stress range is further restricted with back pressure application, as the back pressure value must be added the required effective stress to give the applied cell pressure.

If the deviator stress required to fail the sample is larger than the excess pressure in the line then the back pressure must be reduced. This is more significant at large effective cell pressures. For example, at an effective cell pressure of 200kPa and a standard back pressure of 300kPa the applied stress acting on the loading ram is 500kPa. Therefore, the maximum deviator stress which can be applied is 2.6 x (600 - 500) = 260kPa. This will enable failure of a sample with a peak angle of shearing resistance $\leq 23.2°$. At 100kPa back pressure a sample with a strength $\leq 41.3°$ can be brought to failure. 5% bentonite-sand mixtures only were tested in this cell and the smallest measured strength was 44.2°. As a consequence, back pressures of 0kPa and 200kPa were applied at effective cell pressures of 200kPa and 100kPa respectively. For all other samples, a standard back pressure of 300kPa (e.g. Dunn, 1985) was used.

APPENDIX 2

Calculation of required compaction for Rowe cell samples

A2.1 Scope

250mm Rowe cell hydraulic conductivity tests were conducted on mixtures compacted into the cell using the modified Proctor method (or BS 'heavy' compaction). Therefore, samples were compacted to a specified density which was commensurate with that determined from the compaction tests into a Proctor mould. This is straightforward because a known mass has to fill a specified volume which is calculated from the required sample height (between 20-30mm), and the number a blows to be applied depends on this volume. A calculation relating to the 250mm cell is given below. The pattern of blows was the same as that suggested by Head (1980), compacting first the edge, then the middle, then giving systematic overall coverage.

A2.2 Calculation of required number of blows

Assuming a cell of 252.3mm diameter, the area is 50000mm^2. The height to give a volume of 1 litre (10^6mm^3), i.e. the volume of a Proctor compaction mould, is 20mm. For 'heavy' compaction the number of blows is 25 x 5 = 135 using the 4.5kg rammer. If the compacted height of the sample in the cell is h mm, the volume of soil is h/20 litres, and the total number of blows required are (h/20) x 135 = 6.75h. Because the height to diameter ratio of a Rowe cell sample is less than that of the Proctor mould, Head (1986) suggests that the soil is compacted in 3 layers for a final sample height of 90mm. In the test programme, specimen thicknesses were in the range 20-30mm and were therefore compacted in 1 layer only.

APPENDIX 3

Pore pressure measurement and saturation of samples

Skempton (1954) has shown theoretically that at constant water content, the change in pore pressure, Δu, due to a change in total stress, $\Delta\sigma$, is given by

$$B=\frac{\Delta u}{\Delta\sigma}=\frac{1}{1+n\frac{C_w}{C_s}} \qquad \text{A3.1}$$

where B is a pore pressure coefficient, n is the porosity, C_W is the compressibility of the pore fluid, and C_S the compressibility of the soil skeleton. Equation A3.1 assumes the individual soil particles to be incompressible.

In completely saturated soils the compressibility of the pore fluid is about 5.6×10^{-4} m^2/MN (Wissa, 1969). Therefore, according to Skempton, C_W/C_S is approximately equal to zero, since the compressibility of water is negligible compared to that of the soil structure, and B = 1, when the degree of saturation = 1. However, as the compressibility of the soil decreases, the theoretical B values become less than 1. Wissa (1969) gives B-values for different soil stiffnesses calculated using equation A3.1. At soil stiffnesses of $1 m^2/MN$ and the $10^{-4} m^2/MN$ the theoretical B-values are 0.9997 and 0.6452 respectively.

In addition to the soil stiffness, the degree of saturation, S_r, has a significant effect on the measured B-value. The computed variation in B-value with an increasing degree of saturation for four classes of soil are shown in figure A3.1 (after Black and Lee, 1973). Reference to these curves provides a basis for evaluating the significance of measured values of B or S_r, or both, less than 1. If B = 0.95 was accepted as indicating full saturation, reference to figure A3.1 indicates that this criteria might be satisfactory for stiff soils because S_r is indicated to be at least 99.9%. However, for soft soils, S_r may only be about 96%. Black and Lee (1973) suggest that it may be satisfactory to test soils at S_r = 99.5% or 99.0% and treat them as fully saturated. Table A3.1 gives B-values for the four classes of soil in figure A3.1 at complete and nearly complete saturation. From these results it was concluded that for soft and medium stiff soils it may be acceptable to use S_r values of 99.5% or 99.0%, however, for stiff or very stiff soils, 100% saturation is probably required to assure adequate pore pressure response. The required times to reach full saturation are indicated in figure A3.2 (after Black and Lee, 1973)

Class of soil	Saturation = 100%	Saturation = 99.5%	Saturation = 99.0%
Soft (N.C. clays)	0.9998	0.992	0.986
Medium (compacted clays)	0.9988	0.963	0.930
Stiff (stiff clays - sands)	0.9877	0.69	0.51
Very Stiff (very high consolidation pressures)	0.9130	0.20	0.10

Note: N.C. = normally consolidated

Table A3.1. B-values of different types of soil at complete and nearly complete saturation (after Black and Lee, 1973).

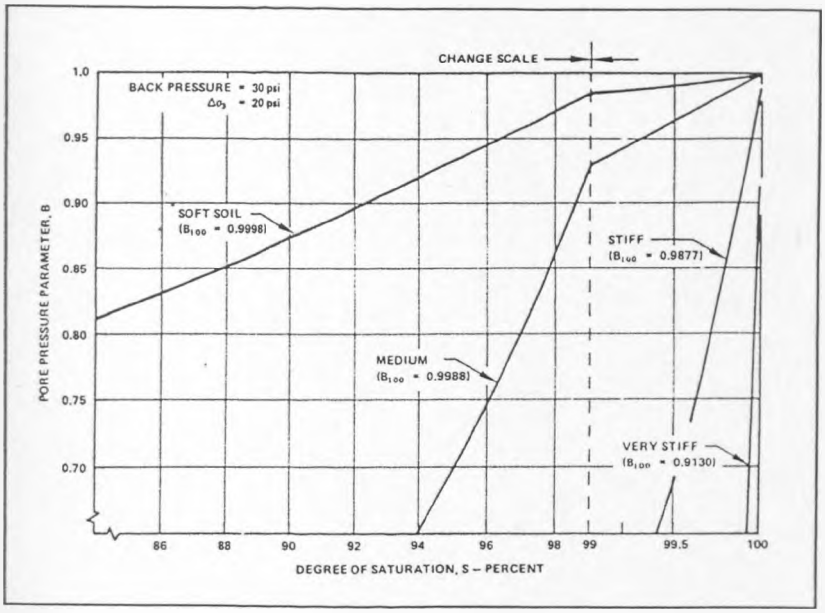

Figure A3.1: Range of B-values for different degrees of saturation (after Black and Lee, 1973).

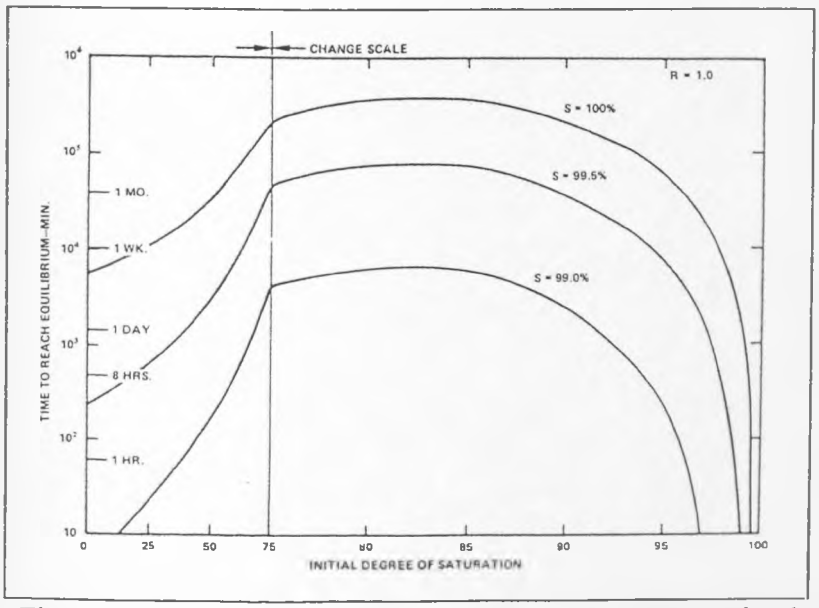

Figure A3.2: Time to reach an equilibrium saturation using back pressure (after Black and Lee, 1973).

APPENDIX 4

Calculated pore pressure dissipations for triaxial samples

Based on the idealised one-dimensional swelling behaviour and hydraulic conductivity of bentonite-sand mixtures, the average degree of consolidation at failure of samples tested in triaxial compression under drained conditions was calculated using the equations given in 4.5.4[1]. The calculated values are given in table A4.1.

Initial and final clay void ratios corresponding to ±10% of the surcharge values quoted in the table (the applied stress range used for triaxial samples) were determined using equation 5.9 for effective stresses below the threshold values and equations 5.14 - 5.16 for effective stresses above the threshold values. This enabled calculation of the coefficient of volume compressibility, m_v. Hydraulic conductivity was calculated using equations 5.27 and 5.28 for 20% and 10% mixtures, and a value of 10^{-10} m/s was assumed for all 5% mixes[2]. The calculated required time to failure, actual time to failure and degree of consolidation at failure U_f are given in table A4.1.

Similar calculations using the overall void ratio instead of the clay void ratio yield higher values of U_f. Therefore, the values quoted are expected to be the worst case.

---

[1]The analysis was conducted using one-dimensional relationships due to the substantially larger amount of data and better characterisation of the behaviour.

[2]Because a clay void ratio - hydraulic conductivity relationship was not established for 5% bentonite-sand mixtures it was considered satisfactory to use the lowest measured value to give a conservative estimate of the pore pressure dissipation.

% bentonite	Surcharge (kPa)	Initial e_c (-10%)	Final e_c (+10%)	a_v (m^2/kN)	m_v (m^2/kN)	k (m/s)	c_v (m^2/s)	T_f (days)	actual T_f (days)	U_f (%)
20	200	3.13	3.01	2.34E-03	5.66E-04	2.13E-12	3.83E-10	21.59	35.75	97.0
20	100	3.53	3.41	4.67E-03	1.03E-03	3.18E-12	3.15E-10	26.30	39.83	96.7
20	50	4.52	4.13	3.19E-02	5.77E-03	6.51E-12	1.15E-10	71.91	75.46	95.2
20	25	5.90	5.50	6.37E-02	9.23E-03	1.6E-11	1.77E-10	46.81	67.75	96.6
10	200	5.77	5.65	2.34E-03	3.45E-04	5.03E-12	1.49E-09	5.57	22.87	98.8
10	100	6.17	6.05	4.67E-03	6.51E-04	6.45E-12	1.01E-09	8.19	14.46	97.2
10	50	6.57	6.46	9.34E-03	1.23E-03	8.15E-12	6.74E-10	12.28	21.67	97.2
10	25	6.98	6.86	1.87E-02	2.34E-03	1.01E-11	4.42E-10	18.73	37.88	97.5
5	200	11.58	11.46	2.34E-03	1.86E-04	1.00E-10	5.49E-08	0.15	15	99.9
5	100	11.98	11.86	4.67E-03	3.60E-04	1.00E-10	2.83E-08	0.29	12	99.9
5	50	12.38	12.27	9.34E-03	6.98E-04	1.00E-10	1.46E-08	0.57	15	99.8
5	25	12.79	12.67	1.87E-02	1.36E-03	1.00E-10	7.52E-09	1.10	7.5	99.3

Table A4.1. Calculated average degrees of consolidation at failure of bentonite-sand mixtures in triaxial compression.

APPENDIX 5

Line fitting procedure for idealised swelling of bentonite-sand mixtures

A.1 Calculation of gradient

Logarithmic regression analysis of data for mixtures whose clay void ratios lay above the bentonite swelling line, gave the following equations:

20%: $e_c = 5.54 - 1.08 \log \sigma'_v$ A5.1

10%: $e_c = 8.43 - 1.15 \log \sigma'_v$ A5.2

5%: $e_c = 14.98 - 1.63 \log \sigma'_v$ A5.3

The number of data points used in the analysis are, 5, 12 and 13 for 20, 10 and 5% bentonite-sand mixtures respectively. A weighted average of the three gradients was calculated by multiplying the gradient of each swelling line by the corresponding number of data points and dividing by the total number as follows:

$[(5 \times 1.08) + (12 \times 1.15) + (13 \times 1.63)]/30 = 1.34$

and this was taken as the gradient of each swelling line.

A.2 Calculation of constant at 1kPa vertical effective stress

An example of the constant fitting procedure for 5% bentonite-sand mixtures is given below. The same procedure was used for 10 and 20% mixtures.

The vertical effective stress range over which the tests were performed was 1.25 - 453kPa. The best fit equation to the data from logarithmic regression analysis (equation A5.3) was used to calculate the clay void ratio at the middle of this stress range on a logarithmic scale (as shown in figure A5.1), i.e., at a vertical effective stress of $10^{[(\log 1.25 + \log 453)/2]} = 23.8$kPa, giving a value of 12.75. This value was re substituted into the equation using the corrected gradient of 1.34 to determine the constant at a vertical effective stress of 1kPa as follows:

$12.75 = C - 1.34 \log 23.8$

giving a value of 14.60.

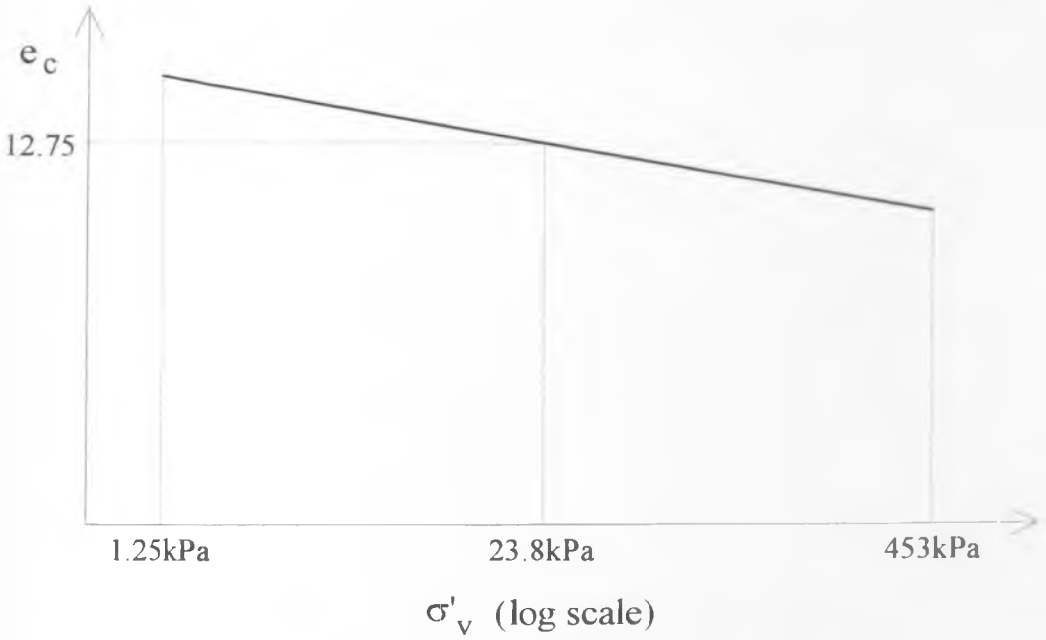

Note: figure is not to scale.

Figure A5.1: Constant fitting procedure for 5% bentonite-sand mixtures

APPENDIX 6

Design examples for hydraulic conductivity and strength criteria

A6.1 Scope

The required clay content or vertical effective stress is calculated for hydraulic conductivity and strength criteria by considering the materials used in this study. For ease of calculation, the predictive equations determined in this study will also be used. In the design examples presented, it will be assumed that the swelling, hydraulic conductivity and strength have been characterised in the laboratory as described in 7.2.1 and 7.3.1.

A6.2 Design example for a hydraulic conductivity criteria

Assuming that a hydraulic conductivity specification of 10^{-11} m/s is required, and the combined sand porosity-tortuosity factor was found to be approximately 0.05 from oedometer swelling tests for an appropriate mixture and surcharge, then the required clay content or vertical effective stress can be determined as follows: The required bentonite hydraulic conductivity is determined using equation 6.6, i.e.,

$$\frac{k_{mix}}{k_{clay}} = n_s \tau_s$$

which gives $k_{clay} = 2 \times 10^{-10}$ m/s.

The maximum permissible clay void ratio is determined from equation 5.26, i.e.,

$k = 10^{-11.07} . e_c^{1.77}$

Therefore, $e_c = 5.95$

The mixture swelling behaviour determined in the laboratory will then indicate the required clay content for a particular vertical effective stress, or, the vertical effective stress required for a specified clay content.

A6.3 Design example for a strength criteria

A6.3.1 Mixture with strength of clay only

Suppose that the estimated field strain (volumetric) is 10%, and laboratory testing indicated that a sand relative density of -1 gives a strength corresponding to the mineralogy of the clay phase only. The sand void ratio, e_s, corresponding to this relative density can be calculated using the relationship

$$I_D = \frac{e_{max} - e_s}{e_{max} - e_{min}}$$

where e_{max} and e_{min} are the maximum and minimum sand void ratios respectively. This gives $e_s = 1.51$. Since $\varepsilon_v = \Delta e_s/(1 + e_{s0}) = 0.1$ then the required initial sand void ratio $e_{s0} = 1.783$.

Suppose that the field stress is 50kPa then equation 5.35 (isotropic swelling line) can be used to determine the required clay void ratio because no sand particles are in contact, i.e.,

$e_c = 10.55 - 4.57 \log p'$

which gives $e_c = 2.79$.

Now $e_c = e/x$ (equation 5.3) and $e_s = [(e + x)/(1 - x)]$ (equation 5.4), therefore

$$x = \frac{e_s}{e_s + e_c + 1} \qquad \text{A6.1}$$

Therefore, the required clay content is 32% by dry volume

A6.3.2 Mixture with strength of sand

Suppose that a maximum angle of shearing resistance of 40° is desired. Then the sand relative density is calculated using equation 6.7, i.e.,

$\phi'_{max} - \phi'_{cv} = 20.60 I_D - 3.40$

which gives $I_D = 0.63$. The corresponding sand void ratio is 0.65.

The sand void ratio is related to the clay void ratio and the clay content by equation A6.1. Therefore, the mixture swelling behaviour determined in the laboratory will enable selection of a clay content (for a particular effective stress), or an effective stress (for a specified clay content), for the required strength.

Clay Minerals (1996) **31**, 243–252

PREDICTING THE PROPERTIES OF BENTONITE–SAND MIXTURES

L.H. MOLLINS, D.I. STEWART, AND T.W. COUSENS

Department of Civil Engineering, University of Leeds, Leeds, LS2 9JT, UK

(*Received 5 June 1995; revised 2 October 1995*)

ABSTRACT: One-dimensional swelling tests and hydraulic conductivity tests have been performed at vertical effective stresses up to 450 kPa on Na-bentonite powder and compacted sand/Na-bentonite mixtures (5, 10 and 20% bentonite by weight) to investigate the use of bentonite-improved soils for waste containment. It was found that bentonite powder swells to reach a final state described by a single straight line on a plot of void ratio against the logarithm of vertical effective stress, regardless of preparation technique. Swelling of sand/bentonite mixtures expressed in terms of the clay void ratio show a deviation from bentonite behaviour above a stress which depends on the bentonite content. Hydraulic conductivity data for bentonite and sand/bentonite mixtures indicate an approximately linear relationship between logarithm of hydraulic conductivity and logarithm of void ratio. A design model based on the clay void ratio, and the sand porosity and tortuosity is presented enabling the hydraulic conductivity of a mixture to be estimated.

A modern landfill must be designed to prevent fluids in the waste migrating from the site. Currently, engineered liner systems are usually a composite of a compacted clay soil and a synthetic (usually high density polyethylene, HDPE) membrane, together with various drainage and fluid collection layers. The HDPE liner alone is sufficiently impermeable to prevent groundwater contamination by leachate from the waste but such liners are susceptible to puncturing, and an additional low permeability clay liner is essential to ensure containment.

The engineering specifications for a compacted clay liner usually consist of a hydraulic conductivity of $<1 \times 10^{-9}$ m/s, and the need for stability during construction and operation of the landfill. Material selection is usually based on local availability, and many different soil types (both natural soils and processed clay minerals) have been used as liners. However, leakage can result from shrinkage cracking if the clay content of the soil is too high. One material that can meet the hydraulic conductivity criteria without suffering from shrinkage cracking is a sand/bentonite mixture. The sand component decreases the shrinkage on drying (Dixon *et al.*, 1985) and below a limiting clay content the sand particles are in contact, providing mechanical stability and preventing shrinkage. When wet, the clay fills the sand voids producing a very low hydraulic conductivity for the mixture.

Bentonite is a particularly effective clay for producing low permeability barriers because it has a high swelling capacity, which reduces the amount required. Depending on the type of bentonite, it can have a free swell (the volume increase when unconfined bentonite powder is inundated, divided by the volume of the original dry loose powder) between 200 and 1200% (Cowland & Leung, 1991; Wu & Khera, 1990). Processed (ground and dried) bentonite is normally used as the hydraulic conductivity of unprocessed bentonite can be higher (Oscarson *et al.*, 1990).

To minimize cost, and to avoid shrinkage cracking, it is important that the amount of clay added to a mixture is kept close to the minimum required to meet the hydraulic conductivity specification. Permeameter tests using distilled water indicate that mixtures containing more than ~5% bentonite by dry weight achieve the required value, although the hydraulic conductivity may be much higher when a landfill leachate is used as the permeant (Alther *et al.*, 1985; Hocks *et al.*, 1987; Wu & Khera, 1990). In addition there is uncertainty about how hydraulic conductivity varies with bentonite content; Cowland & Leung (1991) found no noticeable relationship, Garlanger *et al.* (1987) found that hydraulic conductivity decreases with

increasing bentonite, whereas Dixon & Gray (1985) found that adding (up to 50%) sand to bentonite decreases the hydraulic conductivity of the compacted material.

This paper discusses the swelling behaviour and hydraulic conductivity of Na-bentonite powder and sand/bentonite mixes. All samples were prepared in a relatively dry state and then saturated with distilled water for testing, as this is representative of the field conditions where mixing and compaction are conducted at a relatively low moisture content controlled by the need for optimum compaction (Cowland & Leung, 1991). Mixtures of 5, 10 and 20% bentonite by dry weight were tested. It will be shown that the hydraulic conductivity of a sand/bentonite mixture can be predicted from the bentonite content, its properties and the externally applied stress.

MATERIALS

The materials used in the study were Conquest grade Wyoming bentonite supplied by Colin Stewart MinChem, and Knapton Quarry sand. Conquest grade Wyoming bentonite originates from Newcastle, Wyoming, and is ground, dried and air classified during processing. X-ray diffraction spectra (Fig. 1) indicate that it is predominantly a montmorillonite with some quartz and trace cristobalite and chemical analysis (Table 1) confirms that it is predominantly a Na-montmorillonite. Knapton Quarry sand is a slightly silty fine angular quartz sand (containing some iron oxides and silicate minerals). Other properties of these materials are given in Table 2.

TEST PROCEDURE

Swelling tests

A swelling test was developed to investigate the behaviour of bentonite powder and three sand/bentonite mixtures (5, 10 and 20% bentonite by dry weight). Dry samples were placed in a consolidometer ring, subjected to a vertical stress, and distilled water allowed to be drawn into the cell from a reservoir while the sample height was monitored until swelling ceased. Comparative tests showed that the final void ratio is independent of initial compaction. Tests were performed at various vertical effective stresses, ranging from 1 to 450 kPa. Standard consolidation tests on bentonite slurry (prepared at the liquid limit) were conducted for comparison.

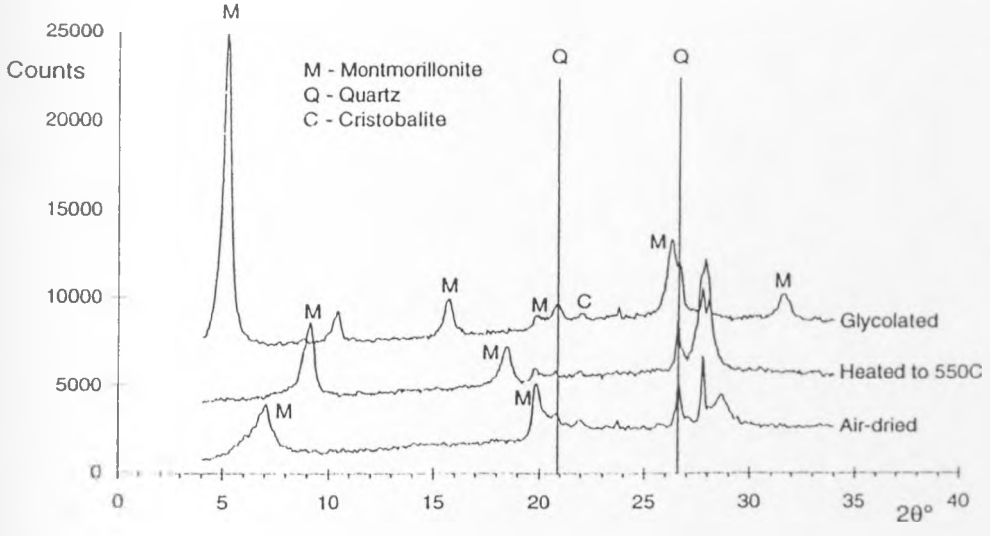

FIG. 1. X-ray diffraction spectra for Conquest Wyoming bentonite; Cu Kα radiation.

TABLE 1. Chemical composition (wt%) of Conquest Wyoming bentonite determined by X-ray fluorescence spectroscopy.

SiO_2	62.91
TiO_2	0.15
Al_2O_3	20.63
Fe_2O_3	3.75
MgO	2.45
CaO	1.16
Na_2O	2.29
K_2O	0.57
LOI*	5.83
Total	99.74

*Loss on ignition (1000°C for 1h).
Note: Sample dried at 105°C prior to testing

Hydraulic conductivity tests

Three methods were used to determine the hydraulic conductivity of the bentonite and sand/bentonite mixes. These were Rowe cell constant head tests, standard compaction permeameter falling head tests, and an indirect method where the hydraulic conductivity was calculated from consolidation data (Terzaghi, 1943), using the logarithmic method (Casagrande & Fadum, 1940). In all tests, hydraulic flow was orthogonal to the bedding direction during sample preparation, and distilled water was used as the permeant.

Bentonite specimens were tamped into the Rowe cell as dry powder, whereas mixtures (with one exception) were compacted into the cell at optimum moisture content (~12% moisture for all the mixtures). One mixture was prepared in the manner of the powders to investigate the influence of the sample preparation technique. All samples were confined by a vertical stress, vacuum de-aired, and allowed access to water. A back pressure of 300 kPa was used in all the Rowe cell tests to improve saturation. Hydraulic conductivity was calculated from inflow and outflow measurments under constant head conditions once equilibrium was reached.

Several workers have observed non-Darcian flow of water through soils (Englehardt & Tunn, 1955, Schwarzendruber, 1962; Irmay, 1965), and high hydraulic gradients can cause particle migration and irreversible decreases in hydraulic conductivity (Dunn, 1985). Therefore the first Rowe cell test investigated the effect of hydraulic gradient on the hydraulic conductivity. Darcy's law was found to be valid for hydraulic gradients between 14 and 340, the range used in this experimental programme.

Rowe cell constant head tests can take a long time to perform and require relatively specialized equipment. Therefore two alternative methods for measuring hydraulic conductivity, falling head compaction permeameter tests and an indirect method based upon consolidation rate on loading, were evaluated by comparison with the Rowe cell data. Both methods use equipment found in most soil mechanics laboratories. It was found that falling head compaction permeameter was suitable for measuring the hydraulic conductivity of the sand/5% bentonite mixture (higher clay contents caused significant swelling that masked the flow data), whereas the method based on consolidation rate required significant, time dependent volume change and was therefore appropriate for specimens with higher clay content.

TABLE 2. Properties of Wyoming bentonite and Knapton Quarry sand[1]

Wyoming bentonite	Knapton Quarry sand
Liquid limit = 407%	Percentage fines = 7%
Plastic limit = 48%	Effective size (D_{10})[2] = 0.07 mm
Specific gravity[3] = 2.76	Specific gravity = 2.67
Moisture content[4] ~13.5% (as supplied)	Moisture content ~4.5% (as supplied)

[1] All tests performed in accordance with B.S. 1377: 1975 Methods of test for soil for civil engineering purposes.
[2] 10% of the soil particles are finer than this effective diameter
[3] Determined by the small pyknometer method on clay oven dried at 105°C
[4] Measured by oven drying at 105°C

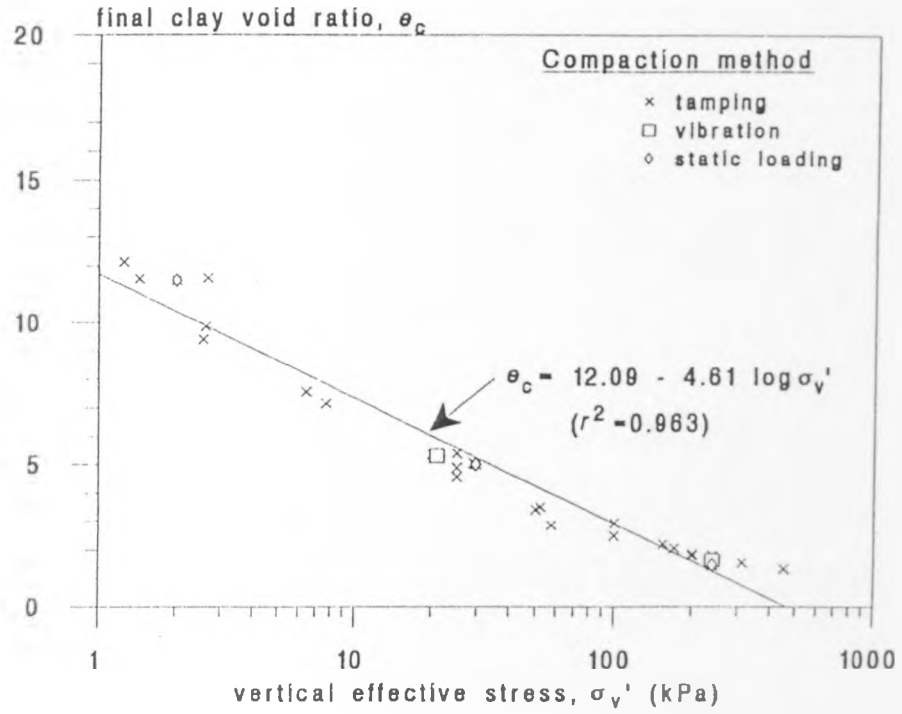

FIG. 2. Swelling of bentonite powder with distilled water.

RESULTS

Swelling: 100% bentonite

Figure 2 shows a linear relationship between the final void ratio of the clay, e_c, and the logarithm of vertical effective stress, σ_V'. The reported void ratios are the average of the value calculated from initial sample parameters (allowing for change in sample height), and the value calculated from post-test parameters. The difference between the two values was, on average, 1.2%, in all cases <3.5%, and consistent with a small amount of fluid being drawn into the specimens upon unloading after testing. Data for compaction by tamping, vibration and static loading were indistinguishable, indicating that the final void ratio is insensitive to sample preparation.

When the data from the consolidation tests on bentonite prepared as a slurry were plotted on axes of void ratio against the logarithm of vertical effective stress, the slope of the initial loading line (the compression index, C_c), and an unloading line (the rebound index, C_r) were 6.92 and 2.82, respectively. It is apparent from the difference between C_c and C_r and the gradient of the line in Fig. 2 that the final fabric of bentonite powder that has swollen from a dry state differs from that of normally consolidated and overconsolidated samples.

Swelling: sand/bentonite mixtures

The mixtures reported in this paper will be conceptualized as a two-phase sand-bentonite gel system, and the state of the bentonite will be described in terms of the clay void ratio, e_c:

$$e_c = \frac{V_w}{V_c} \qquad (1)$$

as shown on the right hand side of Fig. 3 (the conventional void ratio is shown on the left hand side of Fig. 3). The fraction of the total soil volume

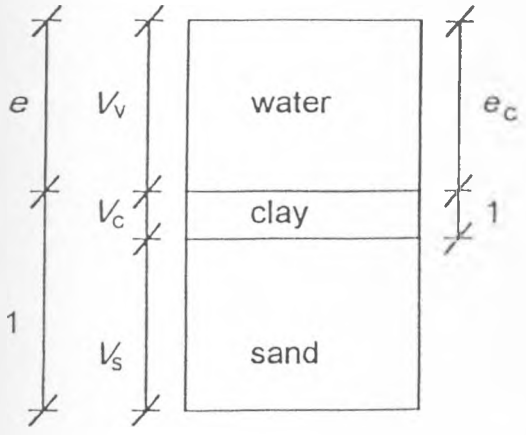

FIG. 3. Phase diagram for a saturated sand–clay mixture; V_v = volume of voids; V_c = volume of clay; V_s = volume of sand.

occupied by the bentonite gel is given by the sand porosity, n_s:

$$n_s = \frac{V_w + V_c}{V_T} \tag{2}$$

where $V_T = V_w + V_c + V_s$ is the total volume.

Figure 4 shows data from the swelling tests on the sand/bentonite mixtures on a graph of final clay void ratio against the logarithm of vertical effective stress. At low effective stress levels the behaviour of the mixtures was indistinguishable from the clay alone, and thus it can be inferred that the externally applied stress is supported by the clay. When the externally applied stress exceeds a threshold value there is little variation in the clay void ratio with increasing effective stress, and it can be inferred that the difference between the externally applied

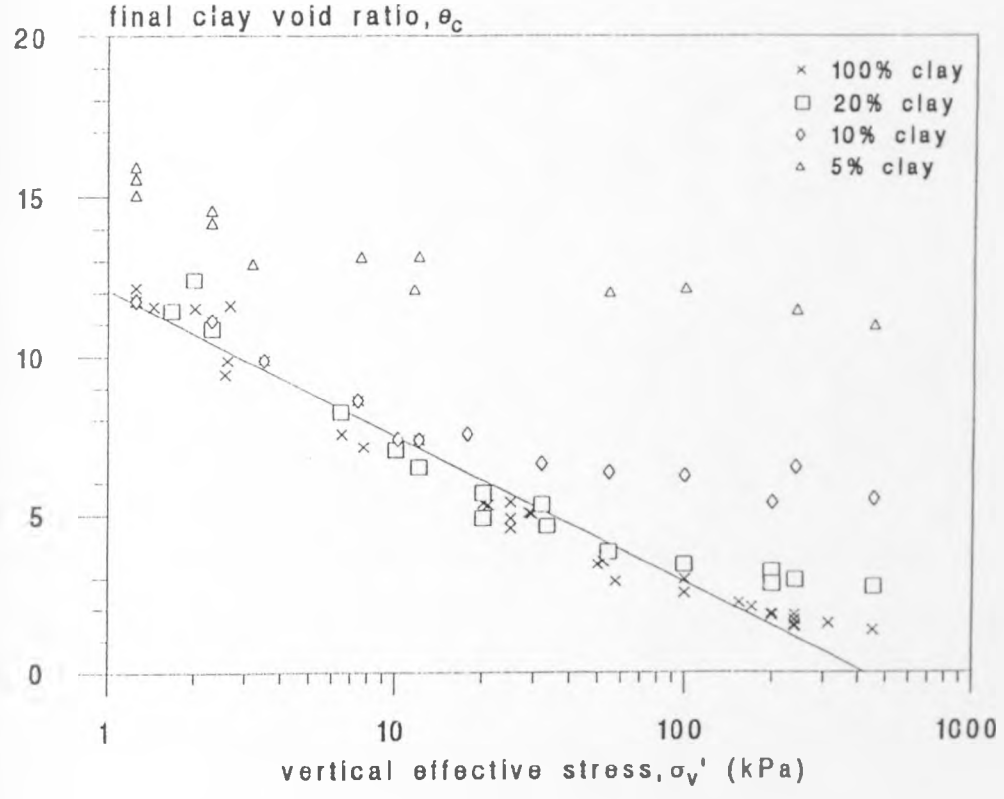

FIG. 4. Final clay void ratio of sand/bentonite mixtures after swelling with distilled water

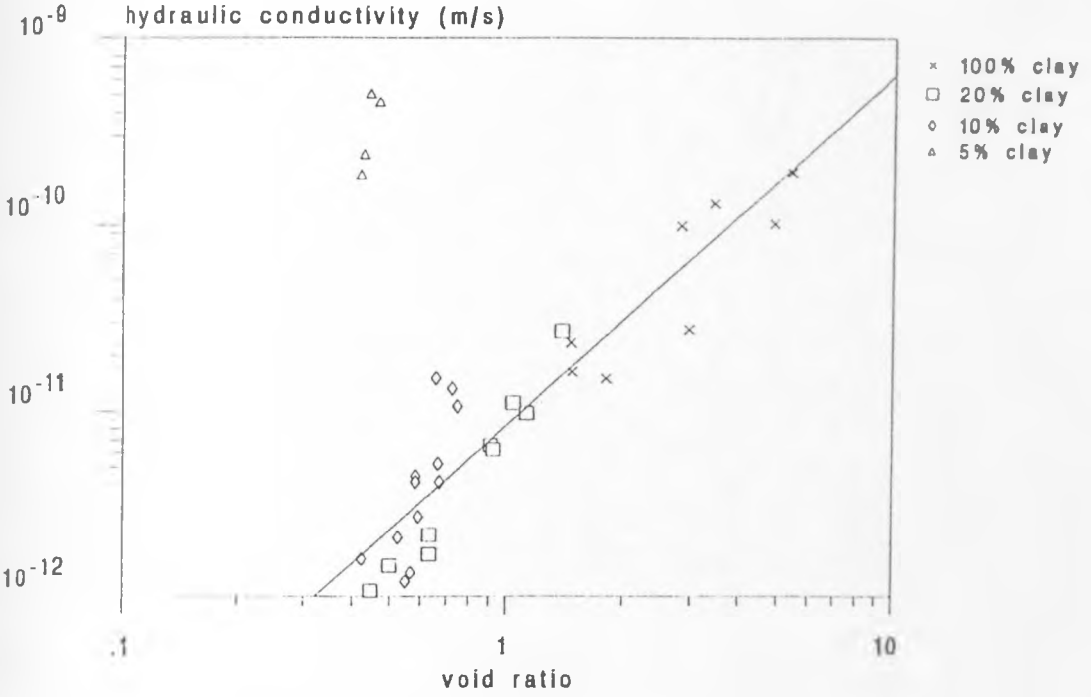

FIG. 5. Hydraulic conductivity of sand/bentonite mixtures

stress and the threshold value is supported largely by the sand, whose particles must now be in contact. The threshold value at which this change in the mixture's behaviour occurs appears to be a function of the clay content of the mixture.

Graham *et al.* (1986) proposed a similar explanation of the mechanical behaviour of sand/bentonite mixtures. They assumed that the internal stress distribution is a combination of inter-particle forces between sand grains and osmotic pressure between clay particles. In such a model, the osmotic pressure between the clay particles decreases as the clay void ratio increases. Therefore, at low confining stress, the clay in the mixture is able to swell against the surcharge and separate the sand particles to reach the same void ratio, for a given surcharge, as 100% bentonite powder. Whereas at high confining stress, the clay void ratio upon filling the sand pores is greater than the clay void ratio in equilibrium with surcharge stress, and the sand particles remain either partially or fully in contact.

Hydraulic conductivity

Terzaghi & Peck (1967) suggest a linear relationship between the logarithm of hydraulic conductivity and the logarithm of void ratio for a particular soil type. Similarly, the Kozeny-Carmen equation (Bear, 1972) indicates that the relationship tends to linearity at large void ratios. Figure 5 shows the hydraulic conductivity data (measured by three different methods) on such a plot. The data for 100, 20 and 10% bentonite mixtures fall on a single straight line indicating that these mixtures are behaving as the same soil type (the pore size term in the Kozeny-Carmen equation is the same).

The data for the hydraulic conductivity of the 5% bentonite mixtures shown in Fig. 5 do not show the same trend as the other data. The probable explanation is that the very low bentonite content leads to an uneven distribution of bentonite within the sand matrix (either due to the mixing method or an effect of compaction), and this resulted in preferential flow-paths. Cowland & Leung (1991)

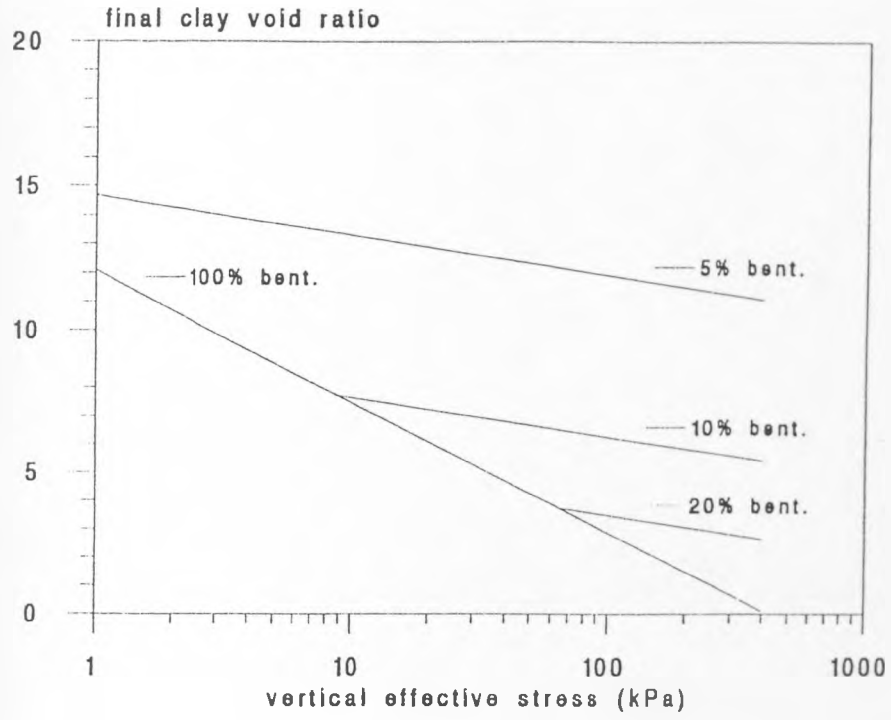

FIG. 6. Idealized swelling behaviour of sand/bentonite mixtures.

reported inhomogeneous mixtures at 5% bentonite content, and recommend a minimum bentonite content of 7% to avoid inhomogeneity.

DISCUSSION

When designing barriers of sand/bentonite mixtures, it is necessary to conduct a laboratory test programme before the final mix is selected. Therefore, it is necessary to characterize the swelling behaviour of sand/bentonite mixtures shown in Fig. 4. For a given mixture, the threshold stress (the maximum surcharge that can be supported solely by the clay) can be calculated from the 100% bentonite swelling behaviour, the bentonite content and an estimate of the sand porosity. The gradients of the right-hand section of each mixture swelling line are similar (Fig. 4), so it is reasonable to assume that they are equal. This is illustrated in Fig. 6, where a weighted average of the three gradients has been back-fitted to the data. Thus the swelling behaviour of a particular mixture can be estimated from experimental data for another similar mixture.

The straight-line relationship shown in Fig. 5 cannot be used directly to estimate the hydraulic conductivity of a mixture under a given surcharge because the conventional void ratio of a mixture will depend on its swelling behaviour. Therefore, the same data have been replotted in Fig. 7 on a logarithmic plot of the hydraulic conductivity against the clay void ratio. Now three distinct trends for 100, 20 and 10% bentonite mixtures are apparent (indicated with best-fit straight lines). The advantage of plotting the data as shown in Fig. 7 is that the clay void ratio can be determined from the idealized swelling behaviour for a particular mixture under a specified surcharge.

Figure 8 is a schematic diagram of a sand–bentonite mixture, showing bentonite gel occupying a tortuous pore within a sand matrix. Adopting the approach taken by Porter *et al.* (1960) to define the effective diffusion coefficient of an ion in saturated soil from it's diffusion coefficient in dilute solution,

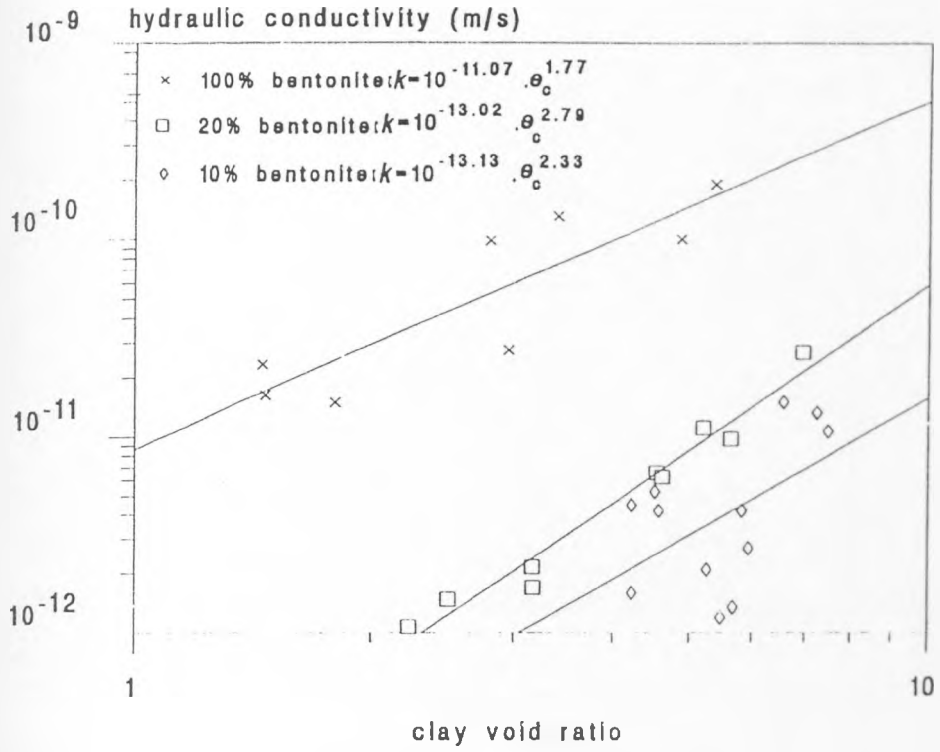

FIG. 7. Hydraulic conductivity of sand–bentonite mixtures (5% data omitted).

Darcy's flow law can be written as:

$$Q = k_{mix} A \frac{\Delta h}{\Delta L} = k_{clay} A_e \frac{\Delta h}{\Delta L_e} \qquad (3)$$

where Q is the flow volume, k is hydraulic conductivity, Δ_h is the head difference, ΔL is the macroscopic length over which flow takes place, ΔL_e is the average length of a flow tube through the sand, A is the cross-sectional area, A_e is the effective cross-sectional area available for flow normal to the flow direction. As $(A_e \cdot \Delta L_e / A \cdot \Delta L)$ is equal to n_s, and the sand tortuosity, τ_s, is defined as $(\Delta L / \Delta L_e)^2$, the relationship between the mixture and clay hydraulic conductivity is:

$$\frac{k_{mix}}{k_{clay}} = \frac{A_e}{A} \cdot \frac{\Delta L}{\Delta L_e} = n_s \tau_s \qquad (4)$$

Therefore the separation of the lines in Fig. 7 will depend on the sand porosity and tortuosity.

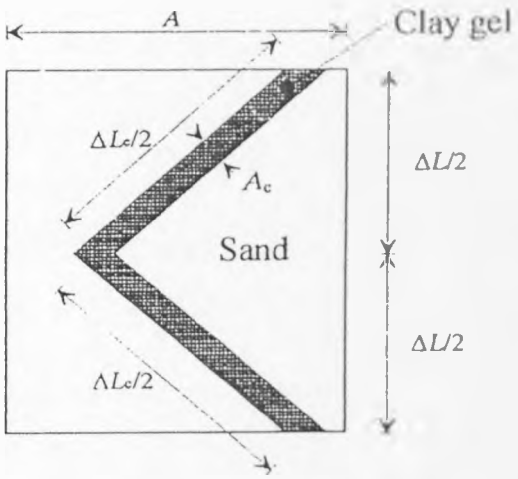

FIG. Simplified porous media.

At a clay void ratio of 5, Fig. 7 indicates that the combined sand porosity/tortuosity factors for the 20% and 10% bentonite mixtures are 0.06 and 0.02, respectively. At such a clay void ratio the sand porosities are 0.6 and 0.4 for the 20% and 10% clay mixtures, respectively, suggesting tortuosity values for the sand matrix of 0.10 and 0.05. This range is very low for a saturated sand (Shackleford & Daniel, 1991), although the effective particle size (D_{10}) of this sand is towards the lower limit of the sand range.

If a proposed mixture fails to meet a specified hydraulic conductivity then the mixture modification that is required depends on whether the sand particles are in contact under the applied stress. If they are in contact, increasing the clay content will decrease the hydraulic conductivity. However, when the clay is supporting the surcharge (i.e. the applied stress is below the threshold level) the only way to reduce the hydraulic conductivity of the mixture is to reduce the sand's porosity and value of tortuosity, and therefore the clay content of the mixture.

APPLICATIONS IN PRACTICE

It is proposed that rational design of a sand/bentonite mixture (to meet a hydraulic conductivity criteria at a particular surcharge stress) can be accomplished by: (1) measuring the swelling behaviour and hydraulic conductivity of the selected bentonite subjected to various surcharge stresses; (2) estimating the clay content for a suitable mixture based on typical sand porosity and tortuosity values; (3) testing of a mixture containing the estimated clay content to determine more appropriate sand porosity and tortuosity values; and (4) testing of a mixture with a clay content calculated from the measured sand porosity and tortuosity.

The bentonite swelling behaviour can be established conveniently in an oedometer cell (without a loading frame for lower surcharge stresses). At the end of each swelling test, a small loading increment can be applied to the bentonite specimens to determine the relationship between the void ratio and hydraulic conductivity (using Terzaghi's consolidation theory).

For a given mixture, the sand porosity at a particular surcharge stress can be calculated from the final volume reached in a oedometer swelling test. Sand tortuosity can then be calculated from the difference in mixture and bentonite hydraulic conductivities at the same clay void ratio using eqn. 4. If clay swelling separates the sand particles, a consolidation increment in an oedometer cell is sufficient to calculate the hydraulic conductivity, otherwise a more sophisticated apparatus (such as the Rowe cell reported here) must be used.

Economically, it is desirable to minimize the clay content of a sand/bentonite mixture. Other factors in favour of a low clay content are: (a) a mixture with the sand particles in contact is unlikely to exhibit macroscopic shrinkage cracks on drying; and (b) the mechanical stability of the mixture is provided by the sand matrix, and therefore it is desirable that some stress is carried by the sand after saturation. Factors against a low clay content are: (a) mixture ductility will decrease as the amount of stress carried by the sand increases; (b) contaminants from the landfill may permeate the mixture reducing the potential swelling of the bentonite; and (c) very low bentonite contents can lead to mixture inhomogeneity and a higher than expected hydraulic conductivity. A design compromise requires some stress to be carried by the sand matrix, whilst leaving the clay with reserve swelling capacity.

The data were obtained using water as the pore fluid. Despite this, the proposed design approach may still be applicable where the permeant is an aqueous solution (e.g. rain water that has leached other substances from the waste), provided that fluid is used for the testing programme. Swelling tests similar to those reported here have been conducted using various aqueous solutions as a pore fluid (P.G. Studds, pers. comm.). Similar linear swelling lines were found (on a plot of void ratio against logarithm of vertical effective stress), whose gradient and intercept (at 1 kPa) depended on the solution composition and concentration.

In the tests reported here, the vertical effective stress range imposed on the specimens was in the range 1 to 450 kPa. Such a stress range is sufficient for studying of the engineering behaviour of landfill liner materials, but extrapolation of the reported trends beyond this range may be inappropriate.

CONCLUSIONS

(1) Sodium bentonite powder swells on access to distilled water to reach a unique void ratio under a particular confining stress, and this void ratio varies linearly with the logarithm of vertical effective

stress. The gradient of this linear relationship is intermediate between the consolidation and rebound indices for consolidated bentonite slurry, indicating a difference in fabric from an initially 'wet' clay.

(2) The swelling behaviour of the mixtures can be characterized by a threshold stress that is a function of clay content. Below the threshold stress the clay in the mixture is able to swell against the surcharge and separate the sand particles to reach the same clay void ratio, for a given surcharge, as 100% bentonite powder. When the confining stress exceeds the threshold value, the clay void ratio upon filling the sand pores is greater than that in equilibrium with surcharge stress and the sand particles remain either partially or fully in contact.

(3) The relationship between hydraulic conductivity and void ratio for Wyoming Bentonite can be represented by a power law.

(4) Once the properties of a particular bentonite are known, the hydraulic conductivity of sand/bentonite mixtures can be predicted from the bentonite content, sand porosity and tortuosity, and the vertical effective stress.

(5) A very low bentonite content can lead to an uneven bentonite distribution within the mixture, and this can result in a higher hydraulic conductivity than would be estimated for a uniform mixture.

ACKNOWLEDGMENTS

The authors would like to thank Professor J.G. Cabrera for his help in preparing this paper, and gratefully acknowledge the support provided by EPSRC through a studentship to L. H. Mollins.

REFERENCES

Alther G., Evans J.C., Fang H.-Y. & Witmer, K. (1985) Influence of inorganic permeants upon the permeability of bentonite. *Hydraulic Barriers in Soil and Rock, ASTM STP* 874, 64–73.

Bear J. (1972). *Dynamics of fluids in porous media.* America Elsevier publishing Company, Inc. New York, London, Amsterdam.

Casagrande A. & Fadum R.E. (1940). *Notes on Soil Testing for Engineering Purposes: Soil Mech. Series* No. 8, Harvard Graduate School of Engineering.

Cowland J.W. & Leung B.N. (1991) A field trial of a bentonite landfill liner. *Waste Management and Research*, 9, 277–291.

Dixon D.A. & Gray M.N. (1985) The engineering properties of buffer material-research at Whiteshell Nuclear Research Establishment. *Proc. 19th Information Meet. Nuclear Waste Management Program.* AECL Technical Report, vol. 3, 513–530.

Dixon D.A, Gray M.N. & Thomas A.W. (1985) A study the of compaction properties of potential clay-sand buffer mixtures for use in nuclear fuel waste disposal. *Eng. Geol.* **21**, 247–255.

Dunn R.J. (1985) Laboratory measurement of a fine grained soil fluid conductivity. *Eng. Geol.* **21**, 215–223.

Englehardt W. Von & Tunn W.L.M. (1955) Flow of Fluids Through Sandstones. *Illinois State Geol. Survey - Cir*, n **194**, 16pp.

Garlanger J.E., Cheung F.K. & Tannous B.S. (1987) Quality control testing for a sand-bentonite liner *Geotechnical Practice for Waste Disposal*, 488–499.

Graham J., Gray M.N., Sun B.C.-C. & Dixon D.A. (1986) Strength and volume change characteristics of a sand-bentonite buffer. *Proc. 2nd Int. Conf. Radioactive Waste Management, Winnipeg, Manitoba*, 188–194.

Hoeks J., Glas H., Hofkamp J. & Rythner A H. (1987) Bentonite liners for isolation of waste disposal sites *Waste Management and Research*, **5**, 93–105.

Irmay S. (1965) Modèles théroiques d' écoulement dans. les corps poreux. *RILEM Bul* n **29**, Dec. 1965, 37–43.

Oscarson D.W., Dixon D.A. & Gray M.N. (1990) Swelling capacity and permeability of an unprocessed and processed bentonitic clay. *Eng Geol* **28**, 281–289.

Porter L.K., Kemper W.D., Jackson R.D. & Stewart B.A. (1960) Chloride diffusion in soils as influenced by moisture content. *Proc. Soil Sci. Soc. Amer.*, **24**, 400–403.

Schwarzendruber D. (1962) Non-Darcy flow behaviour in liquid saturated porous media. *J. Geophys. Res.*, **67(13)**, 5205–5213.

Shackleford C.D. & Daniel D.E. (1991) Diffusion in saturated soil. I: Background. *J. Geotechn. Eng.* **117(3)**, 467–484.

Terzaghi K. T. (1943). *Theoretical Soil Mechanics* Wiley, New York.

Terzaghi K. & Peck R.B. (1967). *Soil Mechanics in Engineering Practice*. A Wiley International Edition

Wu J.Y. & Khera R.P. (1990) Properties of a treated-bentonite/sand mix in contaminant environment. Pp. 47–59 in: *Physico-Chemical aspects of soil and related materials, ASTM STP* **1095**, (K.B. Hoddinott & R.O. Lamb, editors.), American Society for Testing and Materials.